



A Super-Capacitor Based Energy Storage for Quick Variation in Stand-Alone PV Systems

Khaled Sehil

A thesis submitted for the Degree of Doctor of Philosophy
at Brunel University London, UK

Department of Electronic and Computer Engineering
College of Engineering, Design and Physical Sciences
Brunel University London
United Kingdom.

January 2018

©This copy of the thesis has been supplied on condition that anyone who consults it is understood to recognise that its copyright rests with the author and that no quotation from the dissertation, nor any information derived therefrom, may be published without the authors prior, written consent.

Abstract

PHOTOVOLTAIC (PV) system is one of the most prominent energy sources, producing electricity directly from sunlight. In additionally, it is easy to install and is supported financially by many governments as part of their strategy to reduce *CO*₂ gas emissions, and to achieve their agreed set of reduction targets by 2020. In the meantime, researchers have been working on the PV system to make it more efficient, easy to maintain, reliable to use and cost effective.

In the stand-alone PV system, a battery is required. This is due to the fluctuating nature of the output energy delivered by the PV arrays owing to the weather conditions and the unpredictable behaviour of uses with regard to the consumption of energy. During the hours of sunshine, the PV system is directly feeding the load and any surplus electrical energy is stored in the battery at a constant current. During the night, or during a period of low solar irradiation, the energy is supplied to the load from the battery. However, the stand-alone PV system is designed to provide an acceptable balance between reliability and cost, which is a major challenge to the designer owing to the approaches used to size the PV arrays and the battery bank. As a result, the unpredictable, quick daily changes on the PV output is not dependable. Moreover, battery performance, length of life and energy efficiency depends on the rate at which it is discharged. Therefore, it is essential to use other methods to deal with any quick variation in energy.

In this thesis, a super capacitor is used to solve this problem, as it can deal with the fast-changing weather, or a rapid variation in the energy requirements of the customer. A critical evaluation with in-depth analysis of the placement and the implementation for the super-capacitor in the PV stand-alone system has been carried out. The results show, super-capacitor capacitance and the converter efficiency affect the delivered load energy. However, the bi-directional topology performs better than uni-directional under the same conditions.

Finally, a further improvement of the system at component level, has been developed through an energy recovery snubber for the switching transition and achieved a recovery of energy for the resistive load, 94.44% for the turn on transition and 92.86% for the turn off transition. Moreover, for the inductive load, 78.33% and 97.33% of energy has been recovered for the turn on and for the turn off transition respectively.

DECLARATION

I hereby declare that except where specific reference is made to the work of others, the contents of this thesis are original and have not been submitted in whole or in part for consideration for any other degree or qualification in this, or any other university. This thesis is my own work and contains nothing which is the outcome of work done in collaboration with others, except as specified in the text and Acknowledgements.

Signed By

Khaled Sehil

January 2018

Acknowledgements

وَفَوْقَ كُلِّ ذِي عِلْمٍ عَلِيمٌ

First of all, I am infinitely thankful to Allah for continuously blessing me and for providing me with strength and perseverance to achieve this work. Secondly, I would like to express my appreciation and gratefulness to the Engineering and Physical Sciences Research Council (EPSRC) for funding my PhD, I would also like to thank Dr Michael Theodoridis from Brunel University for giving me the opportunity to pursue my research.

It is difficult to put in words my gratitude to my supervisor Dr Mohamed Darwish, his invaluable research experience has been of great assistance for the successful completion of my research work. Dr Darwish's enthusiasm, care and motivation have helped to make my PhD experience much more interesting and productive. He has provided me with encouragement, inspiration, friendship and support. Dr Darwish, I am in debt to you and your kindness will not be forgotten.

I am also thankful to my second supervisor Dr Bary Rawn for his time and advice during my research. And, would like to show appreciation to my colleagues at Brunel University and my gratitude to all the staff at Brunel University as well. I would like to put a special thanks to my friend Dr Kamal Saadi for his support and encouragement.

Mostly, I wish to express my gratitude and loving thanks to my great mother and to the spirit of my father, which I wish the Almighty God to grant him His great mercy Amen. Without them I would never have been able to make it up to a PhD degree. I wish to dedicate this work to my father who wished the attainment of the highest standard in Education for me.

Contents

- 1 Introduction 1**
 - 1.1 Background 1
 - 1.2 Motivations 3
 - 1.2.1 PV System Efficiency 3
 - 1.2.2 Reliability of PV Systems 4
 - 1.3 Research Aim and Objectives 7
 - 1.4 Methodology 7
 - 1.5 Thesis Outline 8

- 2 Review of PV Systems 9**
 - 2.1 Introduction 9
 - 2.2 Overview of Photovoltaic Cells Configurations 9
 - 2.2.1 The Development of the PV System 9
 - 2.2.2 PV Cell Classification 10
 - 2.2.3 Mathematical Photovoltaic Model 12
 - 2.2.4 Photovoltaic Configurations 15
 - 2.3 Electrical Energy Storage System Overview 19
 - 2.3.1 Parameters of an Energy Storage Device 19
 - 2.3.2 Classification of an Electrical Energy Storage System 19
 - 2.3.2.1 Electrochemical Storage Systems 21
 - 2.3.2.2 Electromagnetic and Electrostatic Storage Systems 26
 - 2.4 Maximum Power Point Tracking Algorithms 31
 - 2.4.1 MPPT Techniques Comparison 43

2.5	Summary	44
3	Mathematical Modelling of Converter Topologies and SC as Storage Unit in PV System	45
3.1	Overview	45
3.2	Converter Topologies	45
3.2.1	Buck Converter	46
3.2.2	Boost Converter	50
3.2.3	Buck - Boost Converter	52
3.3	Snubber Circuits	57
3.3.0.1	Electrical Snubbers Circuit Classification	58
3.4	Super-Capacitor	62
3.4.1	Equivalent Circuits	62
3.4.2	Charge-Discharge Method	65
3.4.2.1	Super-Capacitor Charging	65
3.4.2.2	Super-Capacitor Discharge	66
3.4.3	Voltage Balancing	67
3.4.3.1	Voltage Balancing Type	68
3.5	Summary	69
4	Result and Discussions	70
4.1	Introduction	70
4.2	Stand-alone PV System Layout	70
4.2.1	Unidirectional Topology:	71
4.2.2	Bidirectional Topology:	71
4.3	Methodology	72
4.3.1	Storage Effect on the System Performance	77
4.3.1.1	Uni-directional Topology	77
4.3.1.2	Bi-directional Topology	80
4.3.2	Load Effect on the System Performance	83
4.3.3	The effect of Converter Efficiency	85
4.3.4	Comparisons Between Both Topologies	88
4.3.4.1	Capacity Storage	88

4.3.4.2	Load Power	90
4.3.4.3	Converter Efficiency	91
4.4	Summary	95
5	Simulation and Implementation of the Proposed PV System	96
5.1	Introduction	96
5.2	Stand-alone PV System without Storage	97
5.3	Proposed System with Power Management	101
5.3.1	Discussion	104
5.4	Energy Recovery Snubber Circuit	113
5.4.1	Resistive Load	113
5.4.2	Inductive Load	121
5.5	Summary	128
6	Conclusions and Future Work	129
6.1	Conclusions	129
6.2	Future Work	133
	Appendix A Extra Storage types in Power System	151
	Appendix B Super-Capacitor Model In MATLAB	156
	Appendix C MOSFET Datasheet	166

List of Figures

1.1	Incremental Global Renewables-based Electricity Generation [1]	2
1.2	Energy Generation from Solar PV Globally [2]	2
1.3	Cost of PV Electricity VS Utility Peak and Bulk Electricity [3]	3
2.1	PV Cell Technology	11
2.2	Equivalent Circuit of a Solar Cell	12
2.3	PV System Elements [4]	16
2.4	Centralized PV System	17
2.5	String PV System	17
2.6	Multi-String PV System	18
2.7	Module Integrated PV System	18
2.8	Main form of EESS [5]	20
2.9	Battery Representation [6]	22
2.10	The Operating Principle of Flow Batteries. [5]	26
2.11	Comparison of the Energy Densities of Aqueous and Non-Aqueous Batteries [7]	27
2.12	SC Interior Illustration [5, 8]	30
2.13	PV Cell Performance	33
2.14	PV Electrical Characteristics	33
2.15	Block Diagram of MPPT Implementation	34
2.16	Fixed step-size P&O method flowchart	37
2.17	Incremental Conduction Flowchart	39
2.18	General Diagram of Fuzzy Logic Controller	41
2.19	Neural Network Representation	42

3.1	Buck Converter	46
3.2	Buck Converter Representation when Switch Closed	47
3.3	Buck Converter Representation when Switch Opened	47
3.4	Boost Converter	51
3.5	Boost Converter Representation when Switch Closed	51
3.6	Boost Converter Representation when Switch Opened	51
3.7	Back Boost Converter Circuit	53
3.8	Buck Boost Switch On	53
3.9	Buck Boost Switch Off	54
3.10	Instantaneous Power in Switch On Transition	56
3.11	Dissipative Snubber Topology [9, 10]	58
3.12	Combined energy recovery Snubber	61
3.13	Active Snubber	61
3.14	The Three Branch Model	62
3.15	SC Multiple Branches Model	63
3.16	SC Transmission Line Model	63
3.17	SC Electrical and Thermal Model [11]	63
3.18	Equivalent Electrical Circuit Model for Super-Capacitor [12]	64
3.19	Super-capacitor Model [13]	64
3.20	SC Charge Process	65
3.21	Super-Capacitor Discharge Process	66
3.22	Active Balancing [14]	69
4.1	Unidirectional Topology	71
4.2	Bidirectional Topology	72
4.3	Super-capacitor Equivalent Circuit	74
4.4	Real Data [15]	74
4.5	Program Overall Process	75
4.6	Flowchart of Data Processing Algorithm	76
4.7	Unidirectional Results.	78
4.8	Unidirectional Results.	79

4.9	Bidirectional results.	81
4.10	Bidirectional Results.	82
4.11	Load Effect for Both Topologies	84
4.12	Efficiency Effect on Both Topologies.	86
4.13	Efficiency Effect on Both Topologies.	87
4.14	Comparison Between Both Topologies for Capacity Affect.	89
4.15	Comparison Between Both Topologies with same Capacity Storage Under Different Loads	90
4.16	Comparison Between Both Topologies for Converter Efficiency Affect Under Different Capacitance	94
5.1	Power Overview in Stand-alone PV System Without Storage unit	98
5.2	Comparison between produced energy & delived in PV system without storage	99
5.3	Energy flow in Stand-alone System with SC	100
5.4	Overall System	102
5.5	Bidirectional converter	103
5.6	Power management	104
5.7	Power Management Flow	105
5.8	Super-Capacitor Behaviour of Electrical parameter	106
5.9	Converter Switches Controlled Signal	107
5.10	Discharge Idle Discharge	107
5.11	Switch Control Signal in Case 2	108
5.12	Super-capacitor Electrical Parameters Behaviour	108
5.13	Power Management with 50F of Capacitance	109
5.14	Super-Capacitor Performance for 50F of Capacitance	110
5.15	Switches Control Signal of Capacitance for 50F of Capacitance	110
5.16	Power Management with 5F of Capacitance	112
5.17	Super-Capacitor Performance for 5F of Capacitance	112
5.18	Boost Converter and Resistive Load	114
5.19	Boost Converter with Energy Recovery Snubber & Resistive Load	114
5.20	Switch Turn on/off without Snubber Circuit	115

5.21	Switch Turn on/off with Snubber Circuit	116
5.22	Switch Turn on Transition zoom-in without Snubber Circuit	116
5.23	Switch Turn on Transition zoom-in with Snubber Circuit	117
5.24	Switch Turn off Transition zoom-in without Snubber Circuit	118
5.25	Switch Turn off Transition zoom-in with Snubber Circuit	119
5.26	Switch Wave form Improvement at Turn on Transition	120
5.27	Boost Converter with Energy Recovery Snubber and RC Snubber	120
5.28	Switch Wave form Improvement at turn off Transition	121
5.29	Boost Converter	122
5.30	Boost Converter with Energy Recovery Snubber Circuit	123
5.31	Switch Turn on/off Inductive Load	124
5.32	Switch Turn on/off Inductive Load with Snubber Circuit	125
5.33	Switch Turn on Transition Inductive Load zoom-in	126
5.34	Switch Turn on Transition Inductive Load zoom-in With Snubber Circuit	126
5.35	Switch Turn off Transition Inductive Load zoom-in	127
5.36	Switch Turn off Transition Inductive Load zoom-in with Snubber Circuit	127
5.37	Conduction Losses for the Switch	128
A.1	The operating principle of compressed air energy storage [5]	152
A.2	The illustrative topology of a flywheel-based ESS	153
A.3	Characteristics of storage technologies	155

List of Tables

1.1	Photovoltaic cell technology	5
1.2	Li-Ion Battery and Super-Capacitor Comparison	6
2.1	Electrical Power System Storage Type [5, 8, 16–24]	32
2.2	MPPT Comparison	43

Abbreviations

AC	Alternating Current
ANN	Artificial Neural Network
CIGS	Copper Indium Gallium Diselenide
CLSP	Continuous Load Supply Period
CNT	Carbon Nanotubes
CPV	Concentrator Photovoltaic
CV	Constant Voltage
DC	Direct Current
EESS	Electrical Energy Storage System
EPIA	European Photovoltaic Industry Association
ESR	Equivalent Series Resistance
eV	electron Volts
MJ	Multi-Junction
MPP	Maximum Power Point
MPPT	MPP Tracking
OV	Open Voltage
P&O	Perturbation and Observe
PV	Photovoltaic
RC	Resistor Capacitor
SC	Super Capacitor
SMES	Super-Conducting Magnetic Energy Storage
TFSC	Thin Film Solar Cells
UN	United Nation
UN-IPCC	UN Intergovernmental Panel on Climate Change

Chapter 1

Introduction

1.1 Background

THE 2007 Nobel Prize winning organisation united nation intergovernmental Panel on Climate Change (UN-IPCC) estimates that the world will need the equivalent of 32000 *TWH* of electrical energy by 2030 to meet social and economic development. As a result, environmental problems will increase if we keep using fossil fuels as source of energy owing to the production of high level of carbon dioxide CO_2 when they are burnt. However, the growing awareness of climate change, and the requirement to meet the target reduction of greenhouse gas emission polices (as prescribed by the Kyoto Protocol) means that a substantial fraction of our energy must be generated without any CO_2 emissions. This should be achieved within the next 10 to 20 years for energy security and the reduction of global greenhouse-gas emissions [25, 26].

The achievable 2030 set target of CO_2 emission reduction by the world leaders significantly increases the implementation of renewable energy such as wind, solar, biomass, tidal power, geothermal and hydroelectric power as shown in Figure 1.1. However, solar energy (photovoltaic (PV)) has some advantages over the others; it has no moving parts, it is not noisy, requires less maintenance and is harmless in comparison to the wind turbine. It is also capable of recycling its modules, and provides a clean source of energy transformed directly from sunlight into electricity. Photovoltaic energy can bring electricity to a rural home-maker who lives far from the nearest grid connection. Furthermore, the panels are easy to install (on roofs, parking areas, vertical facades on skyscrapers or on adjacent land). The European Photovoltaic Industry Association (EPIA) predicts that PV could provide 12%

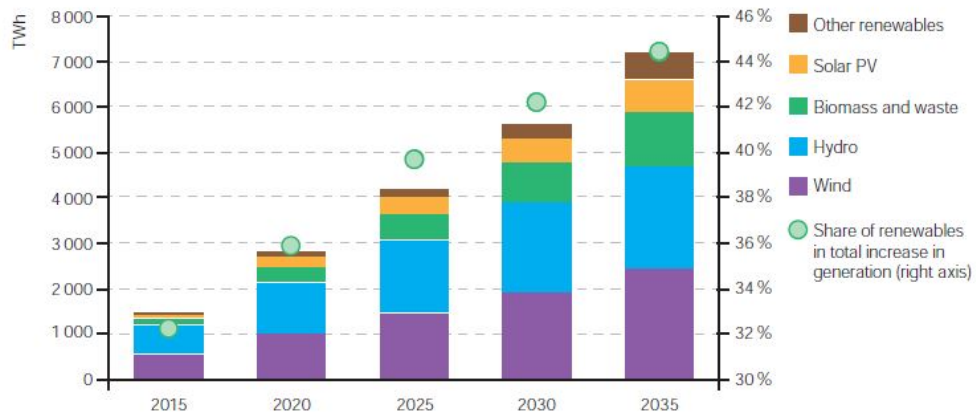


Fig. 1.1: Incremental Global Renewables-based Electricity Generation [1]

of Europe’s energy by 2020, and the International Energy Agency anticipates that PV could provide over 11% of the world’s electricity by 2050 [26].

The correlation between public awareness of climate change and the vital role of renewable energies in combating it, along with government subsidies and feed-in tariffs, has encouraged residential and investors to enhance PV system [27, 28]. Furthermore, with the new policies, power generated from PV systems in 2035 is over 26 times that of 2011 and is predicted to increase from 67 *GW* in 2011 to 600 *GW* in 2035 [2, 26].

Figure 1.2 illustrates the use of PV system around the world by 2035 [2, 29]

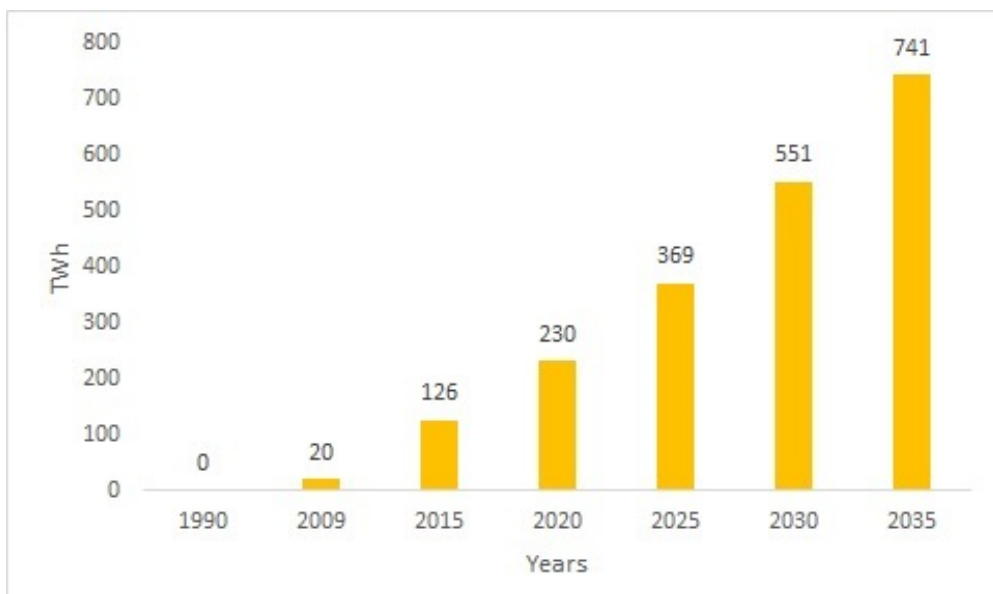


Fig. 1.2: Energy Generation from Solar PV Globally [2]

1.2 Motivations

The last ten years has seen significant technology development make the PV system economically competitive and more efficient. Manufacturing cost of generators has also declined by around 58% between 2010 and 2015, and this trend is likely to continue [30]. The International Renewable Energy Agency estimates that the cost of solar PV will fall by another 57% by 2025, as Figure 1.3 shows [3,30].

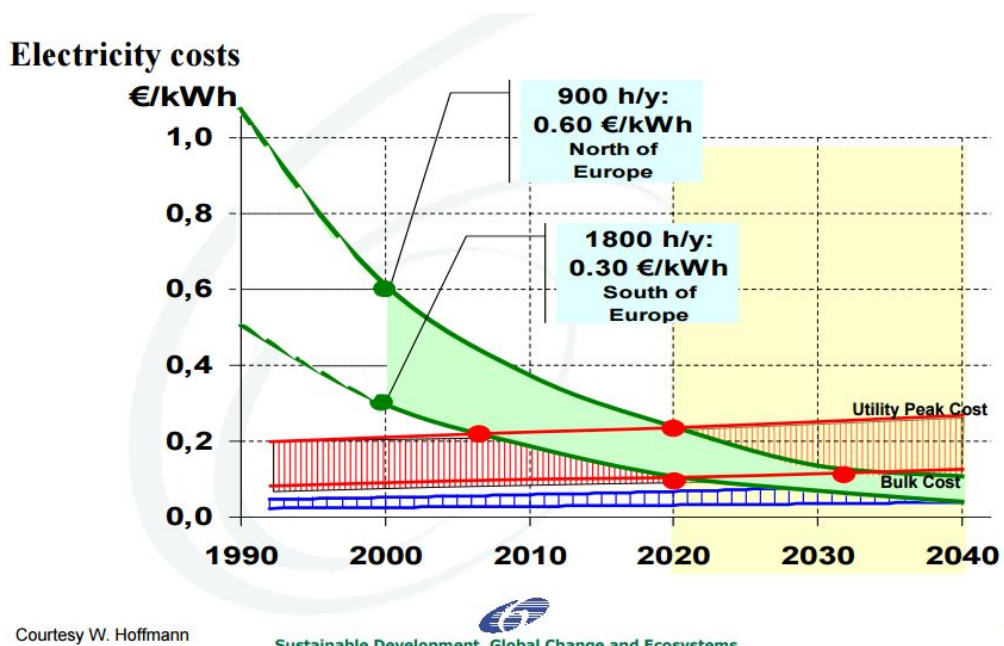


Fig. 1.3: Cost of PV Electricity VS Utility Peak and Bulk Electricity [3]

However, the PV system as a whole is still less efficient and less reliable in comparison to other type of power generation system owing to unpredictable hourly or daily output.

1.2.1 PV System Efficiency

The low efficiency PV system is an aggregation of many factors, which starts with the PV cell material (which allows the conversion of the sunlight to electricity) and ends with the converter technology.

To improve the conversion efficiencies, ongoing research is performed in the material aspect of the cell such as crystalline silicon solar cells ($c - Si$) and is often referred to as "first generation". Thin film solar cells ($TFSC$), which comprise a variety of technologies: amorphous silicon ($a -$

Si), copper indium gallium diselenide (*CIGS*, $Cu(InGa)S_2$), cadmium telluride (*CdTe*), and also concentrator photovoltaic (*CPV*), where expensive and efficient multi-junction (*MJ*) solar cells receive a high intensity of sunlight focused by concentrators made of lenses or mirrors. Thin film solar cells are often referred to as "second generation" tandem cells thanks to nanotechnology, Quantum Dots and organic PV. Overall, materials with high light absorption and higher band gap energy are more efficient, as shown in the Table (1.1) which summarises commercial PV cell technology [29, 31–35]. Thus, in solar cells the efficiency is strongly related to the generation of electronhole pairs caused by light.

The interface between the PV cell and the load presents another efficiency issue, as the interface consists of power electronic components to allow the stepping up or down of the voltage. Passing the current through a conductor or an electrical component creates some heat. This heat is a waste of electrical energy and, as a result, the interface has a low efficiency. However, much research has been done to improve this interface efficiency and up to 98% is now achievable. Lastly, the extraction of the maximum power from the PV cell at all times, regardless of weather conditions, is desirable. A lot of research has been conducted in this area and many algorithms been developed.

1.2.2 Reliability of PV Systems

The dependency of generated power on the presence of light is the main drawback of the PV system. To overcome this issue the improvement of energy storage has a crucial role. By improving the storage method, the reliability of the PV system increases dramatically especially in stand-alone systems with regard to the consistency of the output power. However, standalone PV systems use battery power to provide support when solar energy is insufficient to satisfy load demand. Moreover, in stand-alone systems, the battery capacity is calculated to the average annual use, and also for at least three days of island autonomy. This means that the daily quick change in PV output is not dependable and, as a result, battery life is significantly reduced. Introducing a super-capacitor as storage unit, in a complementary manner, to deal with this quick power variation owing to the changing weather and the load power demand, together with or separately of the power used, reduces the drawback of the battery through high power density, longer life cycles, and high efficiency. This will prolong battery life and overall system reliability.

Table 1.2 shows a comparison between a super-capacitor and the best battery on the market at the present time [36–44].

Tab. 1.1: Photovoltaic cell technology

Technology	Crystalline wafer based		Thin Film		Multi-junction
	Monocrystalline (%)	Multicryst. silicon (%)	Amorphous silicon (%)	Cadmium telluride (%)	
Cell technology shares	42.2	45.2	5.2	4.7	0.5
in 2007					
Cell Efficiency	16 - 19	14 - 15	5 - 7	8 - 11	7 - 11
Module Efficiency	13 - 17	12 - 14	-	-	-
Module Efficiency (laboratory)	22.97 ± 0.6	15.57 ± 0.4	10.47 ± 0.5	10.97 ± 0.5	13.57 ± 0.7
	-	-	-	-	55.9

<i>Type</i>	<i>Li-ion battery</i>	<i>Super-capacitor</i>
Storage Method	Faradic Reaction	Electrostatic interactions
Energy level	High (150 – 250 Wh/kg)	Limited (1 – 10 Wh/kg)
Specific power	1000 – 3000	Up to 10,000
Power level	Limited by mass transport	Limited by electrolyte conductivity
Cost per capacity	\$500 – 3,800 $/kWh$	\$300 – 20,000 $/kWh$
Cycle life	500 – 2,000 <i>cycles</i>	$\geq 10^6$ cycles
Cycle efficiency	94% – 95%	97% – 98%
Cell voltage	3.6 – 3.7 V	2.3 – 2.75 V
Charge time	10 – 60 <i>Min</i>	1 – 10 S
Temperature range	20 – 60 $^{\circ}C$	40 – 70 $^{\circ}C$
Internal resistance	150 – 200 $m\Omega$	0.1 – 1 $m\Omega$
Self-discharge rate	10%/month	20% – 40%/day
Thermal runaway risk	Yes	No
High-temperature performance	Cannot operate long at high temperatures	Can operate long times at 50 To 65 $^{\circ}C$
Low -temperature performance	Cannot operate long at low temperatures	Can operate long times at –30 To –40 $^{\circ}C$

Tab. 1.2: Li-Ion Battery and Super-Capacitor Comparison

1.3 Research Aim and Objectives

The aim of this research is to improve the overall reliability and efficiency of stand-alone PV systems by proposing a new storage system which incorporates a super-capacitor to overcome the mismatch of energy between the PV production the load consumption for short periods of time. Furthermore, a reduction of the switching losses at the electronic switches and the reuse of this energy was implemented through an energy recovery snubbers circuit.

In order to achieve this aim the following objectives were set:

1. To undertake an extensive literature review through books, journals and conference papers concerning a stand-alone PV system and its storage units.
2. To critically review the main converter topologies used in a stand-alone PV system.
3. To critically classify the storage techniques in a stand-alone PV system.
4. To investigate and critically review the placement of the super-capacitor as a storage unit in a stand-alone PV system.
5. To propose a power management method in stand-alone PV system with a super-capacitor.
6. To propose and implement an energy recovery snubber circuit to reduce the power losses in the converter switches.
7. To propose a system in order to provide a smooth power transfer between the PV source and the storage unit with load.
8. To implement an energy recovery snubber with a $DC - DC$ converter.
9. To empirically validate the simulation results.

1.4 Methodology

In this thesis the methodology used is a modelling and simulation approach. Each of the circuit-blocks in the proposed work are modelled and simulated on Matlab / Simulink for the energy management algorithm , and SIMetrix/SIMPLIS software for the switching losses.

1.5 Thesis Outline

This thesis is organized into six chapters, with the relationships to the thesis objectives presented in section 1.3. Each chapter will start with a brief introduction to provide an overview and highlight the main contributions of the chapter. At the end of each chapter a brief summary is presented.

Chapter 1: Provides a brief background about renewable energy, especially a *PV* system, and is followed by a description of the research motivation, aims, objectives and the layout of the thesis.

Chapter 2: Starts with a short review of how PV systems have evolved, and is followed by the mathematical model of the PV cell and the main storage system used in stand-alone PV system respectively. This is followed by storage system classification and, lastly, a definition of the maximum power point tracking (MPPT) principle and a list of MPPT methods.

Chapter 3: Covers the main PV converter topologies and PV storage system. This includes converter functionality, with individual mathematical models displayed via block diagrams. Comparisons of the converters is followed by snubber circuit descriptions, mathematical derivation, modelling types and functionalities. Super-capacitor modelling type and voltage balancing between cells are also carried out.

Chapter 4: Gives a detailed critical analysis of the placement of the super-capacitor in stand-alone PV systems with conventional power conversion topologies.

Chapter 5: Illustrates the proposed energy management configuration simulated in Matlab/Simulink and the simulation outcomes. The different scenarios presented are supported by the appropriate graphs and results. Additionally a further enhancement on the system in the component level were presented and simulated with SIMetrix/SIMPLIS and PSPICE.

Chapter 6: Concludes the thesis and explores suggestions for future research.

Chapter 2

Review of PV Systems

2.1 Introduction

This chapter briefly reviews PV system technology starting with a short history of PV technology development. An illustration of a PV model is mathematically explained, followed by an example of a PV configuration and an overview of storage techniques used in power system. Lastly, the maximum power point tracking (*MPPT*) principle is defined.

2.2 Overview of Photovoltaic Cells Configurations

2.2.1 The Development of the PV System

The modern era of photovoltaics started in 1954 when researchers at Bell Laboratories in the USA accidentally discovered that *pn* junction diodes generated a voltage when the room lights were on, which led to the identification of the photoelectric properties of silicon. Within a year, they had produced a 6% efficient *Si pn* junction solar cell [45]. In the same year, the group at Wright Patterson Air Force Base in the US published results of a thin film heterojunction solar cell based on *Cu₂S/CdS* also having 6% efficiency [46]. A year later, a 6% *GaAs pn* junction solar cell was reported by radio corporation of America (RCA) Lab in the US [47]. By 1960, several key papers by Prince, Loferski, Rappaport and Wysocki [48–50], Shockley (a Nobel laureate) and Queisser [51], developed the fundamentals of *pn* junction solar cell operation, including the theoretical relation between energy band gap, incident spectrum, temperature, thermodynamics, and efficiency. Since then, there

has been a tremendous advance in the technology of the cells and all the associated PV power plant components [5].

PV is the technology that generates direct current (DC), and an electrical power measured in watts (W) or kilowatts (kW) from semiconductor materials, when they are illuminated by photons. As long as light is shining on the solar cell, it generates electrical power. When the light stops, the electricity stops.

Semiconductor materials have weakly bonded electrons occupying a band of energy called the valence band. When energy exceeding a certain threshold, called the band gap energy, is applied to a valence electron, the bonds are broken and the electron is free to move around in the conduction band where it can conduct electricity through the material. Thus the energy needed to free the electron can be supplied by photons, which are particles of light.

$$E_{\lambda} = \frac{hc}{\lambda} \quad (2.1)$$

where E_{λ} is the photo energy, h is Planks constant, c is the speed of light and λ is wavelength. Only photons with sufficient energy can create an electron. However, the size of the band gap is a great influence on solar cell efficiency. If the band gap is too large many photons possess insufficient energy to create electron - hole pairs. However, if they are too small, many photons have a lot of excess energy that must be dissipated as heat. It is found that efficient harvesting of the suns energy requires band gap in the range of 1.0 - 1.6 electron volts (eV).

2.2.2 PV Cell Classification

The first generation of terrestrial PV crystalline Si wafers the second generation of PV thin films of amorphous Si , $CdTe$, or $CuInGaSe_2$ and the third generation PV organic dye-sensitized junctions mimicking photosynthesis, advanced very high efficiency theoretical concepts such as multiphoton and intermediate band solar cells. However, solar cell materials are chosen largely on the basis of how well their absorption characteristics match the solar spectrum and upon their cost of fabrication [26, 34]. A classification diagram of current PV cell technology illustrated in Figure 2.1

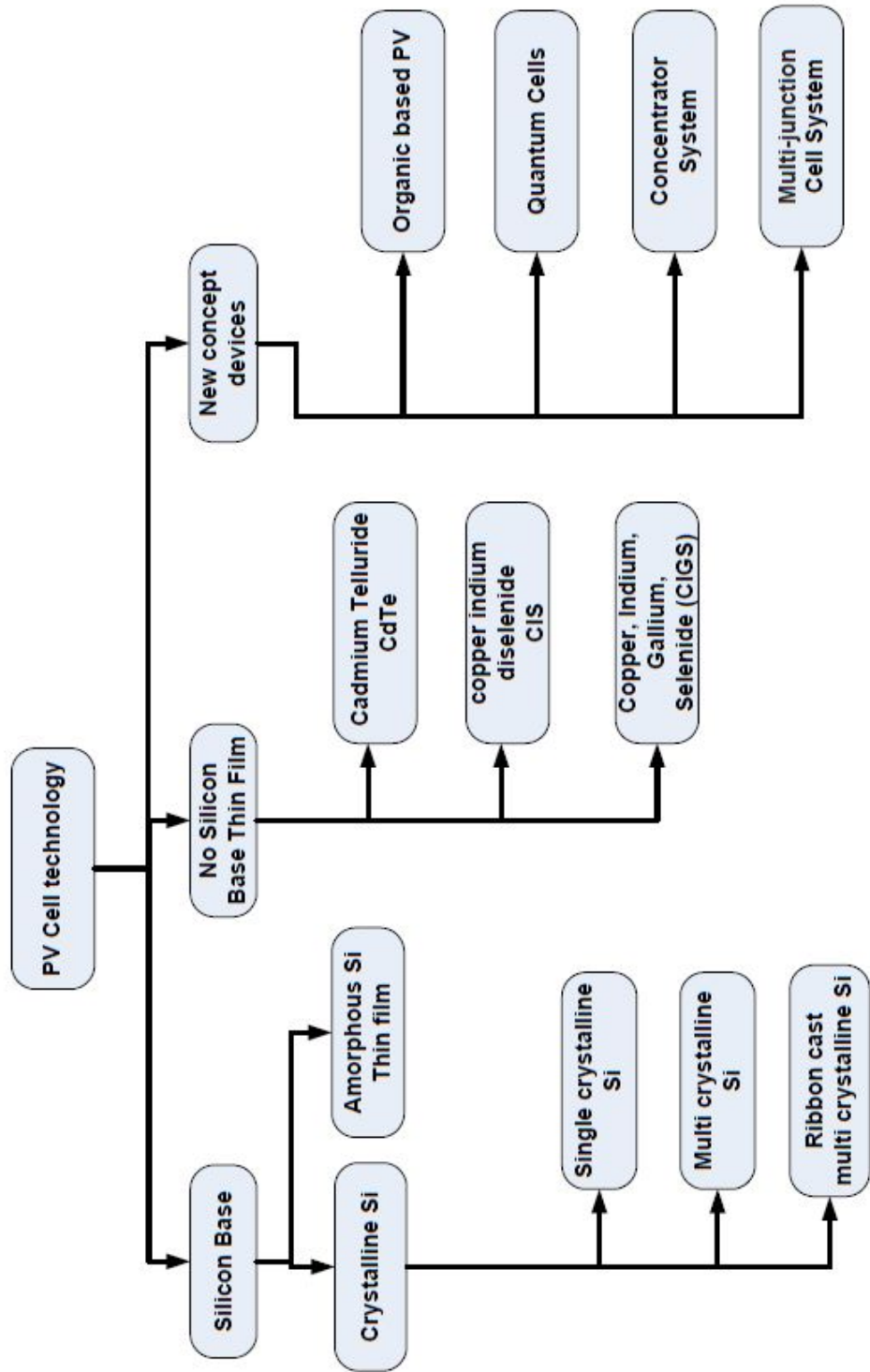


Fig. 2.1: PV Cell Technology

2.2.3 Mathematical Photovoltaic Model

PV system power characteristics output varies and crucially influenced by the temperature and the irradiation which are a non-linear function [52–54]. Figure 2.2 shows the equivalent circuit of single cell PV Walker Model.

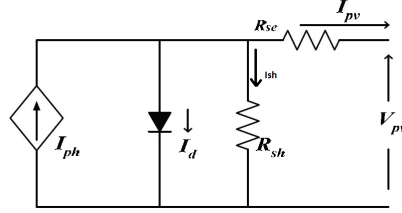


Fig. 2.2: Equivalent Circuit of a Solar Cell

The following equation describes the PV system [53, 55, 56]

$$\begin{aligned}
 I_{pv} &= I_{ph} - I_d - I_{sh} \\
 &= I_{ph} - I_{sat} \left(\exp \left(\frac{qV_{pv}}{AkT} \right) - 1 \right); \quad \text{For ideal photovoltaic cell} \\
 &= I_{ph} - I_{sat} \left(\exp \left(\frac{q(V_{pv} + R_{se}I_{pv})}{AkT} - 1 \right) - \frac{V_{pv} + I_{pv}R_{se}}{R_{sh}} \right); \quad \text{practical PV cell}
 \end{aligned} \tag{2.2}$$

$$\begin{aligned}
 I_{ph} &= (I_{sc} + k_I[T - 298]) \frac{G}{G_n} \\
 &= n_p I_{ph} - n_p I_{sat} \left(\exp \left(\frac{q}{AkT} \left(\frac{V_{pv} + R_{se}I_{pv}}{n_s} + \frac{R_{se}I_{pv}}{n_p} \right) - 1 \right) - \frac{1}{R_{sh}} \left(\frac{V_{pv}}{n_s} + \frac{I_{pv}R_{se}}{n_p} \right) \right); \quad \text{practical PV array}
 \end{aligned} \tag{2.3}$$

where

T : Cell temperature [K]

I_{pv} : The current output of the PV array [A]

I_{ph} : Photo-current (light generating current)[A]

I_d : Leakage current owing to diode effect [A]

I_{sat} : Cell reverse-saturation current [A], the effect of increasing this value corresponding to the decrease in the open circuit voltage.

V_{pv} : Voltage output of the PV array [V]

n_s : Number of PV module in series connection

n_p : Number of PV module in parallel connection

q : Charge of electron $1.602 * 10^{-19}[C]$

A : Ideality factor (for amorphous =1, crystalline=2), If this value increases the open circuit voltage increases

k : Boltzmanns constant $1.381 * 10^{-23}[Nm/K]$

I_{sc} : Short circuit current at $25^{\circ}C$

G : Solar irradiance [w/m^2]

G : Nominal Solar irradiance level [$1000w/m^2$]

$k_I = 0.0017A/^{\circ}C$ is the cells short circuit current temperature coefficient

R_{se} : Series resistance of the PV [Ω], caused by the movement of current through the emitter and base of the solar cell; and the contact resistance between the metal contact and the silicon; and the resistance of the top and rear metal contacts [57]. These factor have a marked effect on the $I - V$ characteristic near the open circuit condition which means that the power output of the cell will be reduced, although high values (very large) may also reduce the short-circuit current

R_{sh} : Parallel leakage resistance [Ω], acts on the slope of the characteristic near the short circuit condition and so causes PV cell current to fall more steeply indicating a high loss of power.

PV arrays are formed by connecting multiple PV modules in various configurations (series, parallel and mixed). A bypass diode is connected in parallel with each PV module to protect the solar cells against efficiency degradation and hot spot failure effects. When cells or panels are series connected the produced voltage is increased and when they are connected in parallel there is an increase in current. The number of modules that are connected in series and the number of parallel-connected is determined by the desired electrical energy. Maximum efficiency is the ratio of the maximum power

which is equal to $I_m \times V_m$ over the input power which is the ambient solar irradiance multiplied by the cell area.

However, the higher the irradiance, the greater the current with small variation in voltage under constant temperature. Under temperature variation and constant irradiance, the solar cell generates almost constant current or a slightly higher current, but the output voltage decreases.

Newton-Raphson algorithm used to solve Equation 2.2. In this method an iterative procedure takes place, in which each successive iterate can be computed based on the following equation $x_{n+1} = x_n - \frac{f(x)}{f'(x)}$

$$i_{pv(n+1)} = i_{pv(n)} - \frac{-i_{pv(n)} + i_l - i_{sat} \left(\exp \left(\frac{q}{AkT} \left(\frac{V_{pv}}{n_s} + \frac{R_{se} I_{pv}}{n_p} \right) - 1 \right) \right)}{-1 - i_{sat} \left(\frac{q R_{se}}{AkT} \exp \left(\frac{q}{AkT} \left(\frac{V_{pv}}{n_s} + \frac{R_{se} I_{pv}}{n_p} \right) - 1 \right) \right)} \quad (2.4)$$

Overall, the solar cell can be characterized by three parameters:

- Short circuit current I_{sc} : This is the greatest current generated by a cell, produced under short circuit conditions, where the output voltage is equal to zero $V_{sc} = 0$.
- Open circuit voltage V_{oc} : This corresponds to the voltage drop across the diode "p-n junction", namely when the generated current is zero $I_{PV} = 0$. It reflects the the cell in the night and it can be mathematically expressed as:

$$V_{oc} = \frac{mkT_c}{e} \left(\ln \frac{I_{ph}}{I_{pv}} + 1 \right) \quad (2.5)$$

- Fill factor FF is a parameter that characterizes the non-linear electrical behavior of the solar cell, which is the ratio of the maximum power that can be delivered to the load and the product

of I_{sc} and V_{oc}

$$FF = \frac{P_{max}}{V_{oc}I_{sc}} = \frac{V_{max}I_{max}}{V_{oc}I_{sc}} \quad (2.6)$$

The energy conversion efficiency for solar cells is calculated using the following equation :

$$\eta = \frac{V_{max}I_{max}FF}{P_{in}} \quad \text{where } P_{in} \text{ is the total power in the light incident on the cell} \quad (2.7)$$

Overall, the main factors that effect the *PV* cell efficiency are the energy band gap of the semiconductor, the operating temperature, the incident light, the type and purity of the material and parasitic resistances [58].

2.2.4 Photovoltaic Configurations

PV systems consist of many cells which form a module. Thus, a *PV* panel is number of modules connected to each other. A group of such panels is called a *PV* array. These elements can be connected in series or in parallel electrical arrangements to provide the required current or voltage to operate electrical loads. In general, cells connected in parallel increase the current and cells connected in series provide greater output voltages [54].

$$I_{pv} = \sum_{i=1}^{M_p} I_i; \quad M_p \text{ parallel branches} \quad (2.8)$$

$$V_{oc} = \sum_{i=1}^{M_s} V_i; \quad M_s \text{ series branches} \quad (2.9)$$

Figure 2.3 depicts the main elements of the *PV* panel.

PV system can be classified into four groups:

1. Centralized Type: the *PV* panels are connected in series first of all to generate the required high voltage and avoid further amplification; then these series panels are connected in parallel, through string diodes, to obtain the desired high power level as illustrated in Figure 2.4. This type is usually implemented in large scale *PV* farms and connect to interface a large number of *PV* panels [59].

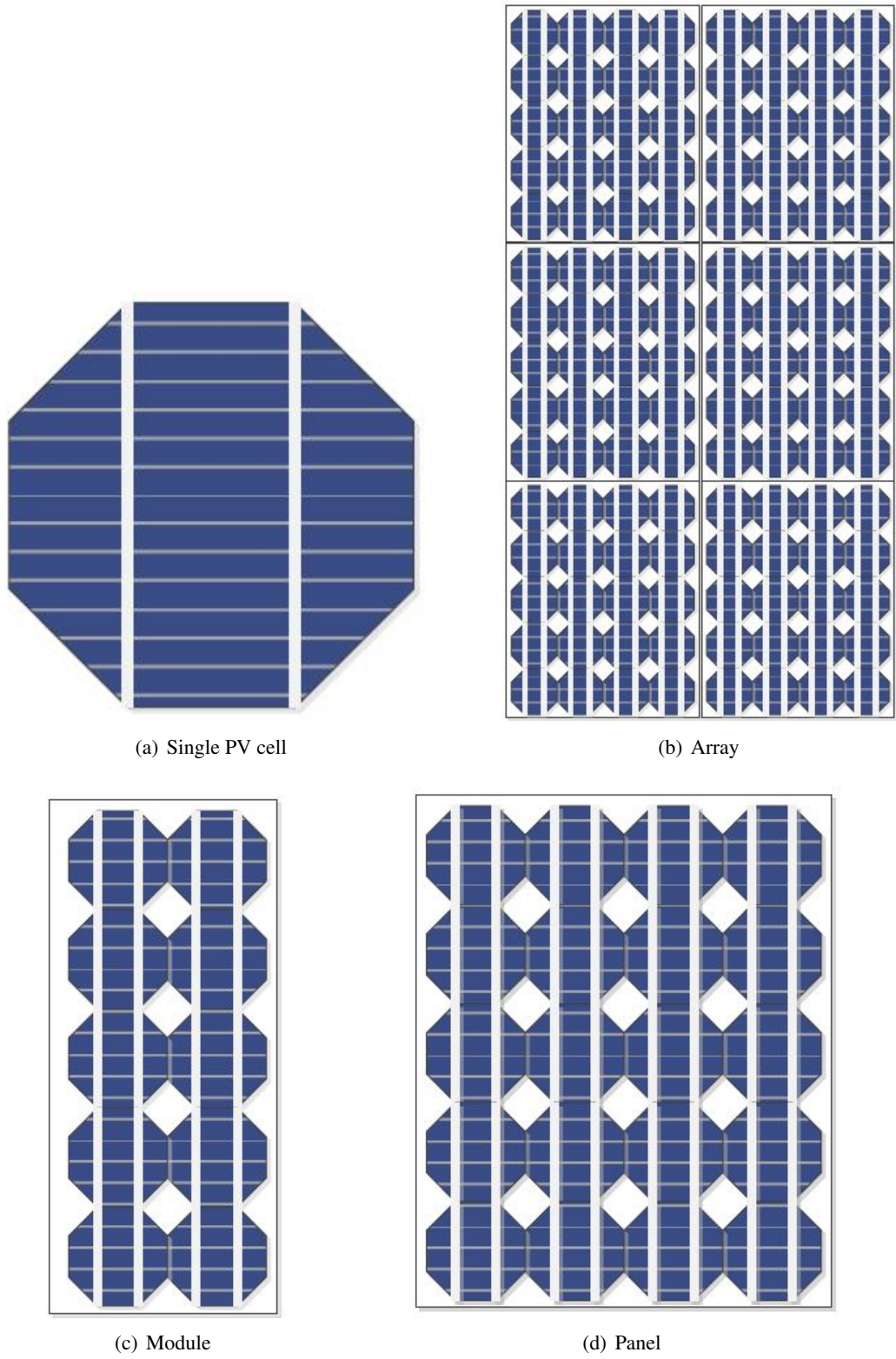


Fig. 2.3: PV System Elements [4]

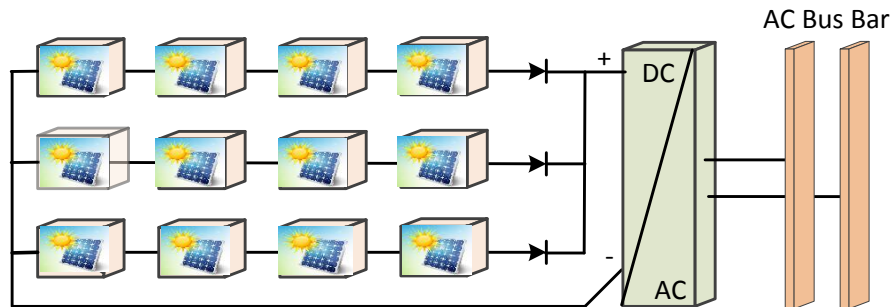


Fig. 2.4: Centralized PV System

2. String Type: several PV panels are connected in series as a string. Each string is connected with a DC/AC converter as Figure 2.5 shows. Expanding of a PV system could be simply realized by inserting additional strings and inverters to the existing platform [59].

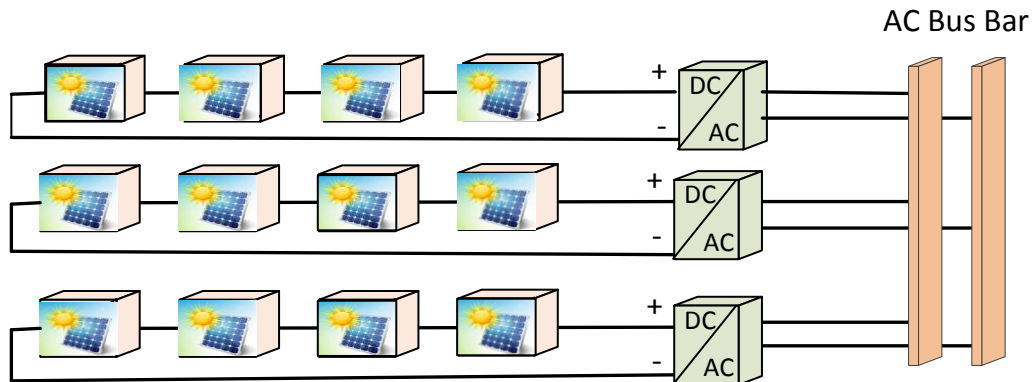


Fig. 2.5: String PV System

3. Multi-String Type: several PV panels are connected in series, and then connected with a low power DC/DC converter as a string, while a number of DC/DC converters, as multiple strings are connected together with one DC/AC converter as shown in Figure 2.6, [59–61].

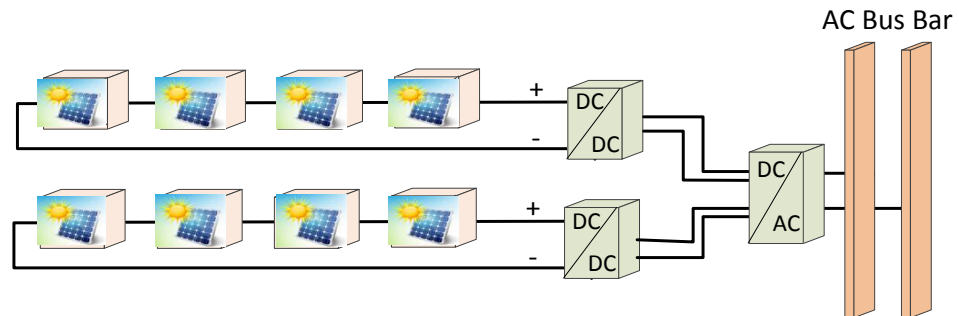


Fig. 2.6: Multi-String PV System

4. Module Integrated Type: each PV panel has a single inverter attached at the back as shown in Figure 2.7. The output from each micro-inverter is connected together to convert raw *DC* power from PV panel to *AC* power [59, 62–64].

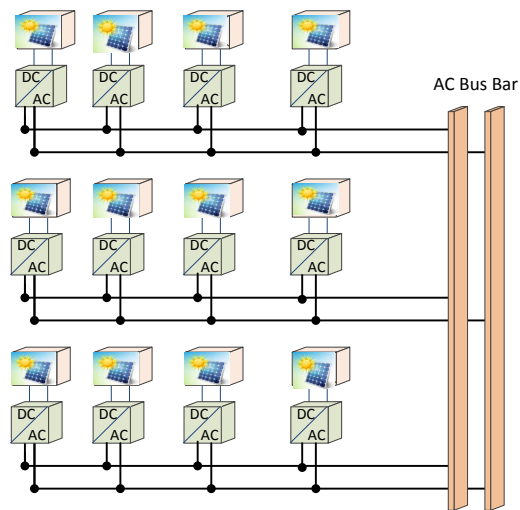


Fig. 2.7: Module Integrated PV System

2.3 Electrical Energy Storage System Overview

The energy storage system is a very important element. It plays a vital role in all parts of the electrical power systems in areas of system stability problems as a result of routine or emergency maintenance, system failure or power system faults by continuity of energy supply, used for Energy management, such as load shifting during the day and store the energy for later use, used for power quality issues, such as unbalance voltage on three phase systems and also used to avoid voltage sags, and maintain the voltage profile within admissible regulatory limits. However, in stand-alone PV system, owing to the natural fluctuation of the output power delivered by the PV arrays, the use of storage system is mandatory. This increases energy utilization by mitigating the temporal mismatch between the power generation and load demand when the load demand is lower than maximum power generation capability. The excess power is stored and is used when the load demand is higher than the maximum power generation capability; this also improves the stability of power generation .

A wide range of different technologies exist to store electrical energy, with a variety of technical characteristics. However, power quality and energy management are the main factors for the use of EESS. The EESS could be a mechanical, electrochemical, chemical, thermal or electrical device. Figure 2.8 summarises the storage system used in an electrical power system.

2.3.1 Parameters of an Energy Storage Device

- Power Capacity: the maximum instantaneous output that an energy storage device can provide.
- Energy Storage Capacity: the amount of electrical energy the device can store.
- Efficiency: indicates the quantity of electricity which can be recovered as a percentage of the electricity used to charge the device.
- Response Time: the needed time of the storage device to start releasing power.

2.3.2 Classification of an Electrical Energy Storage System

In this section a brief classification the types of electrochemical and electrical EESS and their features are listed. More details about other storage system can be seen in Appendix (A).

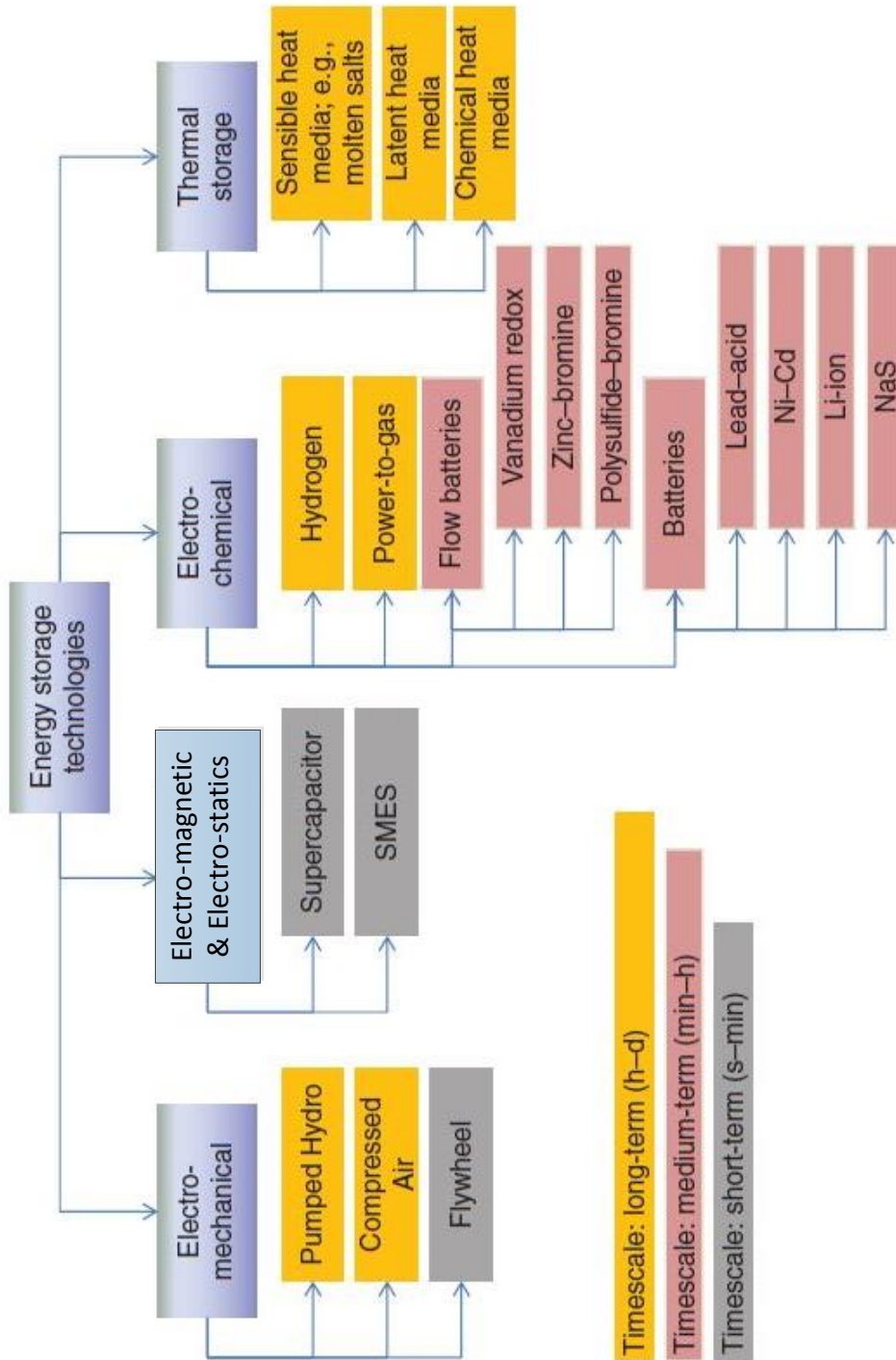


Fig. 2.8: Main form of EESS [5]

2.3.2.1 Electrochemical Storage Systems

Batteries are the most common technology of electrochemical energy storage methods. Batteries convert electrical energy into potential chemical energy whilst charging (store energy in a chemical process) which achieved via reduction and oxidation (redox) reactions which create electron transfers between chemical species and releases electrical energy from chemical energy whilst discharging [8, 65]. This reaction takes place inside the storage cell. Cells are grouped together into a single mechanical and electrical unit to form a module. Many modules are connected electrically to form a battery pack, which has a long charge / discharge time, low power and higher energy density. The energy capacity can be calculated as follows:

$$E_{sp} = \frac{nFV_{th}}{3.6 \sum_{i=1}^m M_i} \quad (2.10)$$

where: E_{sp} is the Energy Capacity [Wh/kg], n is the number of electrons transferred in a chemical reaction, F is the Faraday constant in coulombs per mole, V_{th} is the theoretical thermodynamic voltage of the cell, $\sum_{i=1}^m M_i$ is the sum of the molecular weights of the reactants of the cell.

The major component of any battery cell are:

- ★ **Two pairs of electrochemically active substances:** There is one in the anolyte region while the other is in the catholyte region. The materials composing the anolyte electrode and the component or substance surrounding it have to react, yielding an oxidation reaction (while discharged). Analogously, the electrochemical interaction between the materials comprising the catholyte electrode and the substance or component surrounding it yields a reduction reaction.
- ★ **Two Electrodes:** These are made up of two materials, while discharged, oxidation reactions occur in the anode of the battery (the negative electrode), which is the electrode that captures the electrons lost by the component. Conversely, reduction reactions occur in the cathode of the battery (the positive electrode), which is the electrode that provides the electrons gained by the reduced component; each will be connected to a battery terminal.
- ★ **Separators:** There is an electrical potential between the electrochemically active substances in the anolyte and catholyte regions. The separator avoids direct contact between them, thus protecting the battery from an internal short circuit.

- ★ **Two Terminals:** electrical potential is generated between battery terminals; these terminals are the connection point to the load.
- ★ **Electrolyte:** apart from causing the two pairs of electrochemically active substances to gain or lose electrons, the electrolyte is a liquid (acidic or alkaline) which has been used in traditional batteries; gel or solid material for the battery under development.
- ★ **Enclosure:** the case that hold all of the battery components.

The representation of this major component are illustrated in Figure 2.9

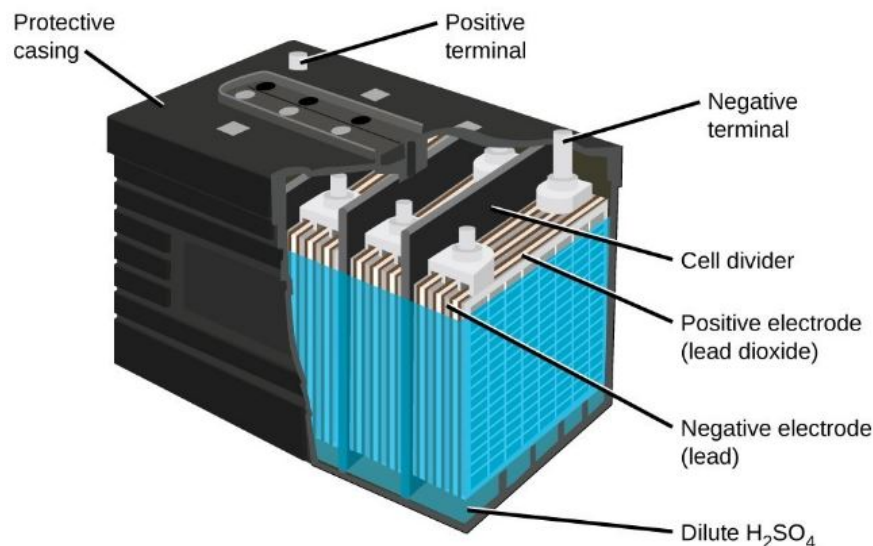


Fig. 2.9: Battery Representation [6]

Electrochemically active substances used for building up battery cells provide different characteristics such as:

- Open-circuit voltages.
- Time response.
- Operational temperature.

The rate of ageing of this battery varies considerably with the technology. However, the main battery type are:

1. Lead-acid battery: Composed of a sponge metallic lead anode, a lead-dioxide cathode and a sulfuric acid solution electrolyte. The typical service life between 6 to 15 years with a cycle life of between 1500 cycles at 80% depth of discharge and achieved cycle efficiency level of around 70% to 80%. A simple charging technology is employed, the cost/performance ratio is favourable and the batteries are easy to recycle [66]. However, there are some draw-backs:

- ★ These batteries are very heavy
- ★ The capacity decreases when discharging at high power
- ★ Not suitable for fast charging
- ★ Lower energy density
- ★ Lead is used, which is a hazardous material that is prohibited or restricted in various jurisdictions

They can be found as vented or sealed housing versions [66, 67]. Typical applications are in emergency power supply systems, stand-alone PV systems, battery systems for mitigation of output fluctuations from wind power and as starter batteries in vehicles [67, 68].

2. Nickel battery: can contain nickel metal hydride (*NiMH*) or nickel cadmium (*NiCd*). Nickel-based batteries have a higher power density, a slightly greater energy density and the number of cycles is higher in comparison to lead-acid batteries. They perform well at low temperatures in the range from -20°C to -40°C .

However, these batteries suffer from memory effects and also lose more energy owing to self-discharge standby than Lead acid batteries. There are also environmental effects owing to the toxicity of cadmium; they have been prohibited for consumer use in Europe and are currently used only for stationary applications.

NiMH batteries have all the positive properties of *NiCd* batteries, and also have much higher energy densities (weight for weight). However, their maximal nominal capacity is still ten times less than *NiCd* and lead acid equivalent. *NiMH* batteries are used in both portable in applications the sealed form, and general stationary industrial applications in flooded form [66, 67, 69, 70].

3. Sodium-Sulfur (*NaS*) battery: The electrodes of *NaS* battery cells are liquid, while the electrolyte, which in turn acts as a separator, is solid. The negative electrode (liquid sodium) is

surrounded by the electrolyte. The material of the electrolyte is ceramic beta-alumina, and the material for the positive electrode is liquid sulfur (usually embedded in a carbon felt). To bring the electrodes to their liquid state, they have to be melted, requiring the operating temperatures for NaS batteries to be maintained between 300°C and 350°C to keep the electrodes molten. The typical life is approximately 4500 cycles with discharge time of 6.0 hours to 7.2 hours. These batteries are 75% – 80% efficient, the energy density is ($151 \text{ kWh}/\text{m}^3$) and have a fast response rate a few milliseconds [69]. The main drawback is the need for a heat source to maintain operating temperatures, which uses the stored energy of the battery, thus, partially reducing the battery performance. Moreover, the system must be protected from reacting with the atmosphere as pure sodium explodes instantly when in contact with air. In addition, the endurance in the harsh chemical environment causes corrosion in the insulators. This means the battery may become conductive, with an increase in the self-discharge rate, which may cause the cracking of the ceramic electrolytic tube [67, 71, 72].

4. Metal-air battery: the battery cell consists of the anode, made from pure metal, and the cathode which is connected to an inexhaustible supply of air. Only the oxygen in the air is used to precipitate the electrochemical reaction. These batteries have a very small self discharge per day comparing to other type of batteries, a cycle life over 100 and very high energy density between $450 - 650 \text{ Wh}/\text{kg}$. However, these batteries are not rechargeable and have a low efficiency of approximately 50% with capital cost $74 - 296 \text{ \$/kWh}$ [69].
5. Lithium battery: Constructed from an active material in the cathode (positive electrode) of *Li-ion* cells and is usually lithium metal oxide, in the form of lithium cobaltate (LiCoO_2). The negative electrode is mainly carbon (*C*) and lithium atoms are actually in the electrode. The electrolyte is an organic solution containing lithium-based dissolved salts, such as LiClO_4 and LiPF_6 ; The electrode areas are separated by porous separators based on polyethylene or polypropylene. owing to the lightness of weight, these materials represent a highly important form of storage technology in the area of portable and mobile applications.

The main advantage of this batteries are:

- ★ High cell voltage levels of up to 3.7 nominal Volts
- ★ High gravimetric energy density $100 - 150 \text{ Wh}/\text{kg}$

- ★ High efficiency, typically in the range of 95% to 98%; the discharge time from seconds to weeks

The main obstacles are the high cost of more than USD 600/*kWh* owing to special packaging and internal overcharge protection circuits, and the metal oxide electrodes are thermally unstable and can decompose at elevated temperatures.

In order to eliminate this risk, the batteries are equipped with a monitoring unit to avoid overcharging and over-discharging; a voltage balance circuit is also installed to monitor the voltage level of each individual cell and prevent voltage deviations among them. Research is focused on the development of cathode materials [69, 73, 74].

6. Flow battery energy storage: A flow battery converts chemical energy directly into electrical energy by using chemical reactions. However, the electroactive material is stored externally in two electrolysis tanks and produces the energy by using a reversible electrochemical reaction between two electrolytes. The efficiency varies between 70% (zinc-cerium) to 85% (vanadium redox).

In this category, it is possible to design the system to have optimal power acceptance and delivery properties without needing to maximize the energy density. The electrodes do not undergo physical and chemical changes during operation and so a more stable and durable performance can be achieved. In addition, the energy capacity of the flow battery is addressed by the size of the external storage components which make it easy to manage the energy density of the battery.

Other advantages are:

- ★ It is safer as the active materials separated from the reactive point source
- ★ A high electricity to electricity conversion efficiency
- ★ Low maintenance
- ★ Tolerance to overcharging
- ★ A deep discharge is possible without affecting the cycle life

However, this system is more complicated and requires more components such as pumps, sensors, flow and power management and secondary containment vessels; this makes these bat-

teries unsuitable for small-scale storage applications [75, 76]. Energy 25 – 35 Wh/kg for the VRB [112] and 70 – 90 Wh/kg for the ZBB [117].

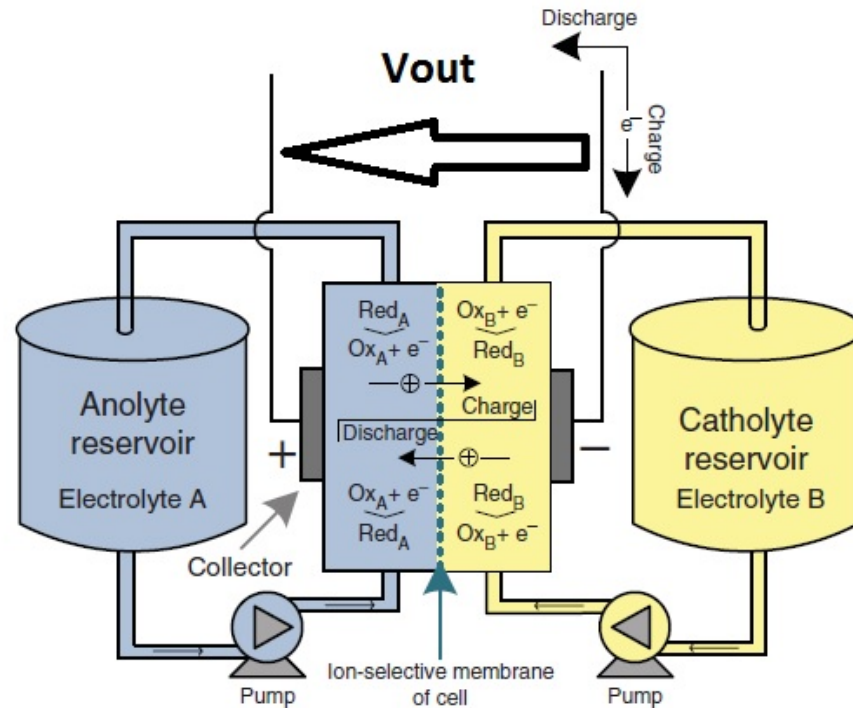


Fig. 2.10: The Operating Principle of Flow Batteries. [5]

Figure 2.11 represents a graphical comparison of the energy densities of aqueous and non-aqueous rechargeable battery systems.

2.3.2.2 Electromagnetic and Electrostatic Storage Systems

1. Super-conducting magnetic energy storage (SMES): these systems function according to an electrodynamic principle. The energy is stored in a magnetic field which is created by the flow of direct current in a super-conducting coil, which is kept below its super-conducting critical temperature; the maximum current flowing through the superconductor is temperature-dependent. The lower the operating temperatures, the higher the operating currents. Moreover, the main component of this storage system is a coil made of super-conducting material. However, additional components are required which include power conditioning equipment and a cryogenically-cooled refrigeration system. The stored energy can be calculated

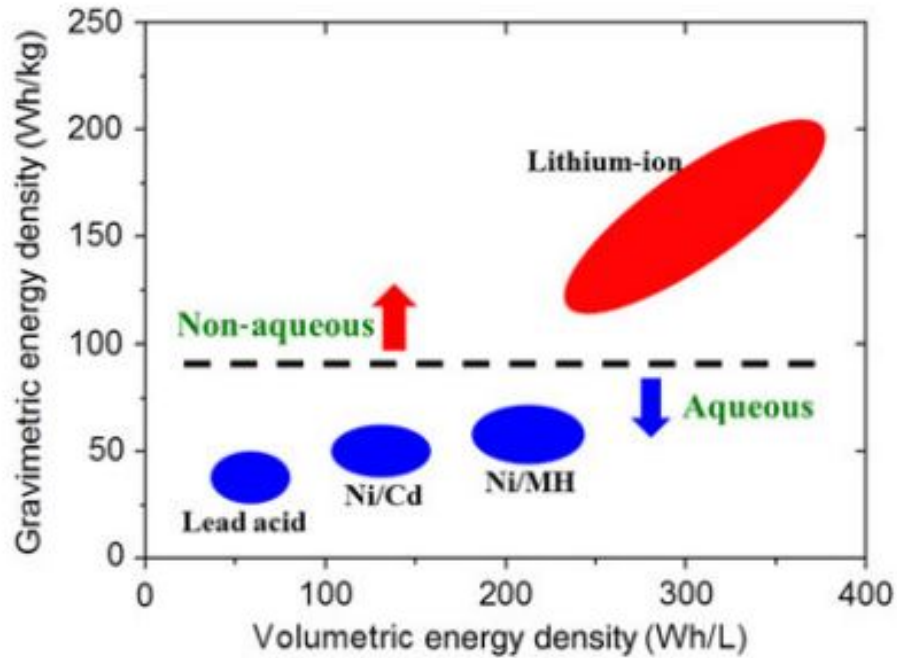


Fig. 2.11: Comparison of the Energy Densities of Aqueous and Non-Aqueous Batteries [7]

using Equation 2.11:

$$E_{SMES} = \frac{1}{2}LI^2 \quad (2.11)$$

where: E_{SMES} The energy stored, $I[A]$ electric current and $L[Henries]$ inductance of the coil

Whilst SMES are limited to short-time storage applications, as the self-discharge rates of the system are relatively high (in the range of 1015% of the rated energy capacity per hour) there are advantages:

- Very quick response time
- High overall round-trip efficiency (85% – 90%)
- Very high power output for a short period of time
- No moving parts in the main portion of SMES

The overall reliability depends on the refrigeration system which is crucial. Large SMES systems, with more than 10MW of power, are mainly used in particle detectors for high-energy physics experiments and nuclear fusion. To date, a few, rather small SMES products, are com-

mercially available: these are mainly used for power quality control in manufacturing plants such as micro-chip fabrication facilities [77].

2. Super capacitor energy storage (SC): Based on the same simple principles applicable to electrostatic capacitors where larger area plates and shorter distance between plates could give a higher effective capacitance, as Equation 2.14 illustrates [8]. However, *SC* incorporates electrodes with much higher effective surface areas and thinner dielectrics, leading to an increase in both capacitance and energy [24]. The energy stored in the capacitors is directly proportional to their capacity and the square of the voltage between the terminals, as the Equation 2.12 illustrates. The capacity is proportional to electrode density ρ and gravimetric capacitance C_g as Equation 2.13 indicates.

Therefore, the overall performance of an super-Capacitor is influenced by two main factors, the choice of the active electrode material [78–81], which will define the capacitance of the device, and the electrolyte utilized, which will determine the operational voltage [24,82–84]. The most practical materials that are used to make the electrode layers, producing charge generation without electrochemical reactions, are:

- ★ Carbon materials such as microporous carbon
- ★ Activated carbon (AC)
- ★ Carbon nanotubes (CNTs) and graphene
- ★ Metal-oxides
- ★ Polymer materials [8,85]

The main factor in the choice of the electrolyte is the wide range of electrochemical stability. For the solvent, the choice is very limited owing to intrinsic electrochemical stability. However, different solvents have different potential windows. For instance, the water electrochemical disassociation window is 1.23 V. The potential window of the ion liquids (which are molten salts that, at higher temperatures, display stability and significantly increased conductivity) can be as high as 4.0 V [8,80,86].

$$E_{SC} = \frac{1}{2}CV^2 \quad (2.12)$$

where: E_{SMES} The energy stored, $V[V]$ voltage between super-capacitor terminal and $C[Farad]$ Capacitance of Super-Capacitor

$$C_v = \rho C_g \quad (2.13)$$

where: C_v volumetric capacitance, ρ electrode density and C_g gravimetric capacitance

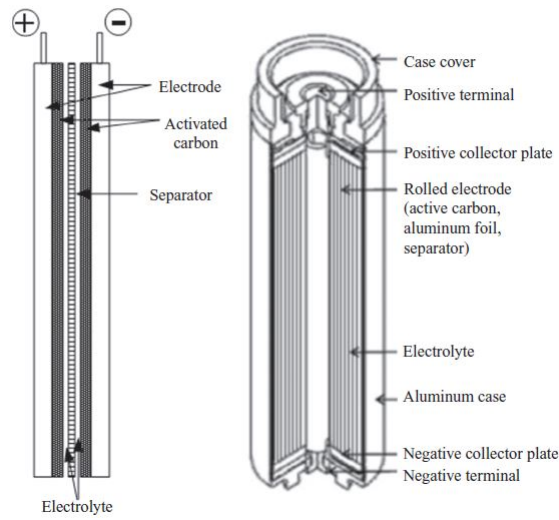
$$C = \epsilon_0 \epsilon_r \frac{A}{d} \quad (2.14)$$

where: C The capacitance in $[Farad]$, A the area of electrodes in $[m^2]$, d the distance between the electrodes in $[m]$, ϵ_0 the vacuum permittivity $8.854 * 10^{-12} F.m^{-1}$ and ϵ_r the relative permittivity of the dielectric electrolyte.

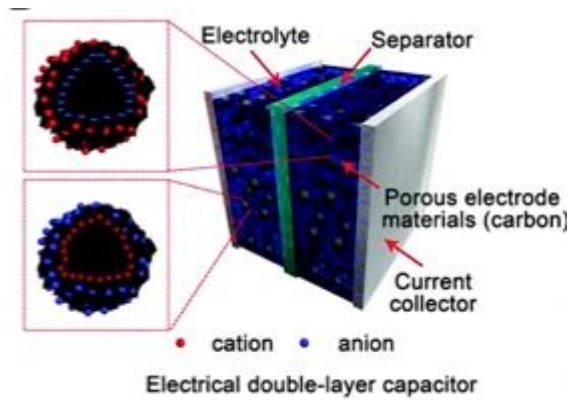
However, electrolyte (usually in a solvent and intimately related to the operating voltage which influences the energy density) and electrode materials have a fundamental influence on the energy, and the power capacity, and on the dynamic behaviour of the super-capacitor. The product of the equivalent resistance of the electrolyte and the capacity of the super-capacitor determine its charge and discharge time constants. This equivalent resistance is very small ($< 10^{-3} \Omega$, therefore short time constants can be achieved. In addition, power densities 10 times higher than batteries can be achieved. Figure 2.12 shows a practical construction of a super-capacitor.

The two main features are the extremely high capacitance values, of the order of many thousands farads, and the possibility of very fast charges and discharges owing to the extraordinarily low inner resistance. These features are not exhibited conventional batteries. The advantages are:

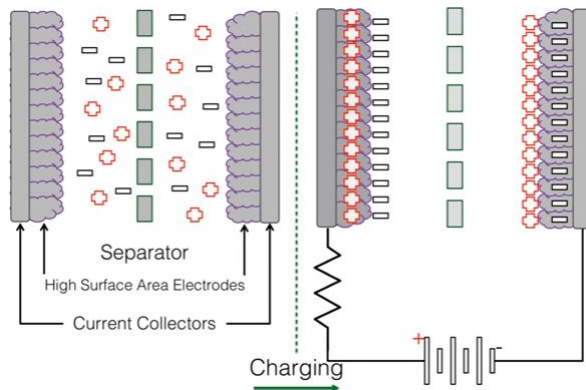
- ★ Durability
- ★ High reliability
- ★ No maintenance
- ★ Long lifetime
- ★ Operation over a wide temperature range and in diverse environments (hot, cold and moist)
- ★ The lifetime is one million cycles (or ten years of operation) without any degradation
- ★ Environmentally friendly and easily recycled or neutralized



(a) Practical Construction of a SC



(b) SC Interior



(c) SC Interior Under Voltage

Fig. 2.12: SC Interior Illustration [5, 8]

The efficiency is typically around 90% and discharge times are in the range of seconds to hours. They can reach a specific power density which is about ten times higher than that of conventional batteries, but the specific energy density is about ten times lower. Owing to these properties, super-capacitors are ideal for providing quick bursts of energy and can be configured in a variety of cell shapes and sizes. They can be assembled into modules to meet the power, energy, and voltage requirements for many specific applications, especially those with a large number of short-charge discharge cycles where their high performance characteristics can be used [8, 18, 73, 87]. EESS are classified on the basis of the suitability for such applications; different applications have different requirements and demand different features from EESS. However, in general, the main criteria applied for the selection of any storage application type are:

- ★ System Energy rating [kWh].
- ★ Discharge time at rated power; a period of time over which an energy storage technology releases its stored energy.
- ★ Energy Density which is the amount of energy that can be supplied from a storage technology per unit weight [Wh/kg]. Combination with the physical size and weight of the storage device, this factor defines the quantity of energy that the device can take in and deliver.
- ★ Costs of energy storage devices are usually quoted in terms of [$cost/kWh$].

Table 2.1 summarises the classifications of all EESS .

2.4 Maximum Power Point Tracking Algorithms

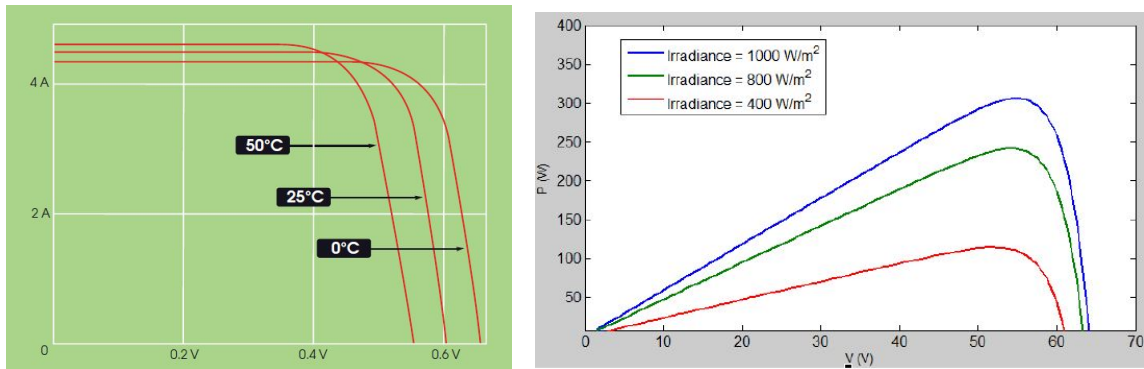
For the effective operation of the PV system, ensuring the extraction of the maximum possible energy from the system at all times is critical.

However, the maximum power available may vary rapidly owing to many factors, such as changing weather conditions and shadows from objects in the environment which cause a change in irradiation or temperature. Determining the maximum power is a time-varying problem.

Furthermore, solar panel characteristics have only one point where the panel provides the maximum power for a given environmental condition which includes the temperature and irradiation; the cell performance under these variations is shown in Figure 2.13.

Tab. 2.1: Electrical Power System Storage Type [5, 8, 16–24]

Energy Storage System	Power Density	Energy Density	Capital Cost	Cycle Efficiency	Cycle Life	Self Discharge
	[W/kg]	[Wh/kg]	[\$/kWh]	%		Per Day
Mechanical						
Pump Hydro	-	-	600 – 2000	65 – 80	40 – 100 years	≈ 0
Compressed Air	-	-	400 – 800	40 – 71	20 – 40 years	≈ 0
Flywheel	11900	5 – 100	250 – 350	85 – 95		
Lead Acid	180	30 – 40	74 – 222	70 – 80	500 – 800 cycles	0.1 – 0.3%
<i>Li – ion</i>	1800	150 – 250	1040 – 1481	77.5 – 90	1200 cycles	0.1 – 0.3%
Electrochemical						
<i>NiMH</i>	250 – 10 ³	30 – 80	450 – 10 ³	66	500 – 10 ³ cycle	2%
<i>NiCd</i>	150	40 – 60	296 – 890	60 – 83	1500 cycles	0.2 – 0.6%
<i>NaS</i>	151	400	1115 – 2250	90	12 – 20 years	≈ 0
Electrical						
Super-Capacitor	10 ³ – 10 ⁴	2 – 10	2000	> 93	> 10 ⁵ +	20 – 40%
Super-Conducting	-	10 – 75	10 ³ – 10 ⁴	85 – 99	10 ⁴	10 – 15



(a) Temperature Effects on I-V Characteristic

(b) Irradiance Effect on PV Cell Power Output

Fig. 2.13: PV Cell Performance

In general, there is a unique point on V & I curve called a maximum power point, at which the the PV system produces maximum power as the Figure 2.14 indicates. The location of the maximum power point (MPP) is not known, but it can be located either through calculation models or search algorithms.

To enable maximum power production under changing environmental conditions, maximum Power

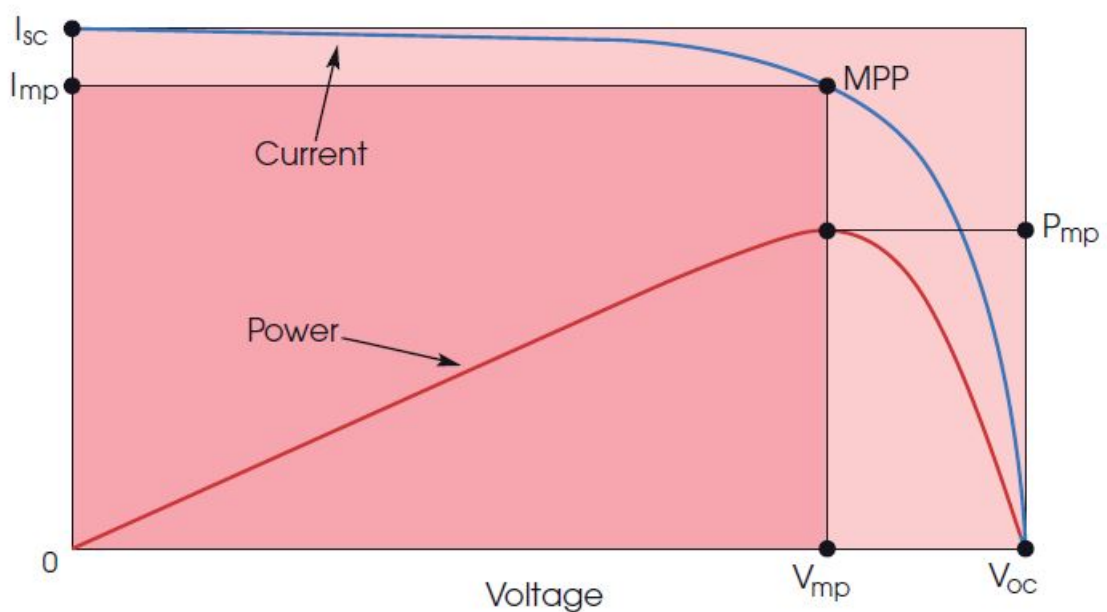


Fig. 2.14: PV Electrical Characteristics

Point Tracking techniques ($MPPT$) are proposed which will track to the optimal power point. Figure 2.15 shows an utilisation of the implementation of ($MPPT$) in the PV system. Several techniques have been developed through the years, and there are wide variations between them, such as:

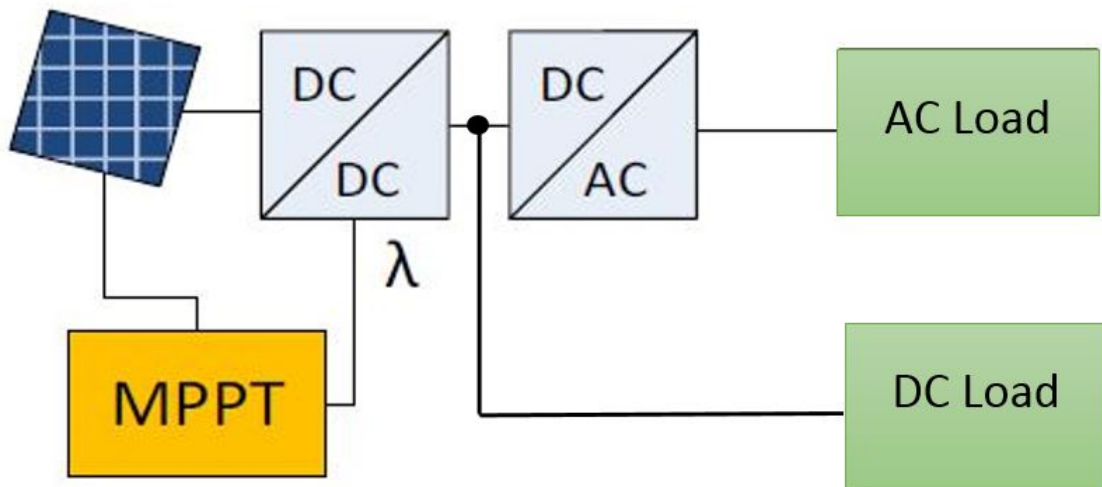


Fig. 2.15: Block Diagram of MPPT Implementation

- ★ Simplicity
- ★ Hardware implementation
- ★ Convergence speed
- ★ Number of sensors required
- ★ Cost effectiveness
- ★ The need for the parametrization and the correct tracking when irradiation and temperature change together or independently
- ★ Hardware needed for the implementation [88] [89].

There are two main methods: Direct control and indirect control.

1. Indirect control: this method is based on the use of a database that includes parameters, or uses mathematical functions from empirical data. The methods that belong to this category are curve fitting, look up tables, open voltage PV generator and short circuit PV generator [88].
 - (a) **Curve fitting:** This method is based on numerical calculations to determine the maximum power point. Because the $V - P$ characteristic curves of solar array are close to parabolas, this method makes a parabola model with the quadratic interpolation using voltage and current parameters of three sampling points; this calculates the peak of the

parabola and finds the voltage value corresponding to MPP.

This method requires accurate knowledge of the physical parameters relating to the cell material, and the manufacturing specifications, or the expression mathematics used are not valid. It also requires a large memory capacity of calculation of the mathematical formulations [88,90,91].

- (b) **Look up table:** the measured current and voltage of PV generators are compared with those stored in the control system, which corresponds to the operation in the MPP, under concrete climatological conditions. This method needs a large memory storage for the data, and the implementation of it must be adjusted for specific PV [88].
- (c) **Open voltage (OV):** this method is based on the voltage of PV generator at the maximum power point is always close to a fixed percentage of the open circuit voltage, this fix percentage is linearly proportional to k . In general, k depends on the fabrication technologies of PV, the fill factor and meteorological conditions ranging from 73% to 80%. The temperature and insulation tolerance is 2% with a sampling interval of $15ms$. To obtain an open voltage circuit, a switch must be added to the circuit in series. Thus, if the system interrupted during the normal operation, there is no power output for a short period of time [32, 88].
- (d) **Short circuit (SC):** this is the maximum current generated by a cell or module and is measured when an external circuit is short circuit. The value depends on the surface area of the cell and the amount of solar radiation incident upon the surface [32, 88]. The operating current is proportional to the short circuit current under various conditions of irradiation level, and the proportional parameter is estimated to be approximately 92% [92]. Therefore, the operating current controls a power converter, so it is necessary to introduce a static switch, in parallel with the PV, in order to measure the short circuit current I_{sc} . Thus, there is no power output during the short circuit period [32, 88].
- (e) **Constant voltage (CV):** The operating point of the PV is kept near to the MPP by regulating the PV output voltage and matching it to a fixed reference voltage V_{ref} . The V_{ref} value is set to the (V_{MPP}) of the characteristic PV module [88]. This method assumes that individual insulation and temperature variations on the PV are insignificant, and that the voltage reference is an adequate approximation of the true MPP.

However, this technique more efficient in low insolation [32], although it can cause power losses when the temperature changes widely [90].

2. Direct control: these algorithms have the advantage of being independent from the prior knowledge of the PV characteristics, which means the operating point is independent of temperature, isolation or irradiation [88].

The methods belonging to this group are sampling, modulation and artificial intelligence.

- Sampling methods:

There are two main methods:

- (a) **Perturbation and observe (P&O)**, known as the hill climbing method.

This is the most widely-adopted method amongst all of the MPPT strategies. This method measures the derivation of power (Δp) and the derivation of voltage (Δv) to determine the movement of the operating point. The derivative of the power with respect to the voltage should be zero at maximum power but, if the sign of ($\Delta p/\Delta v$) is positive, the reference voltage is increased. If the sign of ($\Delta p/\Delta v$) is negative, the reference voltage is decreased [90, 91, 93].

This method requires the solar array voltage (V_{PV}) and the current (I_{PV}) to be measured in order to acquire information about power and conductance. The advantage of this method is the ease of implementation owing to the simple control structure and low cost. Additionally, the operation does not rely on knowledge of the PV module characteristics.

However, the draw-backs of this method [89] [94] [56, 93] are:

- ★ The system oscillates around the MPP; this oscillation can be minimised by reducing the perturbation step size. However, the tracking process will slow down.
- ★ It is hard to acquire the MPP in low irradiance conditions owing to the peak in the power characteristic.
- ★ Good tracking cannot be produced in rapid transition of environmental conditions.

The flow chart of this methods is shown in Figure 2.16.

Owing to the simplicity of it, and the ease of use, it has attracted the attention of the international community in recent years. Attempts are being made to enhance

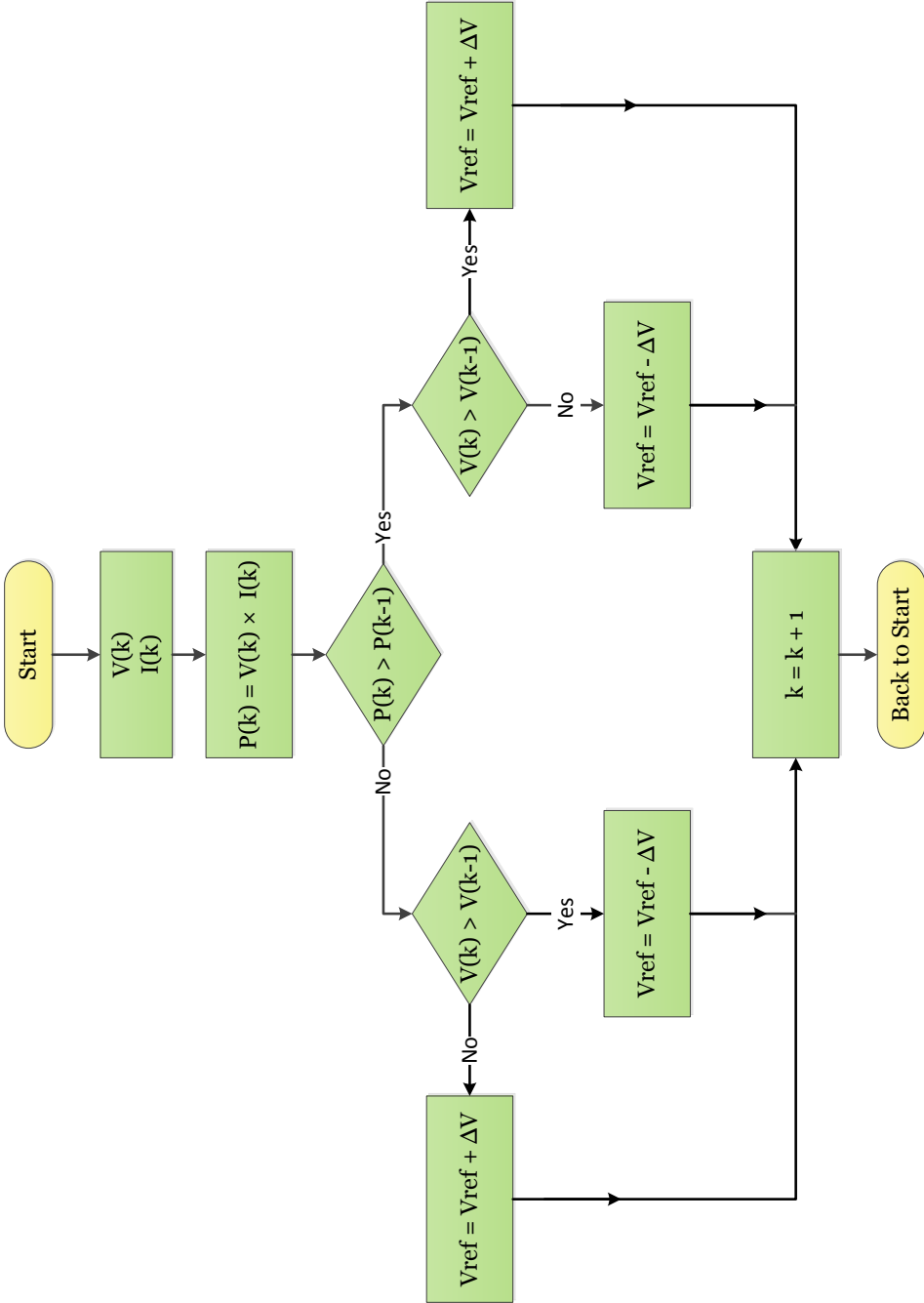


Fig. 2.16: Fixed step-size P&O method flowchart

the performance of this method by implementing $PI - P\&O$ to develop an adaptive perturbation, a variable step-size $P\&O$ method and an Auto-scaling $P\&O$ method [95].

- (b) **Incremental conductance:** The algorithm is based on the fact that the derivative of the PV power with respect to its output voltage is zero at the MPP. The derivative is positive on the left of the MPP and negative on the right. Thus,

$$\frac{dP}{dV} = \frac{d(IV)}{dV} = I + V \frac{dI}{dV} = I + V \frac{\Delta I}{\Delta V} = 0 \quad (2.15)$$

The conditions for the increment Are:

$$\frac{\Delta I}{\Delta V} > -\frac{I}{V} \text{ Left of MPP}$$

$$\frac{\Delta I}{\Delta V} < -\frac{I}{V} \text{ Right of MPP}$$

$$\frac{\Delta I}{\Delta V} = -\frac{I}{V} \text{ at MPP}$$

Once the MPP has been reached, the operation of the PV array is maintained at this point and the perturbation stops unless a change in $\frac{dI_{PV}}{dV_{PV}}$ is noted. In this case, the algorithm decrements or increments to track the new MPP.

However, this technique requires the solar array voltage and current to be measured to acquire information about the power and conductance of the solar array. Furthermore, this tracking method can be applied using a digital signal processor (DSP) and a microcontroller, which have the ability to save the current, and past values, and make the correct decision based on the algorithm. This method solves the oscillation problem around the MPP, and has a good performance under rapidly changing atmospheric conditions. It also has a high tracking accuracy at steady state [96]. A flow chart of this method is shown in Figure 2.17.

- (c) **Current Sweep:** The PV current waveform will be drawn periodically and that waveform is used to operate the PV array at the MPP. The V_{mpp} is computed and driven from that curve. However, this method cannot track the MPP continuously, but does so periodically; the interval time can be adjusted as required. Another consideration is that the increase of the output power should be greater than the losses in power due to the sweeping and manipulating of the PV current [97].

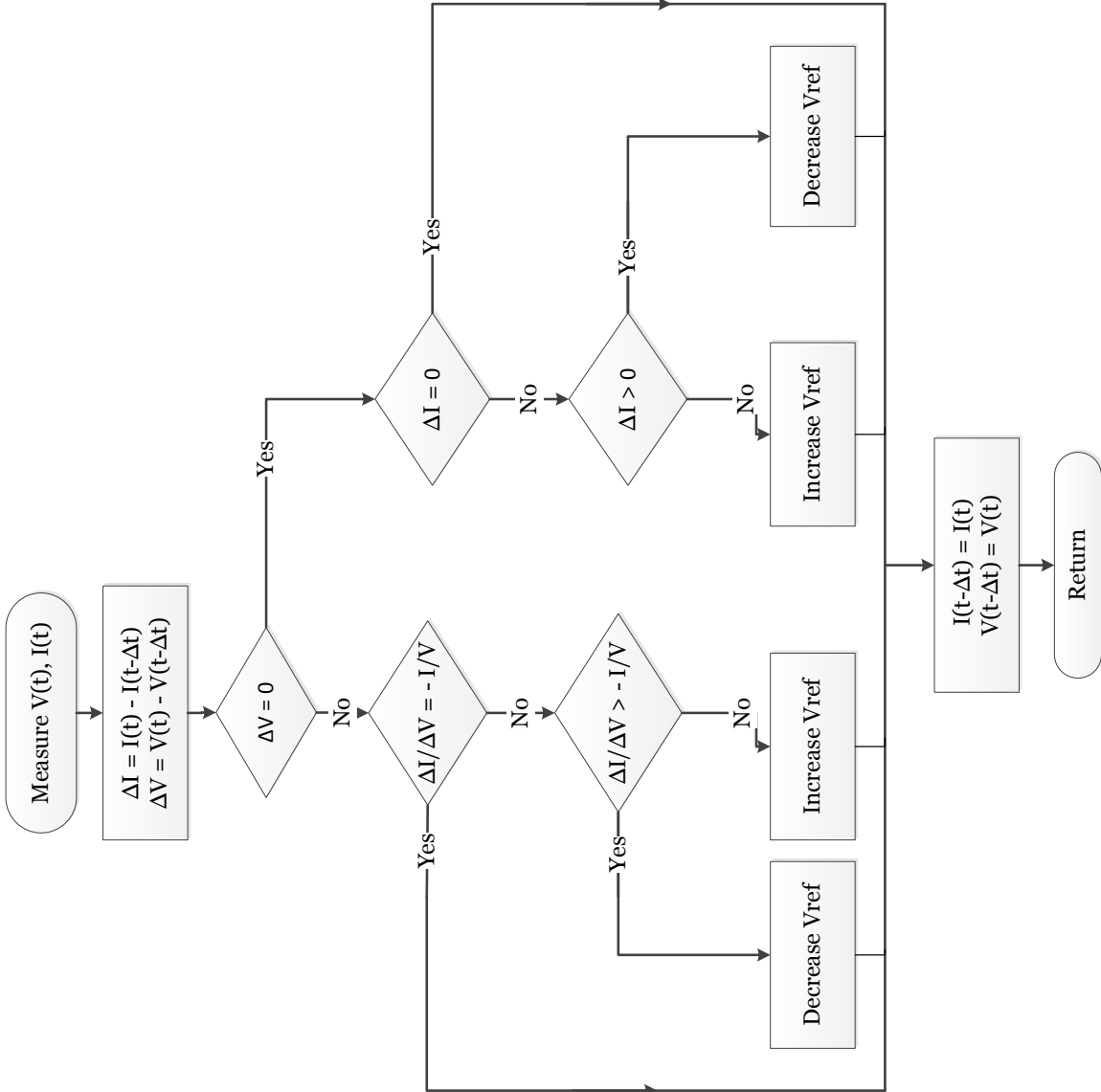


Fig. 2.17: Incremental Conduction Flowchart

- (d) dp/dv Feedback Control: the dp/dv curve is computed from the curve of the PV characteristics. In addition, the MPPT can be conducted by feeding the curve back to the converter and applying some control to drive dp/dv to zero. Shaping the curve can be done using different techniques. A few cycles are computed and stored; each cycle has a unique sign. The MPP is reached after the controller optimises the duty ratio, depending on these signs, and so ordering the converter to either increase or decrease [97–99].
- Modulation methods: in these sampling methods, there are oscillations around the MPPT owing to the appropriate adjustment for the maximum voltage point, which leads to a point close to MPP. These oscillations are generated automatically by the feedback control used. However, in modulation methods the oscillation, which is also called forced oscillation method, introduces a small voltage of 100 Hz which is added to the operation voltage of the PV generator. This leads to a ripple of power, the phase and amplitude of which depend on the relative location of the operation point to the MPP [97].
 - Artificial intelligence methods: this methods can be summarized as: **Fuzzy logic, neural network and fuzzy neural.**

These techniques do not need exact mathematical models, they can work with vague input, handle non-linearity and are adaptable, they have a robust performance under parameter variation. However, more processing time and computational power are required, compared to classical control, owing to the necessity to find control rules for MPPT.

- (a) Fuzzy logic : this method has the advantage of being able to deal with non-linear equations and operate with inaccurate inputs. The measurements needed for this method are error (E) and change of error (ΔE). Based on the fact that at MPP $dp/dv = 0$, the following equations have been adapted by the ref [100]. The Fig(2.18) summarized this method.

$$E_n = \frac{P_n - P_{n-1}}{V_n - V_{n-1}} \quad (2.16)$$

$$\Delta E_n = E_n - E_{n-1} \quad (2.17)$$

Developing a fuzzy logic interface system (*FIS*) and applying it to a control problem involves three stages:

- Fuzzification: inputs are converted from numerical to linguistic variables based on a membership function, These variables are adjusted by the user. Moreover, the higher the membership function the more accurate in the result.
- Rule-based table lookup.
- Defuzzification: this is the output stage when transformation to a numerical base occurs. This output changes the duty cycle and forces the PV to operate at the MPP.

ΔE and E are converted to linguistics variables in the fuzzification stage after calculation. In the second stage, the action required is taken based on a rule table. The controller output is a duty cycle change (Δd) of the *DC – DC* converter. The rule-based table and the membership function justification is dependent on the knowledge and experience of the user [90]. The aim of fuzzy logic is to make decisions based

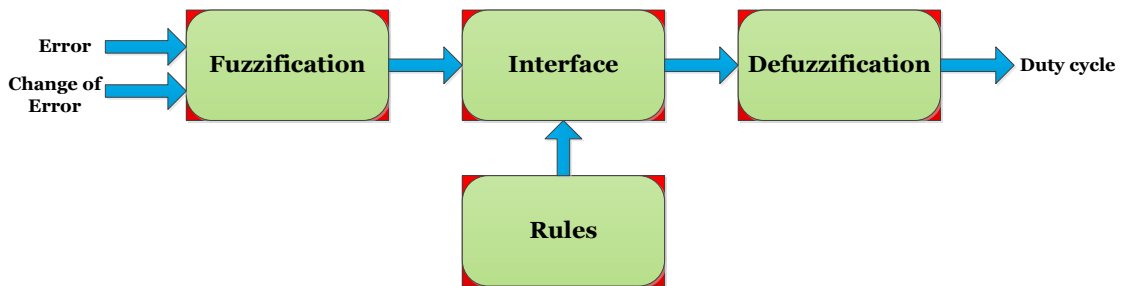


Fig. 2.18: General Diagram of Fuzzy Logic Controller

on a number of learned or predefined rules, rather than numerical calculations.

- (b) neural network (NN): this consist of three stages or layers. The first layer is the input, the last layer is the output and the middle layers are called the hidden layers where the processing takes place, as the Figure 2.19 illustrates. The user has the flexibility to choose the number of nodes in each stage. In The PV system, the user can choose input variables, as PVs electrical parameters, such as voltage V , current I , Power P [101–103] or non electrical parameter such as array temperature T , array irradiance G [104, 105], or a combination of same [106].

After these inputs are processed in the hidden stage, the output most likely is a duty

cycle signal to control the power converter and change the operating voltage to be as close as possible to the MPP [107]. However, the neural network method needs to be well trained to perform at a high quality and operates at the MPP. This training happens on a long run where all the PV data is recorded continuously over months, or even years, into the neural network database. The relationships between the inputs and outputs are obtained and recorded. The result of this training is that, in the algorithm, every link between the points in the hidden layer is weighted precisely. Each PV array has its unique characteristics, so the neural network controller must be trained separately for each array. ANN are trained on some sets of data, which should be representative of the conditions that will be experienced. However, over time, the cells will degrade and the non-linear mapping achieved by the ANN will no longer be representative of the MPP location [16]. For this reason, ANN techniques are often combined with conventional MPPT to enhance their accuracy and improve the speed of techniques such as incremental conductance and *P&O* [108]. In most MPPT applications, the ANN is trained on weather data, which may be difficult to measure [109].

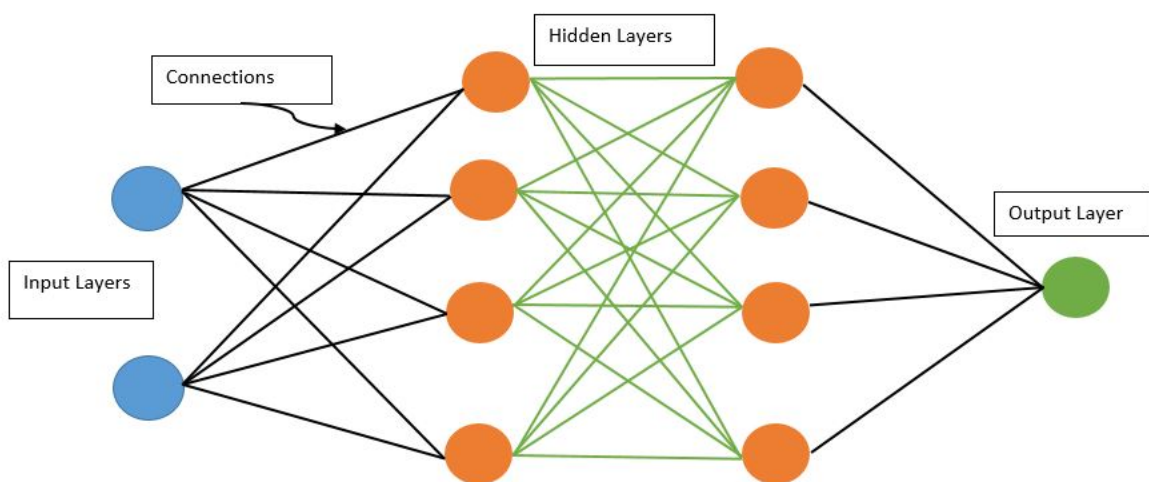


Fig. 2.19: Neural Network Representation

- (c) fuzzy neural: this technique combines the advantages of fuzzy systems and ANN and has been trained using weather inputs to determine the MPP location using a five layer network [110–112].

<i>MPPT Technique</i>	<i>Precision</i>	<i>Regular Adjustment</i>	<i>Tracking Speed</i>	<i>Signal</i>	<i>Complexity</i>	<i>measured Variable</i>
Open Voltage	No	Yes	Medium	Both	Low	V
Short Circuit	No	Yes	Medium	Both	Medium	I
Perturb and Observe	Yes	No	Differs	Both	Low	V, I
Incremental conductance	Yes	No	Differs	Digital	Medium	V, I
Fuzzy logic	Yes	Yes	Fast	Digital	High	Varies
Neural network	Yes	Yes	Fast	Digital	High	Varies
Current sweep	Yes	Yes	Slow	Digital	High	V, I
dp/dv feedback control	Yes	No	Fast	Digital	Medium	V, I

Tab. 2.2: MPPT Comparison

2.4.1 MPPT Techniques Comparison

Table 2.2 illustrates a critical comparison of MPPT with regard to precision ability, the need for regular adjustment, tracking speed, technology used, complexity and the variables that must to measured.

2.5 Summary

This chapter provided an overview of PV development through the years: the mathematical model, the electrical storage systems used in power systems and, lastly, the MPPT algorithms. First of all, a brief historical view about the development of the PV was presented. Secondly, the PV cell was analysed and mathematically modelled, with the storage system and including a definition of it. The types and classifications, followed by the MPPT was reviewed, including the definition, purpose and the different algorithms implemented. Each of the most useful methodologies was presented.

In Chapter 3 a discussion on the mathematical modelling of PV converter topologies, snubber circuits, followed by super-capacitor modelling.

Chapter 3

Mathematical Modelling of Converter

Topologies and SC as Storage Unit in PV

System

3.1 Overview

This chapter covers the characteristics of the main $DC - DC$ converter, incorporating functionality, block diagrams, mathematical models, and the methods implemented to reduce power losses. Super-capacitor modelling is also discussed.

Three main sections are covered in this chapter. The first section illustrates the main power converter topologies including functionality, block diagrams, mathematical models, followed by snubber circuit descriptions, type and implementation. The last section covers super-capacitor electrical models and the techniques implemented for voltage-balancing between cells. The chapter is summarised at the end.

3.2 Converter Topologies

The $DC - DC$ converter plays an important role in the PV system configuration, executing the roles of stepping up or down and regulating the output voltage; regardless of variation in the input power source or to the load variation the maximum preserved power is delivered. Stepping the voltage

up or down, through the converter, is normally achieved by controlling the on and off time of the switches. Moreover, this control can be conducted at a medium or high frequency. The ratio between the converter switches closing T_{on} , and open T_{off} , is called the converter duty cycle D . Therefore, the duty cycle can be calculated from Equation 3.1.

$$D = \frac{T_{on}}{T_{on} + T_{off}} = \frac{T_{on}}{T} = T_{on}f_s \quad (3.1)$$

where T is the period of the control signal, and f_s is the switching frequency.

Three different types of power converters are most frequently used within a given PV system: buck converters, boost converters and buck-boost converter [113]. All these topologies use power semi-conductors as switches operate.

3.2.1 Buck Converter

This is a device which steps down the input voltage $DC - DC$. The input and output are both direct currents and share the same polarities. Figure 3.1 depicts the basic arrangement of the main electronics component in the buck converter. This consists of a DC input voltage source V_{in} , a buck inductor L_{buck} , a controlled switch S_{buck} , a diode D_{buck} , filter capacitor C_{buck} , and the load resistance R_{load} .

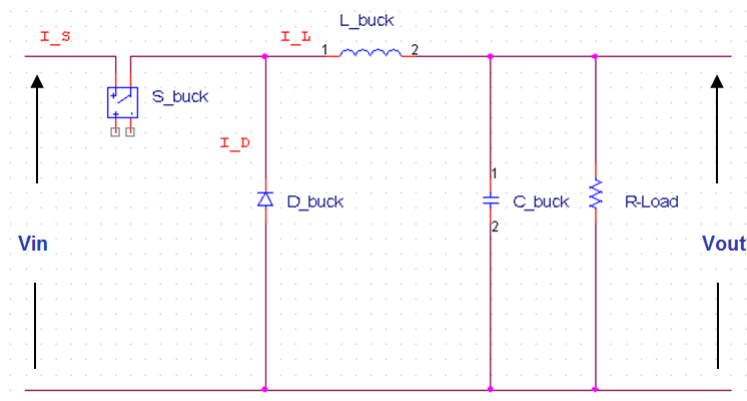


Fig. 3.1: Buck Converter

In the analysis the circuit will be represented twice depending on the switch status. The inductor current will be evaluated and the relationship between the input and output of the converters will be studied.

However, few assumptions are to be considered, such as: the capacitor has a huge capacitance, the

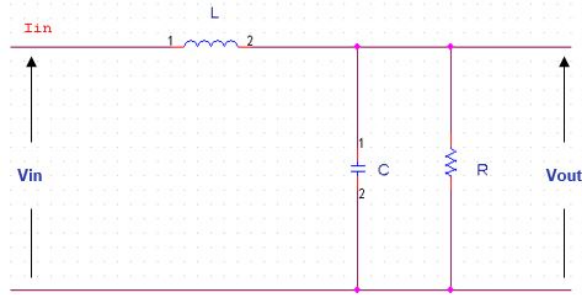


Fig. 3.2: Buck Converter Representation when Switch Closed

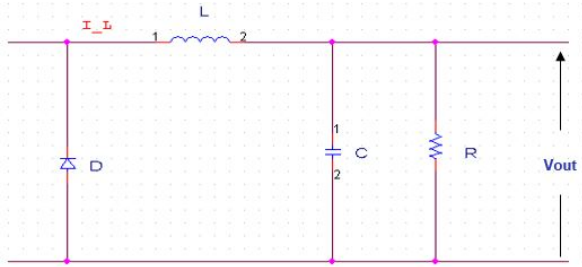


Fig. 3.3: Buck Converter Representation when Switch Opened

converter functions at steady state, the inductor has a continuous current and all the component are ideals. When the switch is closed as Figure 3.2 indicates, a constant voltage ($V_{in} - V_{out}$) is applied across the inductor for a time T_{on} . From a switching period T , T_{on} can be defined as DT where D is the duty ratio. Therefore the net increase in the inductor current can be defined in Equation 3.2

$$\begin{aligned}
 L \frac{\Delta I_L}{\Delta t} &= V_{in} - V_{out} \\
 \frac{\Delta I_L}{\Delta t} &= \frac{V_{in} - V_{out}}{L} \\
 \Delta I_L &= \frac{V_{in} - V_{out}}{L_{buck}} DT
 \end{aligned} \tag{3.2}$$

Figure 3.3 shows the circuit when the switch is opened. Equation 3.3 obtained when the switch is both on and off.

$$\begin{aligned}
 L \frac{\Delta I_L}{\Delta t} &= V_{out} \\
 \frac{\Delta I_L}{\Delta t} &= \frac{V_{out}}{L_{buck}} \\
 \Delta I_L &= \frac{V_{out}}{L_{buck}} (1 - D)T \Rightarrow L_{buck} = \frac{V_{out}(1 - D)}{\Delta I_L f}
 \end{aligned} \tag{3.3}$$

Since the net change in current over a cycle is zero

$$\frac{V_{in} - V_{out}}{L_{buck}}DT - \frac{V_{out}}{L_{buck}}(1 - D)T = 0 \Rightarrow V_{out} = DV_{in} \quad (3.4)$$

It can be seen from Equation 3.4 that the output voltage is always smaller than the input voltage. The buck converter can operate in two distinct modes with respect to the inductor current I_L : a continuous conduction mode CCM or in a discontinuous conduction mode DCM . In CCM , the inductor current flows for the entire cycle whereas, in DCM , the inductor current flows for only a part of the cycle [9, 114].

- $I_{min} > 0$ the converter operates in the continuous conduction mode CCM , which means that the average inductor voltage is zero, because the inductor current is periodic, the current at end time period is equal at the current at starting period. As a result of this, the the inductance required in this mode will be in Equation 3.5

$$L_{CCM} = \frac{(1 - D)R_{load}}{2f}; \quad \text{Where } D \text{ the duty ratio} \quad (3.5)$$

After few mathematical manipulation, we found a relationship between Equation 3.4 and Equation 3.5 as follows:

$$L_{buck} = \frac{L_{CCM}}{1 - \frac{I_{min}}{I_o}}; \quad \text{where } I_o \text{ is the load current.} \quad (3.6)$$

The Equation 3.6 can be expressed as follows

$$\frac{L_{buck}}{L_{CCM}} = \frac{I_o}{I_o - I_{min}} \quad (3.7)$$

All of the calculations were based on the assumption of infinite capacitance. However, by taking a finite value of capacitance from a given specification, which is typically the peak to peak load voltage variation (known as ripple voltage). To calculate the value of this capacitor

the current value during the switch on and off time is the starting point

$$\begin{aligned}
 i_{C_{t_{on}}}(t) &= i_{L_{buck}} - i_{load} \\
 &= \frac{V_s - V_o}{L_{buck}}t + I_{min} - I_o; \quad 0 \leq t \leq t_{on} \\
 &= \frac{V_s - V_o}{L_{buck}} \left[t - \frac{D}{2f} \right]; \quad \text{Let } t_1 = \frac{D}{2f} \\
 i_{C_{t_{off}}}(t) &= \frac{V_o}{L_{buck}}(T - t) + I_{min} - I_o; \quad t_{on} \leq t \leq T \\
 &= \frac{V_o}{L_{buck}} \left(\frac{1 + D}{2f} - t \right); \quad \text{Let } t_2 = \frac{1 + D}{2f}
 \end{aligned} \tag{3.8}$$

$$\Delta V_0 = V_{max} - V_{min}$$

$$\Delta Q = C \Delta V_0$$

$$= \frac{1}{2}(t_1 - t_2)I_{peak} \tag{3.9}$$

$$= \frac{V_o(1 - D)}{8L_{buck}f}; \quad I_{peak} \quad \text{obtained from Eq(3.8)}$$

$$C = \frac{1 - D}{8rL_{buck}f^2}, \quad \text{where } r = \frac{\Delta V_0}{V_0} \tag{3.10}$$

Note: The capacitor calculation must be based on the minimum duty ratio.

- $I_{min} < 0$: the converter operates in discontinuous conduction mode (*DCM*), when the inductor current is not sustained throughout the switching cycle and becomes zero before the end of the period. As a result, a significantly greater capacitance is required to hold the load current for a long period of time. However, the converter works in discontinuous mode if the switching frequency is small, the conducting duty cycle is small, the inductance is small and the load current is high.

In practice, the choice between continuous and discontinuous conduction modes of operation is often dictated by the power rate application. Continuous conduction mode is more suited for high power applications, whereas discontinuous conduction mode is limited to low power applications owing to the relatively high device stresses.

3.2.2 Boost Converter

The output voltage is greater than the input voltage; refer to Figure 3.4 for the circuit diagram. The arrangement for the step up converter, which consists of a DC input voltage source V_{in} , a boost inductor L_{boost} , a controlled switch S_{boost} , a diode D_{boost} , a filter capacitor C_{boost} , and load resistance R_{load} . Before starting to analyse the circuit, some assumptions need to be mentioned:

- ★ The converter operates in steady-state mode.
- ★ The switching period is T_{on} , and DT is the time when the switch is *ON* and $(1 - D)T$ is the time when the switch is *OFF*.
- ★ The capacitor has a very large value so the output voltage remains constant .
- ★ The inductor current is continuous.
- ★ All components are ideal.
- ★ Input voltage is V_{in} and output voltage is V_{out} ; both are constant.

The operation of the circuit can be summarized in two modes.

When the switch S_{boost} is closed, as shown in Figure 3.5, the source voltage is applied across the inductor for a time T_{on} . For a switching period T , T_{on} can be defined as DT where D is the duty ratio. Therefore, the net increase in the inductor current can be defined as follows:

$$\begin{aligned}
 L \frac{\Delta I_L}{\Delta t} &= V_{in} \\
 \frac{\Delta I_L}{\Delta t} &= \frac{V_{in}}{L} \\
 \Delta I_L &= \frac{V_{in}}{L} DT
 \end{aligned} \tag{3.11}$$

When the switch S_{boost} is opened as the Figure 3.6 shows

$$\begin{aligned}
 L \frac{\Delta I_L}{\Delta t} &= V_{in} - V_{out} \\
 \frac{\Delta I_L}{\Delta t} &= \frac{V_{in} - V_{out}}{L} \\
 \Delta I_L &= \frac{V_{in} - V_{out}}{L} (1 - D)T
 \end{aligned} \tag{3.12}$$

Since the net change in current over a cycle is zero.

$$\frac{V_{in}}{L}DT + \frac{V_{in} - V_{out}}{L}(1 - D)T = 0 \Rightarrow V_{out} = \frac{V_{in}}{1 - D} \quad (3.13)$$

Boost converter acts like a *DC* transformer with a variable output voltage, which depends on the duty cycle *D*, that is usually $0.1 < D < 0.9$. It is suitable for low irradiance and low power applications [115]. At 33% duty cycle, the ripple vanishes identically. [116].

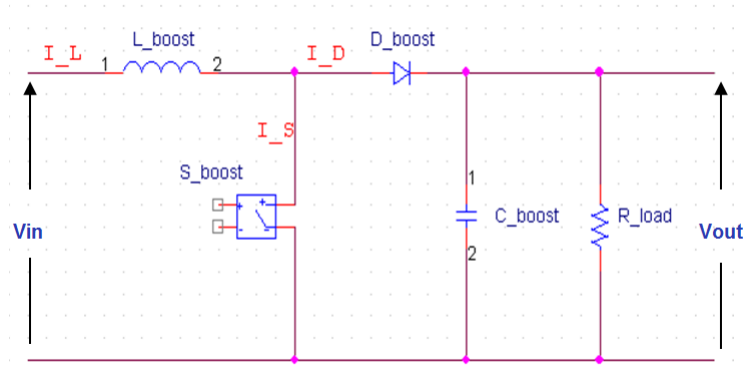


Fig. 3.4: Boost Converter

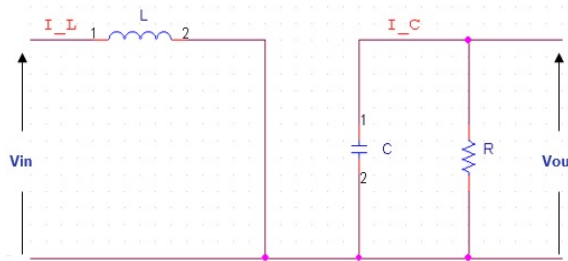


Fig. 3.5: Boost Converter Representation when Switch Closed

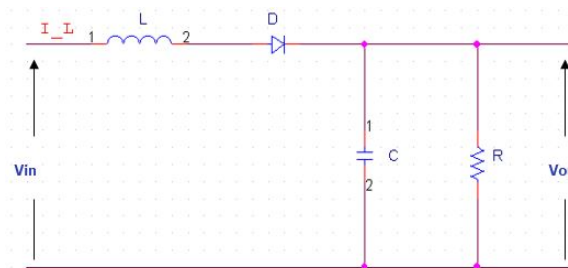


Fig. 3.6: Boost Converter Representation when Switch Opened

The design of the boost converter must take into consideration the value of the inductor, in order to maintain a continuous mode of operation, and also take account of the peak current and frequency

to avoid saturation. Knowing the inductor changing current is key to determining the inductor value [117]. By replacing the time period by the frequency From Equation 3.11 the value of the inductance L can produced.

$$L = \frac{V_{in}D}{f\Delta I_L} \quad (3.14)$$

The other component that requires careful handling by the designer is the capacitor. The capacitance acts as a sink for the voltage ripple and unwanted harmonics. The voltage ripple can be calculated from Equation 3.15

$$\begin{aligned} \frac{\Delta V_{out}}{V_{out}} &= \frac{DT}{RC} \\ &= \frac{D}{RCf} \end{aligned} \quad (3.15)$$

$$C = \frac{D}{R\frac{\Delta V_{out}}{V_{out}}f} \quad (3.16)$$

Many studies have used boost converters in PV system, either for grid-connected or stand-alone applications, such as refs [118–121]

3.2.3 Buck - Boost Converter

This can be obtained by making the cascade connection of the two basic converters: buck and boost converters. The output voltage can be either greater than or less than the input voltage. The output voltage polarity is opposite to the input voltage polarity [116, 122–124]. Figure 3.7 illustrates this converter, Which consists of direct current input voltage source V_{dc} , inductor $L1$, controlled switch $FET1$, Diode $D1$, filter capacitor $C1$, and load resistance $R1$. In the analysis the circuit will be represented twice depending on the switch status. The inductor current will be evaluated and the relationship between the converters input and output will be studied. However, the following assumptions must be considered [123–125]:

1. The converter is running in a steady-state mode.
2. The inductor current is continuous.
3. The capacitor has a huge value.

4. The switching period is T_s , and DT_s is the time when the switch is ON and $(1 - D)T_s$ is the time when the switch is OFF.
5. Input voltage is V_s and output voltage is V_0 and both are constant.
6. All components are ideal.

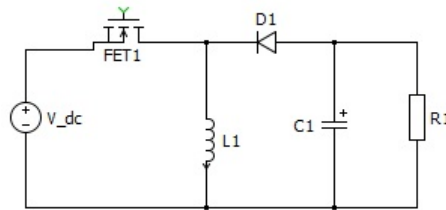


Fig. 3.7: Buck Boost Converter Circuit

- ★ **Step 1:** When the switch $FET1$ is closed, as Figure 3.8 shows, the source voltage is applied across the inductor for a time T_{on} . As the diode acts with a reverse bias, the inductor current flows from the source to the inductor.

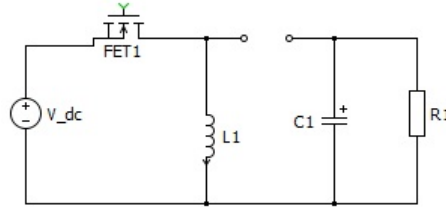


Fig. 3.8: Buck Boost Switch On

$$\begin{aligned} V_{dc} &= V_{L_1} \\ &= L_1 \frac{di_{L_1}}{dt} \end{aligned} \quad (3.17)$$

$$\frac{V_{dc}}{L_1} = \frac{di_{L_1}}{dt} \quad (3.18)$$

Equation 3.18 shows the change in the inductor current is constant, and the ratio increases linearly while the switch is on. Therefore, the equation becomes as follow.

$$\begin{aligned} \frac{\Delta i_{L_1}}{\Delta t} &= \frac{\Delta i_{L_1}}{DT_s} \\ &= \frac{V_{dc}}{L_1} \end{aligned} \quad (3.19)$$

The linear change of the inductor current is

$$(\Delta i_{L_1})_{on} = \frac{V_{dc}DT_s}{L_1} \quad (3.20)$$

- ★ **Step 2:** when the switch is off as the Figure 3.9 shows, The inductor will be a source of energy. It starts releasing its current to the load through the diode, which acts in a forward-biased mode. The current decreases gradually.

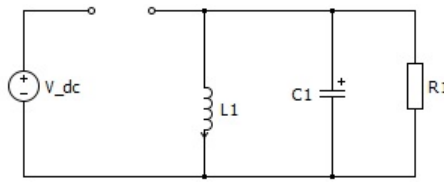


Fig. 3.9: Buck Boost Switch Off

The inductor voltage in this situation is:

$$\begin{aligned} V_0 &= V_{L_1} \\ &= L_1 \frac{di_{L_1}}{dt} \end{aligned} \quad (3.21)$$

$$\frac{V_0}{L_1} = \frac{di_{L_1}}{dt} \quad (3.22)$$

As mention in the previous step, Equation 3.22 shows a linear changing rate in the inductor current. This change can be represented by

$$\begin{aligned} \frac{\Delta i_{L_1}}{\Delta t} &= \frac{\Delta i_{L_1}}{(1-D)T_s} \\ &= \frac{V_0}{L_1} \end{aligned} \quad (3.23)$$

The changing rate of the inductor current is

$$(\Delta i_{L_1})_{off} = \frac{V_0(1-D)T_s}{L_1} \quad (3.24)$$

Sine

$$(\Delta i_{L_1})_{on} = (\Delta i_{L_1})_{off} \quad (3.25)$$

Applying Equation (3.20) and Equation (3.24) in Equation (3.25)

$$\frac{V_0(1-D)T_s}{L_1} = \frac{V_{dc}DT_s}{L_1} \quad (3.26)$$

From Equation (3.26) The output voltage V_0 will be as follows

$$V_0 = -V_{dc} \frac{D}{1-D} \quad (3.27)$$

From Equation (3.20)

$$L_1 = \frac{V_{dc}D}{\Delta i_{L_1} f} \quad (3.28)$$

$$C_1 = \frac{V_0 D}{R_1 \Delta V_o f} \quad (3.29)$$

An electronic switch has several states during an operating cycle. On, transition to Off, Off and transition to On; these states are repeated in each cycle. As a result, the electrical current through the switch and the voltage across it varies during the operating cycle. Furthermore, during the transition interval, both the current through the device and the voltage across the device are substantially larger than zero. This leads to large, instantaneous, power losses (instantaneous power dissipation during the transition period to the *Off* or to the *On* state could be very high) as illustrated in Figure 3.10. This instantaneous power dissipation could damage the switching device or drive it to work outside the safe operating area of the component.

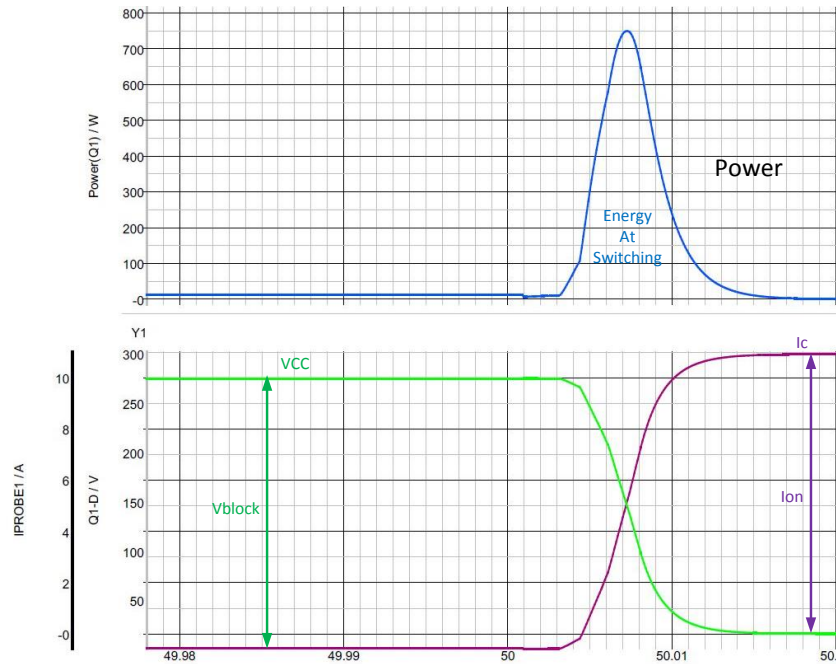


Fig. 3.10: Instantaneous Power in Switch On Transition

1. Switching losses for soft load (resistor):

$$\begin{aligned}
 W &= \int_0^{t_{on}} P dt \\
 &= \int_0^{t_{on}} e i dt \\
 &= \int_0^{t_{on}} V I \frac{t}{t_{on}} \left(1 - \frac{t}{t_{on}}\right) dt \\
 &= \frac{V I t_{on}}{6} \\
 &= \frac{1}{6} V I t_{on} \quad \text{Total turn on switching loss per cycle}
 \end{aligned} \tag{3.30}$$

The same logic is applied to find turn off losses:

$$W = \frac{1}{6} V I t_{off} \quad \text{Total turn off switching loss per cycle} \tag{3.31}$$

The total switching losses per cycle:

$$W = \frac{1}{6} V I (t_{on} + t_{off}) \quad \text{Total turn off switching loss per cycle} \tag{3.32}$$

And, finally, the total losses for soft load can be calculated from Equation 3.33

$$W = \frac{1}{6}VI(t_{on} + t_{off})f_{sw} \quad (3.33)$$

2. Switching losses for hard load:

$$\begin{aligned} W &= \int_0^{t_{on}} P dt \\ &= \int_0^{t_{on}} e i dt \\ &= \int_0^{t_{on}} VI\left(1 - \frac{t}{t_{on}}\right) dt \\ &= \frac{VI t_{on}}{2} \\ &= \frac{1}{2}VI t_{on} \quad \text{Total turn on switching loss per cycle} \end{aligned} \quad (3.34)$$

Same logic apply to find turn off losses

$$W = \frac{1}{2}VI t_{off} \quad \text{Total turn off switching loss per cycle} \quad (3.35)$$

The total switching losses per cycle

$$W = \frac{1}{2}VI(t_{on} + t_{off}) \quad \text{Total turn off switching loss per cycle} \quad (3.36)$$

and finally the total losses for hard load can be calculated by 3.37

$$W = \frac{1}{2}VI(t_{on} + t_{off})f_{sw} \quad (3.37)$$

To deal with these problems, various circuits, called snubber circuits, have been developed.

3.3 Snubber Circuits

In power switching circuits, snubber circuits comprise a small network, the function of which is to control the effects of circuit reactance [126]. The main aim is to reshape the voltage and/or the current waveforms of a switch during the turn On and turn Off, or combination of both. Moreover, the snubbers introduced in order to overcome the limitation of the switch, such as maximum rates

of change of voltage and current (dv/dt & di/dt), reduces over-voltage during turn-on and turn-off, reduces the current at starting by making an alternate path, reduces switching losses and ensures that the switch does not operate outside its safe operating area (*SOA*).

The use of snubbers can greatly enhance the switch circuit performance and results in high reliability, high switching frequency, an increased power handling of a given device, lower electromagnetic interference (*EMI*) (by the damping of voltage and current ringing of a switching devices). It also helps to maintain a uniform distribution of voltages across the switches that are connected in series, to increase the effective voltage rating or currents in the switches that are connected in parallel and to increase the effective current rating.

3.3.0.1 Electrical Snubbers Circuit Classification

Snubber circuits can be categorised into two classes: Dissipative energy or energy recovery.

1. Dissipative Electrical Snubbers Circuit: a snubber is called dissipative when the stored energy at the turn On or turn Off of the switch is dissipated through a resistor. Figure 3.11 illustrates a general dissipative snubber.

During the turn on process, the inductance L_1 reduce the effect of di/dt by storing the extra

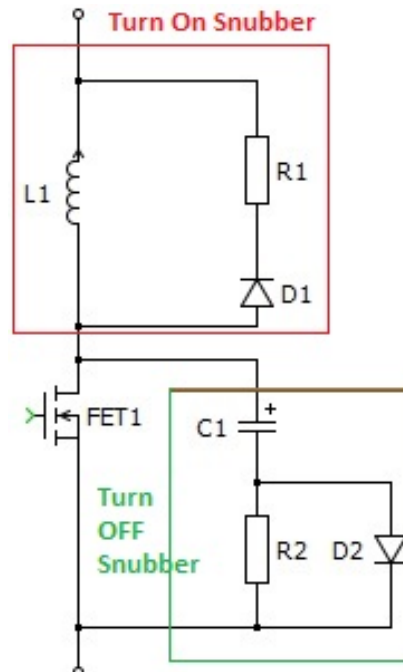


Fig. 3.11: Dissipative Snubber Topology [9, 10]

energy. The R_1 and D_1 allow the discharging of L_1 when the electronic switch is turned off, so that the snubber is reset by the start of the next cycle.

During the turn off process, capacitor C_1 reduces the effect of dv/dt , R_2 and D_2 allow the discharge of C_1 when the electronic switch is turned on. The amount of dissipated energy in the snubber resistance is equal to the amount of stored energy in the inductance L_1 during the turn on process, or in the capacitor C_1 during the turn off process.

TURN-OFF Snubber [127]

The fall time, $0 \leq t \leq t_{off}$

$$i = I\left(1 - \frac{t}{t_{off}}\right) \quad (3.38)$$

$$\begin{aligned} e &= \frac{1}{c} \int_0^t (I - i) dt \\ &= \frac{I}{c} \int_0^t \frac{t}{t_{off}} dt \\ &= \frac{It^2}{2Ct_f} \end{aligned} \quad (3.39)$$

when $t = t_{off} \Rightarrow e = V$

The size of the capacitor can be calculated from the Equation 3.43

$$C = \frac{It_{off}}{2V} \quad (3.40)$$

where t_{off} is the switch fall time, which can be obtained from manufacturers data sheet, and V is the rated switch voltage of the switch.

The whole stored energy in the snubber capacitor must be dissipated in the snubber resistor during each cycle. Thus, RC time constant must ensure that, after turn on the capacitor discharges before the next turn off is required [122]. Hence:

$$t_{off(min)} = 5RC \quad (3.41)$$

The power rating of the resistor is dependent on the switching frequency as Equation 3.42 shows:

$$P_R = \frac{1}{2} CV_C^2 f \quad \text{where: } f \text{ is the switching frequency} \quad (3.42)$$

TURN-ON Snubber [127]

The fall time, $0 \leq t \leq t_{on}$

$$e = V\left(1 - \frac{t}{t_{on}}\right) \quad (3.43)$$

$$\begin{aligned} i &= \frac{1}{L} \int_0^t (V - e) dt \\ &= \frac{V}{L} \int_0^t \frac{t}{t_{on}} dt \\ &= \frac{Vt^2}{2Lt_{on}} \end{aligned} \quad (3.44)$$

when $t = t_{on} \Rightarrow i = I$

The size of the Inductance L can be calculated form Equation 3.45

$$L = \frac{Vt_{on}}{2I} \quad (3.45)$$

$$t_{on(min)} = 5L/R \quad (3.46)$$

The power rating of the resistor is dependent on the switching frequency, as Equation 3.42 shows:

$$P_R = LI_m^2 f \quad \text{where: } L \text{ represents the inductance} \quad (3.47)$$

However, the power dissipation increases in high power application, and also with the switching frequency, and thus reduces the power efficiency of a high-frequency switching converter. To remedy this drawback, a energy recovery snubber introduced [122, 124].

2. Energy Recovery Electrical Snubber circuit : The snubbing action on the switch is exactly the same as for the dissipative snubbers. The difference is the way in which the stored energy in the snubber is delivered back to either the input source, or into the load. Alternatively, the energy may be circulated to prepare for the next cycle. Two classifications of energy recovery circuit exist:

- ★ Passive recovery circuit: this involves passive components with diode. Figure 3.12 shows a passive recovery snubber which provide a combined of turn-on and and turn-off.

L_{s1} is the turn-on snubber inductance and C_{s1} is the turn-off snubber capacitor. D_{s2} ,

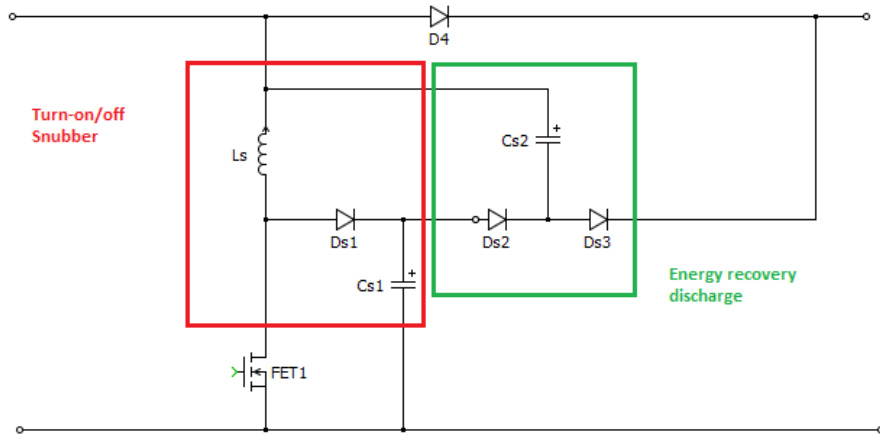


Fig. 3.12: Combined energy recovery Snubber

D_{s3} and C_{s2} form an energy recovery network which delivers the recovered energy to the load.

★ Active recovery techniques which involves switching devices: this type of snubber employs an auxiliary active switch, with few passive components, as shown in Figure 3.13 [128]. The auxiliary switch and the main switch share the same *PWM* signal. Operation

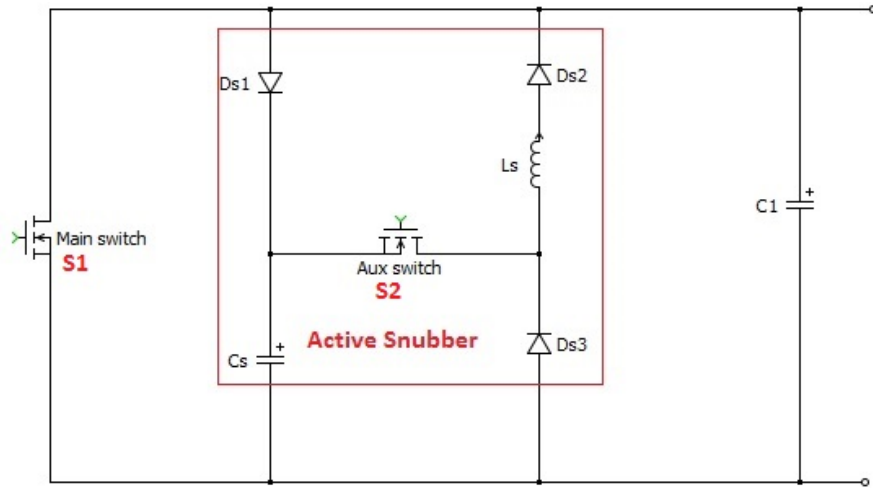


Fig. 3.13: Active Snubber

principle:

- ★ First Stage: Both switches S_1 and S_2 are OFF; the current passes through the diode D_{s1} to charge the capacitor C_s . Diode D_{s2} and D_{s3} are both off.
- ★ Second Stage: switches S_1 and S_2 are turned on during this period, whereas the diodes D_{s1} and D_{s3} are blocked by the reverse voltage across them, which is applied

individually. Energy stored in the capacitor C_s during stage 1 is discharged through the inductor L_s , and the diode D_{s2} , to charge C_1 . When the voltage VC_s is larger than VC_1 , the inductor current increases and, when the voltage VC_s drops below VC_1 , the inductor current decreases. During this period, diode D_{s1} will prevent VC_s from going negative, and D_{s2} will prevent the inductor current from going negative.

- ★ Third stage: switches S_1 and S_2 are OFF and the inductor current flows through diodes D_{s2} and D_{s3} to keep charging C_1 , until the inductor current decreases to zero. Diodes D_{s2} and D_{s3} would block the inductor current from going negative. On the other side the capacitor C_s start charging as analysed in first stage.

3.4 Super-Capacitor

3.4.1 Equivalent Circuits

Many equivalent circuit models have been proposed:

1. The classical RC model: this represents the super-capacitor model as a series combination of a resistor and a capacitor. The resistor represents the equivalent series resistance (ESR), which is the loss term that will cause internal heating in the capacitor, and an ideal capacitance [129–131].
2. The three branch model: This represents the super-capacitor model as a three branch model, as Figure 3.14 illustrates. The first branch is in the time range of seconds, the second branch is in the range of minutes and the third one is for time longer than 10 minutes [132–135].

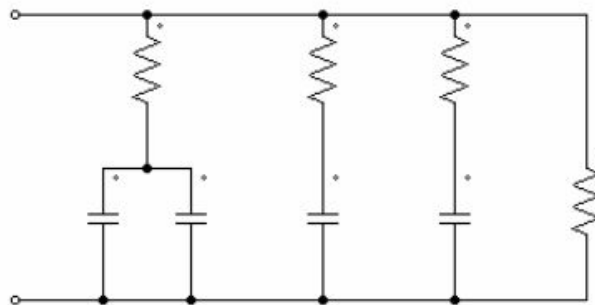


Fig. 3.14: The Three Branch Model

- The multiple branch model: this can describe the behaviours of super-capacitors in a very wide range of frequencies. The author of [136] believes this model is the general model of the super-capacitor and the models listed above (classical RC and the three-branch) are only two specific cases of this mode. This model is shown in Figure 3.15

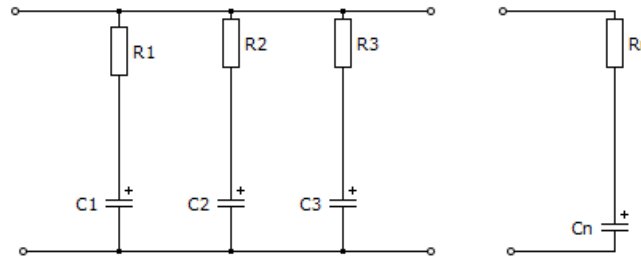


Fig. 3.15: SC Multiple Branches Model

- The transmission line model: This exhibits several RC constants and involves distributed capacitance C_i and resistance R_i , R_i . C_i can be considered as resistance and capacitance of the pores with certain pore size. [137–143].

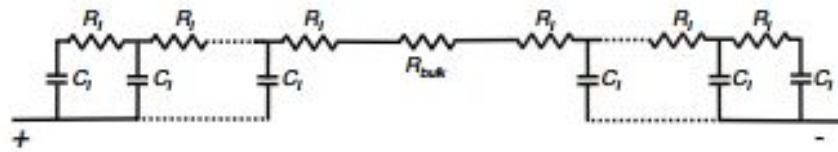


Fig. 3.16: SC Transmission Line Model

- Another equivalent circuit is proposed by [11], which includes the thermal and electrical behaviour of the super-capacitors. Thermal variations of the device and its environment were applied and analysed owing to the application of super-capacitor in transportation. Figure 3.17 shows the proposed model.

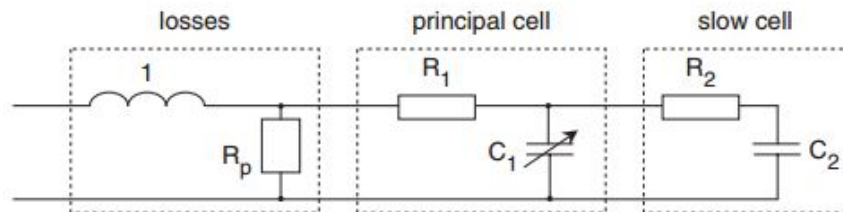


Fig. 3.17: SC Electrical and Thermal Model [11]

6. The two branch model with five parameters [12] proposed two branch equivalent circuit, with time-dependent diffuse circuit, which is based on five parameters as shown in Figure 3.18. In this figure, C_1 corresponds to Helmholtz capacitance, C_2 corresponds to diffuse capacitance, R_1 represents the equivalent series resistance (ESR), R_L represents the leakage resistance and $R_2(t)$ represents the resistance between the Helmholtz and diffuse capacitances. This resistance is time dependent.

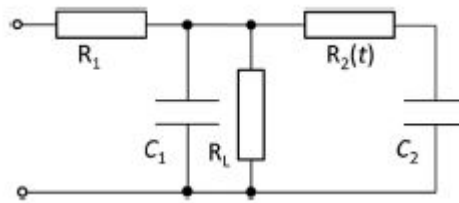


Fig. 3.18: Equivalent Electrical Circuit Model for Super-Capacitor [12]

However, an equivalent circuit model is usually preferred by a design engineer owing to its simplicity, simulation time is reduced when compared to the models listed above. This model also holds the most common model representation as an equivalent electrical circuit, according to [13, 135, 144] and as Figure 3.18 illustrates. The model consists of a capacitor representing the SC capacitance, an equivalent series resistor (ESR) representing the ohmic losses and an equivalent parallel resistor (EPR) representing the SC self-discharge [138], due to:

- Faradaic reaction of electrolyte impurities.
- Parasitic redox reactions involving impurities (oxygen groups and metals).
- Non-uniformity of charge acceptance along the surface of electrode material pores.
- Possible short-circuit of the anode and cathode from improperly sealed bipolar electrodes

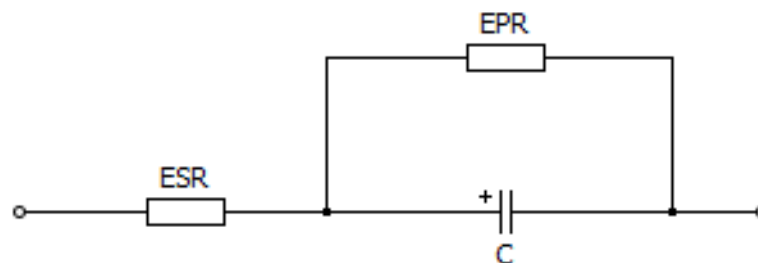


Fig. 3.19: Super-capacitor Model [13]

Furthermore, those parameters can be determined by Gouy and Chapman theories [145, 146].

3.4.2 Charge-Discharge Method

3.4.2.1 Super-Capacitor Charging

The equivalent circuit of charge super-capacitor with calculation notation are illustrated in Figure 3.20.

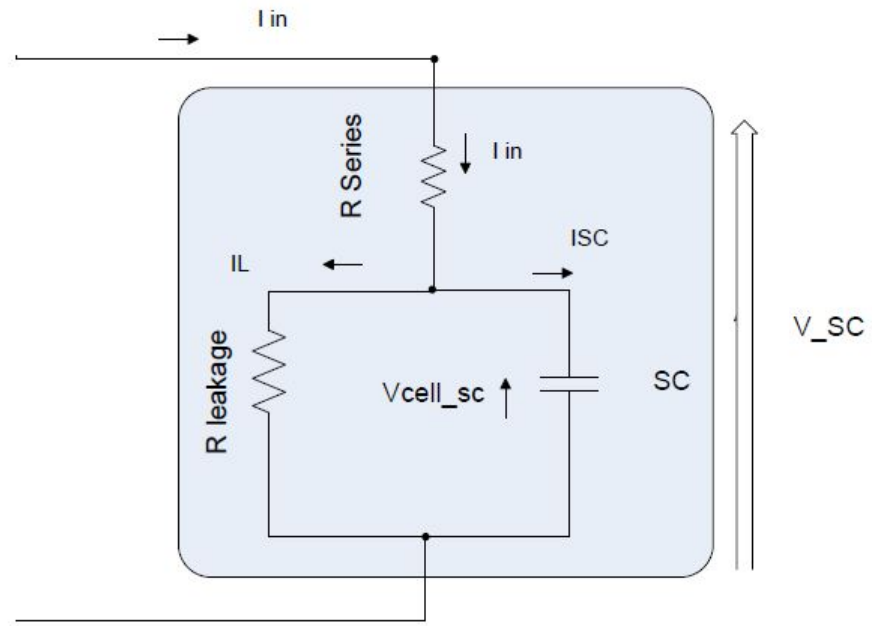


Fig. 3.20: SC Charge Process

$$\left. \begin{array}{l}
 I_{in} = I_{SC_{cell}} + I_L \quad \text{SC charging Current} \\
 I_{in} = C \frac{dV_{cell_{SC}}}{dt} + \frac{V_{cell_{SC}}}{R_{Leakage}} \quad \text{with initial condition } t = 0, V_{cell_{SC}} = 0 \\
 V_{cell_{SC}} = I_L R_{Leakage} \left(1 - \exp\left(\frac{-t}{CR_{Leakage}}\right) \right) \quad \text{SC charging process} \\
 V_{SC} = R_{series} I_{in} + I_L R_{Leakage} \left(1 - \exp\left(\frac{-t}{CR_{Leakage}}\right) \right) \quad \text{SC terminal voltage at charging process} \\
 V_{SC} = R_{series} I_{SC} + \frac{t}{C} I_{SC} \quad \text{Charge process with } R_{Leakage} \rightarrow \infty, I_L = 0 \\
 V_{SC} = R_{series} I_{in} + \frac{t}{C} I_{in} \quad \text{Charge process with } R_{Leakage} \rightarrow \infty, I_L = 0 \\
 V_{SC} = \frac{t}{C} I_{in} \quad \text{SC Voltage with } R_{Leakage} \rightarrow \infty, R_{series} = 0
 \end{array} \right\} \quad (3.48)$$

From Equation 3.48 the charging voltage is linearly proportional to the charge time when the leakage resistance is neglected, and in exponential form otherwise, at $t = 0$, $V_{SC} = R_{series}I_{in}$ and when $t \rightarrow \infty$, $V_{SC} = R_{series}I_{in} + I_L R_{Leakage}$. In this case the voltage across the super-capacitor increasingly approaches its maximum value. If charging an ideal super-capacitor $R_{series} = 0$, $R_{Leakage} \rightarrow \infty$ the voltage will become:

$$V_{SC} = V_{cell_{SC}} = I_{in} \frac{t}{C} + V_{initial} \quad (3.49)$$

The reused stored energy in Super-capacitor can be calculated by the following equation

$$E_{SC} = \frac{1}{2}C[V_{max}^2 - V_{min}^2] \quad (3.50)$$

3.4.2.2 Super-Capacitor Discharge

The calculation notation are shown in Figure 3.21, which also illustrated the discharge process.

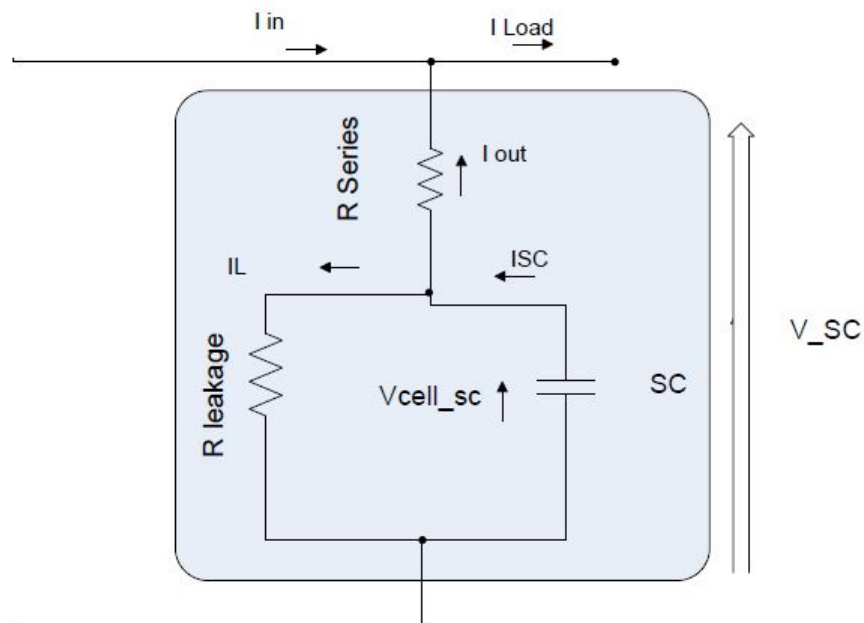


Fig. 3.21: Super-Capacitor Discharge Process

$$\left. \begin{array}{l}
 V_{SC} = V_{cell_{SC}} - V_{R_{series}} \quad \text{SC terminals Voltage} \\
 V_{cell_{SC}} = V_{cell_{SC}}^{max} - \frac{1}{C} \int_{t_0}^t I_{SC} dt \\
 V_{cell_{SC}} = V_{cell_{SC}}^{max} - (V_{cell_{SC}}^{max} + I_{out} R_{leakage}) \left[1 - \exp\left(-\frac{t}{CR_{leakage}}\right) \right] \\
 V_{SC} = V_{cell_{SC}}^{max} - I_{out} R_{series} - (V_{cell_{SC}}^{max} + I_{out} R_{leakage}) \left[1 - \exp\left(-\frac{t}{CR_{leakage}}\right) \right] \\
 I_{SC} = \frac{(V_{cell_{SC}}^{max} + I_{out} R_{leakage})}{R_{leakage}} \exp\left(-\frac{t}{CR_{leakage}}\right) \quad \text{SC Discharge current} \\
 V_{SC} = V_{cell_{SC}}^{max} - I_{out} R_{series} - I_{out} \frac{t}{C} \quad R_{leakage} \rightarrow \infty \\
 t_{dsc} = -CR_{leakage} \ln \frac{I_{out} R_{leakage}}{V_{cell_{SC}}^{max} + I_{out} R_{leakage}} \quad t_{dsc} \text{ fully discharge time}
 \end{array} \right\} \quad (3.51)$$

3.4.3 Voltage Balancing

In order to operate at higher application voltages, super-capacitors are connected in series and in parallel configurations to form a module. This module meets the DC voltage, energy capability and the total ESR value, which determine the maximum power capability of the bank. However, if the cells have a variation in capacitance, individual cell voltages will vary based on capacitance. The cells with greater capacitance will be charged to lower voltages, and the cells with smaller capacitance will be charged to higher voltages. This is due to the fact that each cell conducts the same charging current, and the voltage is a function of current and capacitance. Those undesired and unequal capacitances could contribute to the following:

- Tolerances of 5 – 10%.
- Temperature gradient in the system.
- Cell ageing

This can lead to some super-capacitors having an over voltage, with an associated decrease of their lifetime. For the other super-capacitors, the maximum voltage will be under the voltage limit; the energy storage in super-capacitors will not be at its maximum level. However, capacitors with a smaller capacitance need a shorter charging time and so reach the maximum voltage faster than a larger capacitor. To avoid damaging the smaller capacitor, voltage equalization circuits have to be employed.

3.4.3.1 Voltage Balancing Type

There are two, common, approaches to cell balancing in super-capacitor modules: passive balancing and active balancing.

1. Passive balancing techniques: in general these can be classified into two types:
 - (a) Resistance balancing: this is simple approach to equalize the super-capacitor stacks by using a bypass resistor in parallel with the super-capacitor. The amount of current drawn by the resistors is proportional to the cell voltage, which results in more current being diverted to the resistor as the cell voltage decreases. This will tend to reduce the voltage variations between the different cells within the stack, since higher voltage cells will be further discharged by the resistors which are in parallel. The drawback of this approach is that the energy is converted into additional losses in the resistors and the amount of current drawn by the resistors is not regulated. As a result, the cell voltages are not fully regulated and the system efficiency is lower [8].
 - (b) Switched-resistors balancing circuits: this includes adding a controlled switch to an equalization resistor in order to limit the energy dissipation. The switch turns on when cell voltage goes beyond the operating voltage and then turns off when the level is lower than this voltage. The efficiency of this solution is much better than the technique mentioned above [147].
 - (c) Zener diode balancing: to overcome the drawback of the previous technique, a Zener diode is placed in parallel across the super-capacitor and is used as a voltage regulator when a capacitor reaches its maximum voltage. If the voltage is almost at the value of the breakdown voltage of the diode, it starts conducting and deviates the charging current. However, the amount of lost energy is minimized, compared to the previous technique, since the shunt circuitry is only active when the cell voltage exceeds the pre-set breakdown level. On the other hand, this approach suffers from the temperature dependency of the Zener diodes [148].

To minimize lost energy and optimize the performance of the cells, passive balancing is best suited for low power applications or low current charge / discharge rates.

2. Active balancing: Figure 3.22 summarize this technique. Which focuses on buck-boost topology for active voltage balancing. If the voltage U_{c1} is detected as being significantly greater than voltage U_{c2} , transistor $T1$ will be switched at a certain frequency to generate a positive equalizing current, $2I_{eq}$. If U_{c2} is greater than U_{c1} , then $T2$ will be switched to generate a negative equalizing current. This process continues until the voltages are balanced.

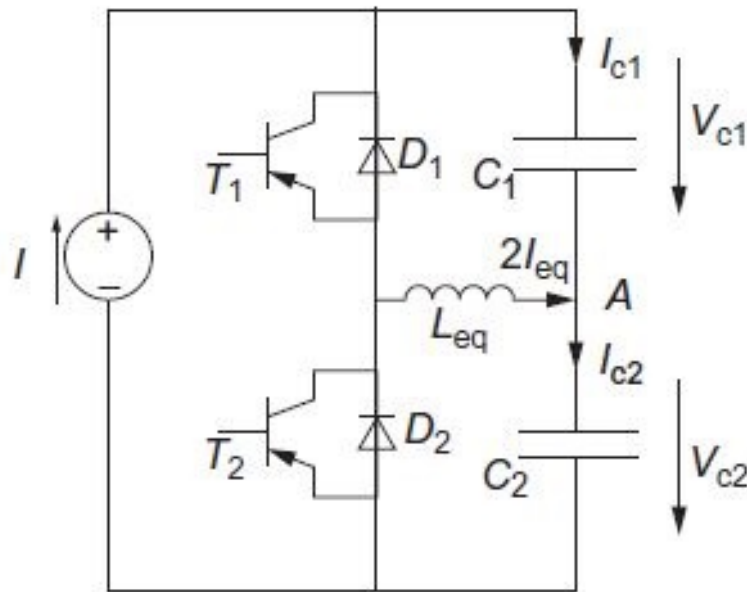


Fig. 3.22: Active Balancing [14]

3.5 Summary

In this chapter a review of the main $DC - DC$ converter topologies (buck, boost, buck-boost); Functionality is presented and the circuit analysis supported by the circuit diagram is delineated. Additionally, an over-view and classification of the snubber circuit design and implementation in $DC - DC$ converter has been presented. Finally, Super-capacitor models and balancing techniques have been presented. The following chapter present result and discussion of the Comparison between unidirectional and bidirectional Topologies for the placement of the super-capacitor.

Chapter 4

Result and Discussions

4.1 Introduction

This chapter presents an overview of stand-alone *PV* system, with a multi-string layout, followed by the results and discussions on the critical analysis between the power conversion topologies used for this conventional *PV* structures [16].

The analysis has been run for a range of parameters, which are: the capacitance of a super-capacitor when used as storage unit, converter efficiency and the load power. Moreover, the load power variation is related to the input mean power by a proportional constant, k , and also for every single load a wide range of capacitance values has been considered. However, the criterion of the comparison is the longest continuous load supply period without interruption CLSP, for both topologies in changing weather. The effect of each element variation on the performance of the whole PV system will be discussed.

4.2 Stand-alone *PV* System Layout

A typical standalone *PV* system structured with multi-string type, when several PV panels are connected in series and then connected with a low power DC/DC converter as a string. Several DC/DC converters, as multiple strings, are connected together with one DC/AC converter. The multi string structure type can realize optimal MPP for each string and is flexible with string design, an extra diode connected in series with a string is not required (less power losses), each string operates inde-

pendently so if one fails all other strings can still feed the load. The configuration of this structure with the super-capacitor as a storage system can be as follows:

4.2.1 Unidirectional Topology:

the illustration of this topology is shown in Figure 4.1. The power generated from the PV system flows in one direction throughout the whole system. However, the first $DC - DC$ converter is used to step down the voltage for the super-capacitor unit owing to its low operating voltage, whilst controlling the charging requirement. The second one is used to step the voltage up and maintain it at a fix level for the DC load. The super-capacitor unit is placed between the two converters, absorbing the extra energy produced by the PV and delivering it back when the energy produced is not enough for the load.

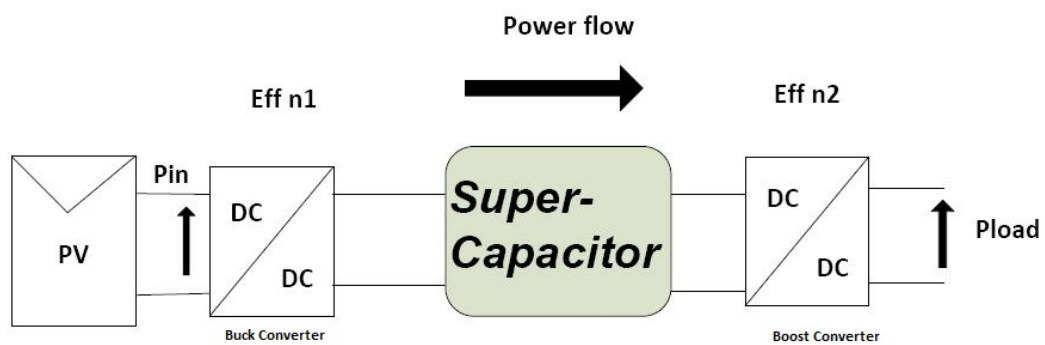


Fig. 4.1: Unidirectional Topology

4.2.2 Bidirectional Topology:

The overall power flow of this topology shown in Figure 4.2.

In this structure, the generated power from the PV system passes through the first $DC - DC$ converter in order to maintain the voltage fixed at the load level. Any surplus energy will pass through into another converter to the super-capacitor unit, and back through the same converter when there is a shortage of energy. Thus, this $DC - DC$ converter must be a bidirectional one, working as buck boost converter, stepping down the voltage for the super-capacitor unit side owing to the charge / discharge cycle, stepping it up in the load side and maintaining a fixed voltage.

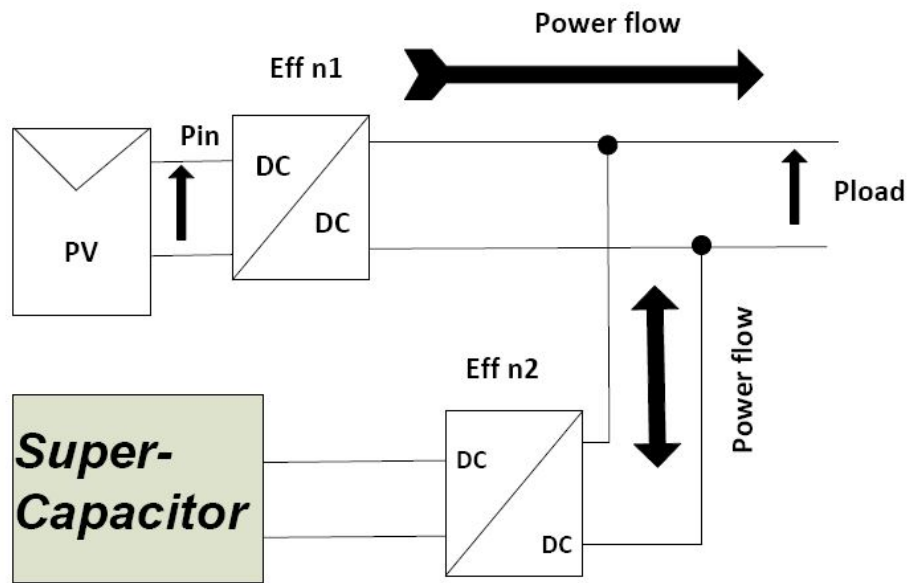


Fig. 4.2: Bidirectional Topology

4.3 Methodology

The comparative analysis of real data from cloudy day was used [15], as shown in Figure 4.4. In order to get an accurate comparison of the performance of each topology in dynamic matter, data interpolation was used.

Both converter topologies have identical efficiencies. Matlab software has been used to confirm the performance and effectiveness of each topology.

The control strategy was carried out based on the power flows between a PV as the main source, a super-capacitor bank as storage unit, and the load.

$$\left\{ \begin{array}{ll} P_{in} > P_{load} & \text{SC Charging (Surplus energy stored in SC)} \\ P_{in} < P_{load} & \text{SC Discharging (delivers the extra needed energy to the load)} \\ P_{in} = P_{load} & \text{SC Disconnected (Idle mode)} \\ P_{SC} = P_{load} & \text{SC Discharging (Source disconnected (} P_{in} = 0)) \\ P_{in} + P_{SC} < P_{load} & \text{SC Charging Load disconnected} \end{array} \right.$$

For safe operation of the super-capacitor, the voltage range was constrained by upper and lower limits. The upper limit was considered in order to avoid a surcharge to protect the integrity of Super-Capacitor, so the maximum stored energy in it is:

$$E_{SC_{max}} = \frac{1}{2}CV_{max}^2 \quad (4.1)$$

where $E_{SC_{max}}$ is the maximum Stored energy, C is the super-capacitor capacitance, and V_{max} is the max applied voltage. The lower limit was considered to prevent the converter from drawing excessive current, whilst limiting the high spike current for high output power. As a result, the minimum stored energy in the super-capacitor was fixed by a minimum voltage.

$$E_{SC_{min}} = \frac{1}{2}CV_{min}^2 \quad (4.2)$$

where $E_{SC_{min}}$ is the minimum Stored energy, C is the super-capacitor capacitance , and V_{min} is the minimum applied voltage .

From Equations ((4.1), (4.2)) the reused energy is:

$$E_{SC} = \frac{1}{2}C[V_{max}^2 - V_{min}^2] \quad (4.3)$$

The equivalent - electrical circuit model of super-capacitor used in this study, to predict each topology performance, is shown in Figure 4.3.

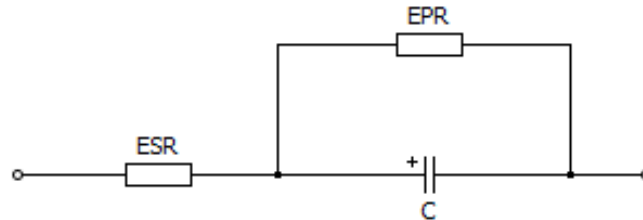


Fig. 4.3: Super-capacitor Equivalent Circuit

Since the input power was changing throughout the time, as Figure 4.4 shows, the investigation of the load power impact on the system is related to the input-mean power by a ratio of k , which varies from 10% to 200%.

$$k = \frac{P_{load}}{P_{inmean}} \quad (4.4)$$

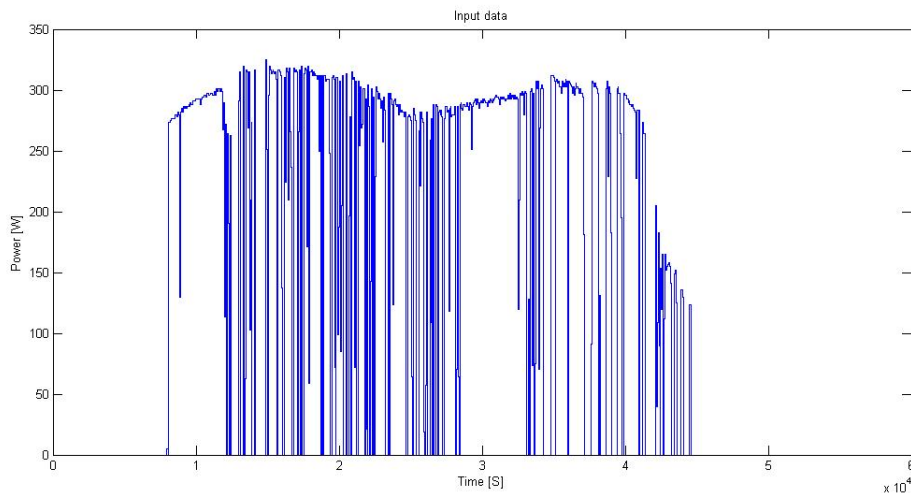


Fig. 4.4: Real Data [15]

The overall computational process is illustrated as a flowchart in Figure 4.5. This flowchart indicates the main steps applied in sequence through the MATLAB code in this investigation.

Data manipulation was needed to get accurate comparison between both topologies. A few different values of converter efficiency was applied in this comparison to observe the impact on the performance of each topology and the influence in the comparison. A wide range of capacitance values has been applied, for every single load, to see the storage effect on the system performance. This process

was repeated for a wide range of load power levels. Moreover, the load power variation was chosen to be varied by a proportional ratio to the input-mean power k .

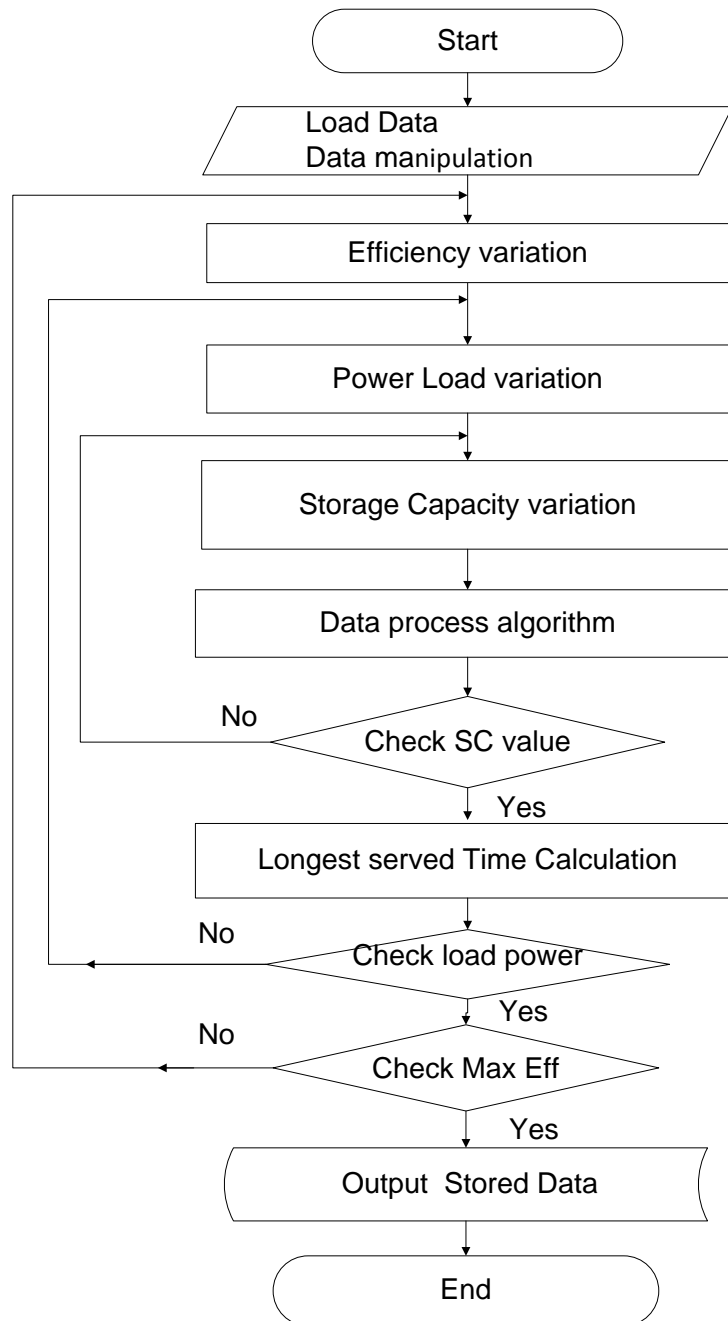


Fig. 4.5: Program Overall Process

The flowchart in Figure 4.6 indicates the real data process and manipulation algorithm used in this investigation. The manipulation was based on the variation of the produced power by the PV system in every single second.

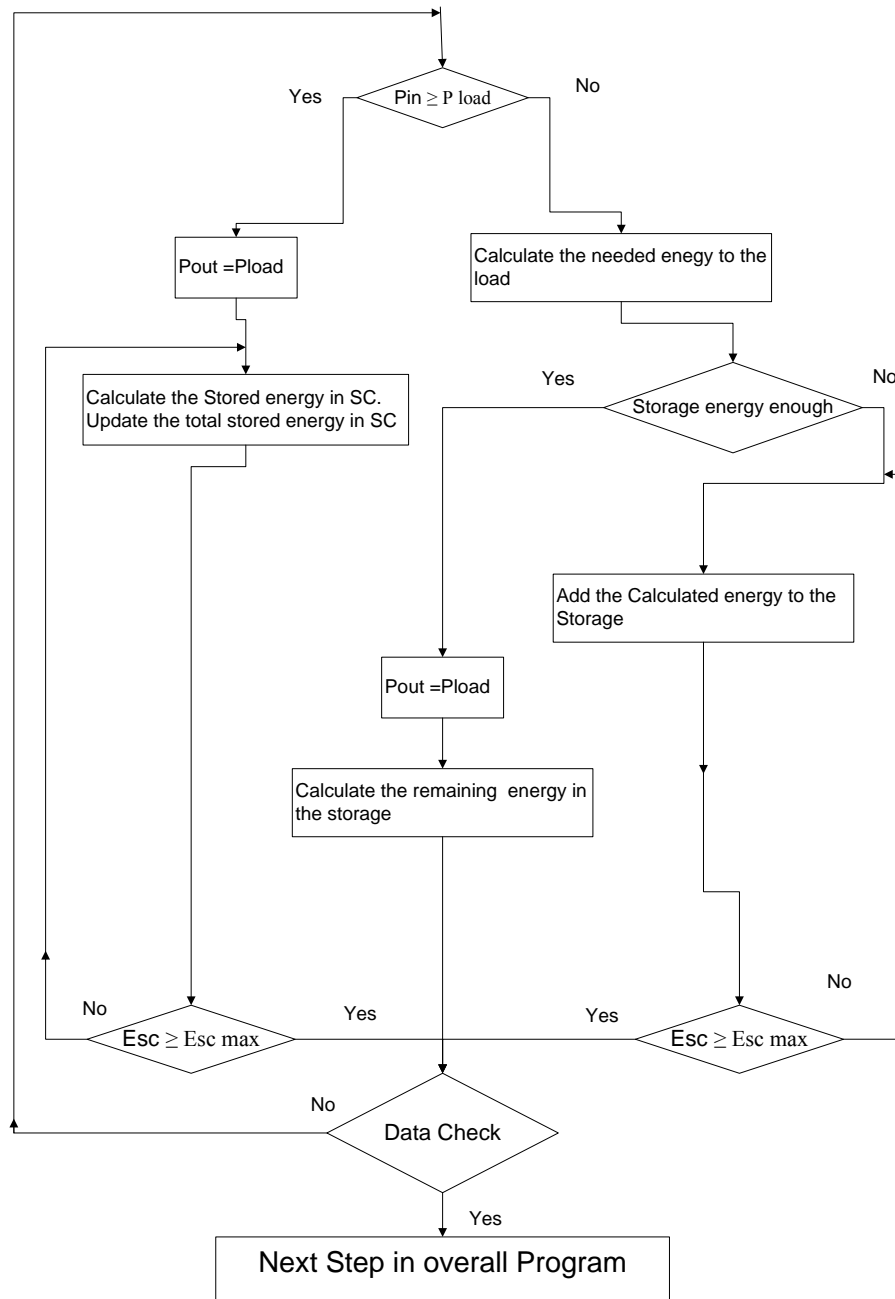


Fig. 4.6: Flowchart of Data Processing Algorithm

4.3.1 Storage Effect on the System Performance

4.3.1.1 Uni-directional Topology

Figures 4.7(a) and 4.7(b) plots the performance of uni-directional topology, with the load power varying from 10% of the input mean power up to 200%, with 1% step, under a wide range of capacitance having a step of one farad. The continuous load supply period (CLSP) in seconds, without interruption, is shown on the y axis.

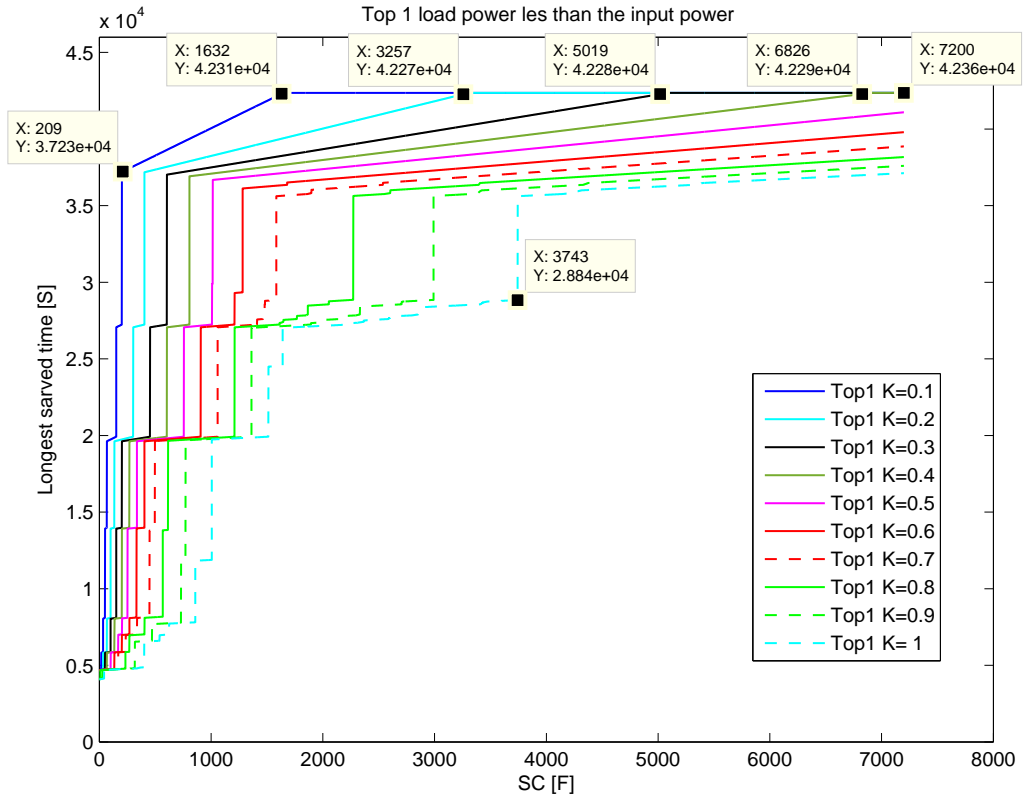
In Figure 4.7(a) some observation could be made:

- The steps shown in the plots were small slopes, owing to the big range of the horizontal axis, and small variation on the vertical axes, it looked like steps. However, because the used data in this comparison was changing throughout the time, and the result was based on CLSP without interruption, a small variation in super-capacity capacitance made a huge impact on the served time at the right time: this is shown in Figures 4.8(a) and 4.8(b).

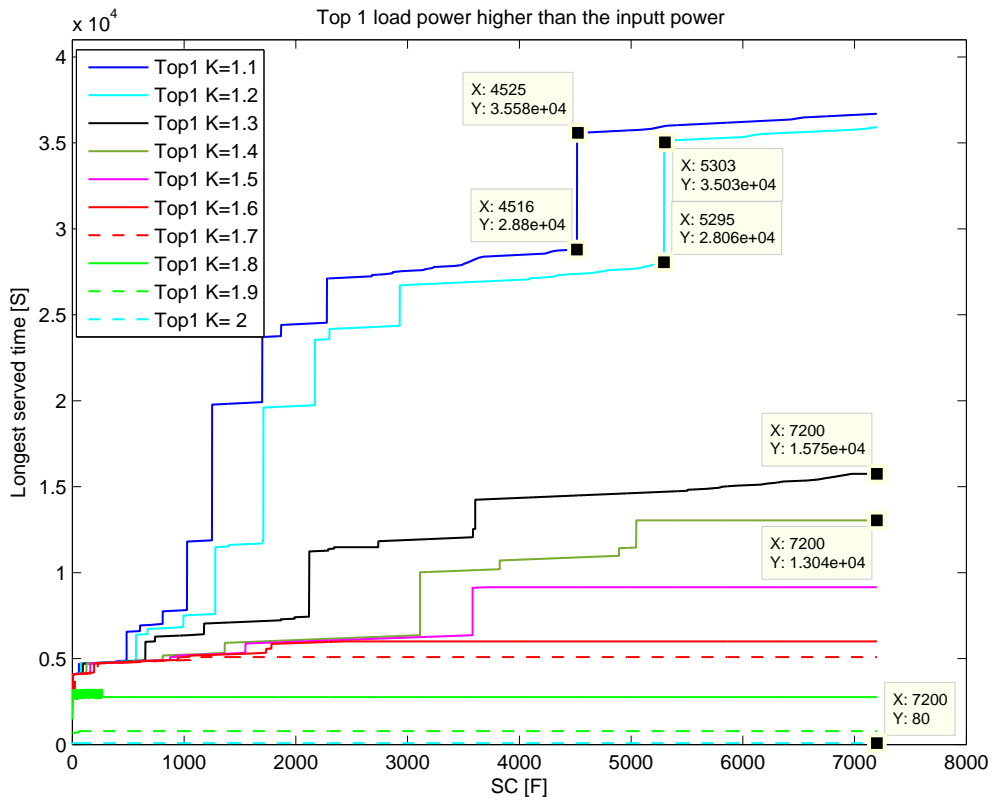
Figures 4.8(a) and 4.8(b) shows the the energy that delivered to the same load which is smaller by 90% of the input mean power ($k = 10\%$), one farad capacitance difference between the to graphs.

Figure 4.8(a) with $SC = 403F$ displays the delivered energy to the load with little interruption, and Figure 4.8(b) with $SC = 404F$, shows the disappearance of that interruption. in other words, a small change in capacitance has a great impact on continuous load supply period owing to the disappearance of the interruption and the merging of two long supply periods.

- When $k \leq 45\%$, the load serving time increased to the peak and stayed at that level, which means the load can be served, without interruption, for the whole period at that capacitance. However, the smaller the load, the smaller capacity storage needed to achieve that.
- When $45\% < k \leq 100\%$, the load served with interruption. However, this interruption can be reduced by increasing the capacitance value.
- The continuous load supply period increases with the increases of the capacitance.

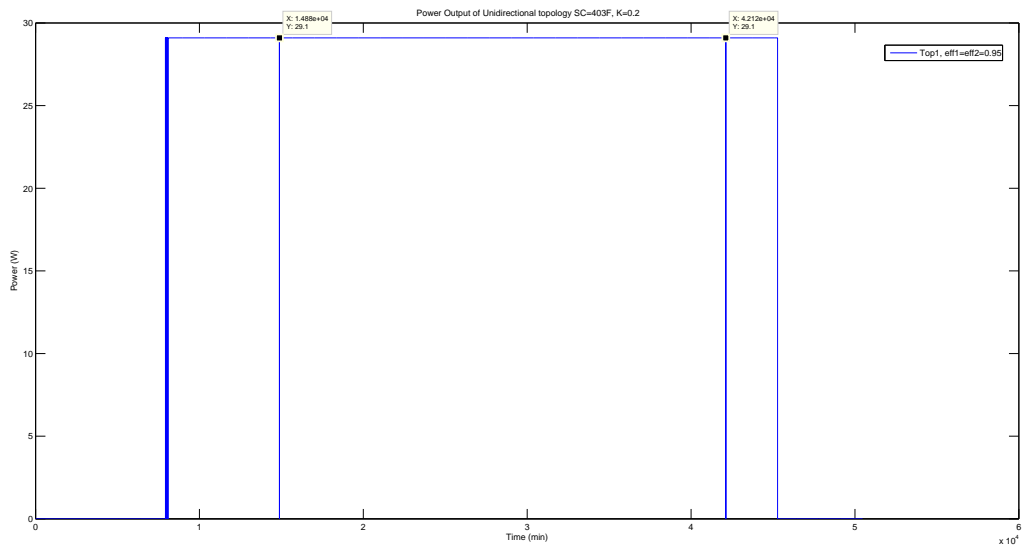


(a) Storage variation under load less than the input mean power

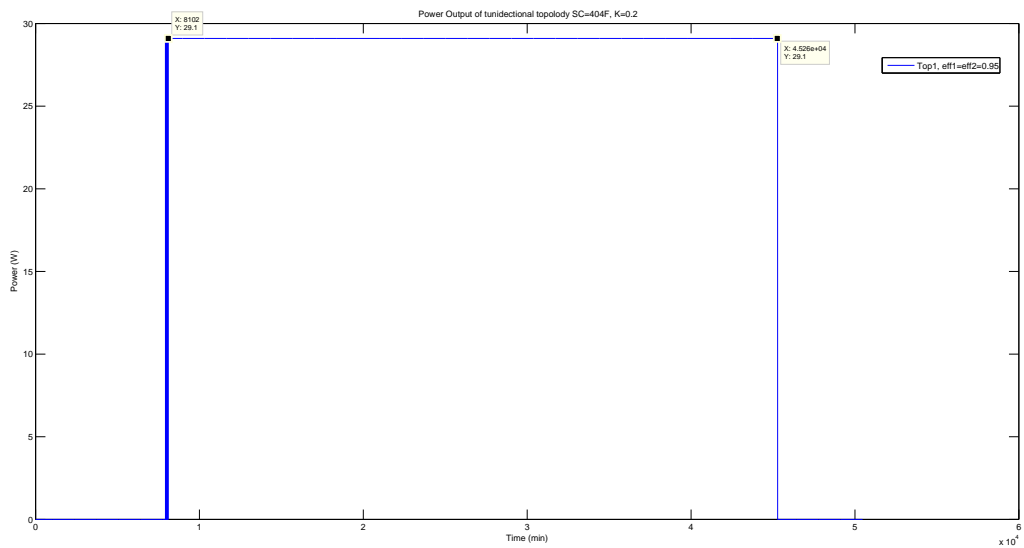


(b) Storage variation under load higher than the input mean power

Fig. 4.7: Unidirectional Results.



(a) Load Served Power SC= 403F & k=0.2



(b) Load Served Power SC=404F & k=0.2

Fig. 4.8: Unidirectional Results.

The graphs in Figure 4.7(b) shows the performance of uni-directional topology for loads that are higher than the input mean power and some observation could be made:

- With $100\% \leq k \leq 120\%$ the CLSP significantly increased with the capacitance.

- With $120\% < k \leq 170\%$ the CLSP decreased considerably, which can be explained by the insufficient available power.
- When k exceeded 170% the changes in the storage capacity had no effect whatsoever on the served time (that is, remained stable), as the super-capacitor capacitance did not fully charge owing to very low availability of energy on the system.

Predictably, the greater the storage capacity and the lower applied load, the higher the CLSP.

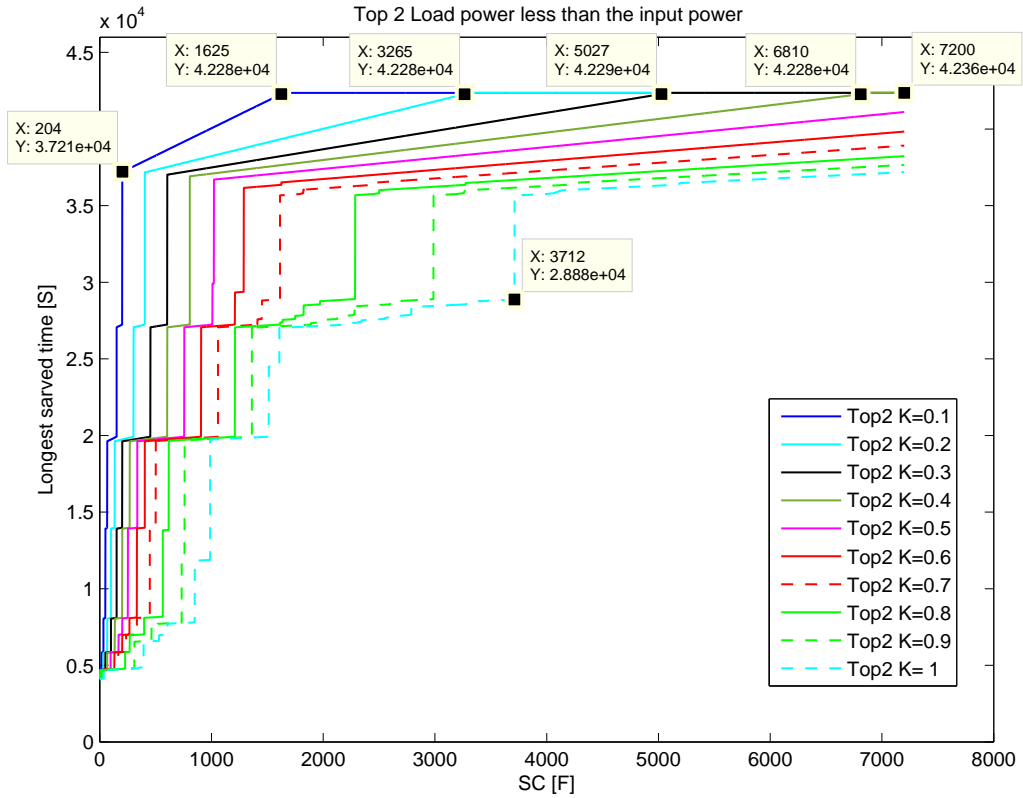
It was clear from the graphs in Figure 4.8 that the storage capacity had an effect on the CLSP, and also any change occurring in the the load would have an effect up to a load level of $k = 170\%$ of the input mean power.

4.3.1.2 Bi-directional Topology

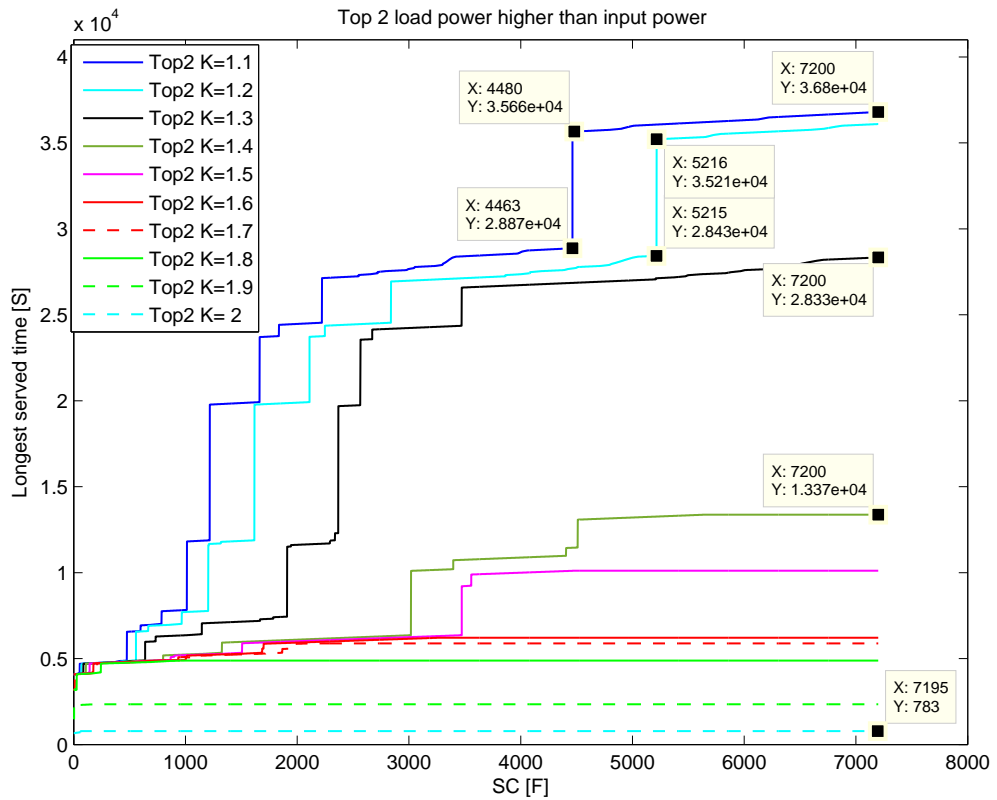
Figures 4.9(a) and 4.9(b) shows the performance of bi-directional topology, with the load increasing from 10% of the input mean power up to 200% with 1% step increment, under a wide range of capacitance of one farad step, while the longest load served time in seconds appeared on the y axis.

From the Figure 4.9(a), the same observations that were made for uni-directional topology can be made for this topology.

Predictably, the greater the storage capacity and the lower applied load, the higher the CLSP the load.

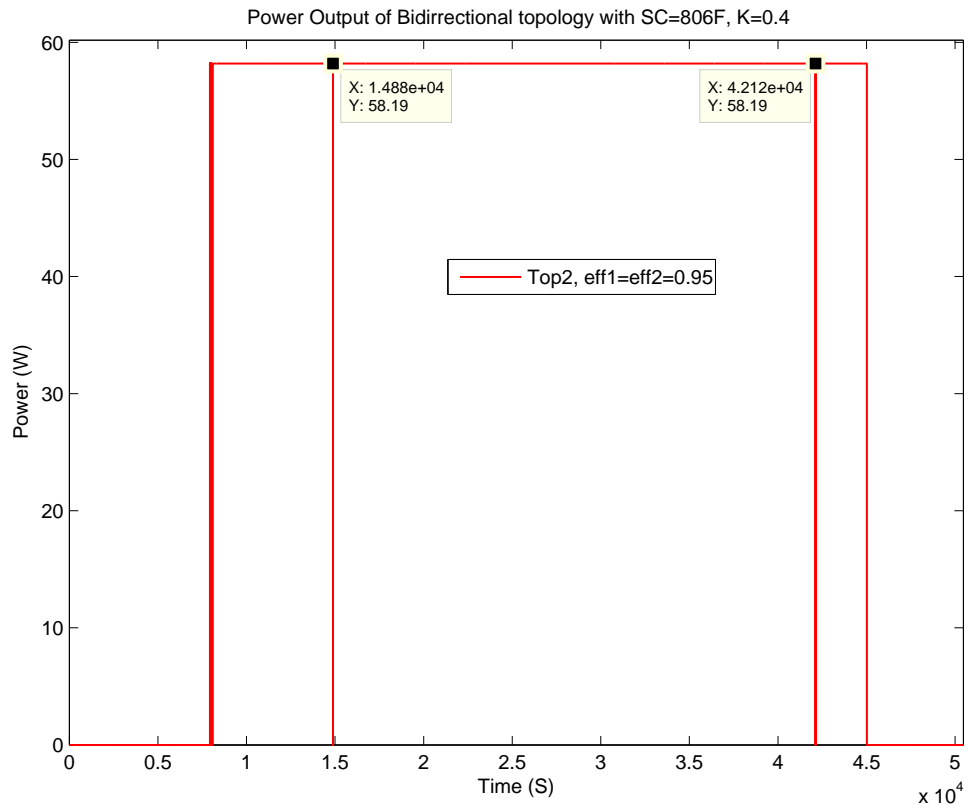


(a) Storage Variation Under Load less than the Input mean Power

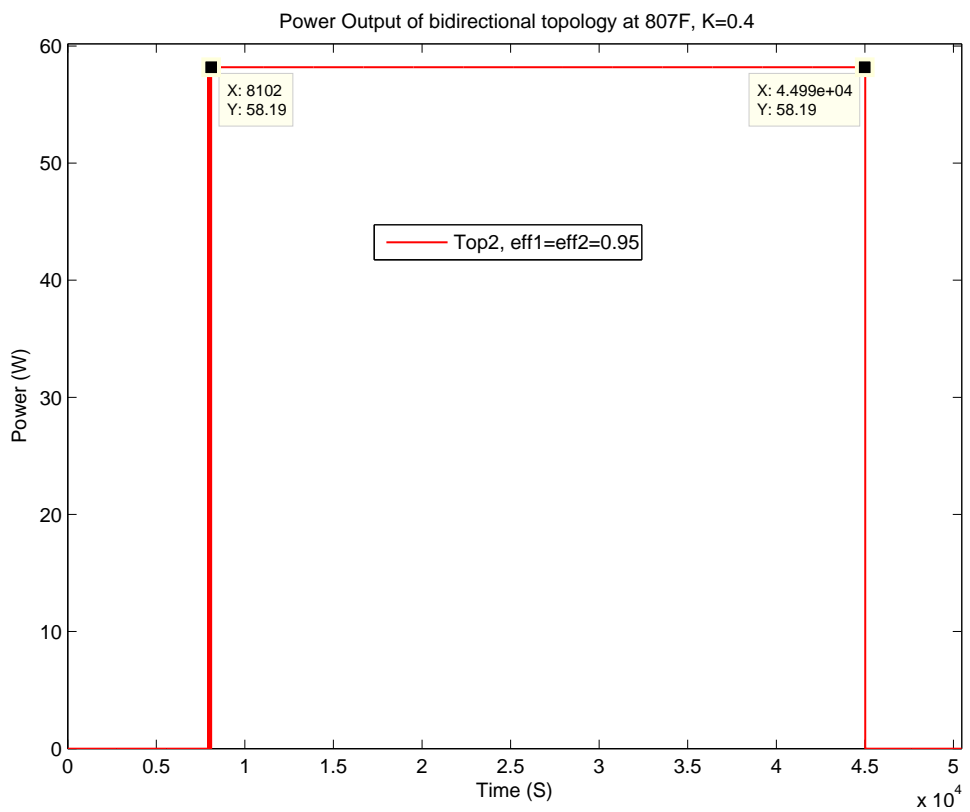


(b) Storage Variation Under Load Higher than the Input mean Power

Fig. 4.9: Bidirectional results.



(a) Load Served Power SC= 806 F



(b) Load Served Power SC=807 F

Fig. 4.10: Bidirectional Results.

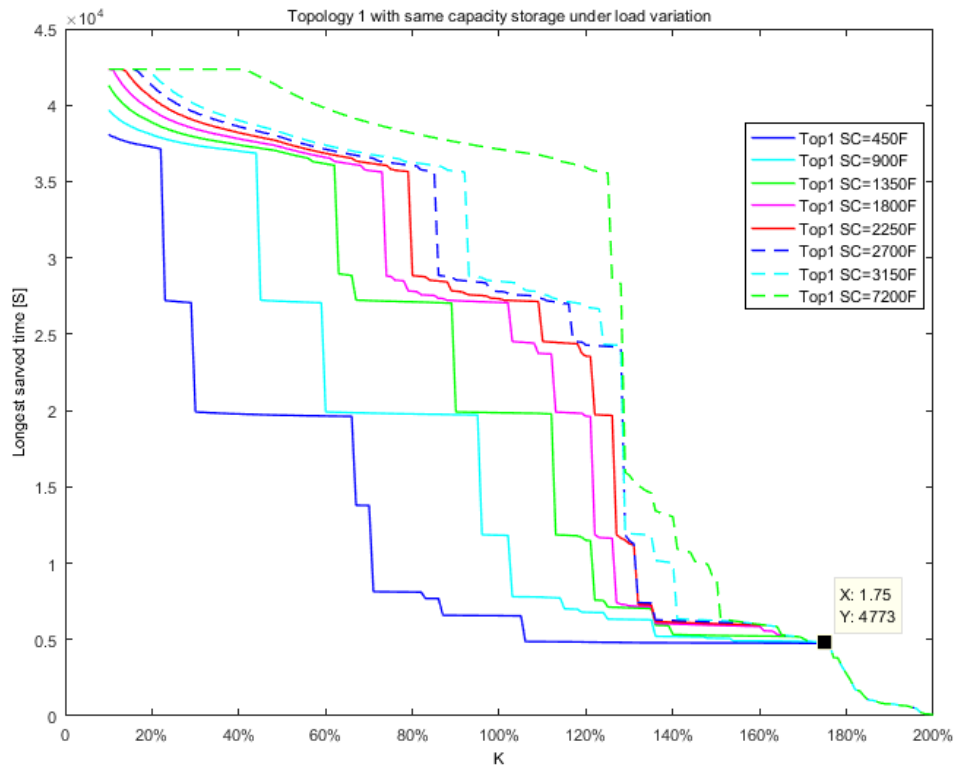
The graphs in Figure 4.9(b) shows the performance of bi-directional topology at load power that is higher than the input mean power. With the load power at less than 130% of the input mean power, there is a significant increase in the CLSP with the storage capacitance. When the load power increases above 130% of the input mean power, the CLSP decreases considerably, which means that the load serving time will be greatly interrupted. Moreover, when the load power exceed 180%, the changes in the storage capacity had no effect whatsoever on the served time (that is ,remained stable); this is due to the fact that the capacitance does not fully charge owing to the low supply of power. It is clear from the graphs in Figure 4.10 that the capacitance of the super-capacitor has an effect of the continuous load supply period CLSP, and also any changes that occurred in the load would affect it.

4.3.2 Load Effect on the System Performance

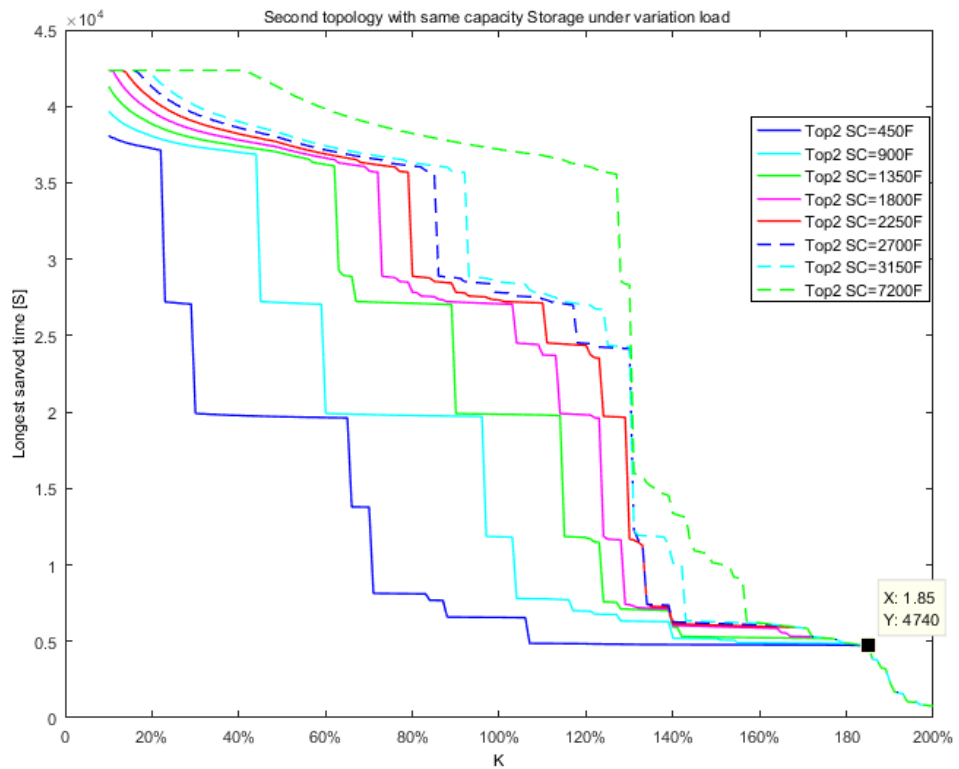
Figures 4.11(a) and 4.11(b) show the performance of uni-directional and bi-directional topologies under load variation respectively .

The loads were increased from 10% of input mean power up to 200% in 1% steps, in proportion to the input mean power as denoted by k in the horizontal axis; the CLSP was plotted on the y axis. Some observations can be made:

- The highest CLSP to the load could be achieved with a small load.
- The biggest capacitance served higher load for longer.
- At high load, $k = 175\%$ for uni-directional topology and $k = 185\%$ for bi-directional topology. The capacitance values did not affect the load serving time; this was due to the insufficient available energy from the source which would have served the load and charged the super-capacitor.



(a) Unidirectional Topology Under Load Variation



(b) Bidirectional Topology Under Load Variation

Fig. 4.11: Load Effect for Both Topologies

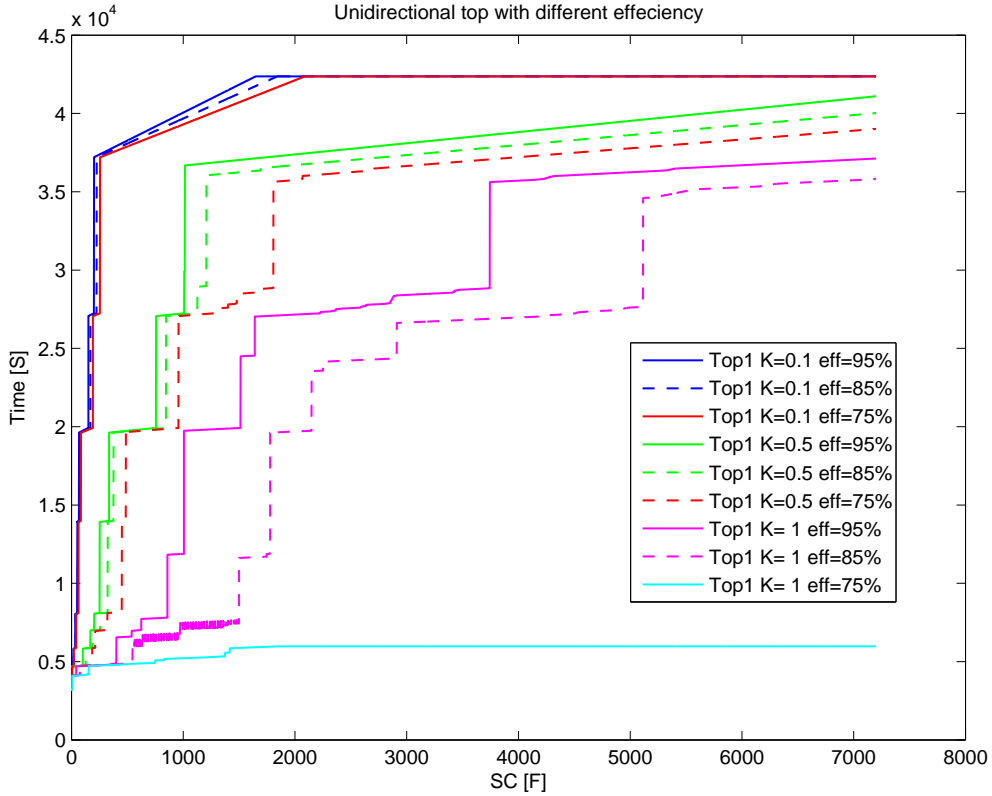
4.3.3 The effect of Converter Efficiency

The plots in the Figures 4.12(a), 4.12(b), 4.13(a) and 4.13(b) show the performance of both topologies under different converter efficiencies. The loads were increased from 10% of the input mean power up to 200% again in 1% steps, under a wide range of storage capacity, of one farad step for each efficiency value, while the longest served time in seconds was plotted on the y axis.

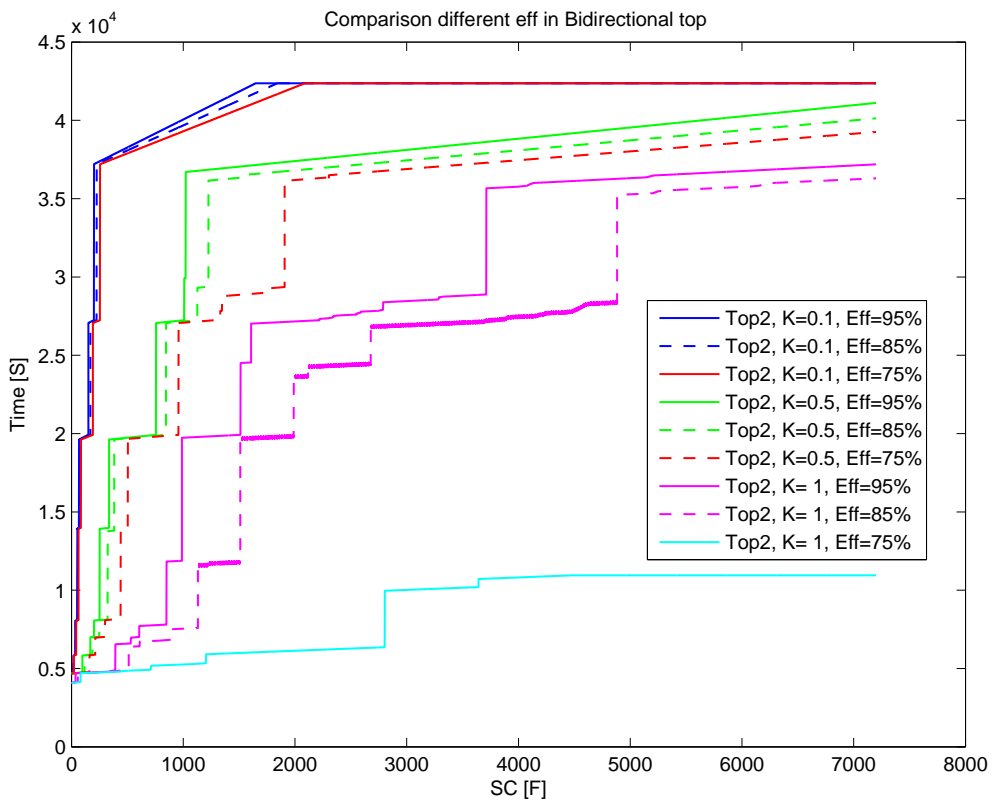
Some observation could be made:

- Figures 4.12(a) and 4.12(b) show unidirectional and bidirectional topology respectively. For $k = 10\%$ there were small differences in the system performance, in relation to the converter efficiency value up to the peak point, after which all converters performed the same way. This can be explained as follows: there was enough available energy and this energy was stored in high capacitance which made the converter losses unnoticeable at this low load.
- As the k increased, the significance of the converter efficiency started to appear.
- At high load ($k \geq 1$) the converter efficiency was low and its performance in the system decreased, as displayed in Figures 4.13(a) and 4.13(b).

Predictably, both topologies perform better with higher efficiency converters. However, at low load power, the converter efficiency had a small impact which could be overcome by high capacitance but, as the load exceeded the mean input power, the converter efficiency became significant to the performance of both systems: this can be explained by the fact that the low converter efficiency produced high losses, which meant that there was less energy available to reach the load.

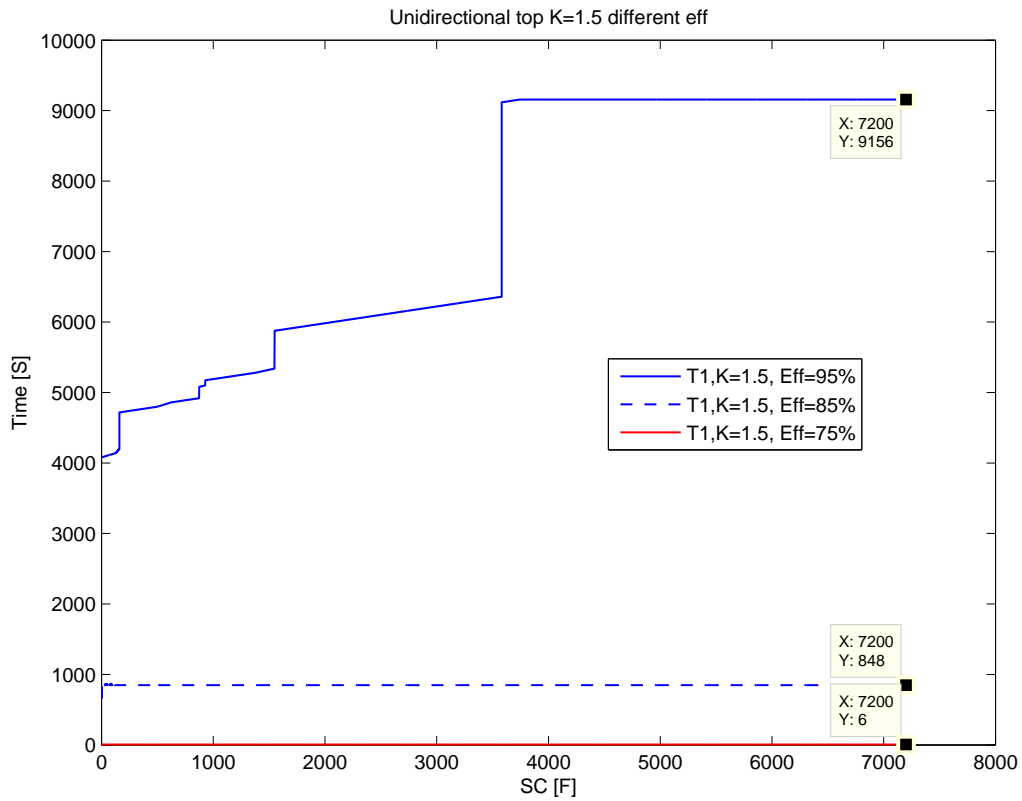


(a) Low Load Unidirectional Topology with Converters under Different Efficiency

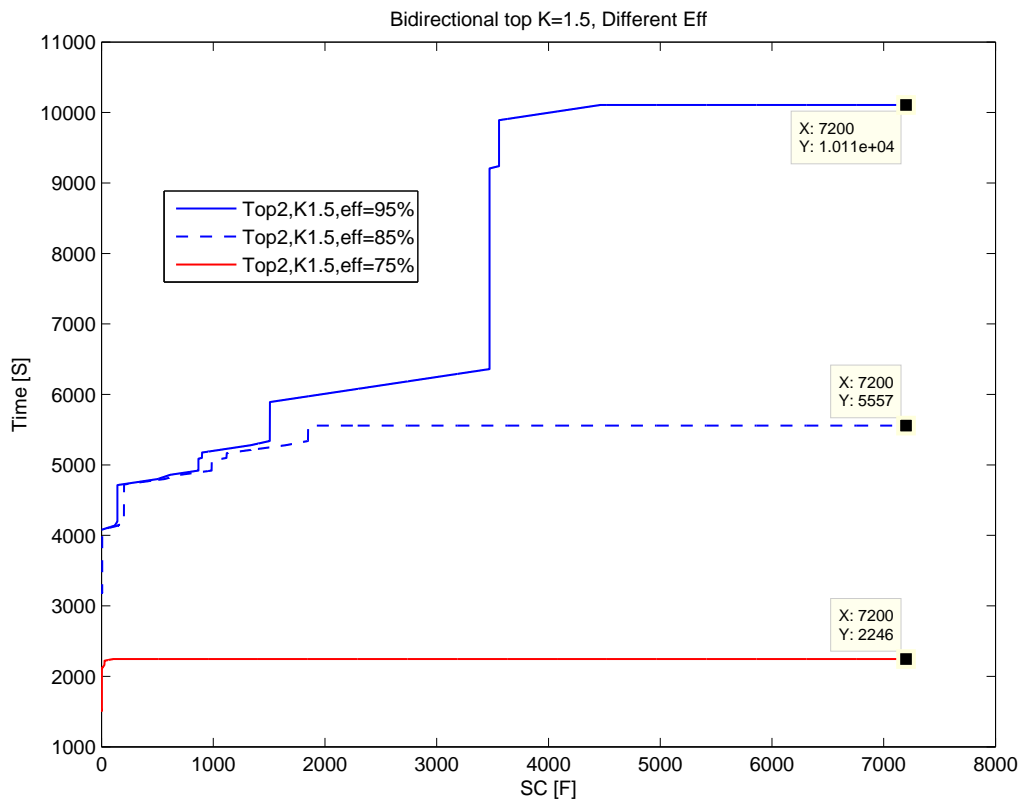


(b) Low Load Bidirectional Topology with Converters under Different Efficiency

Fig. 4.12: Efficiency Effect on Both Topologies.



(a) High Load Unidirectional Topology with Converters under Different Efficiency



(b) High Load Bidirectional Topology with Converters under Different Efficiency

Fig. 4.13: Efficiency Effect on Both Topologies.

4.3.4 Comparisons Between Both Topologies

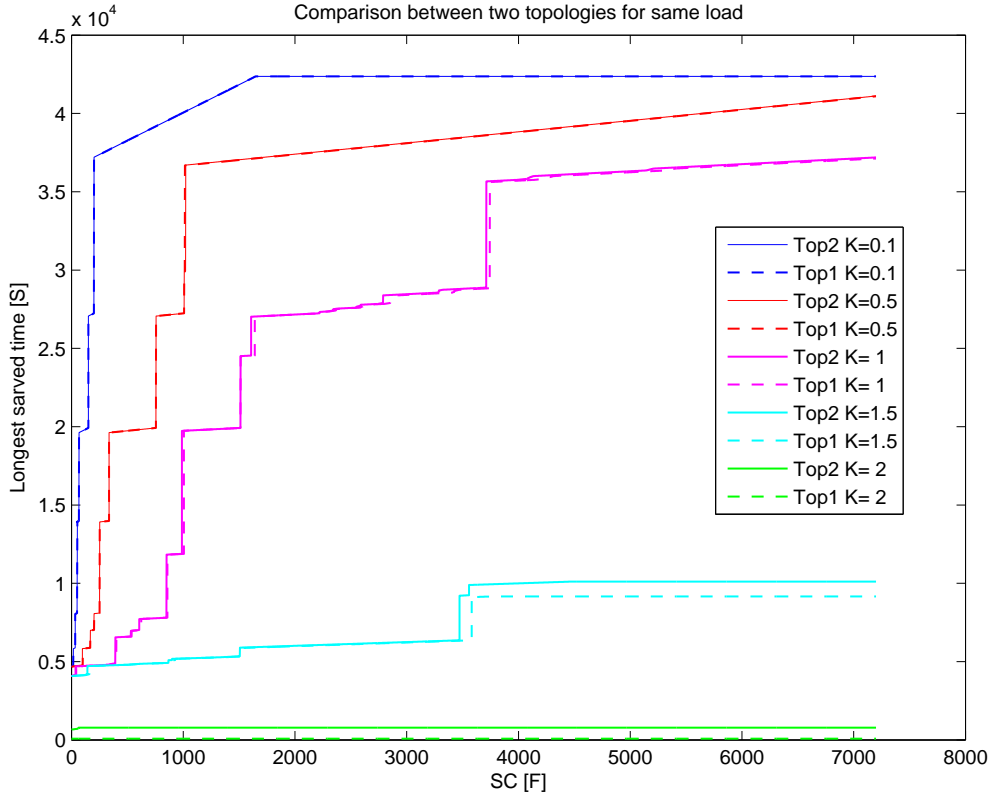
This section provides a comparison between both topologies to show which topology provides the longest served time to the load without any interruption and which criteria has the highest influence on the system design. The criteria used are: Capacitance of super-capacitor, load power, converters efficiency.

4.3.4.1 Capacity Storage

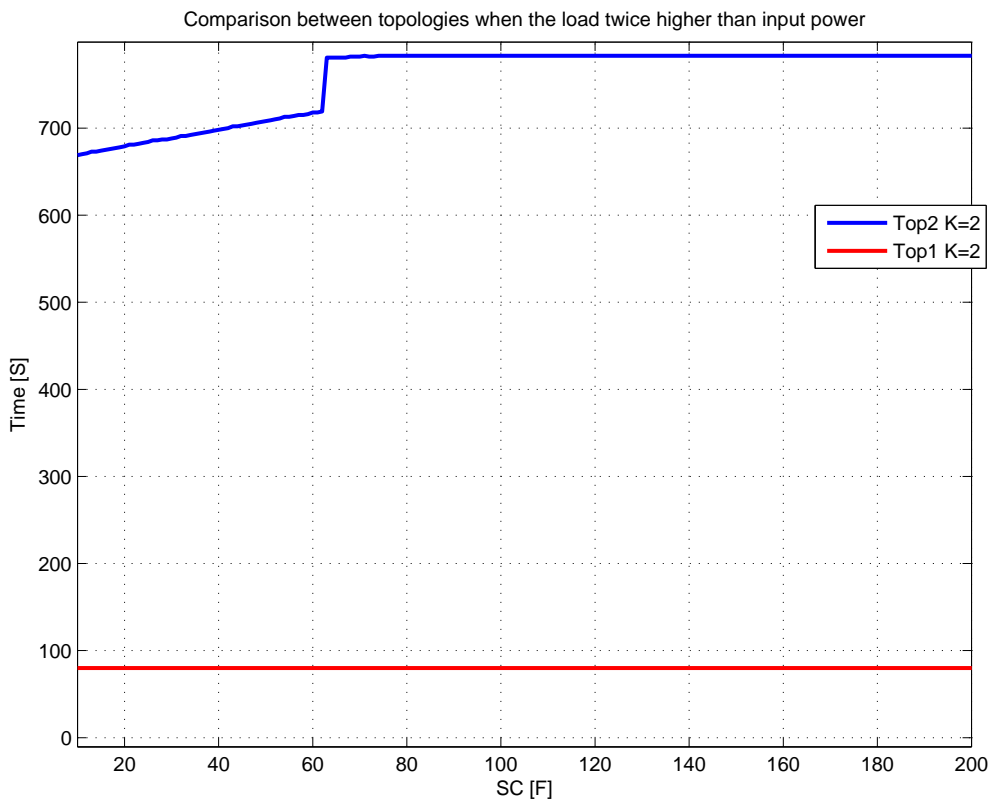
Figure 4.14(a) shows a comparison between the performance of unidirectional and bidirectional topologies under a wide range of capacitance in the x axis in *Farad* [F] and, in the y axis, a longest served time to the load in *seconds*.

- For $k \leq 100\%$ the super-capacitor capacitance achieved the same longest time under the same load comparing both topologies. However, it was smaller for the bidirectional topology than the unidirectional topology by 0.43% and 0.83% for $k = 10\%$ and $k = 100\%$ respectively.
- When k is between 100% and 140%, for capacitance $C \leq 3000F$, the bidirectional topology served the load for less capacitance than the unidirectional by 2.71% to 10.15% for $k = 110\%$ and $k = 140\%$ respectively. However, for high capacitance, the bidirectional capacitance remained less than the unidirectional topology, with a percentage variation from 1.18% for $k = 110\%$ to 3% for $k = 140\%$.
- For k between 140% and 170% and for capacitance $C \leq 3000F$, the bidirectional topology served the load longer by 0.44%, 0.47% and 0.47% for load $k = 150\%$, $k = 160\%$ and $k = 170\%$ respectively. However, at capacitance $C \geq 3000F$ the bidirectional topology served the load longer by 7.87% for $k = 150\%$ and 13.5% for $k = 170\%$, as Figure 4.14(b) indicates.
- At $200\% \leq K \leq 180\%$ the bidirectional topology served the load longer by 43.59%, 66.42% and 89.78% for $k = 180\%$, $k = 190\%$ and 200% respectively. However, at this load level, the capacitance of the super-capacitor did not have any significant effect on the served time to the load.

Predictably, the capacitance values affected both topologies when $k \leq 100\%$. However, the bidirectional topology served the load longer than the unidirectional especially.



(a) Comparison Between Both Topologies with same Load Under Variable Capacitance



(b) Comparison Between Both Topologies when Load Power Double the Input Power

Fig. 4.14: Comparison Between Both Topologies for Capacity Affect.

4.3.4.2 Load Power

Figure 4.15 indicates the performance of both topologies under an increasing load, from 90% of the input mean power up to 200% at 1% steps, under the same converters efficiency, for a four capacitances value of the super-capacitor. The largest load can be served longer by the higher capacitance.

- When $K = 42\%$, it can be served without interruption with capacitance $7200F$ for both topologies with 0.05% better performance of bidirectional topology. However, for the same capacitance the served time reduced significantly by 55% for load after $k = 127\%$ and $k = 125\%$ for bidirectional and unidirectional respectively.
- At $K = 42\%$, the capacitance $7200F$ served the load longer by 8.85%, 12.18%, 113, 96% than the capacitances $3100F$, $1800F$, and $450F$ respectively. However, for the same load the capacitances of $1800F$ served the load longer than $450F$ by 90.73%.
- Bidirectional topology performed better than unidirectional at $k = 100\%$ by 0.28%, 1%, 0.04% and 35% for $7200F$, $3100F$, $1800F$, and $450F$ respectively.

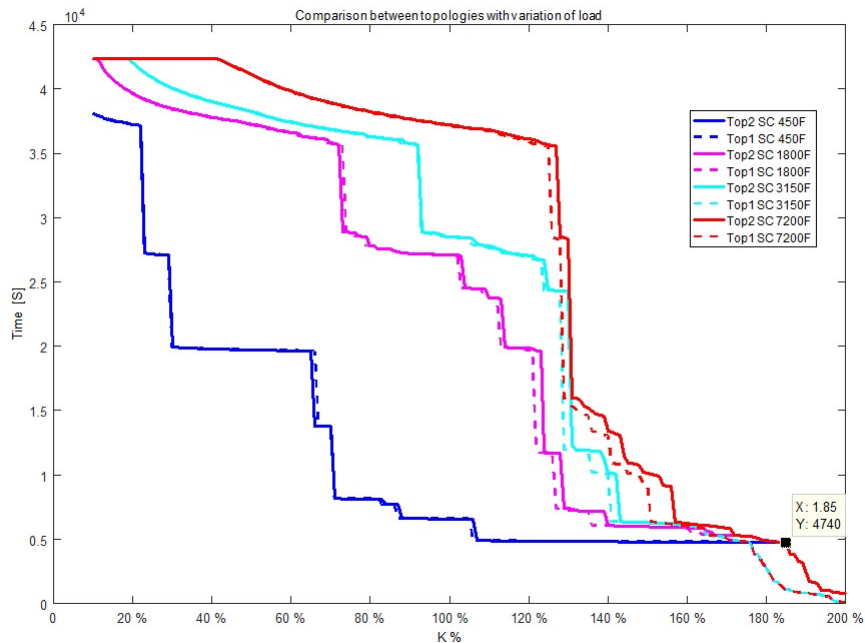


Fig. 4.15: Comparison Between Both Topologies with same Capacity Storage Under Different Loads

4.3.4.3 Converter Efficiency

Figures 4.16(a) and 4.16(b) illustrate the performance of both topologies under different loads, with different converter efficiencies, for four capacitances of the super-capacitor.

Figure 4.16(a) shows the performance of both topologies, with different converter efficiencies, for 900F of capacitance. The following observations were made:

- At 10% of the load, both converters can deliver the energy to the load without any interruption. However, converters with 95% efficiency perform better by 0.84% and 1.70% than converters with efficiency of 85% and 75% respectively.
- The 95% efficient converters deliver more energy to the load by 14.28% and 33.33% than 85% and 75% efficient converters respectively.
- For converters with 75% of efficiency the following observations were made:
 - For a load below 65%, both topologies have identical behaviour.
 - For a load of between 65% and 68%, bidirectional topology served the load longer by 0.35% than unidirectional topology.
 - For a load above 68%, both topologies performance reduced significantly, by 66.38%, when the load increased by 1%.
- For converters with 85% efficiency the following observations were made:
 - For a load below 81%, both topologies have identical behaviour.
 - For a load of between 81% and 82%, bidirectional topology served the load longer by 0.05% than unidirectional topology.
 - For a load above 82%, the performance of both topologies reduced significantly by, 66%, when the load increased by 1%.
- For converters with 95% efficiency, the following observations were made:
 - For a load below 91%, both topologies have identical behaviour.
 - For a load of between 91% and 96%, bidirectional topology served the load longer by 0.05% than unidirectional topology.

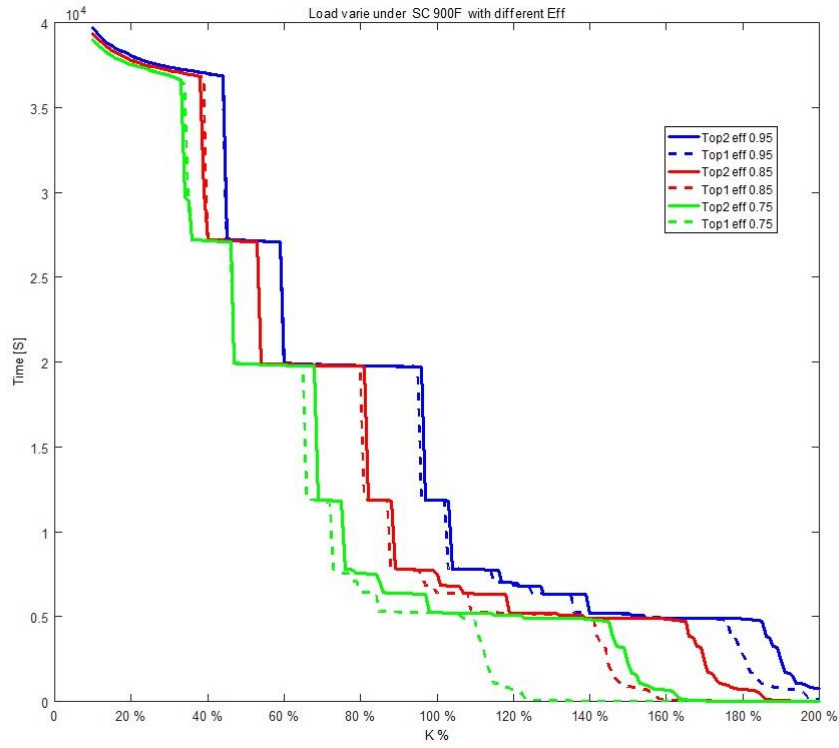
- For a load above 96%, both topologies performance reduced significantly, by 64.66%, when the load increased by 1%.

Figure 4.16(b) shows the performance of both topologies with different converter efficiencies, for 7200F capacitance. The following observations were made:

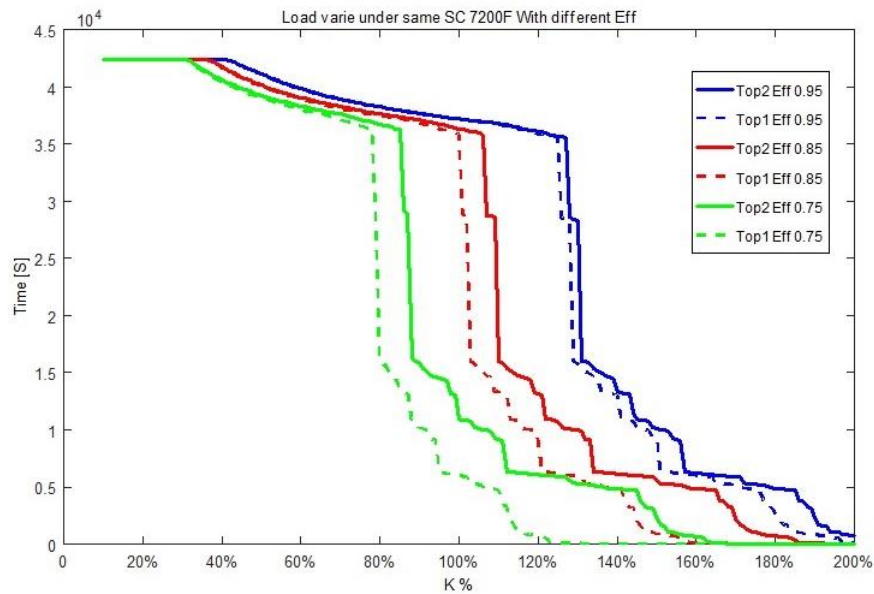
- At low load, when $k \leq 41\%$, both converters can deliver the energy to the load without any interruption. However, this maximum load varies in relation to the converters efficiency 75%, 85% and 95%, as follows $k = 31\%$, $k = 36\%$ and $k = 41\%$ respectively.
- The 95% efficient converters deliver more energy to the load by 10.80% than converter with 85% efficiency and by 32.25% for 75% efficiency converters.
- For converters with 75% efficiency the following observations were made:
 - For a load below 31%, both topologies have identical behaviour.
 - For a load of between 31% and 78%, bidirectional topology served the load longer by 1.76% than unidirectional topology.
 - For a load of between 78% and 85%, bidirectional topology served the load longer by 8.97% than unidirectional topology.
 - For a load above 85%, the performance of both topologies reduced significantly, by 55%, when the load increased by 3.52%.
- For converters with 85% efficiency the following observations were made:
 - For a load below 36%, both topologies have identical behaviour.
 - For a load of between 36% and 100%, bidirectional topology served the load longer by 1.31% than unidirectional topology.
 - For a load of between 100% and 106%, bidirectional topology served the load longer by 6% than unidirectional topology.
 - For a load above 106%, the performance of both topologies reduced significantly, by 55%, when the load increased by 3.77%.
- For converters with 95% efficiency the following observations were made:

- For a load below 41%, both topologies had identical behaviour.
- For a load of between 41% and 125%, bidirectional topology served the load longer by 0.33% than unidirectional topology.
- For a load of between 125% and 127%, bidirectional topology served the load longer by 1.6% than unidirectional topology.
- For a load above 127%, the performance of both topologies reduced significant, by 55%, when the load increased by 3.14%.

However, when the load ratio exceed 100%, the converter efficiencies limited the continuous longest served time without interruption regardless of the capacitance used for storage.



(a) Comparison Under Different Load Different Efficiency with Small Capacitance



(b) Comparison Under Different Load Different Converters Efficiency with Big Capacitance

Fig. 4.16: Comparison Between Both Topologies for Converter Efficiency Affect Under Different Capacitance

4.4 Summary

In this chapter (ch4) a multi-string stand-alone *PV* system layout with storage system has been described, followed by the flow chart of the algorithms used in this critical analysis of the system. The result and discussions of unidirectional and bidirectional converters for low power stand-alone PV systems were also summarized. Some important factors regarding both topologies were discussed in detail, such as the capacitance of super-capacitors, converter efficiencies and load variations. It can be concluded that all the parameters (storage capacitance, load and converter efficiency) were significant to both topologies. However, the bidirectional topology performed better than the unidirectional topology, especially when the load was higher than the produced power. In addition, the longest CLSP can be achieved with less storage capacity than with the unidirectional topology.

Chapter 5

Simulation and Implementation of the Proposed PV System

5.1 Introduction

The super-capacitor represents one of the latest innovations in the field of electrical storage and is an attractive technology. The advantages of it are durability, high reliability, lack of maintenance, a long life-time and operation over a wide temperature range, and in diverse environments (hot, cold and moist). The life-time reaches one million cycles (or ten years of operation) without any degradation and it is environmentally friendly and easily recycled or neutralised. The efficiency is typically around 90% and discharge times are in the range of seconds to hours. Moreover, it can reach a specific power density which is about ten times higher than that of conventional batteries, but the specific energy density is about ten times lower.

This chapter presents the simulation results obtained from a PV system without a storage unit and the results obtained from the proposed PV system model that has a super-capacitor and a *DC – DC* converter with an efficient snubber circuit. The results are analysed and discussed to show the performance validity of the proposed model. MATLAB-R2014b/Simulink was used to set the simulation environment.

Moreover, for further enhancement on the system at the component level and to reduce the thermal energy, an energy recovery snubber circuit has been implemented in the circuit to deal with the produced energy by the switching. The recovered energy is recycled back to the load which improved

the performance, the efficiency and the reliability of the system.

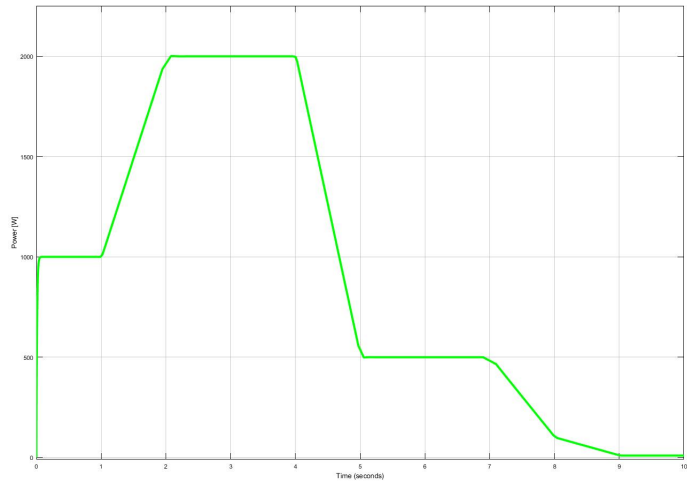
The latest version of SIMetrix/SIMPLIS software was used to show the waves form of the switching transition for an electronic switch under different load, and also verify the importance of the snubber circuit

5.2 Stand-alone PV System without Storage

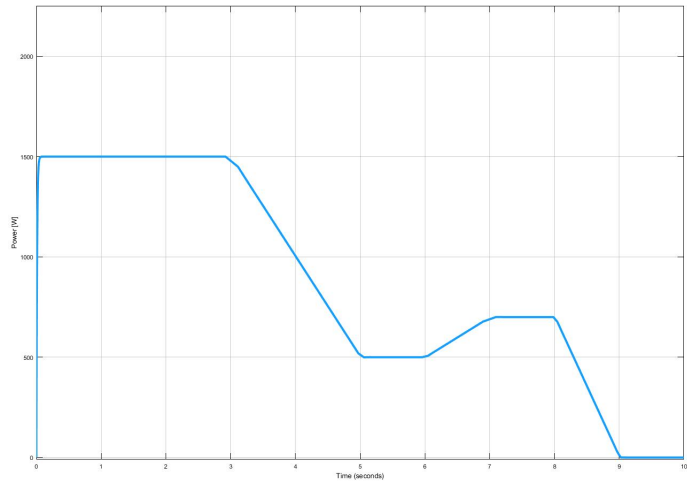
Figure 5.1 presents an overview of the simulated module for a stand-alone PV system without any storage unit. Figure 5.1(a) illustrates the produced electrical energy by the PV system. The power required for the load is as shown in the Figure 5.1(b) and, finally, the energy delivered to the load is presented in Figure 5.1(c).

The applied control strategy as follows:

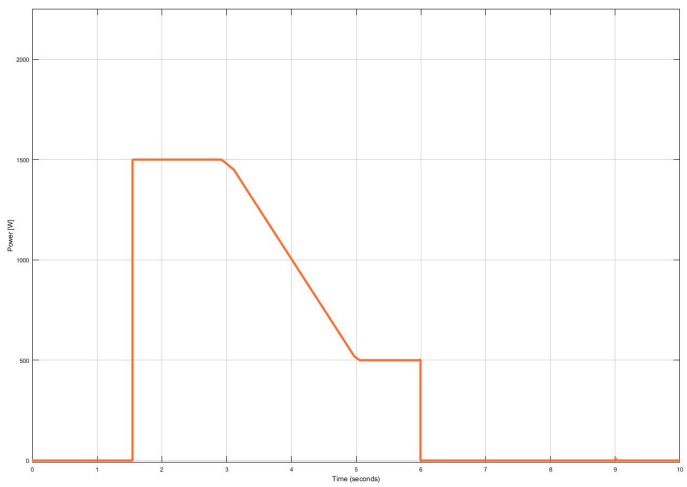
$$\left\{ \begin{array}{ll} P_{PV} \geq P_{load} & \text{The system delivers the power to the load} \\ P_{PV} < P_{load} & \text{The System will shut-down to prevent the load from under-performing} \end{array} \right.$$



(a) PV Power



(b) Load requested Power



(c) Delivered Power

Fig. 5.1: Power Overview in Stand-alone PV System Without Storage unit

In order to show a comparison between the available energy and the wasted energy in a stand-alone PV system without a storage unit, the three sub-graphs from Figure 5.1 are combined in one plot and presented in Figure 5.2.

Figure 5.2, the colour surface high-lighted in green indicates the energy that is delivered to the load by the system. However, the surfaces high-lighted in red represent the available energy that is not used owing to the miss-match of energy between the energy supplied by the PV arrays and the demand load energy. As a result, a significant amount of energy is wasted.

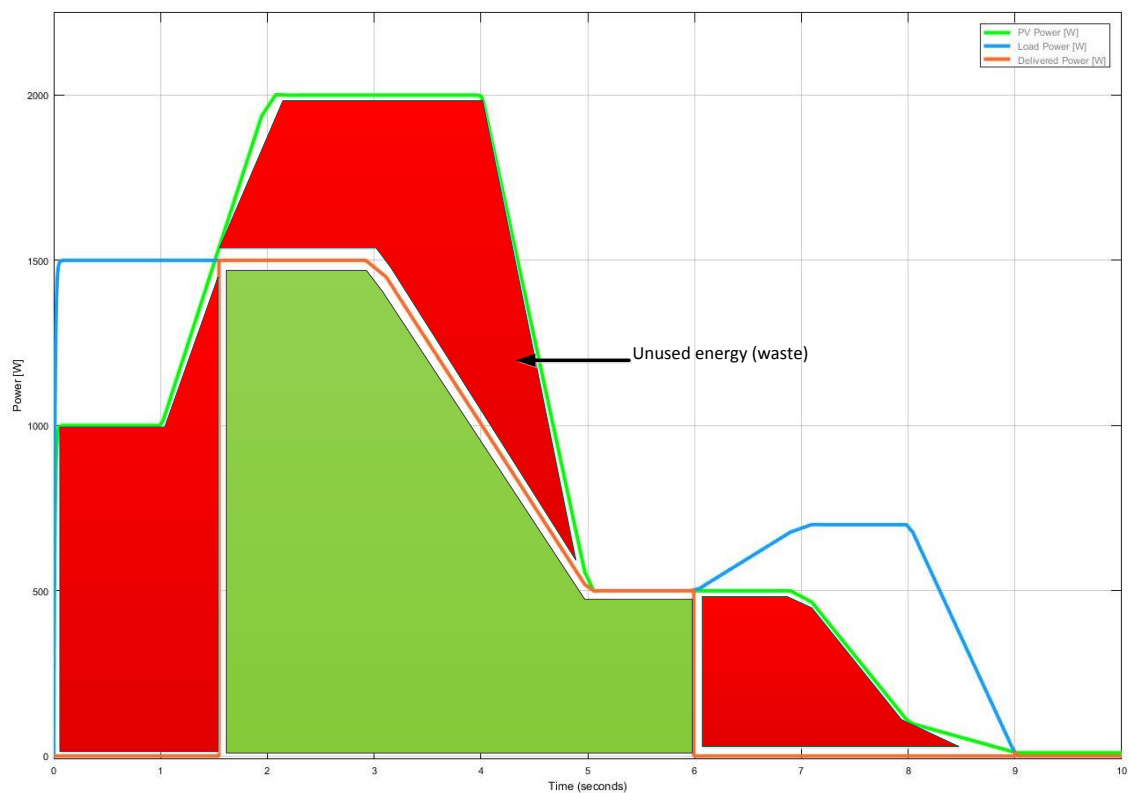


Fig. 5.2: Comparison between produced energy & delivered in PV system without storage

Thus, a stand-alone PV system without a storage unit is inefficient. Any surplus energy will be wasted, in the case of the requested energy, as the load is lower than the energy produced. On the other hand, the delivered power is discontinuous if there is a miss-match between the energy requested by the load and the produced energy (when the produced power is lower than that requested by the load). Solving the miss-match energy problem, by adding a battery in a fast changing environment, is not ideal because the change in the environment will reduce its life time dramatically. This is especially

true in stand-alone systems where oversized battery storage is required to deliver the energy to the system, in the absence of the sun, for up to 7 days.

A more encouraging solution is to introduce a super-capacitor into the system, to deal with this issue, and so improve the system performance of the system and the battery service life.

Figure 5.3, the same power that was used to produce the output in Figure 5.1 has been re-implemented in the simulation. However, a super-capacitor has been added to the stand-alone PV system. As a result the load was supplied with full requested energy without any interruption.

Figure 5.3 illustrates the energy flow in the system, and the super-capacitor power flow behaviour discharge happened when the produced energy by PV is lower than the requested by the load which shows in the graph twice, between $[0s - 1.5s]$ & from $[5 - 10S]$. Super-capacitor charges when the produced energy by PV is higher than the requested by the load as shown in the graph between $[1.5s - 5s]$ all the surplus energy stored in the super-capacitor.

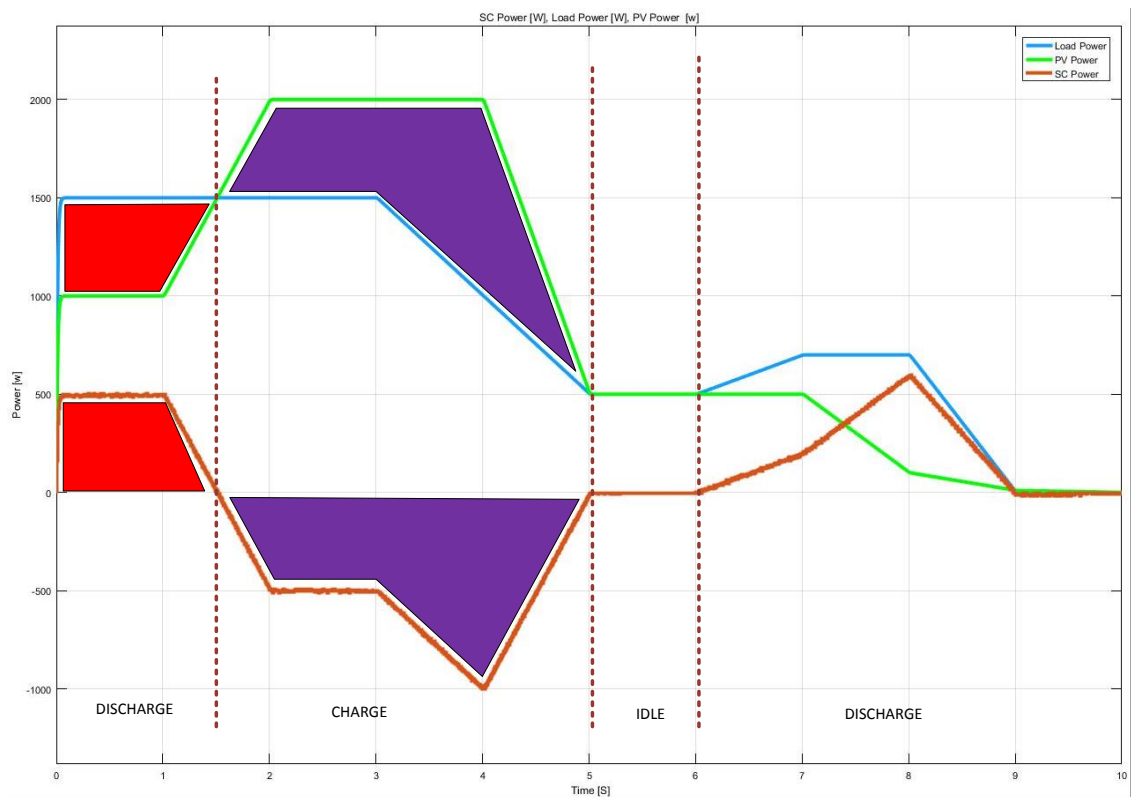


Fig. 5.3: Energy flow in Stand-alone System with SC

The next section presents the result obtained from introducing a super-capacitor into a stand-alone PV system to deal with this fast changing environment, either in the changing of the PV side or the load side.

5.3 Proposed System with Power Management

Figure 5.4 shows the overall proposed system, with a super-capacitor as the storage unit, and the control strategy of the power flow management of the buck-boost converter in MATLAB Simulink.

The requested energy by the load and the produced energy by the PV arrays, are presented as random input data to the system to validate the energy management algorithm strategy.

In Figure 5.4, a bi-directional buck-boost converter is used and Figure 5.5 illustrates the detailed components of the converter. The bi-directional converter is used to charge and discharge the super-capacitor, in relation to the availability of energy . However, this converter contains an inductance and two electronics switches, which are controlled in complementary way (they can be either off or if the first is on the second is off). Figure 5.6 shows the details for the energy data manipulation of the load and the PV arrays which are also used in the proposed system in Figure 5.4.

The control of the energy flow in the system is based on the availability in the system in relation to the load. The PV arrays are an energy source and the super-capacitor as a storage unit, the energy flow from and into it were explained in Chapter 4.

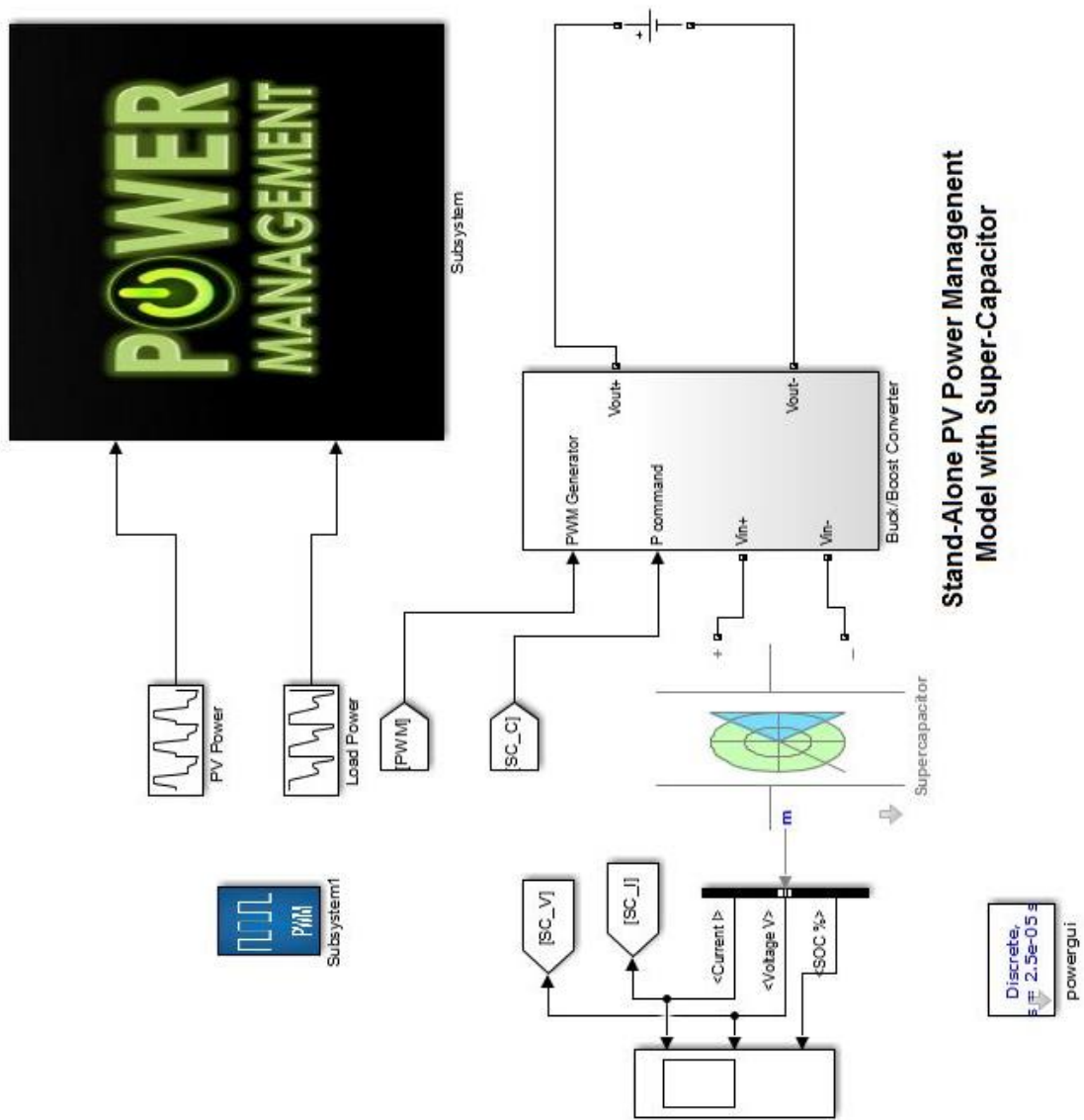


Fig. 5.4: Overall System

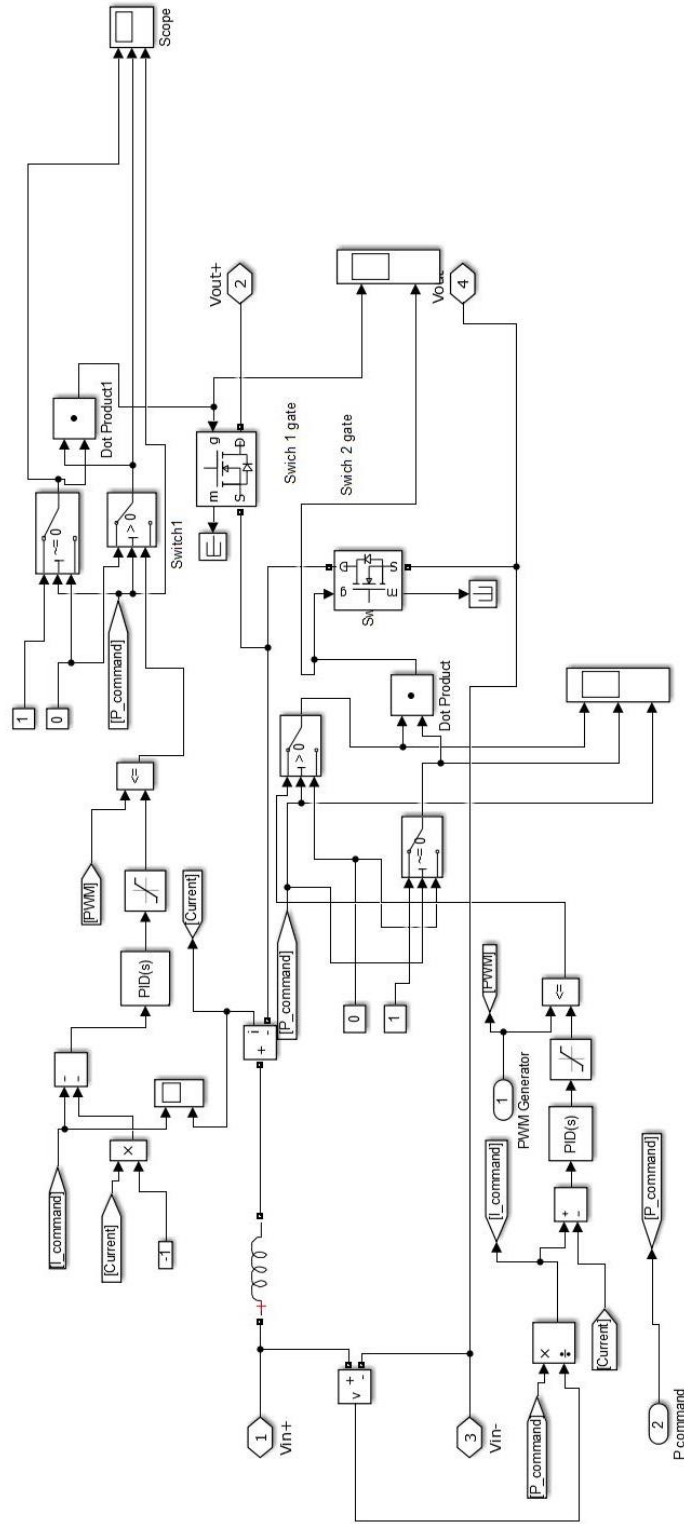


Fig. 5.5: Bidirectional converter

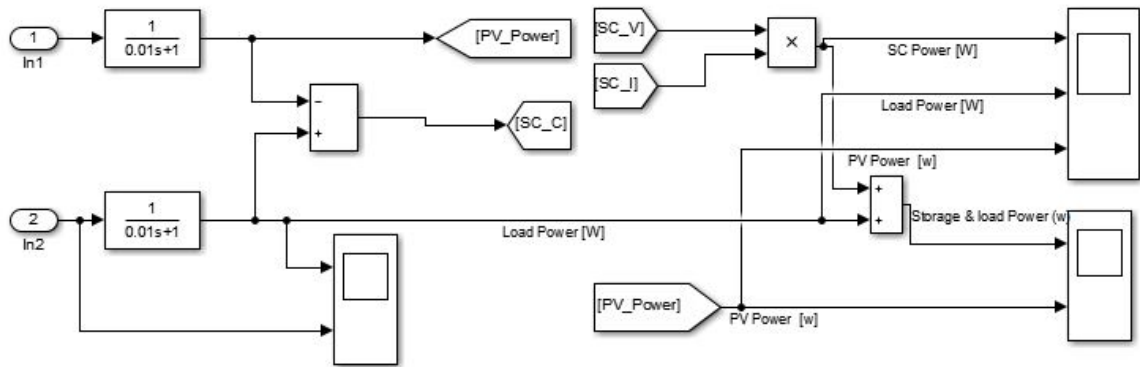


Fig. 5.6: Power management

5.3.1 Discussion

With the aim of presenting the advantages of using a super-capacitor for power management, three cases were considered. In the first case, PV energy lower than the load at the start of simulation. The second case is when PV energy is same as the load at the start of simulation, and the final case represents the response of the super-capacitor to rapid changing to the load with high step up demand on the energy. The simulation settings were as follows: the switching frequency of the switches was 10 KHz , the bus-bar DC voltage is 42 V and the inductance was 1mH . Six super-capacitor were connected on series, each one with 3000 F of capacitance, an $8.4\text{ m}\Omega$ internal resistance and 2.7V maximum voltage for each super-capacitor (this parameters is also applied in section 5.3). Please refer back to Appendix B for more information about super-capacitor MATLAB model and the official data sheet of the super-capacitor on which this simulation is based.

1. **Case 1: PV energy lower than the load at the start.** The super-capacitor goes into discharge mode as the Figure 5.7 illustrates. The difference between variation of the produced PV energy and the variation of the load delivered by the super-capacitor. The first sub-graph shows the energy flow in the system with the super-capacitor behaviour (charge, discharge and disconnected), in relation to the available energy in the system, which can be explained as follows:
 - (a) When the generated PV energy is lower than the load energy, the super-capacitor delivers the difference (discharge mode).
 - (b) When the generated PV energy is higher than the load energy, the surplus energy stored in the super-capacitor (charge mode).

- (c) When the generated PV energy is same as the load energy, the super-capacitor goes to idle mode (disconnected).

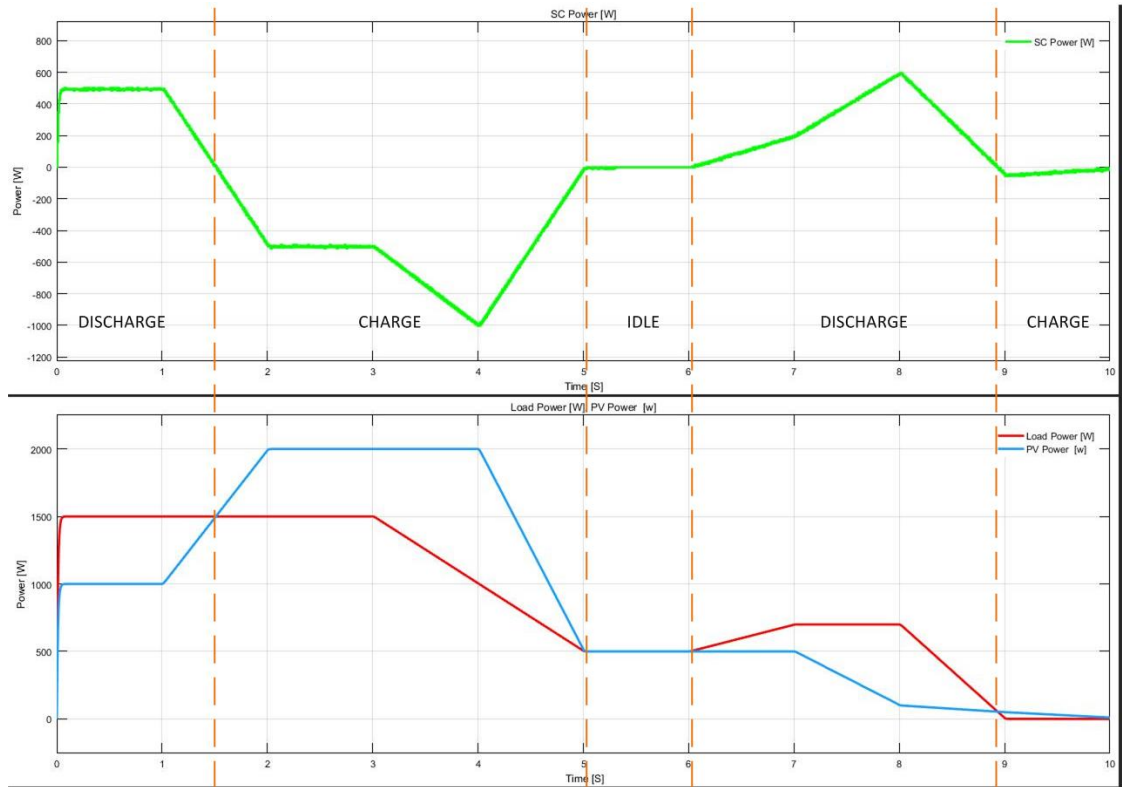


Fig. 5.7: Power Management Flow

The second sub-graph from Figure 5.7 represents the energy variation that can occur in the load and the PV arrays, while Figure 5.8 shows the super-capacitor electrical parameters and their variation in relation to the applied mode. These parameters are: the current which is shown in the first sub-graph in red line; the voltage which is presented in the second sub-graph in blue and the state of charge is shown in the third sub-graph in green.

The following observations can be made from Figures 5.7 & 5.8:

- (a) Discharging mode operation: when the produced PV power is not enough to support the load, the super-capacitor delivers the required energy to the load and this energy is shown as a positive energy. There were two states of discharge which were between time intervals (0s & 1.5s), and between (6s & 9s), as can be seen from Figure 5.7. For the same time intervals in Figure 5.8, the super-capacitor voltage and state of charge electrical

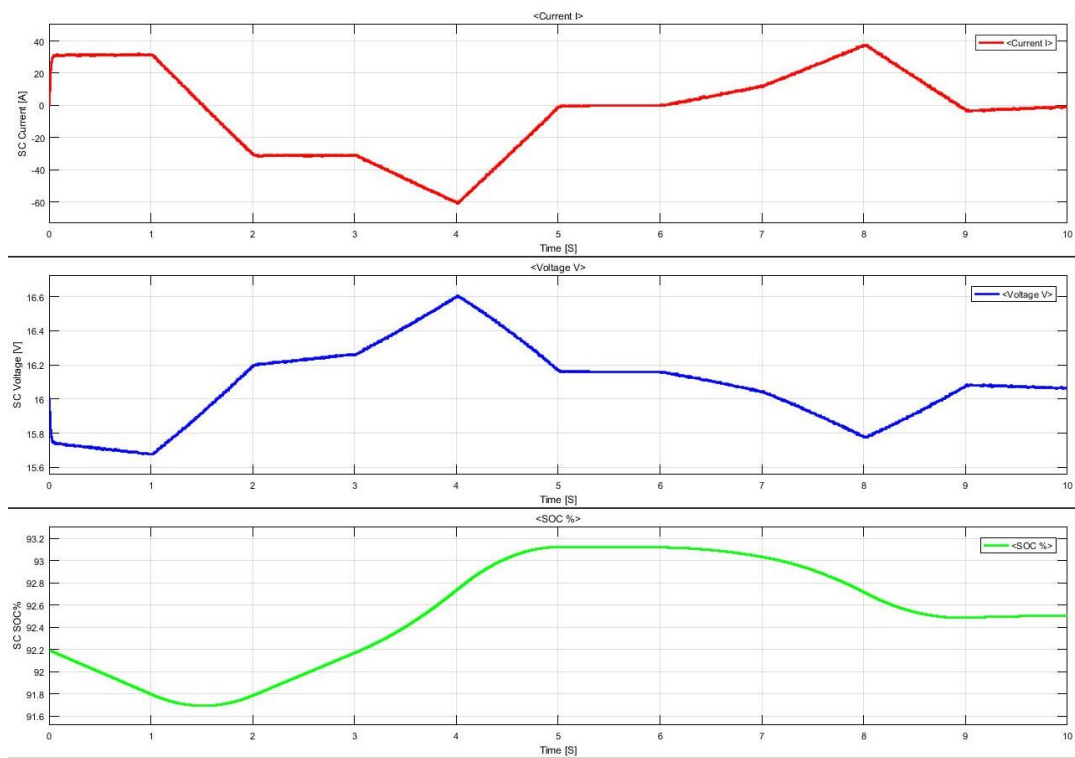


Fig. 5.8: Super-Capacitor Behaviour of Electrical parameter

parameters reduced owing to the delivered power. Furthermore, in Figure 5.9 and for the same time intervals, the converter functioning as boost converter.

- (b) Charging mode operation: when there is surplus energy in the system, the extra energy is stored in the super-capacitor as a negative energy, this is shown in Figure 5.7 between the time intervals (1.5s & 5s) and between (9s & 10s), in Figure 5.8 and for the same time intervals, the voltage and the state of charge of the super-capacitor are getting higher owing to the extra energy supplied into super-capacitor (charging mode). Moreover, the converter is functioning as a buck converter for that time intervals as shown in Figure 5.9.
- (c) Idle mode operation: the idle mode occurs when the energy produced by the PV system is the same as the energy requested by the load. Figure 5.7 illustrates this mode which can be seen during time intervals (5s to 6s). Furthermore, for the same time interval, the current of the super-capacitor is equal to zero, which means no power is delivered to or from the super-capacitor; this can be seen in Figure 5.8. Finally, there is no control signal to the gate of both switches for the same time interval as Figure 5.9 shows.

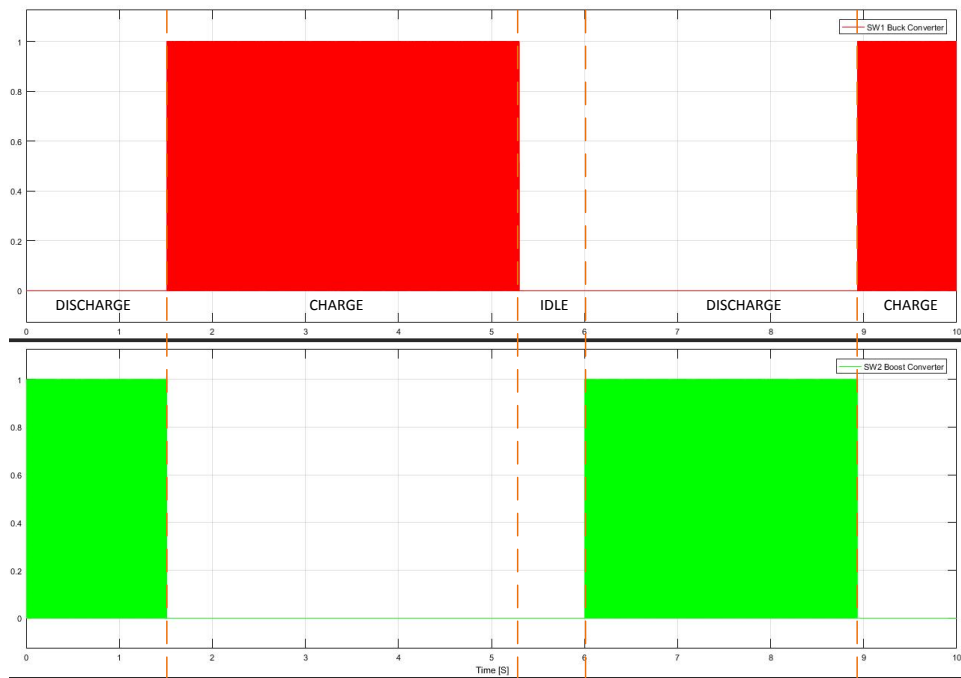


Fig. 5.9: Converter Switches Controlled Signal

2. Case 2 PV energy is same as the load at the start:

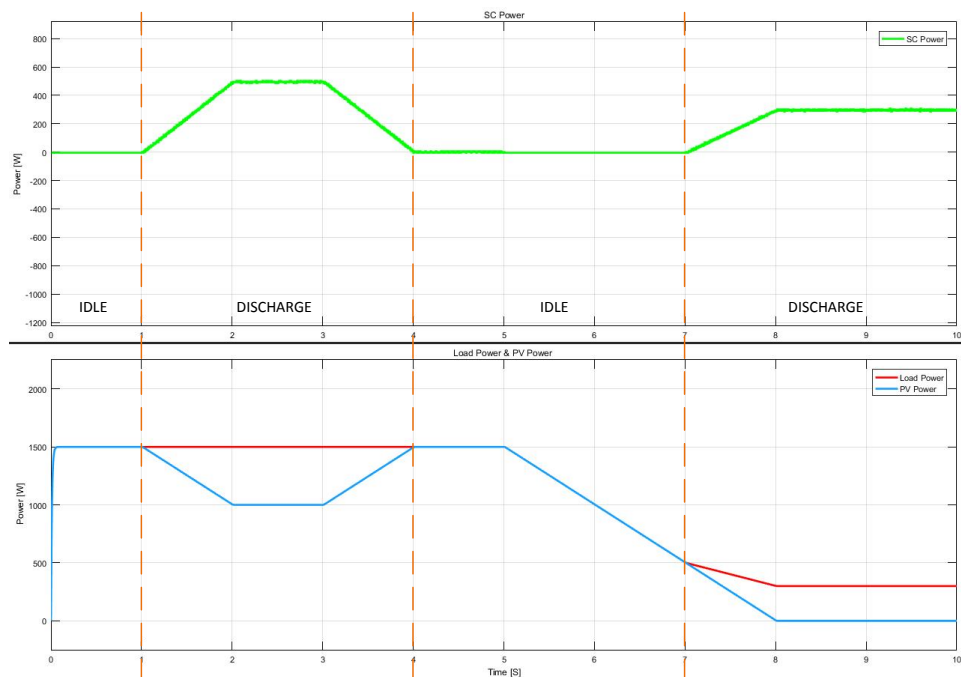


Fig. 5.10: Discharge Idle Discharge

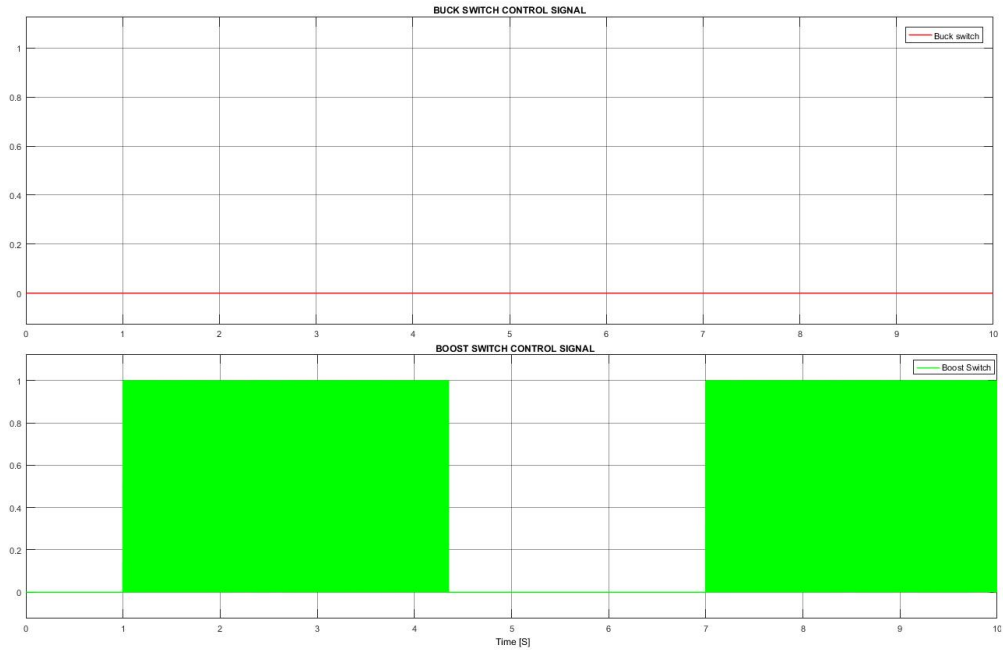


Fig. 5.11: Switch Control Signal in Case 2

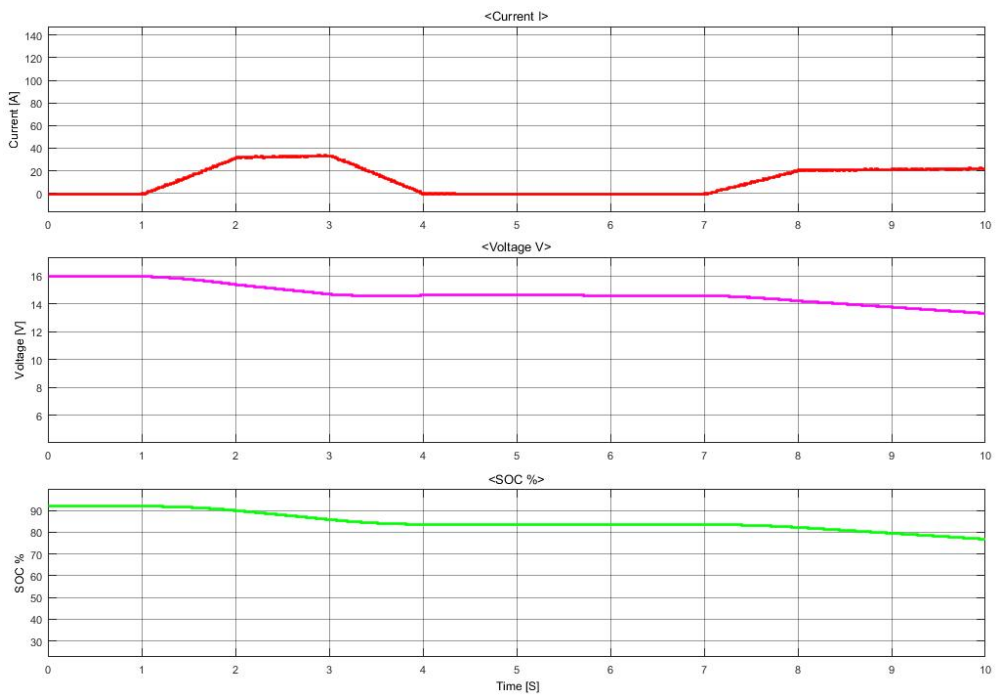


Fig. 5.12: Super-capacitor Electrical Parameters Behaviour

Figure 5.10, 5.11 and 5.12 illustrates two modes of the energy flow in the system:

- Idle mode: The energy produced by the PV arrays is equal to the load. As a result, the super-capacitor goes into idle mode, which occurs twice when $[0s \leq t \leq 1s]$ & $[4s \leq t \leq 7s]$. Figure 5.11 shows that, for that time, no signal has been sent to the switches in the converter.
- Discharge mode: the energy produced by the PV arrays is lower than the load. This occurs twice, when $[1s \leq t \leq 4s]$ & $[7s \leq t \leq 10s]$, and the Super-capacitor supplies the extra energy to the load. Moreover, Figure 5.11 shows the bi-directional converter working only in Boost converter as discharge mode is in operation.

3. **Case 3:** represents a comparison between two different capacitance under same condition (same load and same weather condition) as Figure 5.13 and 5.16 shows

(a) Super-capacitor capacitance $50F$

Figures 5.13, 5.14 and 5.15 illustrates the power flow, super-capacitor electrical parameters behaviours, and the converter switches control signal respectively for $50F$ of capacitance. The results can be explained as follows:

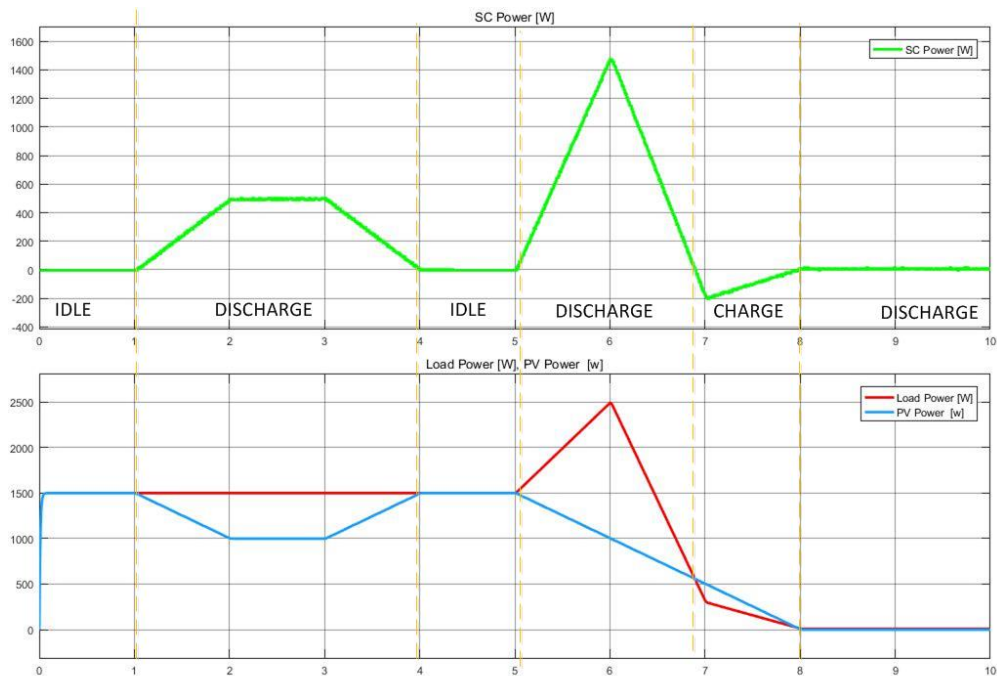


Fig. 5.13: Power Management with 50F of Capacitance

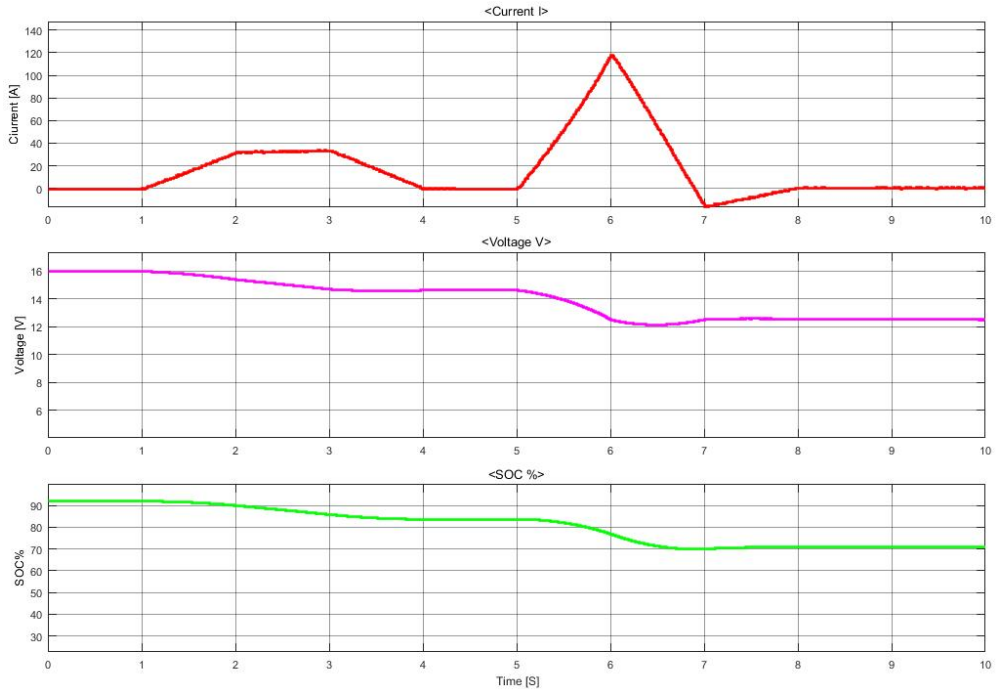


Fig. 5.14: Super-Capacitor Performance for 50F of Capacitance

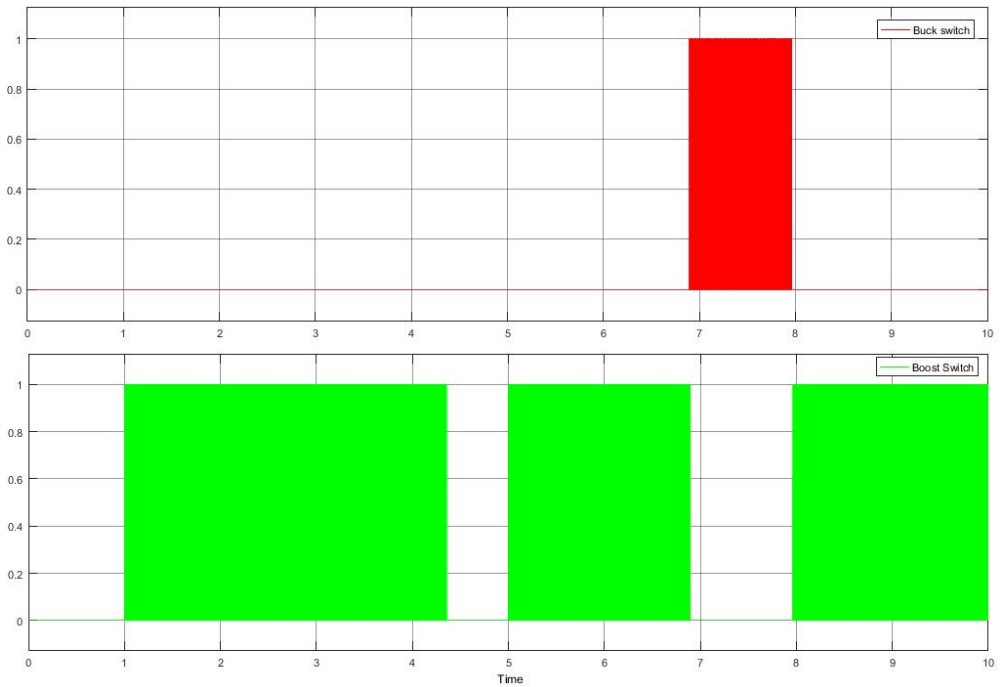


Fig. 5.15: Switches Control Signal of Capacitance for 50F of Capacitance

- In the first period, from 0s to 1s, the PV energy produced was equal to the load requirement and the super-capacitor was in idle mode (disconnected)

- In the second period, from $1s$ to $4s$, the PV energy produced dropped slightly. As a result, the super-capacitor delivered the power requirement in discharge mode.
- In the third period, from $4s$ to $5s$, the PV energy produced returned to the same level as the load and so the super-capacitor entered idle mode.
- In the fourth period, from $5s$ to $6.9s$, the PV energy produced dropped slightly and the requested load increased dramatically. As a result, the super-capacitor delivered high power to support the load.
- In the fifth period, from $6.9s$ to $8s$, the PV system produced more energy the super-capacitor start charging.
- In the fifth period, from $8s$ to $10s$, the PV system didn't produce any energy and so the whole load energy requirement was delivered by the super-capacitor.

Figure 5.14 illustrates super-capacitor electrical parameters variation; the first graph shows the current, followed by the voltage and the state of charge respectively.

Figure 5.15 shows the back-boost converter switches control; the first graph with red colour shows the buck mode that confirm the charging of the super-capacitor, followed by the boost mode to allow the super-capacitor to discharge with green colour respectively.

(b) Super-capacitor capacitance $5F$

Figures 5.16 and 5.17 illustrates the power flow in the system, followed by the super-capacitor electrical parameters behaviours, for capacitance of $5F$. The results can be explained as follows:

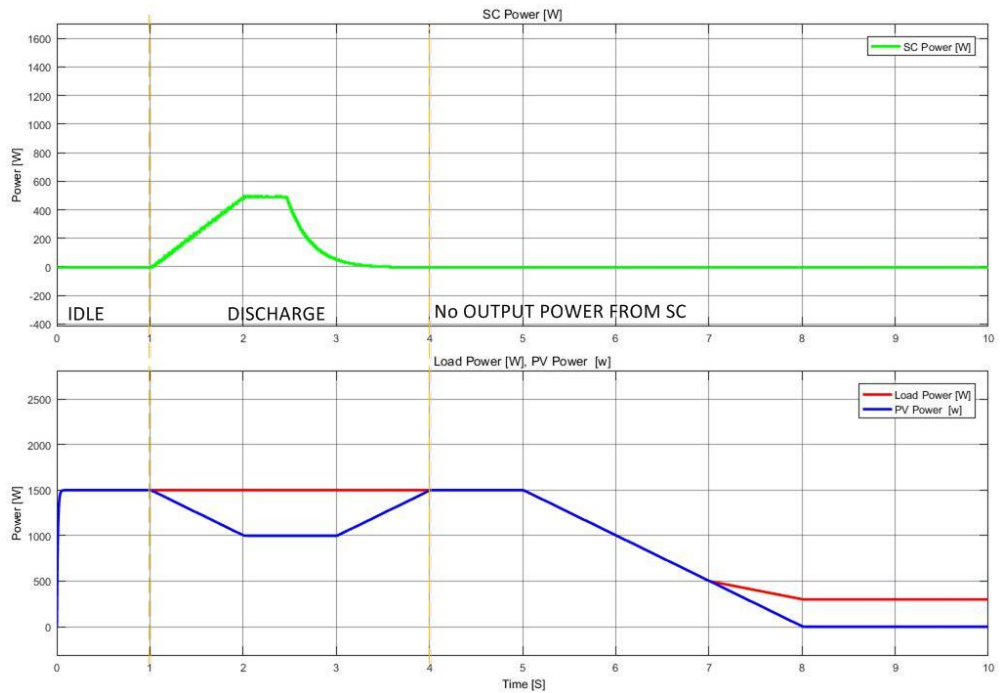


Fig. 5.16: Power Management with 5F of Capacitance

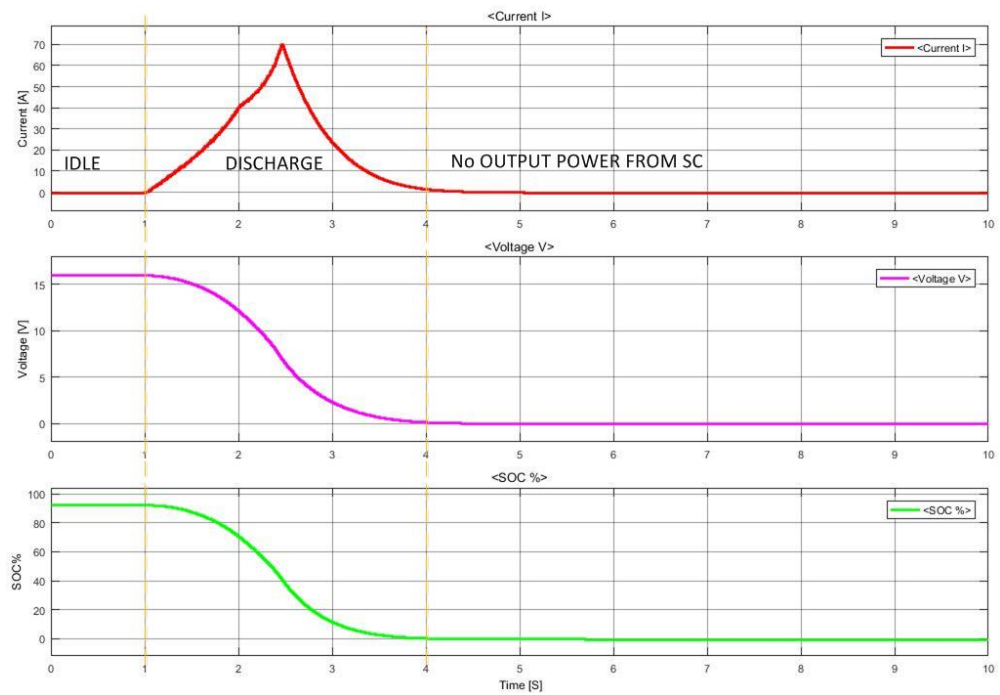


Fig. 5.17: Super-Capacitor Performance for 5F of Capacitance

- In the first period, from 0s to 1s, the PV energy produced was equal to the load requirement and the super-capacitor was in idle mode (disconnected)

- In the second period, from 1s to 4s, the PV energy produced dropped slightly. As a result, the super-capacitor delivered the power requirement in discharge mode.
- In the third period, from 4s to 7s, the PV energy produced returned to the same level as the load and so the super-capacitor entered idle mode.
- In the fourth period, from 7s to 10s, the PV system didn't produce any energy, meanwhile, the super-capacitor is fully discharged, as a result the load will be disconnected (no power delivered to the load).

Figure 5.17 illustrates super-capacitor electrical parameters variation; the first graph shows the current, followed by the voltage and the state of charge respectively.

5.4 Energy Recovery Snubber Circuit

The power level in a stand-alone PV system varies from a few watts to megawatts in range, depending on the application. However, a further improvement to the system can be made at component level, especially with regard to the converter where the energy losses of the switches (during switching) can be recovered and recycled, either to the source or the load. These switching losses vary with the switching frequency and the load type. Such an enhancement can significantly improve the overall system reliability and efficiency.

5.4.1 Resistive Load

Figure 5.18 represents a 3 kW boost converter, with a resistive load and without an energy recovery snubber circuit. Figure 5.19 represents the same converter with an energy recovery snubber circuit. The obtained results are based on an existing component data-sheet; please refer back to Appendix C for MOSFET data-sheet.

The following graphs illustrate the results obtained from Figures 5.19 and 5.18. Figures 5.20 and 5.21 show the overall turn on/off process for the switch, with and without an energy recovery snubber circuit respectively, in relation to the gate signal, the switch power losses, the current and the voltage of the switch.

The switch gate signal is represented by the first sub-figure followed by the switch Power losses (turn on, turn off and conduction losses) and, lastly, the switch current and voltage. It is clear from the

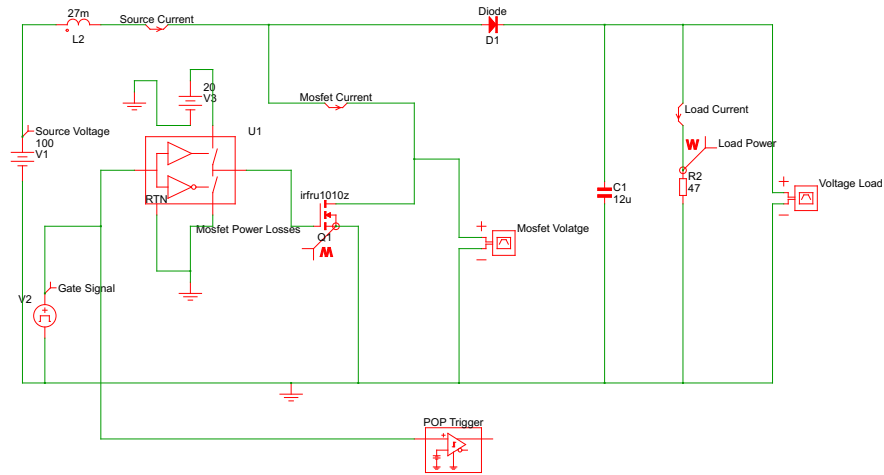


Fig. 5.18: Boost Converter and Resistive Load

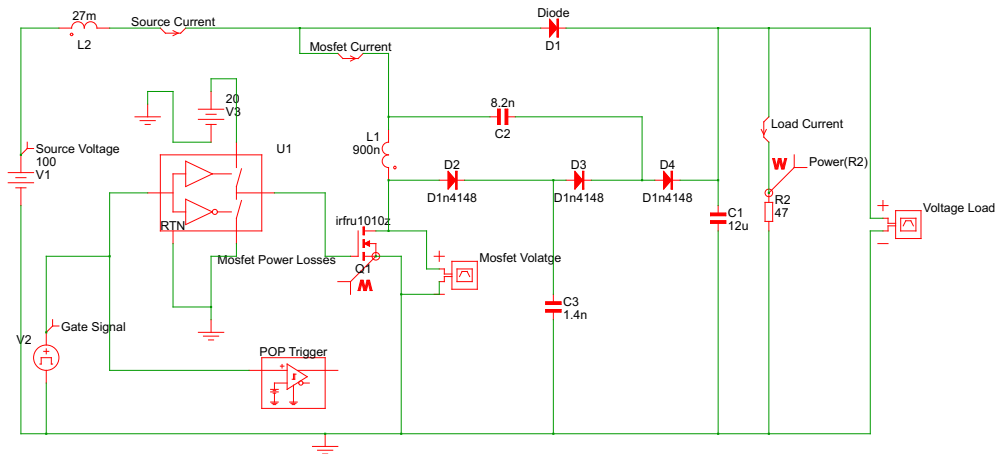


Fig. 5.19: Boost Converter with Energy Recovery Snubber & Resistive Load

switch Power losses sub-figure for Figure 5.20 that the power losses are huge. At turn on transition, the power loss in the switch is 900 W and, at turn off transition, the power loss in the switch is approximately 750 W. However, by implementing the energy recovery snubber circuit, the losses

reduced dramatically to 60 W for turn on transition and 120 W for turn off transition, as can be seen from Figure 5.21.

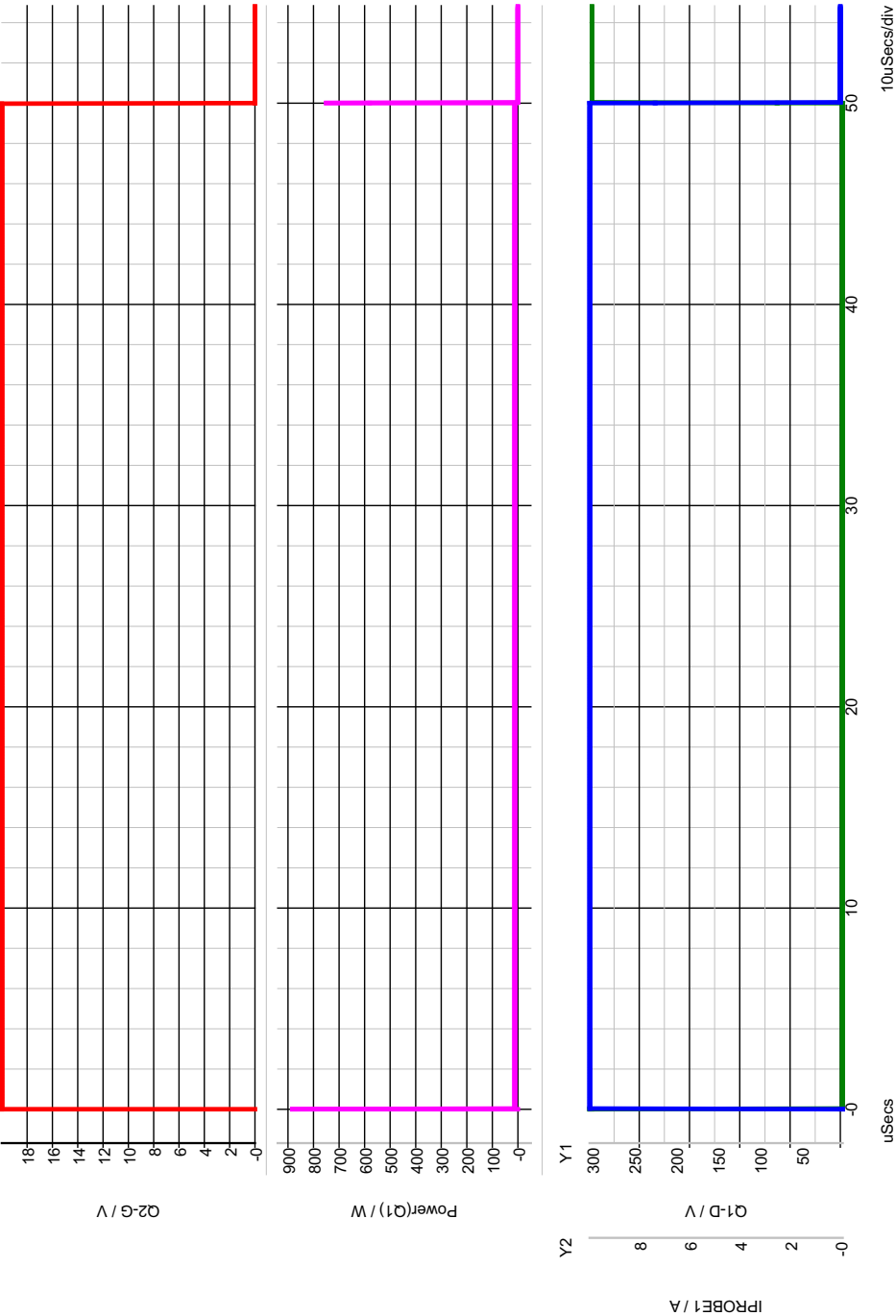


Fig. 5.20: Switch Turn on/off without Snubber Circuit

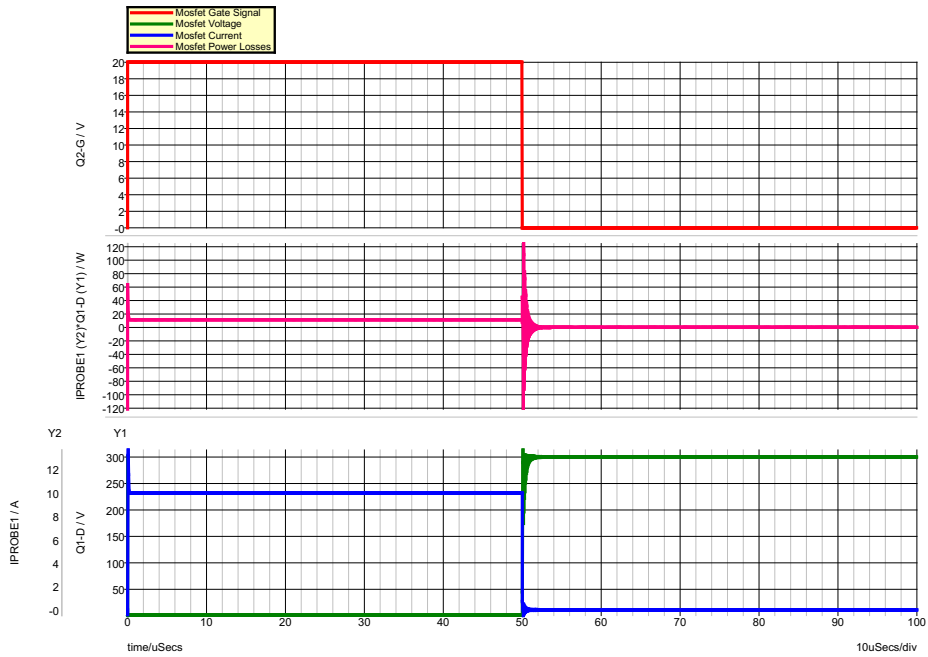


Fig. 5.21: Switch Turn on/off with Snubber Circuit

A zoom-in at the turn on transition period in Figures 5.20 and 5.21 is represented in Figure 5.22 and Figure 5.23 respectively. Figure 5.23 shows a reduction by 94.44% for the turn on transition losses. However, the snubber circuit introduced a substantial ringing on the current and the voltage wave form; as a consequence, the power losses wave form was also ringing.

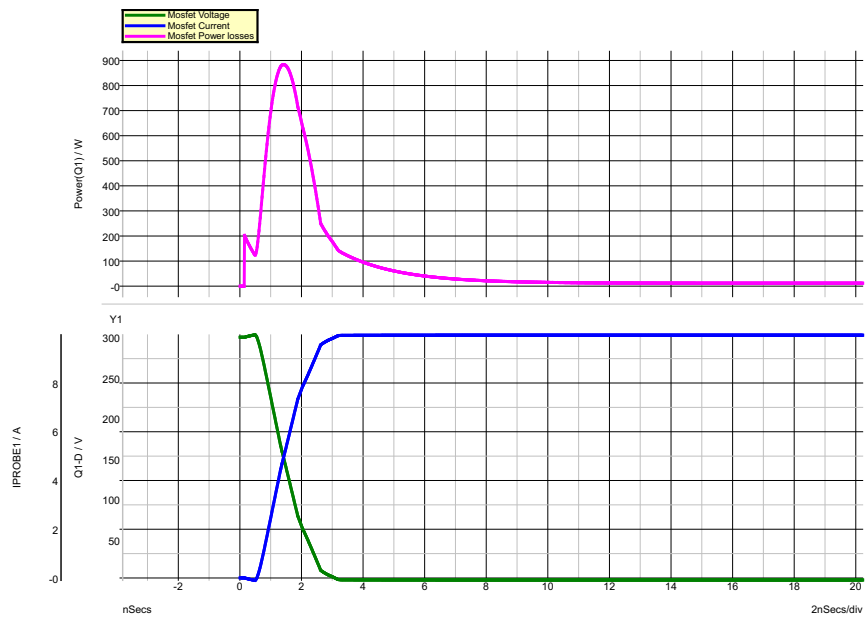


Fig. 5.22: Switch Turn on Transition zoom-in without Snubber Circuit

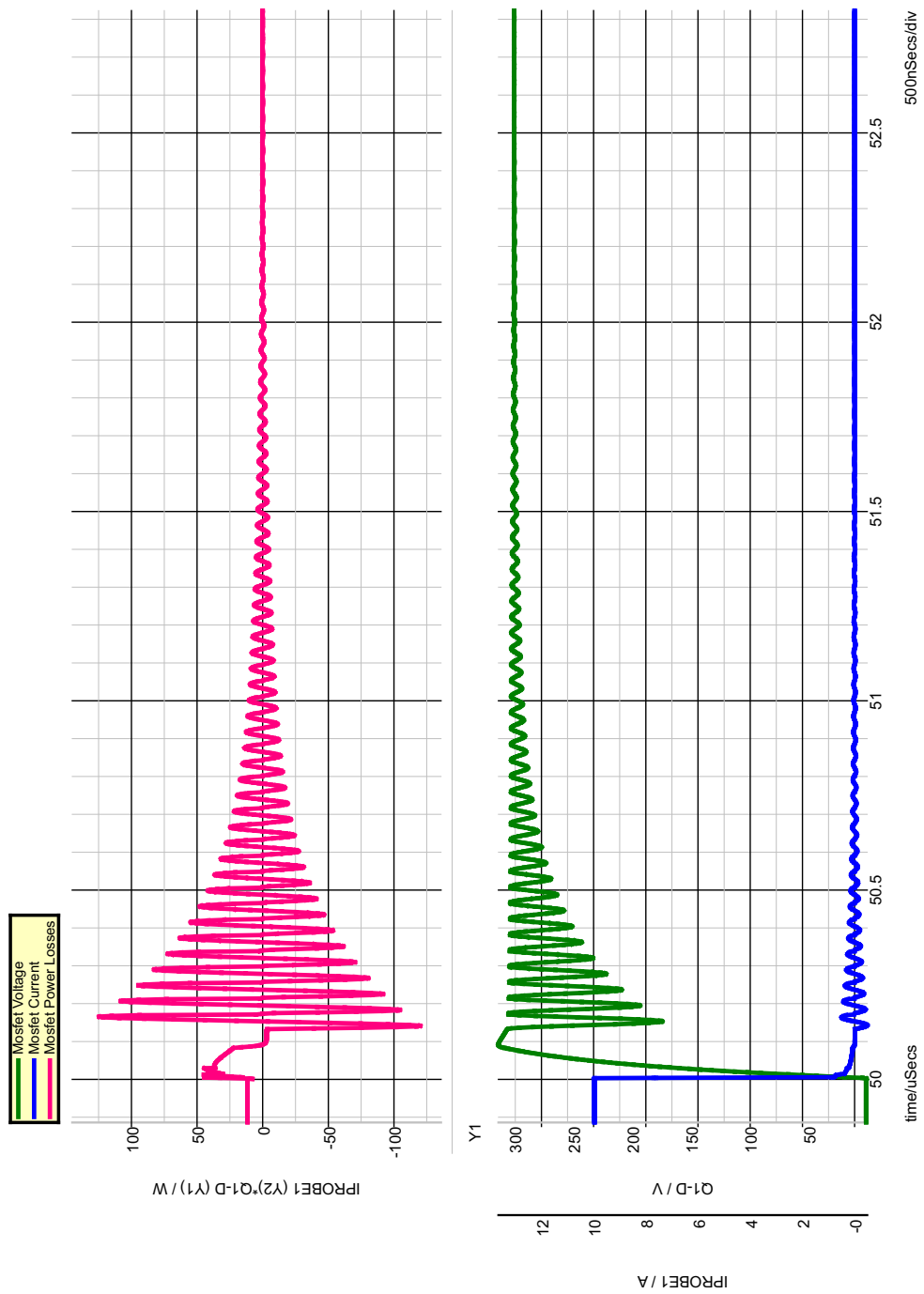


Fig. 5.23: Switch Turn on Transition zoom-in with Snubber Circuit

A zoom-in at the turn off transition period in Figures 5.20 and 5.21 is represented in Figure 5.24 and Figure 5.25 respectively. Figure 5.25 shows a reduction by 92.86% for the turn off transition

losses. However the same, substantial, ringing on the current and voltage wave forms and the power losses wave form was also evident.

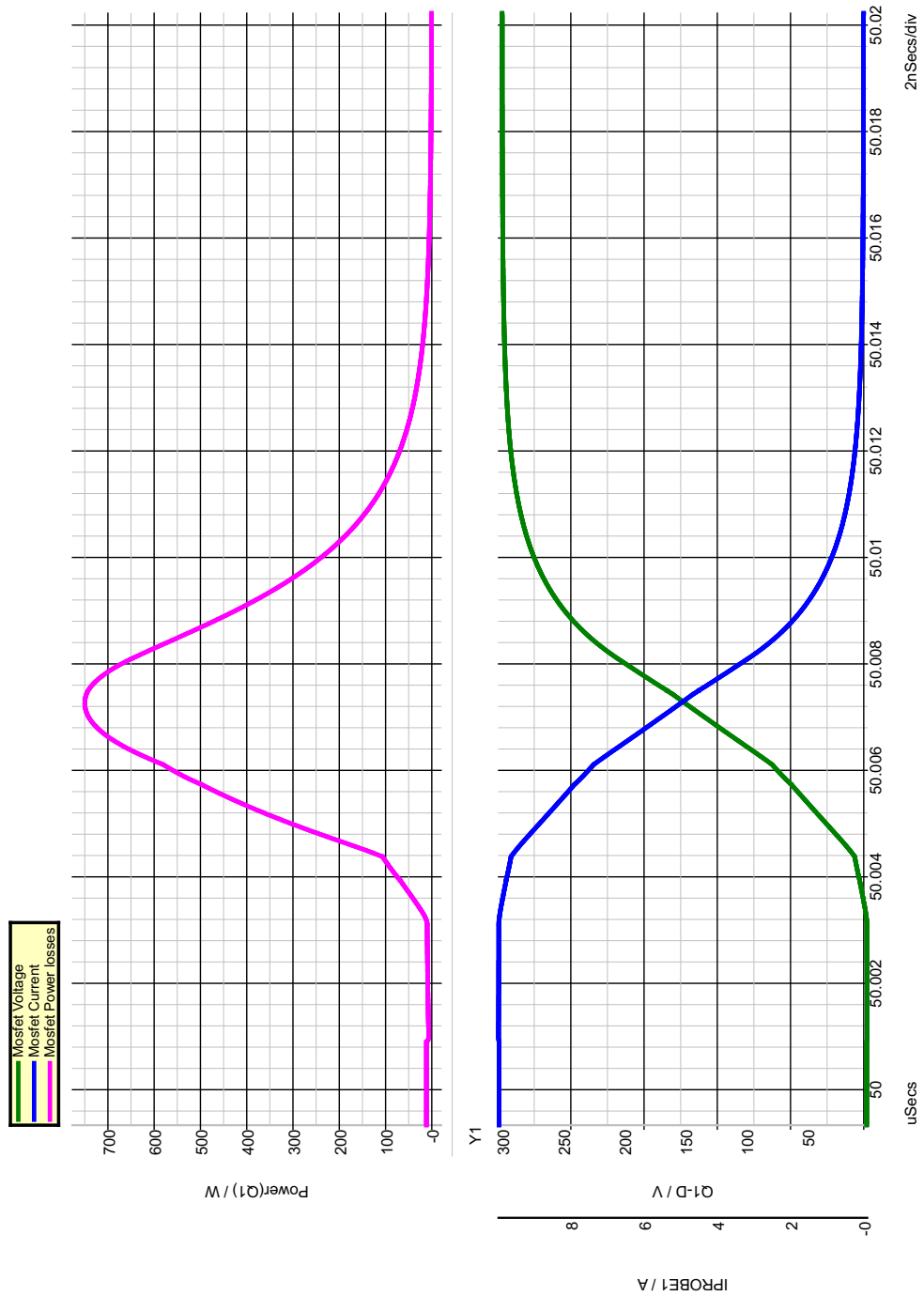


Fig. 5.24: Switch Turn off Transition zoom-in without Snubber Circuit

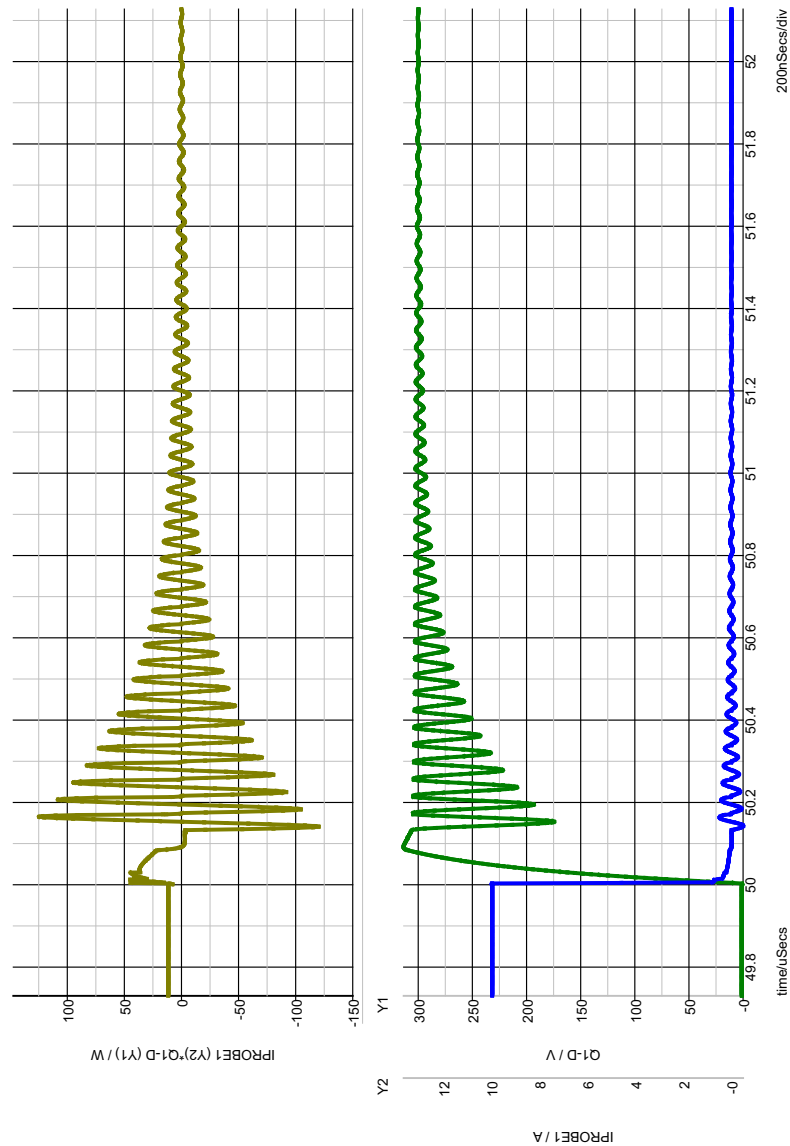


Fig. 5.25: Switch Turn off Transition zoom-in with Snubber Circuit

The substantial ringing was caused by the energy recovery snubber circuit and, in order to suppress the ringing, a resistor capacitor snubber were added across the diode, as shown in Figure 5.26. This can be considered as being a trade-off to the design owing to the additional power losses element (resistor). However, Figures 5.27 and 5.28 show a huge improvement in the wave form for both transitions (on and off).

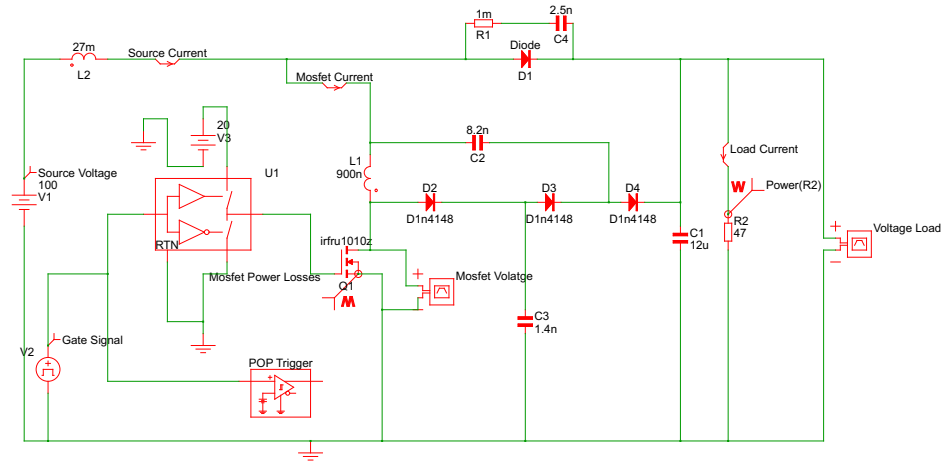


Fig. 5.26: Switch Wave form Improvement at Turn on Transition

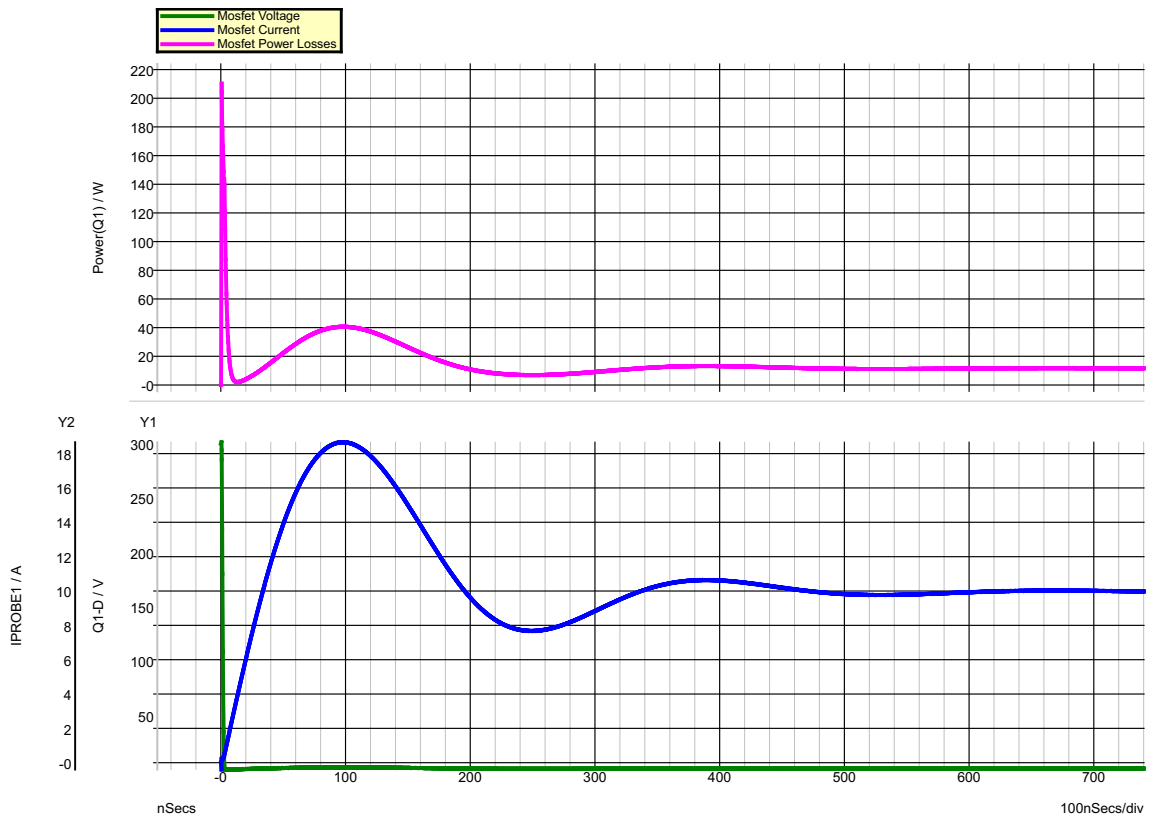


Fig. 5.27: Boost Converter with Energy Recovery Snubber and RC Snubber

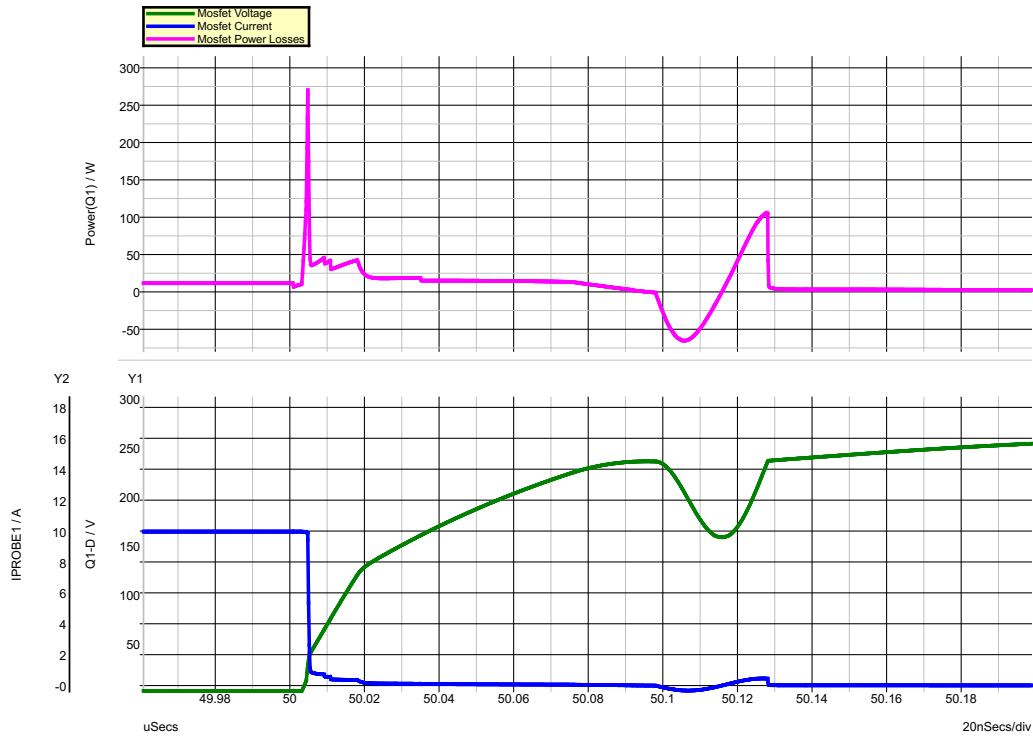


Fig. 5.28: Switch Wave form Improvement at turn off Transition

5.4.2 Inductive Load

The transition time will be very short, comparing to turn on and off time interval, so there is very little change in either the inductor current and the output voltage; and in order to capture the maximum losses and simplify the design. The following simplifications are made: the input voltage source, with the inductance, are represented by the current source and the output response is represented by voltage source.

Figure 5.29 represents the boost converter with an inductive load (hard load) and without an energy recovery snubber circuit. Figure 5.30 represents the same converter with an energy recovery snubber circuit.

The following graphs illustrate the results obtained from Figures 5.29 and 5.30. Figures 5.31 and 5.32 shows the overall turn on/off process for the switch, both with and without an energy recovery snubber circuit respectively, in relation to the gate signal, the current and the voltage of the switch. The switch gate signal represented by the first sub-figure followed by the switch Power losses (turn on and turn off losses) and, lastly, the switch current and voltage are shown. It is clear from the switch power losses sub-figure in Figure 5.31 that the power losses are huge. At turn on and off transition,

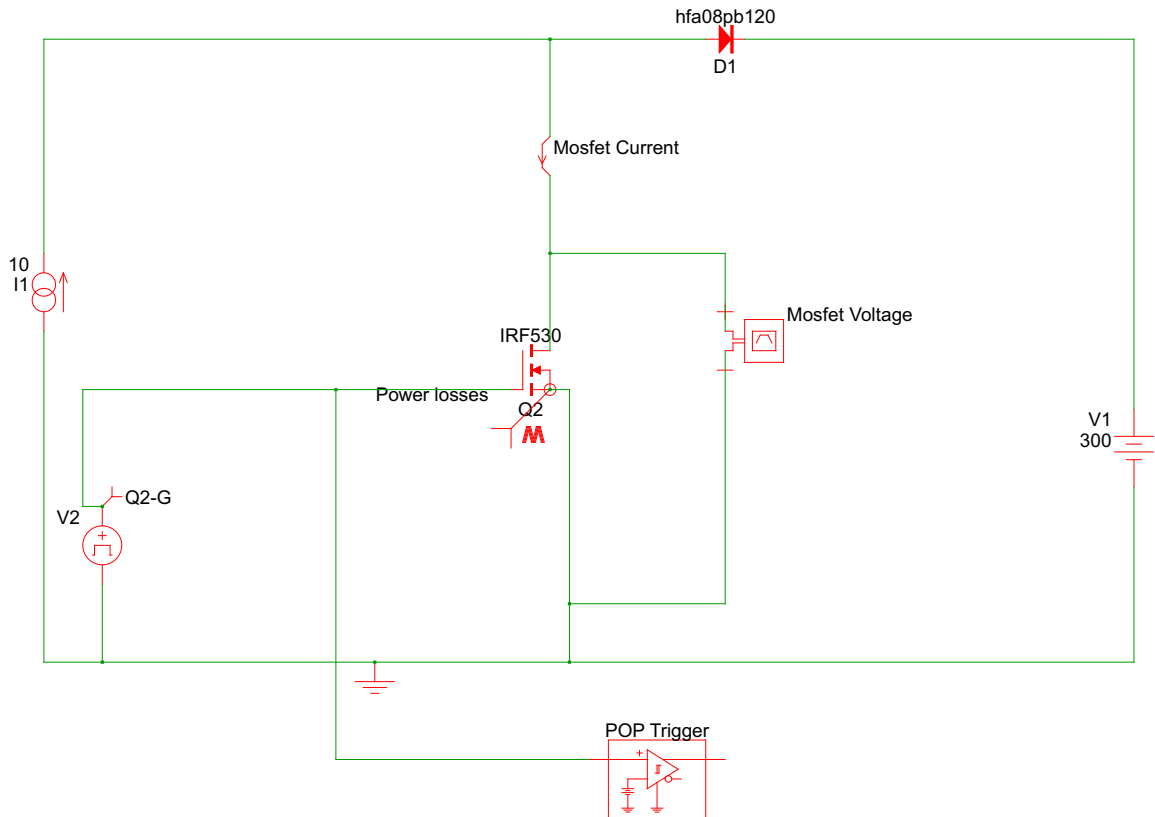


Fig. 5.29: Boost Converter

the power loss in the the switch is 3 kW . However, by implementing the energy recovery snubber circuit, the losses reduced dramatically, to approximately 600 W for turn on transition and 50 W for turn off transition, as can be seen in Figure 5.32.

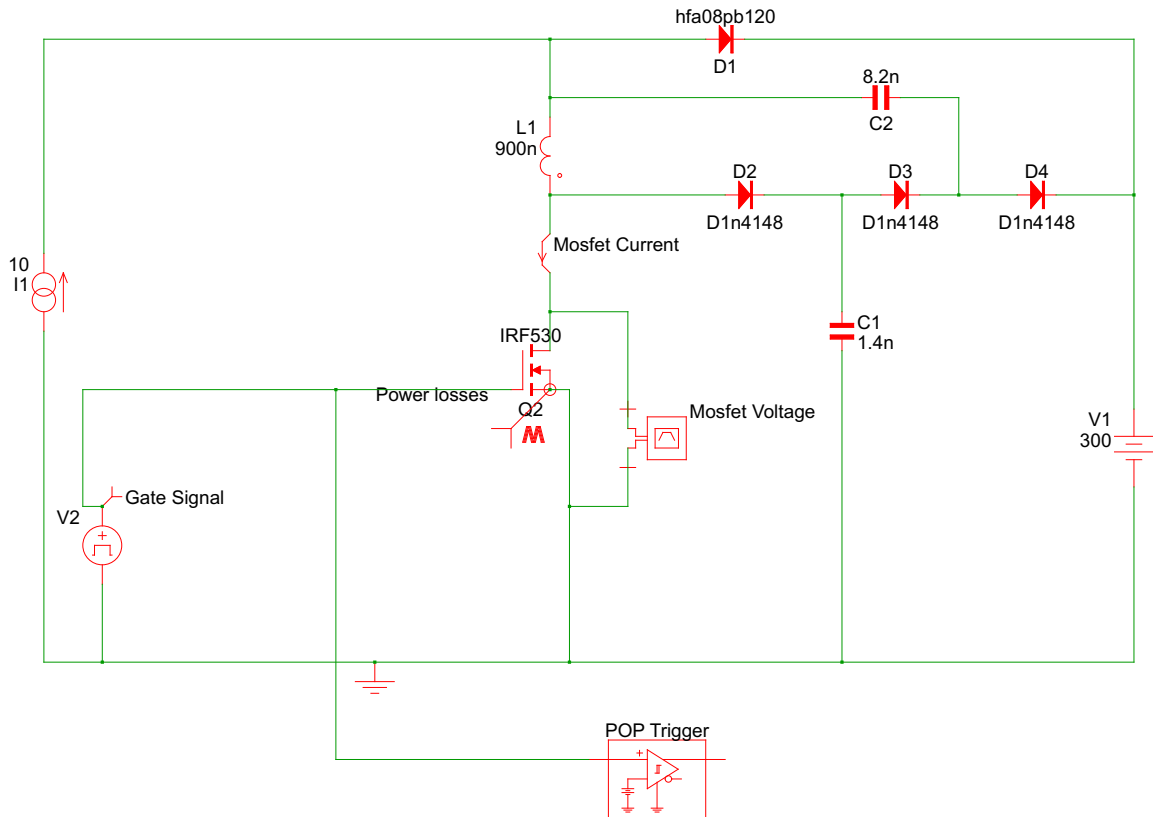


Fig. 5.30: Boost Converter with Energy Recovery Snubber Circuit

A zoom-in at the turn on transition period in Figures 5.31 and 5.32 is represented in Figure 5.33 and Figure 5.34 respectively. Figure 5.34 shows a reduction of 78.33% in the turn on transition losses.

A zoom-in at the turn off transition period in Figures 5.31 and 5.32 is represented in Figure 5.35 and Figure 5.36 respectively. Figure 5.36 shows a reduction of approximately 97.33% in the turn off transition losses.

Note: The conduction losses for the switch are always fixed, regardless of the load type, as can be seen in Figure 5.37.

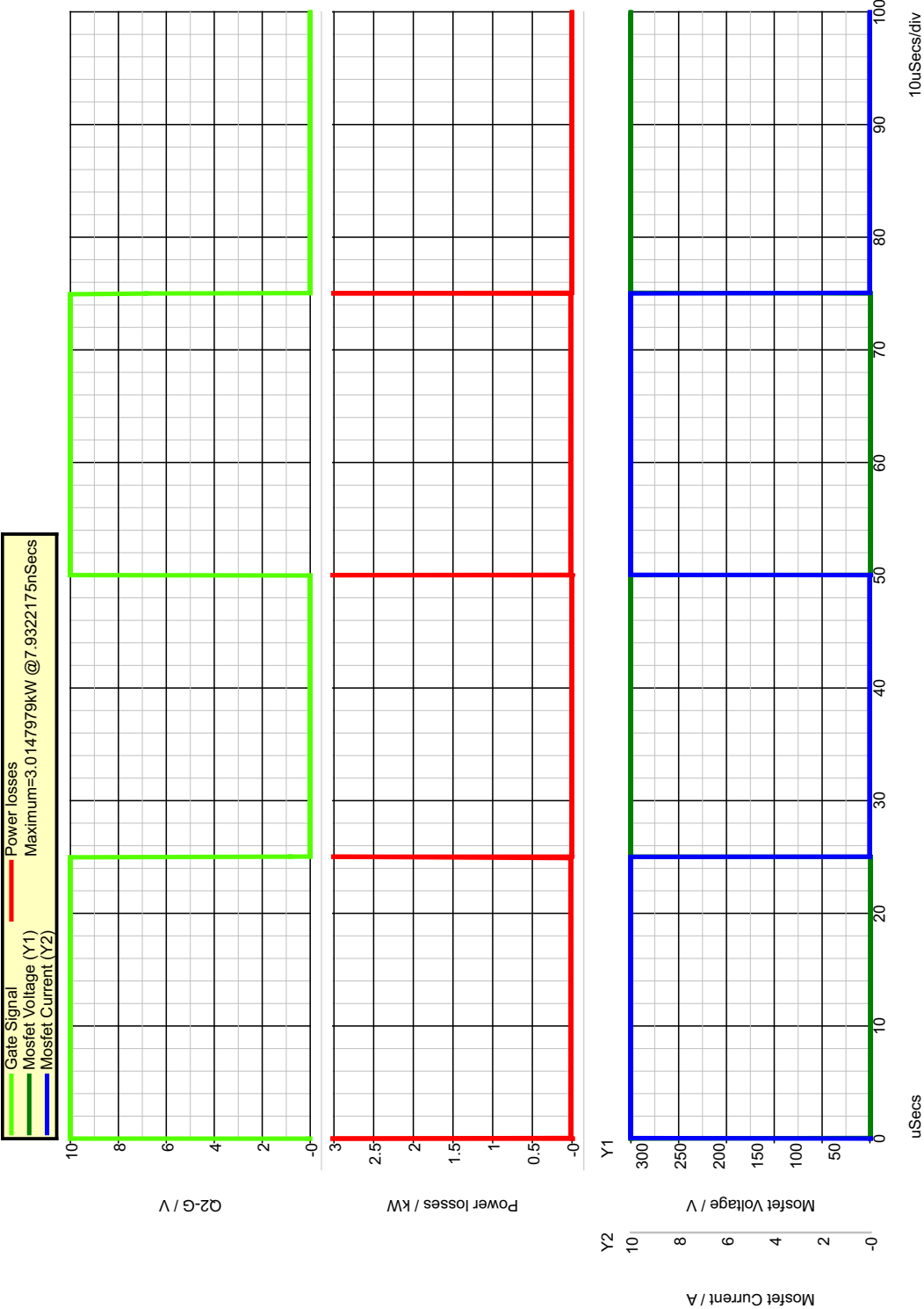


Fig. 5.31: Switch Turn on/off Inductive Load

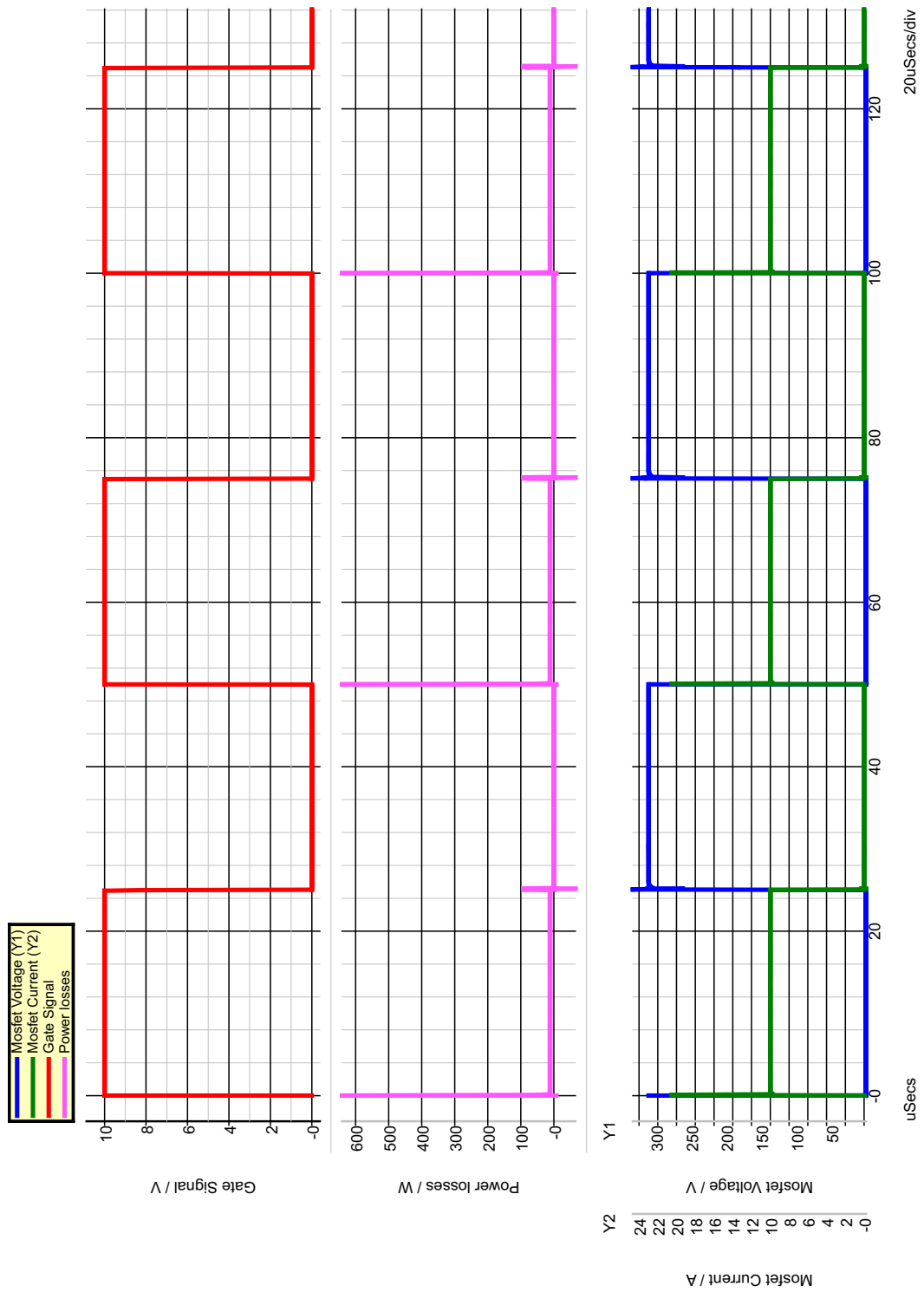


Fig. 5.32: Switch Turn on/off Inductive Load with Snubber Circuit

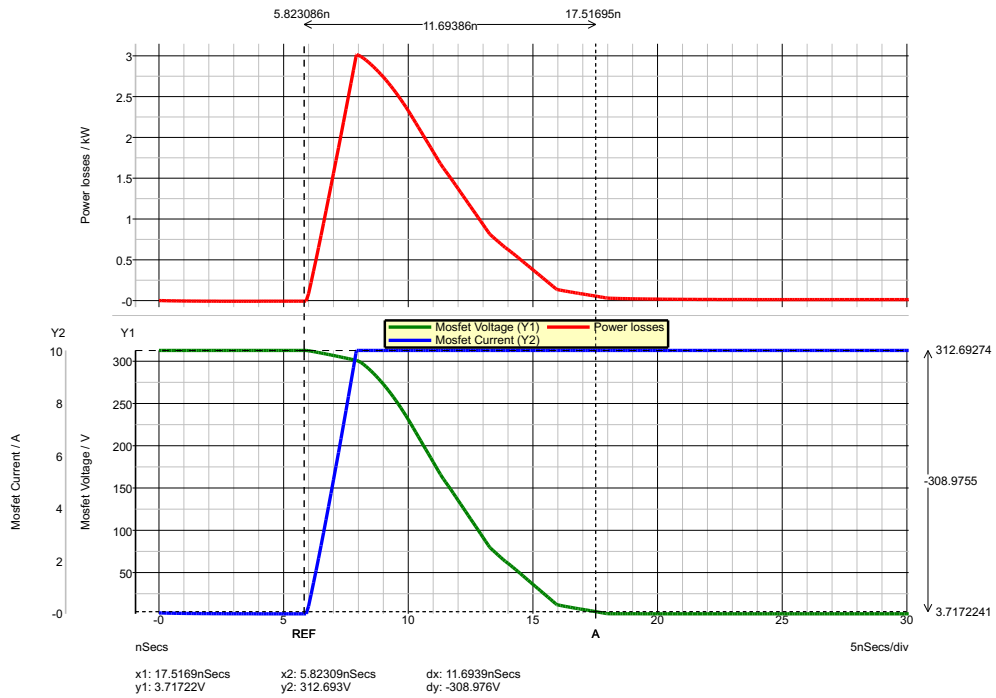


Fig. 5.33: Switch Turn on Transition Inductive Load zoom-in

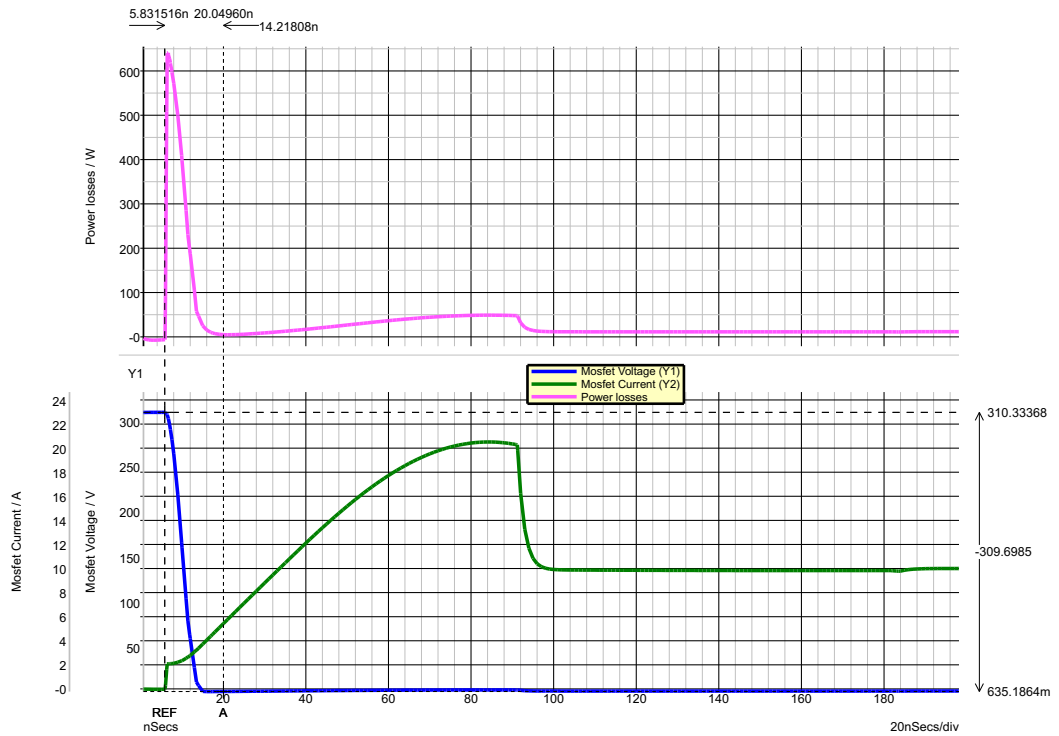


Fig. 5.34: Switch Turn on Transition Inductive Load zoom-in With Snubber Circuit

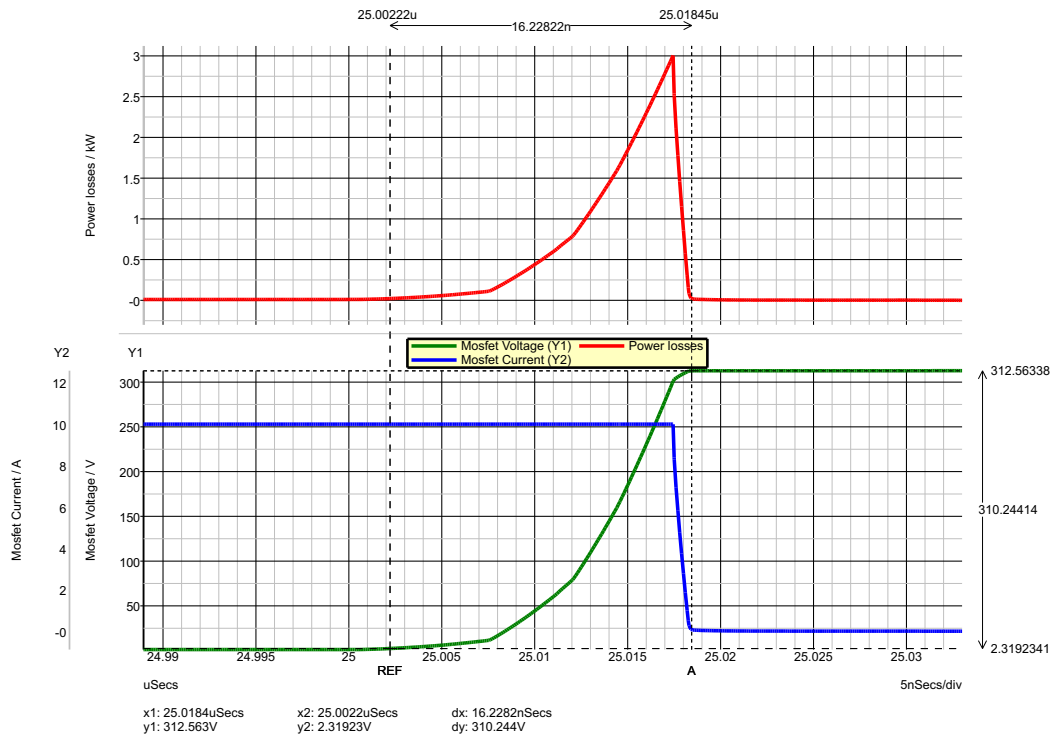


Fig. 5.35: Switch Turn off Transition Inductive Load zoom-in

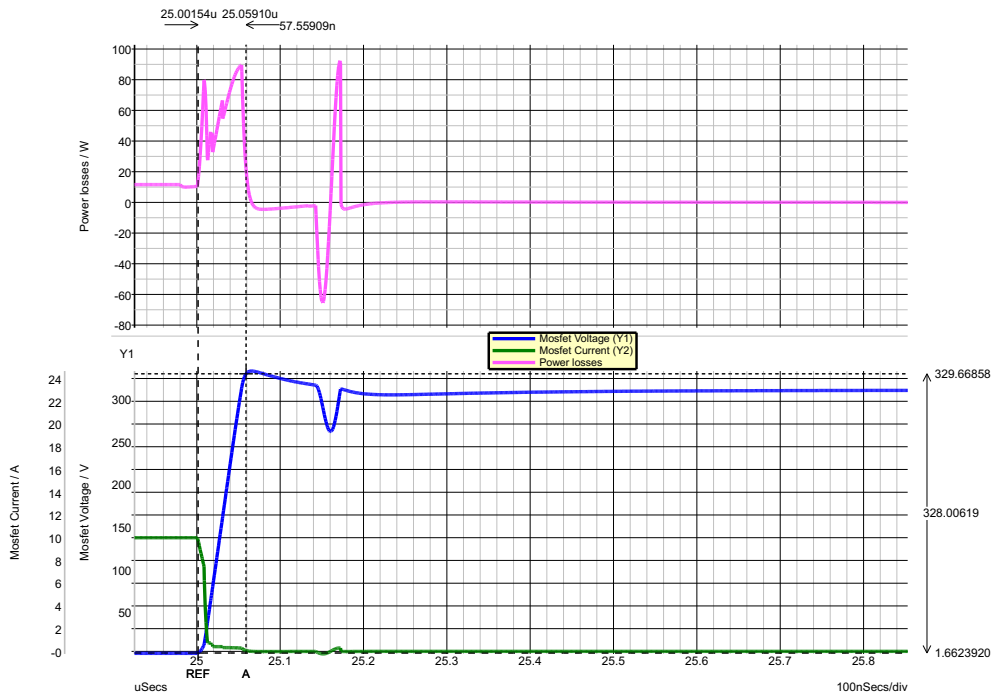


Fig. 5.36: Switch Turn off Transition Inductive Load zoom-in with Snubber Circuit

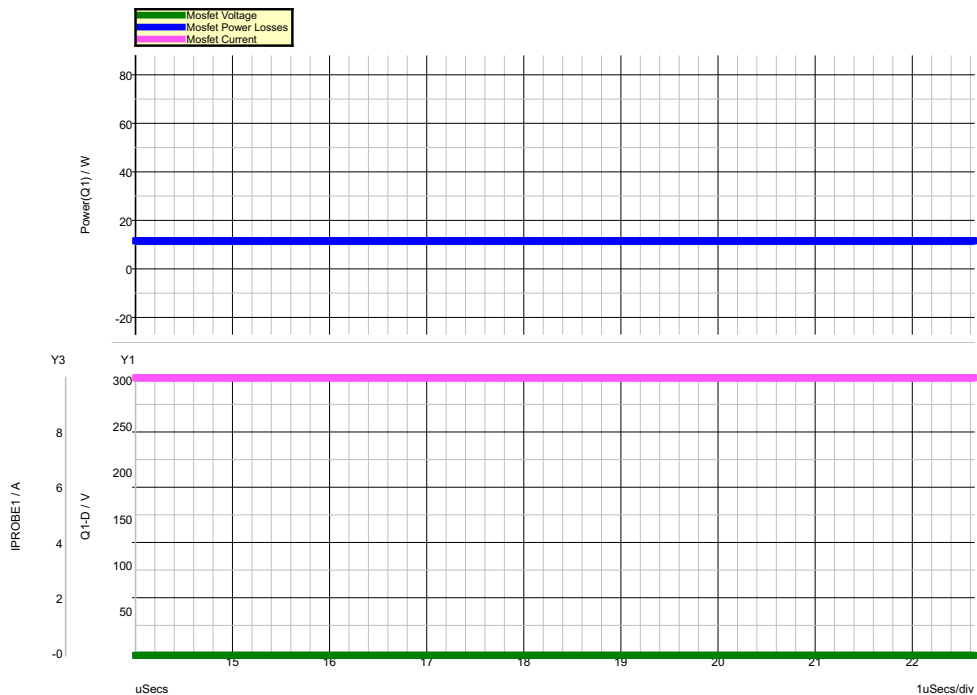


Fig. 5.37: Conduction Losses for the Switch

5.5 Summary

In this chapter, a novel power management in stand-alone *PV* system has been validated through simulation. This management of power incorporated a super-capacitor to negate fast fluctuations in the miss-match of power.

The results showed that a significant amount of power is wasted in a stand-alone *PV* system which did not include a super-capacitor. However, when the super-capacitor was included, any fast fluctuations that led to a miss-match in the energy between the load and the produced power were eliminated.

In addition, a further enhancement of the system at the component level was implemented by the introduction of an energy recovery snubber circuit. The energy lost during each switching event was recovered and delivered back to the load.

As a result, huge thermal losses were avoided and the performance of the switch was enhanced. However, the implementation of an energy recovery snubber circuit induced ringing in the voltage wave form. This issue was eliminated by the addition of a RC snubber circuit; this can be considered to be a trade-off in the design.

Chapter 6

Conclusions and Future Work

6.1 Conclusions

Climate change, environmental pollution and the increased demand on energy and fossil fuel depletion are amongst the issues discussed in the United Nations 21st conference of parties (COP-21) meeting. Thus, a number of countries signed the Kyoto protocol that brings along with binding obligations, such as the limitation of global warming to no more than 2 °C above pre-industrial levels within the next 10 to 20 years.

Renewable energy technologies are essential contributors to the energy supply portfolio which includes generating power from wind or solar sources. Photovoltaic (*PV*) panels convert solar energy into electric power. Voltage and current at *PV* terminals have a complicated, non-linear, relationship depending on the temperature and irradiance of the environment. To best regulate the available power from the *PV* panels, several power electronic technologies have been developed in recent decades. However, the stand-alone *PV* system uses batteries to provide support when the solar energy is insufficient to satisfy load demand. The battery size is calculated for the average annual data, and also for at least three days of island autonomy. Therefore, the daily quick changing in *PV* output is not dependable and as a result, the battery life reduced dramatically.

The correlation between public awareness of climate change and the vital role of renewable energies in combating it, along with government subsidies and feed-in tariffs, has encouraged residential users and investors to enhance *PV* system. In order to overcome the power issue in *PV* systems,

a super-capacitor is introduced in this study to deal with the quick change between the produced electrical power in relation to the consumption.

In order to fulfil the first objective in this thesis, an extensive literature review of the development of *PV* systems through the years, a historical view and a classification of *PV* cell technology that existed in the market was presented in Chapter 2. Moreover, a mathematical model of the *PV* cell was presented, with its electrical presentation, in the same chapter. As the available power generated by *PV* panels are varied by time and are dependent on circumstances, the power to load can fluctuate considerably and so changes can occur within seconds or minutes. To balance the requirements from fluctuating load and the intermittent source, energy storage is introduced into the *PV* system. The *PV* design of the system, and the configuration, has been discussed in detail. Furthermore, the electrical storage unit technology used in power system has been presented with regard to the specific parameters and technology classifications with a detailed comparison between the storage types.

The storage units used in the stand-alone *PV* system mainly is electrochemical batteries. Therefore, a detailed description of the battery technologies, with the types and the functionalities has been demonstrated. Another storage technique, used for short lengths of time, is the electrical storage systems, including the super-conducting magnetic and super-capacitor methodologies which are explained and discussed in details in Chapter 2. Moreover, to keep extracting maximum power at all time with regard to the fluctuation, an overview of maximum power point tracking (MPPT) algorithms definition, the purpose and the different techniques implemented, with comparisons between them are also demonstrated.

To achieve the second and the fourth objectives of this thesis, a critical review and investigation of the main DC-DC converter topologies (buck, boost, buck-boost), functionality and the circuit analysis supported by the circuit diagram, is delineated in Chapter 3. Additionally, an overview and classification of the snubber circuit design and implementation in DC - DC converter has been presented with an in-depth explanation. This is followed by up-to-date super-capacitor mathematical models and electrical representations, with the balancing techniques used when connecting several super-capacitors together in order to obtain a specific voltage and capacitance.

This study proposed two system layouts for the placement of the super-capacitor. The first layout presents a unidirectional topology, where the super-capacitor was placed in between two *DC – DC* converters; the first *DC – DC* converter is used to step down the voltage for the super-capacitor unit owing to its low operating voltage to control the charging requirement. The second *DC –*

DC converter is used to step the voltage up and maintain it at a fix level for the load. The second layout represents a bidirectional topology, where the super-capacitor is placed after a bidirectional *DC – DC* converter. A critical analysis between the two layouts, for a stand alone *PV* systems, was conducted as illustrated by the flow chart presented in the methodology in Chapter 4. The results and discussion of the main important factors regarding both layouts were discussed in detail, such as the capacitance of super-capacitors, converter efficiencies and load variations. From the results obtained by the critical comparison, all the main parameters (storage capacitance, load and converter efficiency) were significant to both topologies. Moreover, the longest served time when the load was 10% of the produced mean power, the bidirectional layout required 43% less capacitance than the unidirectional layout. When the load was 20% of the produced mean power, the bidirectional layout required 25% less capacitance than the unidirectional layout. Furthermore, when the load was 30% of the produced mean power, the bidirectional layout required 16% less capacitance than the unidirectional layout, and this was so throughout the remaining results. This indicates that the bidirectional layout performed better as it achieved the longest continuous load supply period (CLSP) with less storage capacity compared to the unidirectional layout.

Having realised the good performance of the bidirectional over the unidirectional layout in relation to the storage capacitance and the load supply, it was necessary to find the behaviour of both layouts with regards to the efficiency of the system. To achieve this, a simulation was implemented with different converter efficiency values. The results showed that, as the converter efficiency reduced, the energy delivered to the load was reduces with the longest served time for both layouts. At low capacitance of the super-capacitor, a small difference between both layouts was noticed in relation to the efficiency. However, the best result achieved by the bidirectional layout with regard to the converter efficiency at high and low capacitance values.

A super-capacitor was introduced as an attempt to manage the fast fluctuations in the generated stand-alone *PV* energy. Based on the findings in Chapter 4, and in order to prove the enhancement of the power management of the stand-alone *PV* system and to provide a validation for the obtained results, the first part in Chapter 5 presented the validation results obtained for a stand-alone *PV* system without a storage unit. The results for the proposed stand-alone *PV* system model, incorporating the super-capacitor and a *DC* converter were derived using Matlab/Simulink.

A comparison between the available energy and the wasted energy in a stand-alone *PV* system without implementing the super-capacitor, has shown that a significant amount of the power was

wasted. The traditional design of the stand-alone *PV* system was not dependable owing to fast fluctuations in both the supply power and the demands of the consumer. When the proposed system with the super-capacitor was implemented, all of the wasted power was reused, either by storing it in the super-capacitor when the produced energy was higher than the load requirement, or by delivering it to the load when the produced energy was not sufficient. As a result, all of the miss-matched energy, between the produced energy in the stand-alone *PV* arrays and the consumed energy by the consumer, was been re-implemented to the system. This made the stand-alone *PV* system more reliable and efficient with regard to energy management.

The bi-directional converter was used to connect and disconnect the super-capacitor unit to and from the system in response to the availability of energy. Three cases were generated to validate the proposed energy management algorithm. The first case, when the energy generated by the *PV* arrays was lower than the energy required by the load, the super-capacitor entered a discharge mode in order to deliver the required difference in the energy to the load. In the second case, when the *PV* energy was the same as the required load, the super-capacitor went into idle mode and electrically disconnected from the system. In the last case, when the generated energy by the *PV* arrays was higher than the energy required by the load, the super-capacitor absorbed the surplus energy and store it by going into a charging sequence. However, when the *PV* arrays did not produce any energy in the system and the super-capacitor was fully charged, the energy requested by the load was delivered by the super-capacitor.

A validation for the inclusion of the super-capacitor was carried out in Chapter 5. The results showed that a significant amount of power is wasted for the stand-alone *PV* system without the implementation a super capacitor. However, when including the super-capacitor all the wasted power was reused, either by storing it in the super-capacitor when the produced *PV* energy was higher than the consumed energy, or by delivering it to the load when the produced *PV* energy was less than the required energy. Furthermore, the super-capacitor was disconnected when the produced *PV* energy was equal to the load requested by the consumer.

A further enhancement on the stand-alone *PV* system, at the component level, was demonstrated in Chapter 5 by the inclusion of an energy recovery snubber circuit. The results showed that, for the resistive load, the switching loss energy recovery was 94.44% for the turn on transition and 92.86% for the turn off transition. With regard to the inductive load, the switching loss energy recovery was 78.33% for the turn on transition and 97.33% for the turn off transition. However, the implementation

of the energy recovery snubber introduced ringing in the wave form and, as a trade-off, an RC snubber with small resistor was incorporated. In the meantime, the conduction losses were fixed, regardless of the load type.

6.2 Future Work

Based on the proposed use of a super-capacitor to deal with fast fluctuations in the electrical power produced by a *PV* stand-alone system, the following research points can be further investigated:

- Investigate the optimum super-capacitor value for each PV string in relation to the output power, and the cost of the converter, with long-term cost savings.
- Further research could focus on a high switching frequency with the super-capacitor time response; this would fix the optimum switching frequency for the super-capacitor charger without sacrificing power efficiency.
- Implement a dynamic configuration, by changing the super-capacitor value in relation to the weather conditions and the load, by developing a smart algorithm to select the optimum value of the storage in any condition.
- Implement an optimum MPPT technique to work with the super-capacitor charger to establish time variation compatibility.
- Further investigate this area, for example, by including energy storage in the trade-off optimisation for better integration of PV solar. An in-depth technical and economic analysis of different algorithms for the energy storage technologies may also be undertaken.
- Further interesting research topics could include the application of different artificial intelligence techniques, such as PSO, ANN, Neuro-Fuzzy and so forth, to optimize a storage system that incorporates a super-capacitor. This would be considered to be an improvement to the existing applied optimisation algorithms.

Publications

Published

1. K. Sehil and M. Darwish, “Critical analysis of power conversion topologies for stand-alone pv systems with super-capacitor,” *International Journal of Computers and Applications*, vol. 39, no. 4, pp. 179–188, 2017

Submitted

1. K. Sehil and M. Darwish, “Effective power management in stand-alone pv system,” in *53rd International Universities Power Engineering Conference, UPEC 2018*, Sep 2018

References

- [1] I. E. Commission *et al.*, “Grid integration of large-capacity renewable energy sources and use of large-capacity electrical energy storage,” *IEC White Paper, Geneva: International Electrotechnical Commission*, [www. iec. ch/whitepaper/pdf/iecWP-gridintegrationlargecapacity-LR-en. pdf](http://www.iec.ch/whitepaper/pdf/iecWP-gridintegrationlargecapacity-LR-en.pdf) (last accessed March 2015), 2012.
- [2] Iec, “Grid integration of large-capacity renewable energy sources and use of large-capacity electrical energy storage,” *IEC, White Paper*, vol. 39, 2009.
- [3] M. Raugei and P. Frankl, “Life cycle impacts and costs of photovoltaic systems: Current state of the art and future outlooks,” *Energy*, vol. 34, no. 3, pp. 392 – 399, 2009. {WESC} 2006Advances in Energy Studies6th World Energy System Conference5th workshop on Advances, Innovation and Visions in Energy and Energy-related Environmental and Socio-Economic Issues.
- [4] M. A. Alqarni, *A High Efficiency Photovoltaic Inverter System Configuration with Maximum Power Point Tracking*. PhD thesis, Department of Electronic and Computer Engineering, College of Engineering, Design and Physical Science Brunel University London, UK, 2016.
- [5] F. D.-G. O. G.-B. . A. Sumper, *Energy storage in power systems*. John Wiley & Sons, 2016.
- [6] “Battery management an overview.” <http://www.battariat.com/en/Battery-Management/Overview>. Accessed: 2018-04-02.
- [7] J. B. Goodenough and A. Manthiram, “A perspective on electrical energy storage,” *MRS Communications*, vol. 4, no. 4, pp. 135 –142, 2014.
- [8] N. Kularatna, *Energy Storage Devices for Electronic Systems: Rechargeable Batteries and Supercapacitors*. Academic Press, 2014.

- [9] M. H. Rashid, *Power electronics handbook: devices, circuits and applications*. Academic press, 2010.
- [10] C. W. Lander, “8 dc machine control,” *Power Electronics (3rd ed.)*. London: Mc Graw Hill International UK. ISBN 0-07-707714-8, 1993.
- [11] H. Gualous, D. Bouquain, A. Berthon, and J. Kauffmann, “Experimental study of supercapacitor serial resistance and capacitance variations with temperature,” *Journal of power sources*, vol. 123, no. 1, pp. 86–93, 2003.
- [12] V. Sedlakova, J. Sikula, J. Majzner, P. Sedlak, T. Kuparowitz, B. Buegler, and P. Vasina, “Supercapacitor equivalent electrical circuit model based on charges redistribution by diffusion,” *Journal of Power Sources*, vol. 286, pp. 58 – 65, 2015.
- [13] S. Ban, J. Zhang, L. Zhang, K. Tsay, D. Song, and X. Zou, “Charging and discharging electrochemical supercapacitors in the presence of both parallel leakage process and electrochemical decomposition of solvent,” *Electrochimica Acta*, vol. 90, pp. 542–549, 2013.
- [14] P. Barrade, S. Pittet, and A. Rufer, “Energy storage system using a series connection of supercapacitors, with an active device for equalizing the voltages,” in *IPEC 2000: International Power Electronics Conference*, no. LEI-CONF-2005-044, 2000.
- [15] T. U. of Queensland Australia, “Daily instantaneous power from concentrating array at st lucia campus.” <http://solar.uq.edu.au/user/reportPower.php?pa=2-3&dtra=day&dts=2013-04-11&etp=n>, 2013. Online; accessed 6-June-2013.
- [16] Y. Kim and N. A. Ch Ang, *Design and management of energy-efficient hybrid electrical energy storage systems*. Springer International Publishing, 2014.
- [17] P. Thounthong, S. Rael, and B. Davat, “Energy management of fuel cell/battery/supercapacitor hybrid power source for vehicle applications,” *Journal of Power Sources*, vol. 193, no. 1, pp. 376–385, 2009.
- [18] B. Frenzel, P. Kurzweil, and H. Rönnebeck, “Electromobility concept for racing cars based on lithium-ion batteries and supercapacitors,” *Journal of Power Sources*, vol. 196, no. 12, pp. 5364–5376, 2011.

- [19] M. Chowdhury, M. Haque, M. Aktarujjaman, M. Negnevitsky, and A. Gargoom, "Grid integration impacts and energy storage systems for wind energy applicationsa review," in *Power and Energy Society General Meeting, 2011 IEEE*, pp. 1–8, IEEE, 2011.
- [20] A. Evans, V. Strezov, and T. J. Evans, "Assessment of utility energy storage options for increased renewable energy penetration," *Renewable and Sustainable Energy Reviews*, vol. 16, no. 6, pp. 4141–4147, 2012.
- [21] N. E. Mohammad Rozali, S. R. Wan Alwi, Z. A. Manan, J. J. Klemeš, and M. Y. Hassan, "A process integration approach for design of hybrid power systems with energy storage," *Clean Technologies and Environmental Policy*, vol. 17, no. 7, pp. 2055–2072, 2015.
- [22] Y. Kim, Y. Wang, N. Chang, M. Pedram, *et al.*, "Computer-aided design and optimization of hybrid energy storage systems," *Foundations and Trends® in Electronic Design Automation*, vol. 7, no. 4, pp. 247–338, 2013.
- [23] S. J. Kazempour, M. P. Moghaddam, M. Haghifam, and G. Yousefi, "Electric energy storage systems in a market-based economy: Comparison of emerging and traditional technologies," *Renewable energy*, vol. 34, no. 12, pp. 2630–2639, 2009.
- [24] M. Lu, F. Beguin, and E. Frackowiak, *Supercapacitors: materials, systems and applications*. John Wiley & Sons, 2013.
- [25] IPCC, "Climate change 2014: Mitigation of climate change," *Working Group III Contribution to the Fifth Assessment Report of the Intergovernmental Panel on Climate Change*, p. 1454, 2014.
- [26] A. Luque and S. Hegedus, *Handbook of photovoltaic science and engineering*. John Wiley & Sons, 2011.
- [27] A. R. Reisi, M. H. Moradi, and S. Jamasb, "Classification and comparison of maximum power point tracking techniques for photovoltaic system: A review," *Renewable and Sustainable Energy Reviews*, vol. 19, pp. 433 – 443, 2013.
- [28] S. Kouro, J. I. Leon, D. Vinnikov, and L. G. Franquelo, "Grid-connected photovoltaic systems: An overview of recent research and emerging pv converter technology," *IEEE Industrial Electronics Magazine*, vol. 9, pp. 47–61, March 2015.

- [29] F. Birol *et al.*, “World energy outlook,” *Paris: International Energy Agency*, 2008.
- [30] REN21, “100 % Renewable Energy Renewables Global Futures Report,” in *Great debates towards 100% renewable energy*, Paris, REN21 Secretariat, REN21. 2017.
- [31] T. Grau, M. Huo, and K. Neuhoff, “Survey of photovoltaic industry and policy in germany and china,” *Energy Policy*, vol. 51, pp. 20 – 37, 2012. Renewable Energy in China.
- [32] A. C. Robert Foster, Majid Ghassemi, *Solar Energy, Renewable Energy and the Environment*. CRC Press Taylor & Francis Group 6000 Broken Sound Parkway NW, Suite 300 Boca Raton, FL: CRC Press Taylor, 2010.
- [33] V. Fthenakis, S. Morris, P. Moskowitz, and D. Morgan, “Toxicity of cadmium telluride, copper indium diselenide, and copper gallium diselenide,” *Progress in Photovoltaics: Research and Applications*, vol. 7, no. 6, pp. 489–497, 1999.
- [34] A. Martí and A. Luque, *Next generation photovoltaics: High efficiency through full spectrum utilization*. CRC Press, 2003.
- [35] R. King, D. Bhusari, D. Larrabee, X.-Q. Liu, E. Rehder, K. Edmondson, H. Cotal, R. Jones, J. Ermer, C. Fetzer, *et al.*, “Solar cell generations over 40% efficiency,” *Progress in Photovoltaics: Research and Applications*, vol. 20, no. 6, pp. 801–815, 2012.
- [36] M. E. Glavin, P. K. W. Chan, S. Armstrong, and W. G. Hurley, “A stand-alone photovoltaic supercapacitor battery hybrid energy storage system,” in *2008 13th International Power Electronics and Motion Control Conference*, pp. 1688–1695, Sept 2008.
- [37] S. Vazquez, S. M. Lukic, E. Galvan, L. G. Franquelo, and J. M. Carrasco, “Energy storage systems for transport and grid applications,” *IEEE Transactions on Industrial Electronics*, vol. 57, pp. 3881–3895, Dec 2010.
- [38] V. V. Viswanathan and M. Kintner-Meyer, “Second use of transportation batteries: Maximizing the value of batteries for transportation and grid services,” *IEEE Transactions on Vehicular Technology*, vol. 60, pp. 2963–2970, Sept 2011.

- [39] J. Cao and A. Emadi, "A new battery/ultracapacitor hybrid energy storage system for electric, hybrid, and plug-in hybrid electric vehicles," *IEEE Transactions on Power Electronics*, vol. 27, pp. 122–132, Jan 2012.
- [40] Y. Kim, V. Raghunathan, and A. Raghunathan, "Design and management of battery-supercapacitor hybrid electrical energy storage systems for regulation services," *IEEE Transactions on Multi-Scale Computing Systems*, vol. 3, pp. 12–24, Jan 2017.
- [41] Y. Hou, R. Vidu, and P. Stroeve, "Solar energy storage methods," *Industrial & engineering chemistry research*, vol. 50, no. 15, pp. 8954–8964, 2011.
- [42] "Comparison of commercial supercapacitors and high-power lithium-ion batteries for power-assist applications in hybrid electric vehicles: I. initial characterization," *Journal of Power Sources*, vol. 112, no. 1, pp. 236 – 246, 2002.
- [43] V. Musolino, E. Tironi, and P. di Milano, "A comparison of supercapacitor and high-power lithium batteries," in *Electrical Systems for Aircraft, Railway and Ship Propulsion*, pp. 1–6, Oct 2010.
- [44] G. Xiong, A. Kundu, and T. S. Fisher, *Thermal effects in supercapacitors*. Springer, 05 2015.
- [45] D. M. Chapin, C. Fuller, and G. Pearson, "A new silicon p-n junction photocell for converting solar radiation into electrical power," *Journal of Applied Physics*, vol. 25, no. 5, pp. 676–677, 1954.
- [46] D. Reynolds, G. Leies, L. Antes, and R. Marburger, "Photovoltaic effect in cadmium sulfide," *Physical Review*, vol. 96, no. 2, p. 533, 1954.
- [47] D. Jenny, J. Loferski, and P. Rappaport, "Photovoltaic effect in gaas p- n junctions and solar energy conversion," *Physical Review*, vol. 101, no. 3, p. 1208, 1956.
- [48] M. Prince, "Silicon solar energy converters," *Journal of Applied Physics*, vol. 26, no. 5, pp. 534–540, 1955.
- [49] J. J. Loferski, "Theoretical considerations governing the choice of the optimum semiconductor for photovoltaic solar energy conversion," *Journal of Applied Physics*, vol. 27, no. 7, pp. 777–784, 1956.

- [50] J. J. Wysocki and P. Rappaport, "Effect of temperature on photovoltaic solar energy conversion," *Journal of Applied Physics*, vol. 31, no. 3, pp. 571–578, 1960.
- [51] W. Shockley and H. J. Queisser, "Detailed balance limit of efficiency of p-n junction solar cells," *Journal of applied physics*, vol. 32, no. 3, pp. 510–519, 1961.
- [52] M. Alahmad, M. Chaaban, and S.-K. Lau, "An adaptive photovoltaic-inverter topology," in *Innovative Smart Grid Technologies (ISGT), 2011 IEEE PES*, pp. 1–7, 2011.
- [53] K. Ishaque, Z. Salam, S. Mekhilef, and A. Shamsudin, "Parameter extraction of solar photovoltaic modules using penalty-based differential evolution," *Applied Energy*, vol. 99, no. 0, pp. 297 – 308, 2012.
- [54] S. J. Moura and Y. A. Chang, "Lyapunov-based switched extremum seeking for photovoltaic power maximization," *Control Engineering Practice*, vol. 21, no. 7, pp. 971 – 980, 2013.
- [55] I.-S. Kim and M.-J. Youn, "Variable-structure observer for solar-array current estimation in a photovoltaic power-generation system," *Electric Power Applications, IEE Proceedings -*, vol. 152, no. 4, pp. 953–959, 2005.
- [56] K. Il-Song, "Robust state estimator design for a solar battery charging system," *International Journal of Electronics*, vol. 96, no. 3, pp. 229–247, 2009.
- [57] F. Ghani, M. Duke, and J. Carson, "Numerical calculation of series and shunt resistance of a photovoltaic cell using the lambert w-function: Experimental evaluation," *Solar Energy*, vol. 87, no. 0, pp. 246 – 253, 2013.
- [58] R. Foster, M. Ghassemi, and A. Cota, *Solar energy: renewable energy and the environment*. CRC Press, 2009.
- [59] S. B. Kjaer, J. K. Pedersen, and F. Blaabjerg, "A review of single-phase grid-connected inverters for photovoltaic modules," *IEEE transactions on industry applications*, vol. 41, no. 5, pp. 1292–1306, 2005.
- [60] J. Schonberger, "A single phase multi-string pv inverter with minimal bus capacitance," in *Power Electronics and Applications, 2009. EPE'09. 13th European Conference on*, pp. 1–10, IEEE, 2009.

- [61] J. M. Myrzik and M. Calais, "String and module integrated inverters for single-phase grid connected photovoltaic systems-a review," in *Power Tech Conference Proceedings, 2003 IEEE Bologna*, vol. 2, pp. 8–pp, IEEE, 2003.
- [62] J. J. Bzura, "The ac module: An overview and update on self-contained modular pv systems," in *Power and Energy Society General Meeting, 2010 IEEE*, pp. 1–3, IEEE, 2010.
- [63] R. H. Wills, S. Krauthamer, A. Bulawka, and J. P. Posbic, "The ac photovoltaic module concept," in *Energy Conversion Engineering Conference, 1997. IECEC-97., Proceedings of the 32nd Intersociety*, vol. 3, pp. 1562–1563, IEEE, 1997.
- [64] M. Prudente, L. L. Pfitscher, G. Emmendoerfer, E. F. Romaneli, and R. Gules, "Voltage multiplier cells applied to non-isolated dc–dc converters," *IEEE Transactions on Power Electronics*, vol. 23, no. 2, pp. 871–887, 2008.
- [65] F. Wu, R. Li, L. Huang, H. Miao, and X. Li, "Theme evolution analysis of electrochemical energy storage research based on citnetexplorer," *Scientometrics*, vol. 110, no. 1, pp. 113–139, 2017.
- [66] R. Huggins, *Energy storage*. Springer Science & Business Media, 2010.
- [67] T. Mahlia, T. Saktisahdan, A. Jannifar, M. Hasan, and H. Matseelar, "A review of available methods and development on energy storage; technology update," *Renewable and Sustainable Energy Reviews*, vol. 33, pp. 532 – 545, 2014.
- [68] T. Crompton, *Battery reference book*, Newnes. Newnes, OXFORD, UK, 2000.
- [69] C. Naish, I. McCubbin, O. Edberg, and M. Harfoot, "Outlook of energy storage technologies," *European Parliament's committee on Industry, Research and Energy*, no. January 2004, 2008.
- [70] M. Perrin, P. Malbranche, F. Mattera, L. Simonin, D. U. Sauer, P. Lailier, A. Joessen, B. Willer, M. Dahlen, A. Ruddell, I. Cyphelly, N. Tassin, and M. Bruesewitz, "Evaluation and perspectives of storage technologies for pv electricity," in *3rd World Conference on Photovoltaic Energy Conversion, 2003. Proceedings of*, vol. 3, pp. 2194–2197 Vol.3, May 2003.
- [71] K. Divya and J. stergaard, "Battery energy storage technology for power systems - an overview," *Electric Power Systems Research*, vol. 79, no. 4, pp. 511 – 520, 2009.

- [72] A. Nourai, "Installation of the first distributed energy storage system (dessa) at american electric power (aep)," *Sandia Report SAND2007-3580*, 2007.
- [73] B. Espinar and D. Mayer, "Energy Storage for Mini-Grid Stabilization," *5th European PV-Hybrid and Mini-Grid Conference*, vol. 33, pp. 1–8, 2010.
- [74] C. Glaize and S. Genies, *Lithium batteries and other electrochemical storage systems*. John Wiley & Sons, 2013.
- [75] C. David, "A Review of Energy Storage Technologies for the Integration of Fluctuating Renewable Energy," no. August, pp. 1–46, 2009.
- [76] T. V. Nguyen and R. F. Savinell, "Flow batteries," *Electrochemical Society Interface*, vol. 19, no. 3, pp. 54–56, 2010.
- [77] S.-I. Inage, "Prospects for large-scale energy storage in decarbonised power grids," *International Energy Agency*, p. 90, 2009.
- [78] G. Wang, L. Zhang, and J. Zhang, "A review of electrode materials for electrochemical supercapacitors," *Chemical Society Reviews*, vol. 41, no. 2, pp. 797–828, 2012.
- [79] Q. Wu, Y. Xu, Z. Yao, A. Liu, and G. Shi, "Supercapacitors based on flexible graphene/polyaniline nanofiber composite films," *ACS nano*, vol. 4, no. 4, pp. 1963–1970, 2010.
- [80] J. Huang, B. G. Sumpter, and V. Meunier, "Theoretical model for nanoporous carbon supercapacitors," *Angewandte Chemie International Edition*, vol. 47, no. 3, pp. 520–524, 2008.
- [81] B. Ricketts and C. Ton-That, "Self-discharge of carbon-based supercapacitors with organic electrolytes," *Journal of Power Sources*, vol. 89, no. 1, pp. 64–69, 2000.
- [82] A. Lewandowski and M. Galinski, "Practical and theoretical limits for electrochemical double-layer capacitors," *Journal of Power Sources*, vol. 173, no. 2, pp. 822–828, 2007.
- [83] A. Lewandowski, A. Olejniczak, M. Galinski, and I. Stepniak, "Performance of carbon–carbon supercapacitors based on organic, aqueous and ionic liquid electrolytes," *Journal of Power Sources*, vol. 195, no. 17, pp. 5814–5819, 2010.

- [84] B. E. Conway, *Electrochemical supercapacitors: scientific fundamentals and technological applications*. Springer Science & Business Media, 2013.
- [85] S. Wu and Y. Zhu, “Highly densified carbon electrode materials towards practical supercapacitor devices,” *Science China Materials*, vol. 60, no. 1, pp. 25–38, 2017.
- [86] A. Yu, V. Chabot, and J. Zhang, *Electrochemical supercapacitors for energy storage and delivery: fundamentals and applications*. CRC Press, 2013.
- [87] D. Li, F. Meng, X. Yan, L. Yang, H. Heng, and Y. Zhu, “One-pot hydrothermal synthesis of Mn_3O_4 nanorods grown on Ni foam for high performance supercapacitor applications,” *Nanoscale Research Letters*, vol. 8, no. 1, p. 535, 2013.
- [88] V. Salas, E. Olas, A. Barrado, and A. Lzaro, “Review of the maximum power point tracking algorithms for stand-alone photovoltaic systems,” *Solar Energy Materials and Solar Cells*, vol. 90, no. 11, pp. 1555 – 1578, 2006.
- [89] P. S. S. Sumathi, L. Ashok Kumar, *Solar PV and Wind Energy Conversion Systems*. Springer, International Publishing Switzerland: Springer, 2015.
- [90] C. Tavares, K. Leite, W. Suemitsu, and M. Bellar, “Performance evaluation of photovoltaic solar system with different mppt methods,” in *Industrial Electronics, 2009. IECON '09. 35th Annual Conference of IEEE*, pp. 719–724, 2009.
- [91] J. Hu, J. Zhang, and H. Wu, “A novel mppt control algorithm based on numerical calculation for pv generation systems,” in *Power Electronics and Motion Control Conference, 2009. IPEMC '09. IEEE 6th International*, pp. 2103–2107, 2009.
- [92] T. Noguchi, S. Togashi, and R. Nakamoto, “Short-current pulse-based maximum-power-point tracking method for multiple photovoltaic-and-converter module system,” *Industrial Electronics, IEEE Transactions on*, vol. 49, no. 1, pp. 217–223, 2002.
- [93] “Maximum power point tracking techniques for photovoltaic systems: A comprehensive review and comparative analysis,” *Renewable and Sustainable Energy Reviews*, vol. 52, pp. 1504 – 1518, 2015.

- [94] A. Chikh and A. Chandra, "Voltage and frequency controller for a stand alone pv system with battery storage element," in *IECON 2012 - 38th Annual Conference on IEEE Industrial Electronics Society*, pp. 1172–1177, 2012.
- [95] P.-C. Chen, P.-Y. Chen, Y.-H. Liu, J.-H. Chen, and Y.-F. Luo, "A comparative study on maximum power point tracking techniques for photovoltaic generation systems operating under fast changing environments," *Solar Energy*, vol. 119, pp. 261 – 276, 2015.
- [96] F. Liu, S. Duan, F. Liu, B. Liu, and Y. Kang, "A variable step size inc mppt method for pv systems," *Industrial Electronics, IEEE Transactions on*, vol. 55, no. 7, pp. 2622–2628, 2008.
- [97] V. Salas, E. Olas, A. Barrado, and A. Lzaro, "Review of the maximum power point tracking algorithms for stand-alone photovoltaic systems," *Solar Energy Materials and Solar Cells*, vol. 90, no. 11, pp. 1555 – 1578, 2006.
- [98] C.-L. Hou, J. Wu, M. Zhang, J.-M. Yang, and J.-P. Li, "Application of adaptive algorithm of solar cell battery charger," in *Electric Utility Deregulation, Restructuring and Power Technologies, 2004.(DRPT 2004). Proceedings of the 2004 IEEE International Conference on*, vol. 2, pp. 810–813, IEEE, 2004.
- [99] R. Bhide and S. Bhat, "Modular power conditioning unit for photovoltaic applications," in *Power Electronics Specialists Conference, 1992. PESC'92 Record., 23rd Annual IEEE*, pp. 708–713, IEEE, 1992.
- [100] N. Khaehintung, K. Pramotung, B. Tuvirat, and P. Sirisuk, "Risc-microcontroller built-in fuzzy logic controller of maximum power point tracking for solar-powered light-flasher applications," in *Industrial Electronics Society, 2004. IECON 2004. 30th Annual Conference of IEEE*, vol. 3, pp. 2673–2678, IEEE, 2004.
- [101] R. Ramaprabha, B. Mathur, and M. Sharanya, "Solar array modeling and simulation of mppt using neural network," in *Control, Automation, Communication and Energy Conservation, 2009. INCACEC 2009. 2009 International Conference on*, pp. 1–5, IEEE, 2009.
- [102] M. C. Di Piazza, M. Pucci, A. Ragusa, and G. Vitale, "A growing neural gas network based mppt technique for multi-string pv plants," in *Industrial Electronics (ISIE), 2010 IEEE International Symposium on*, pp. 544–549, IEEE, 2010.

- [103] X. Li, Y. Li, J. E. Seem, and P. Lei, "Maximum power point tracking for photovoltaic systems using adaptive extremum seeking control," in *ASME 2011 Dynamic Systems and Control Conference and Bath/ASME Symposium on Fluid Power and Motion Control*, pp. 803–810, American Society of Mechanical Engineers, 2011.
- [104] A. Mathew and A. I. Selvakumar, "Mppt based stand-alone water pumping system," in *Computer, Communication and Electrical Technology (ICCCET), 2011 International Conference on*, pp. 455–460, IEEE, 2011.
- [105] M. Veerachary, T. Senjyu, and K. Uezato, "Neural-network-based maximum-power-point tracking of coupled-inductor interleaved-boost-converter-supplied pv system using fuzzy controller," *IEEE Transactions on Industrial Electronics*, vol. 50, no. 4, pp. 749–758, 2003.
- [106] M. D. Singh, V. Shine, and V. Janamala, "Application of artificial neural networks in optimizing mppt control for standalone solar pv system," in *Contemporary Computing and Informatics (IC3I), 2014 International Conference on*, pp. 162–166, IEEE, 2014.
- [107] T. Eswam and P. L. Chapman, "Comparison of photovoltaic array maximum power point tracking techniques," *IEEE Transactions on energy conversion*, vol. 22, no. 2, pp. 439–449, 2007.
- [108] H. H. Lee, P. Q. Dzung, N. T. D. Vu, *et al.*, "The new maximum power point tracking algorithm using ann-based solar pv systems," in *TENCON 2010-2010 IEEE Region 10 Conference*, pp. 2179–2184, IEEE, 2010.
- [109] L. M. Elobaid, A. K. Abdelsalam, and E. E. Zakzouk, "Artificial neural network-based photovoltaic maximum power point tracking techniques: a survey," *IET Renewable Power Generation*, vol. 9, no. 8, pp. 1043–1063, 2015.
- [110] A. Z. Alabedin, E. El-Saadany, and M. Salama, "Maximum power point tracking for photovoltaic systems using fuzzy logic and artificial neural networks," in *Power and Energy Society General Meeting, 2011 IEEE*, pp. 1–9, IEEE, 2011.
- [111] H. Abu-Rub, A. Iqbal, S. M. Ahmed, F. Z. Peng, Y. Li, and G. Baoming, "Quasi-z-source inverter-based photovoltaic generation system with maximum power tracking control using anfis," *IEEE Transactions on Sustainable Energy*, vol. 4, pp. 11–20, Jan 2013.

- [112] P. Sekhar, S. Mishra, and R. Sharma, "Data analytics based neuro-fuzzy controller for diesel-photovoltaic hybrid ac microgrid," *IET Generation, Transmission & Distribution*, vol. 9, no. 2, pp. 193–207, 2015.
- [113] F. Mocci and M. Tosi, "Comparison of power converter technologies in photovoltaic applications," in *Electrotechnical Conference, 1989. Proceedings. 'Integrating Research, Industry and Education in Energy and Communication Engineering', MELECON '89., Mediterranean*, pp. 11–15, Apr 1989.
- [114] M. K. Kazimierczuk, *Pulse-width modulated DC-DC power converters*. John Wiley & Sons, 2015.
- [115] D. Petreus, T. Patarau, S. Daraban, C. Morel, and B. Morley, "A novel maximum power point tracker based on analog and digital control loops," *Solar Energy*, vol. 85, no. 3, pp. 588 – 600, 2011.
- [116] K. H. Sueker, *Power Electronics Design: A Practitioners Guide*. Newnes is an imprint of Elsevier 30 Corporate Drive, Suite 400, Burlington, MA 01803, USA Linacre House, Jordan Hill, Oxford OX2 8DP, UK: Newnes, 2005.
- [117] D. W. Hart, *Power electronics*. Tata McGraw-Hill Education, 2011.
- [118] A. Khalifa and E. El-Saadany, "Control of three phase grid-connected photovoltaic arrays with open loop maximum power point tracking," in *Power and Energy Society General Meeting, 2011 IEEE*, pp. 1–8, July 2011.
- [119] J. S. Kumari, C. S. Babu, *et al.*, "Comparison of maximum power point tracking algorithms for photovoltaic system," *International Journal of Advances in Engineering & Technology*, vol. 1, no. 5, pp. 133–148, 2011.
- [120] S. Yuvarajan and S. Xu, "Photo-voltaic power converter with a simple maximum-power-point-tracker," in *Circuits and Systems, 2003. ISCAS'03. Proceedings of the 2003 International Symposium on*, vol. 3, pp. III–III, IEEE, 2003.
- [121] M. S. Ngan and C. W. Tan, "A study of maximum power point tracking algorithms for stand-alone photovoltaic systems," in *Applied Power Electronics Colloquium (IAPEC), 2011 IEEE*, pp. 22–27, 2011.

- [122] B. W. Williams, "Power electronics: Devices, drivers, and applications," 1987.
- [123] W. P. Ned Mohan, Tore M. Undeland, *Power Electronics converters, Applications, and design, Second Edition*. The Atrium Southern Gate, Chichester West Sussex PO19 8SQ England: John Wiley & Sons, INC, 2003.
- [124] M. H. Rashid, *Power Electronics Handbook*. A Harcourt Science and Technology Company 525 B Street, Suite 1900, San Diego, California 92101-4495, USA: Academic Press USA, 2001.
- [125] D. M. R.W. Erickson, *Fundamentals of power electronics*. Springer Science+Business Media UK Ltd, London: Springer, 2001.
- [126] P. C. Todd, "Snubber circuits: Theory, design and application," in *Unitrode Switching Regulated Power Supply Design Seminar Manual, SEM-900*. Unitrode, 1993.
- [127] W. McMurray, "Selection of snubbers and clamps to optimize the design of transistor switching converters," in *Power Electronics Specialists Conference, 1979 IEEE*, pp. 62–74, IEEE, 1979.
- [128] Q. Zhang, "Optimization and design of photovoltaic micro-inverter," 2013.
- [129] Y. Zhong, J. Zhang, G. Li, and A. Liu, "Research on energy efficiency of supercapacitor energy storage system," in *2006 International Conference on Power System Technology*, pp. 1–4, Oct 2006.
- [130] S. Castano, L. Gauchia, and J. Sanz-Feito, "Effect of packaging on supercapacitors strings modeling: Proposal of functional unit defined around balancing circuit," *IEEE Transactions on Components, Packaging and Manufacturing Technology*, vol. 3, pp. 1390–1398, Aug 2013.
- [131] L. Shi and M. Crow, "Comparison of ultracapacitor electric circuit models," in *Power and Energy Society General Meeting-Conversion and Delivery of Electrical Energy in the 21st Century, 2008 IEEE*, pp. 1–6, IEEE, 2008.
- [132] L. Zubieta and R. Bonert, "Characterization of double-layer capacitors for power electronics applications," *IEEE Transactions on Industry Applications*, vol. 36, pp. 199–205, Jan 2000.

- [133] M. Corley, J. Locker, S. Dutton, and R. Spee, "Ultracapacitor-based ride-through system for adjustable speed drives," in *Power Electronics Specialists Conference, 1999. PESC 99. 30th Annual IEEE*, vol. 1, pp. 26–31, IEEE, 1999.
- [134] A. Rufer and P. Barrade, "A supercapacitor-based energy-storage system for elevators with soft commutated interface," *IEEE transactions on industry applications*, vol. 38, no. 5, pp. 1151–1159, 2002.
- [135] P. Sharma and T. Bhatti, "A review on electrochemical double-layer capacitors," *Energy Conversion and Management*, vol. 51, no. 12, pp. 2901 – 2912, 2010.
- [136] T. Wei, X. Qi, and Z. Qi, "An improved ultracapacitor equivalent circuit model for the design of energy storage power systems," in *2007 International Conference on Electrical Machines and Systems (ICEMS)*, pp. 69–73, Oct 2007.
- [137] R. De Levie, "On porous electrodes in electrolyte solutions: I. capacitance effects," *Electrochimica Acta*, vol. 8, no. 10, pp. 751–780, 1963.
- [138] B. E. Conway, *Electrochemical Supercapacitors Scientific Fundamentals and Technological Applications*. Plenum Publishing Co., New York, 1999.
- [139] R. De Levie, "Electrochemical response of porous and rough electrodes," *Advances in electrochemistry and electrochemical engineering*, vol. 6, pp. 329–397, 1967.
- [140] E. Karden, S. Buller, and R. W. De Doncker, "A frequency-domain approach to dynamical modeling of electrochemical power sources," *Electrochimica Acta*, vol. 47, no. 13, pp. 2347–2356, 2002.
- [141] H. Miniguano, A. Barrado, C. Raga, A. Lzaro, C. Fernandez, and M. Sanz, "A comparative study and parameterization of supercapacitor electrical models applied to hybrid electric vehicles," in *2016 International Conference on Electrical Systems for Aircraft, Railway, Ship Propulsion and Road Vehicles International Transportation Electrification Conference (ESARS-ITEC)*, pp. 1–6, Nov 2016.
- [142] Y. Parvini, J. B. Siegel, A. G. Stefanopoulou, and A. Vahidi, "Supercapacitor electrical and thermal modeling, identification, and validation for a wide range of temperature and power

- applications,” *IEEE Transactions on Industrial Electronics*, vol. 63, pp. 1574–1585, March 2016.
- [143] C. Pean, B. Rotenberg, P. Simon, and M. Salanne, “Multi-scale modelling of supercapacitors: From molecular simulations to a transmission line model,” *Journal of Power Sources*, vol. 326, pp. 680–685, 2016.
- [144] R. L. Spyker and R. M. Nelms, “Classical equivalent circuit parameters for a double-layer capacitor,” *IEEE Transactions on Aerospace and Electronic Systems*, vol. 36, pp. 829–836, Jul 2000.
- [145] D. L. Chapman, “Li. a contribution to the theory of electrocapillarity,” *The London, Edinburgh, and Dublin philosophical magazine and journal of science*, vol. 25, no. 148, pp. 475–481, 1913.
- [146] M. Gouy, “Sur la constitution de la charge électrique à la surface d’un électrolyte,” *J. Phys. Theor. Appl.*, vol. 9, no. 1, pp. 457–468, 1910.
- [147] D. Linzen, S. Buller, E. Karden, and R. W. De Doncker, “Analysis and evaluation of charge-balancing circuits on performance, reliability, and lifetime of supercapacitor systems,” *IEEE transactions on industry applications*, vol. 41, no. 5, pp. 1135–1141, 2005.
- [148] P. Sharma and T. Bhatti, “A review on electrochemical double-layer capacitors,” *Energy Conversion and Management*, vol. 51, no. 12, pp. 2901–2912, 2010.
- [149] K. Sehil and M. Darwish, “Critical analysis of power conversion topologies for stand-alone pv systems with super-capacitor,” *International Journal of Computers and Applications*, vol. 39, no. 4, pp. 179–188, 2017.
- [150] K. Sehil and M. Darwish, “Effective power management in stand-alone pv system,” in *53rd International Universities Power Engineering Conference, UPEC 2018*, Sep 2018.
- [151] S. Christine, *Wind and Pumped-Hydro Power Storage : Determining Optimal Commitment Policies with Knowledge Gradient Non-Parametric Estimation*. PhD thesis, 2010.

- [152] A. Gonzalez, B. Gallachoir, E. McKeogh, and K. Lynch, "Study of electricity storage technologies and their potential to address wind energy intermittency in Ireland," *Sustainable Energy Ireland*, 2004.
- [153] I. Arsie, V. Marano, M. Moran, G. Rizzo, and G. Savino, "Optimal management of a wind/caes power plant by means of neural network wind speed forecast," in *European Wind Energy Conference and Exhibition, The European Wind Energy Association (EWEA), Milan, May 7*, vol. 10, 2007.
- [154] Z. Kohari and I. Vajda, "Losses of flywheel energy storages and joint operation with solar cells," *Journal of Materials Processing Technology*, vol. 161, pp. 62 – 65, 2005. 3rd Japanese-Mediterranean Workshop on Applied Electromagnetic Engineering for Magnetic and Superconducting Materials and 3rd Workshop on Superconducting Flywheels.
- [155] L. Truong, F. Wolff, N. Dravid, and P. Li, "Simulation of the interaction between flywheel energy storage and battery energy storage on the international space station," *Proceedings of the Intersociety Energy Conversion Engineering Conference*, vol. 2, pp. 848–854, 2000.
- [156] T. J. Pieronek, D. K. Decker, and V. A. Spector, "Spacecraft flywheel systems-benefits, and issues," in *Proceedings of the IEEE 1997 National Aerospace and Electronics Conference. NAECON 1997*, vol. 2, pp. 589–593 vol.2, Jul 1997.
- [157] G. Ries and H.-W. Neumueller, "Comparison of energy storage in flywheels and {SMES}," *Physica C: Superconductivity*, vol. 357360, Part 2, pp. 1306 – 1310, 2001.
- [158] *Thermal Energy Storage*, no. November 2008, (Berlin, Germany), 2008.

Appendix A

Extra Storage types in Power System

1. **Mechanical storage systems:** This type of storage mostly combined with grid connection, three types of storage can be illustrated under this category which are:

- **Pumped hydro storage:** Two water reservoirs been used at different elevations to pump water during off-peak hours from the lower to the upper reservoir (charging). And when required, the water flows back from the upper to the lower reservoir, powering a turbine with a generator to produce electricity (discharging), The energy stored is proportional to the volume of water in the upper reservoir and the height of the waterfall. However, its efficiency between 70% & 85%, has very long lifetime and practically unlimited cycle stability of the installation and has a large capacity comparing to other mechanical storage system. Main drawbacks are the dependence on topographical conditions, large land use and also is the need to wait prior to reversing direction from charge to discharge as a result waiting period of several minutes every time the operating mode change. However, is the most used technology for high-power applications [5, 151].
- **Compressed air energy storage (CAES):** Introduced in 1970 to provide load following and to meet the electrical energy peak demand. Energy is stored in the form of compressed air in an underground storage cavern, at pressures between 40 – 70 bar at near-ambient temperature or to store the air in above-ground tanks [5]. When needed the compressed air is mixed with natural gas, burned and expanded in a modified gas turbine. However, this system able to produce electricity three times larger than a conventional gas turbine for a same amount of fuel [75], and In addition, fast reaction time usually less than 10min

and capable to undertake frequent start-up and shut down [152]. In other-hand The overall system coupled with other energy sources may increase the total cost of investment due to the complexity of the large plant [153]. Due to the use of natural gas to heat the incoming air before entering the turbine the technology is not free from producing carbon footprint [67]. Fig(A.1) show this storage technique.

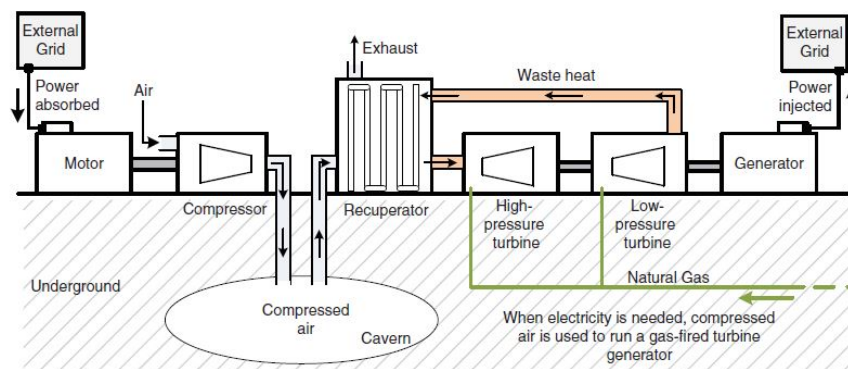


Fig. A.1: The operating principle of compressed air energy storage [5]

- **Flywheel energy storage:** Is a method of storing mechanical kinetic energy by accelerated rotor , to a massive rotating cylinder at a very high speed. It made up of a central shaft that holds a rotor and a flywheel. This central shaft rotates on two magnetic bearings to reduce friction. These are all contained within a vacuum to reduce aerodynamic drag losses. However, The energy is maintained in the flywheel by keeping the rotating body at a constant speed. An increase in the speed results in a higher amount of energy stored and decreases of the speed stored energy is distracted to the load. Furthermore, The energy capacity of the system is thus limited by the maximum and minimum operating speeds of the flywheel and the power capacity is limited by the maximum torque produced at the shaft of the electrical machine, which is directly translated into an electric current as the Fig(A.2) illustrated. However, The main advantage of flywheels are the excellent cycle stability and a long life cycle (up to 10^7 cycles, low maintenance cost,high efficiency (around 90% at rated power), high power density, free from depth of discharge effects, wide operating temperature and the use of environmentally inert material.In other-hand, flywheels have a high level of self-discharge due to air resistance and bearing losses and suffer from low current efficiency [154–157].

$$E_{fw} = \frac{1}{2}J\omega^2 = \frac{1}{2}m_f v_{circular}^2 = m_f \frac{\sigma}{\rho} \quad (\text{A.1})$$

where $J[\text{kgm}^2]$ is the inertia of the rotating parts, that is, the flywheel itself and the rotor of the machine to which it is connected and $\omega[\text{rad/s}]$ is the rotational speed, m_f is mass of the flywheel in kg , σ the specific strength of the material in Nm/kg , ρ of the material in kg/m^3 , $v_{circular}$ is the circular velocity of the flywheel in m/s^2 .

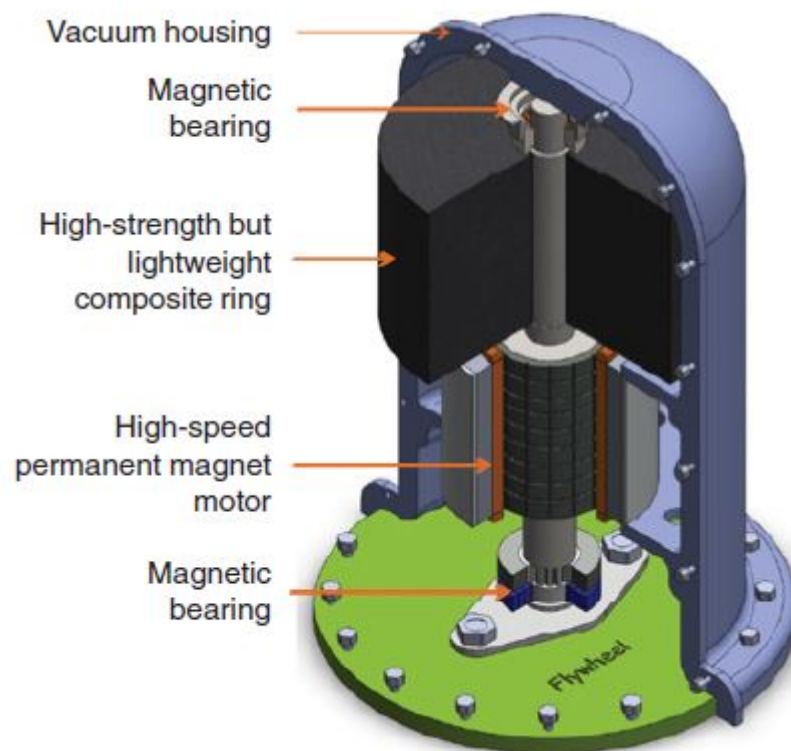


Fig. A.2: The illustrative topology of a flywheel-based ESS

2. **Thermal storage systems:** Store available heat by different means in an insulated repository for later use in different industrial and residential applications, such as space heating or cooling, hot water production or electricity generation [158]. This storage system is convenient for plants primarily produce heat, and this can be stored easily before conversion to electricity.
3. **Chemical energy storage:** The main purpose of such a chemical energy storage system is to use surplus electricity to produce hydrogen via water electrolysis. Once hydrogen is produced different ways are available for using it as an energy carrier, either as pure hydrogen or as

synthetic natural gas. Although the overall efficiency of hydrogen and synthetic natural gas is low compare to other storage techniques, cell voltage of around $0.8V$, efficiency 42%, storage systems $100MWh/10MW$.

	Power rating	Discharge duration	Response time	Efficiency	Parasitic losses	Lifetime	Maturity
Pumped hydro	100 – 4000MW	4 – 12 h	sec – min	0.7 – 0.85	evaporation	30 y	commercial
CAES (in reservoirs)	100 – 300MW	6 – 20 h	sec – min	0.64	-	30 y	commercial
CAES (in vessels)	50 – 100MW	1 – 4 h	sec – min	0.57	-	30 y	concept
Flywheels (low speed)	< 1650 kW	3 – 120 s	< 1 cycle	0.9	~1%	20 y	commercial products
Flywheels (high speed)	< 750 kW	< 1 h	< 1 cycle	0.93	~3%	20 y	prototypes in testing
Super-capacitors	< 100 kW	< 1 m	< 1/4 cycle	0.95	-	10,000 cycles	some commercial products
SMES (Micro)	10 kW – 10MW	1 s – 1 m	< 1/4 cycle	0.95	~4%	30 y	commercial
SMES	10 – 10MW	1 m – 30 m	< 1/4 cycle	0.95	~1%	30 y	design concept
Lead-acid battery	< 50MW	1 m – 8 h	< 1/4 cycle	0.85	small	5 – 10 y	commercial
NaS battery	< 10MW	< 8 h	n/a	0.75 – 0.86	5 kW/kWh	5 y	in development
ZnBr flow battery	< 1MW	< 4 h	< 1/4 cycle	0.75*	small	2,000 cycles	in test / commercial units
V redox flow battery	< 3MW	< 10 h	n/a	70 – 85*	n/a	10 y	in test
Poly sulphide Br flow battery	< 15MW	< 20 h	n/a	60 – 75*	n/a	2,000 cycles	in test
Hydrogen (Fuel Cell)	< 250 kW**	as needed	< 1/4 cycle	0.34 – 0.40*	n/a	10 – 20 y	in test
Hydrogen (Engine)	< 2MW**	as needed	seconds	0.29 – 0.33*	n/a	10 – 20 y	available for demonstration

*AC-AC efficiency

**Discharge device. An independent charging device (electrolyser) is required

Fig. A.3: Characteristics of storage technologies

Appendix B

Super-Capacitor Model In MATLAB

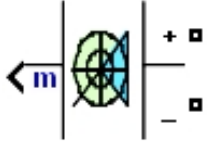
Supercapacitor

Implement generic supercapacitor model

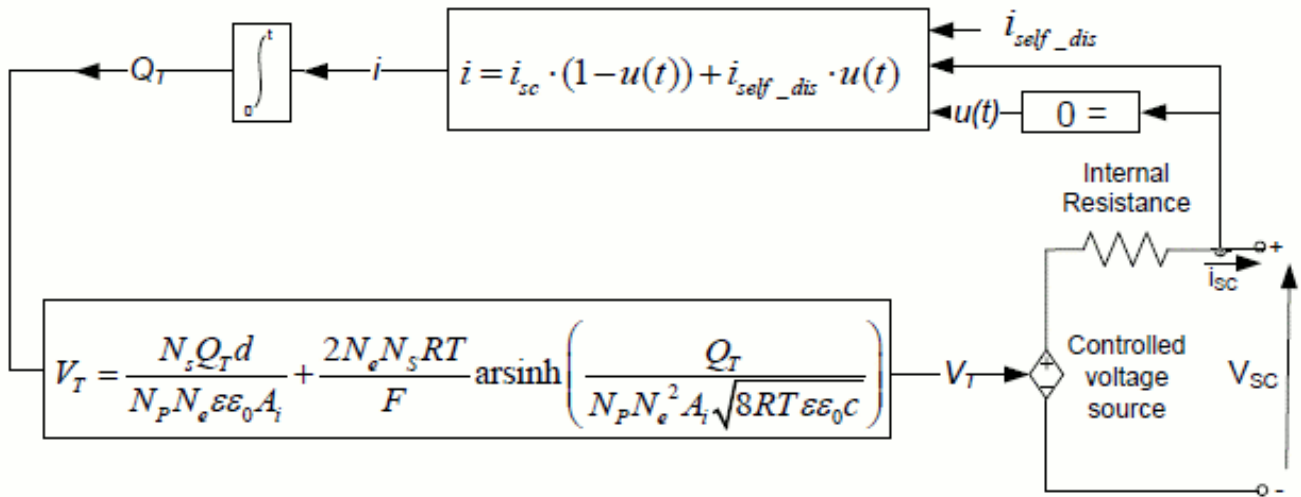
Library

Electric Drives/Extra Sources

Description



The Supercapacitor block implements a generic model parameterized to represent most popular types of supercapacitors. The figure shows the equivalent circuit of the supercapacitor:



The supercapacitor output voltage is expressed using a Stern equation as:

$$V_{SC} = \frac{N_s Q_T d}{N_p N_e \epsilon \epsilon_0 A_i} + \frac{2 N_e N_s R T}{F} \sinh^{-1} \left(\frac{Q_T}{N_p N_e^2 A_i \sqrt{8 R T \epsilon \epsilon_0 C}} \right) - R_{SC} \cdot i_{SC}$$

with

$$Q_T = \int i_{SC} dt$$

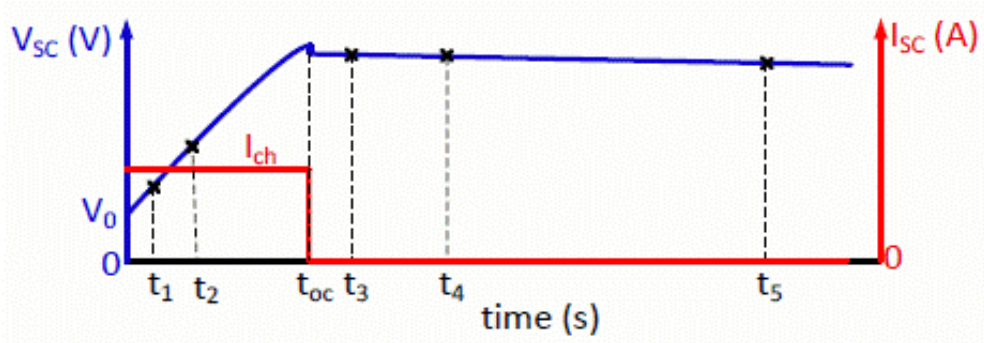
To represent the self-discharge phenomenon, the supercapacitor electric charge is modified as follows (when $i_{SC} = 0$):

$$Q_T = \int i_{self_dis} dt$$

where

$$i_{self_dis} = \begin{cases} \frac{C_T \alpha_1}{1 + s R_{SC} C_T} & \text{if } t - t_{oc} \leq t_3 \\ \frac{C_T \alpha_2}{1 + s R_{SC} C_T} & \text{if } t_3 < t - t_{oc} \leq t_4 \\ \frac{C_T \alpha_3}{1 + s R_{SC} C_T} & \text{if } t - t_{oc} > t_4 \end{cases}$$

The constants α_1 , α_2 , and α_3 are the rates of change of the supercapacitor voltage during time intervals (t_0, t_1) , (t_1, t_2) , (t_2, t_3) , (t_3, t_4) , and (t_4, t_5) respectively, as shown in the figure:



Variable	Description
A_i	Interfacial area between electrodes and electrolyte (m^2)
c	Molar concentration (mol/m^3) equal to $c = 1/(8N_A r^3)$
r	Molecular radius (m)
F	Faraday constant
i_{sc}	Supercapacitor current (A)
V_{sc}	Supercapacitor voltage (V)
C_T	Total capacitance (F)
R_{sc}	Total resistance (ohms)
N_e	Number of layers of electrodes
N_A	Avogadro constant
N_p	Number of parallel supercapacitors
N_s	Number of series supercapacitors
Q_T	Electric charge (C)
R	Ideal gas constant
d	Molecular radius
T	Operating temperature (K)
ϵ	Permittivity of material
ϵ_0	Permittivity of free space

Dialog Box and Parameters

Parameters Tab

Block Parameters: Supercapacitor

Supercapacitor (mask)

Implements a generic supercapacitor model which allows the simulation of Electric Double Layer Capacitors (EDLCs)

Parameters | Stern | Self-discharge

Rated capacitance (F)
99.5

Equivalent DC series resistance (Ohms)
8.9e-3

Rated voltage (V)
48

Number of series capacitors
18

Number of parallel capacitors
1

Initial voltage (V)
0

Operating temperature (Celsius)
25

OK Cancel Help Apply

Rated capacitance (F)

Specify the nominal capacitance of the supercapacitor, in farad.

Equivalent DC series resistance (Ohms)

Specify the internal resistance of the supercapacitor, in ohms.

Rated voltage (V)

Specify the rated voltage of the supercapacitor, in volts. Typical rated voltage is equal to 2.7 V.

Number of series capacitors

Specify the number of series capacitors to be represented.

Number of parallel capacitors

Specify the number of parallel capacitors to be represented.

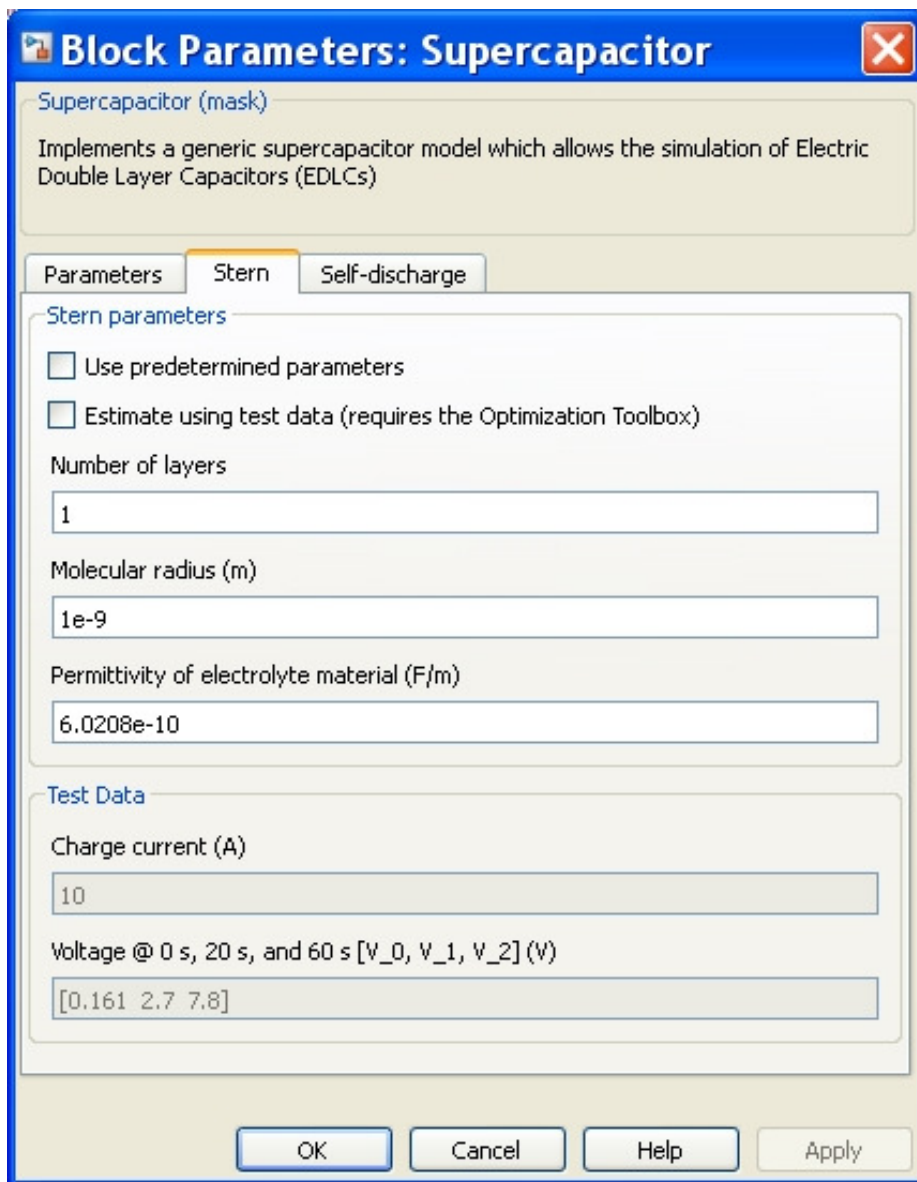
Initial voltage (V)

Specify the initial voltage of the supercapacitor, in volts.

Operating temperature (celsius)

Specify the operating temperature of the supercapacitor. The nominal temperature is 25° C.

Stern Tab



Use predetermined parameters

When this check box is selected, loads predetermined parameters of the Stern model into the mask of the block. These parameter values have been determined from experimental tests, and they can be used as default values to represent a common supercapacitor. Experimental validation of the model has shown a maximum error of 2% for charge and discharge when using the predetermined parameters.

When this check box is selected, the **Number of layers**, **Molecular radius (m)**, **Permittivity of electrolyte material (F/m)**, and **Estimate using test data** parameters appear dimmed.

Estimate using test data

When this check box is selected, you provide test data required for the estimation of the Stern model parameters. This parameter is available only if the Optimization Toolbox™ of MATLAB® is installed.

When this check box is selected, the **Charge current (A)** and **Voltage @ 0 s, 20 s, and 60 s [V_0, V_2, V_3] (V)** parameters are enabled. The **Use predetermined parameters**, **Number of layers**, **Molecular radius (m)**, and **Permittivity of electrolyte material (F/m)** parameters appear dimmed.

Number of layers

Specify the number of layers related to the Stern model.

Molecular of radius (m)

Specify the molecular radius related to the Stern model, in meters.

Permittivity of electrolyte material (F/m)

Specify the permittivity of the electrolyte material, in farad/meter.

Charge current (A)

Specify the charge current during a constant current charge test, in amperes.

Voltage @ 0 s, 20 s, and 60 s [V_0, V_2, V_3] (V)

Specify the supercapacitor voltage, in volts, at 0 s, 20 s, and 60 s, when the supercapacitor is charged with a constant current equal to the value provided in the **Charge current (A)** parameter.

Self-discharge Tab

Block Parameters: Supercapacitor

Supercapacitor (mask)
Implements a generic supercapacitor model which allows the simulation of Electric Double Layer Capacitors (EDLCs)

Parameters Stern **Self-discharge**

Discharge

Simulate self-discharge

Current prior open-circuit (A)
10

Voltage @ 0 s, 10 s, 100 s, and 1000 s [V_{oc}, V₃, V₄, V₅] (V)
[48 47.8 47.06 44.65]

Charge

Plot charge characteristics

Charge current [i₁, i₂, i₃, ...] (A)
[10 20 100 500]

Time units sec

OK Cancel Help Apply

Simulate self-discharge

When this check box is selected, you provide test data required for modeling the self-discharge phenomenon.

Current prior open-circuit (A)

Specify the current prior to an open-circuit event, in amperes.

Voltage @ 0 s, 10 s, 100 s, and 1000 s [V_{oc}, V₃, V₄, V₅] (V)

Specify the supercapacitor voltage, in volts, at 0 s, 10 s, 100 s, and at 1000 s, when the supercapacitor is open-circuit. The corresponding current prior to open-circuit is given in the **Current prior open-circuit (A)** parameter.

Plot charge characteristics

When this check box is selected, the block plots a figure containing the charge curves at the specified charge currents and time units.

Charge current [i₁, i₂, i₃, ...] (A)

Specify the charge currents, in amperes, used to plot the charge characteristics.

Time units

Specify the time units (seconds, minutes, hours) used to plot the charge characteristics.

Inputs and Outputs

m

Outputs a vector containing measurement signals. You can demultiplex these signals using the [Bus Selector](#) block.

Signal	Definition	Units	Symbol
1	The supercapacitor current	A	Current
2	The supercapacitor voltage	V	Voltage
3	The state of charge (SOC), between 0 and 100	%	SOC

The SOC for a fully charged supercapacitor is 100% and for an empty supercapacitor is 0%. The SOC is calculated as:

$$SOC = \frac{Q_{init} - \int_0^t i(\tau) d\tau}{Q_T} \times 100$$

Model Assumptions

- Internal resistance is assumed constant during the charge and the discharge cycles.
- The model does not take into account temperature effect on the electrolyte material.
- No aging effect is taken into account.
- Charge redistribution is the same for all values of voltage.
- The block does not model cell balancing.
- Current through the supercapacitor is assumed to be continuous.

Example

The [parallel_battery_SC_boost_converter](#) example shows a simple hybridization of a supercapacitor with a battery. The supercapacitor is connected to a buck/boost converter and the battery is connected to a boost converter. The DC bus voltage is equal to 42V. The converters are doing power management. The battery power is limited by a rate limiter block, therefore the transient power is supplied to the DC bus by the supercapacitor.

References

[1] Oldham, K. B. "A Gouy-Chapman-Stern model of the double layer at a (metal)/(ionic liquid) interface." *J. Electroanalytical Chem.* Vol. 613, No. 2, 2008, pp. 131–38.

[2] Xu, N., and J. Riley. "Nonlinear analysis of a classical system: The double-layer capacitor." *Electrochemistry Communications.* Vol. 13, No. 10, 2011, pp. 1077–81.

FEATURES

- » High performance product with low RC time constant
- » Long lifetimes with over 1,000,000 duty cycles
- » Rated capacitance of 3000F
- » Threaded terminals for easy integration
- » Compliant with RoHS and REACH requirements



* Image is not to scale

SPECIFICATIONS

Electrical		ESHSR-3000C0-002R7A5T
Rated Voltage (V_R) at 65°C		2.7 VDC
Surge Voltage ¹		2.85 VDC
Rated Capacitance ²		3000 F
Capacitance Tolerance	Max.	-0% / +20%
	Avg. ⁴	+5% / +12%
DC-ESR, Initial ³	Max.	0.26 mΩ
	Avg. ⁴	0.14 mΩ
Max. Leakage Current ⁵		5.2 mA
Maximum Continuous Current	at $\Delta T = 15^\circ\text{C}$	148 A
	at $\Delta T = 40^\circ\text{C}$	243 A
Maximum Peak Current, Non-repetitive ⁶		2,270 A
Max. Stored Energy (E_{max}) at V_R ⁷		3.03 Wh
Usable Specific Power ⁷		6.28 kW/kg
Impedance Match Specific Power ⁷		13.10 kW/kg
Max. Gravimetric Specific Energy ⁷		5.67 Wh/kg

Temperature	
Operating Temperature Range	-40 ~ 65°C (up to 85°C with de-rated voltage) ($\Delta\text{CAP} < 5\%$ and $\Delta\text{ESR} < 100\%$ of initial value measured at 25°C, with linear voltage de-rating to 2.3V @ 85°C)
Storage Temperature Range	-40 ~ 70°C (storage without charge)

Life	
Endurance (at 65°C, 2.7V) ^{8,9}	2,500 hours
Room Temperature (at V_R and 25°C) ⁸	10 years
Cycle Life (at 25°C) ⁸	1,000,000 cycles (Cycled from V_R to $1/2V_R$ using 100mA/F constant current with 10 second rest between charge and discharge steps)
Shelf Life	2 years (Stored without charge at or under 70°C and under 40% RH)

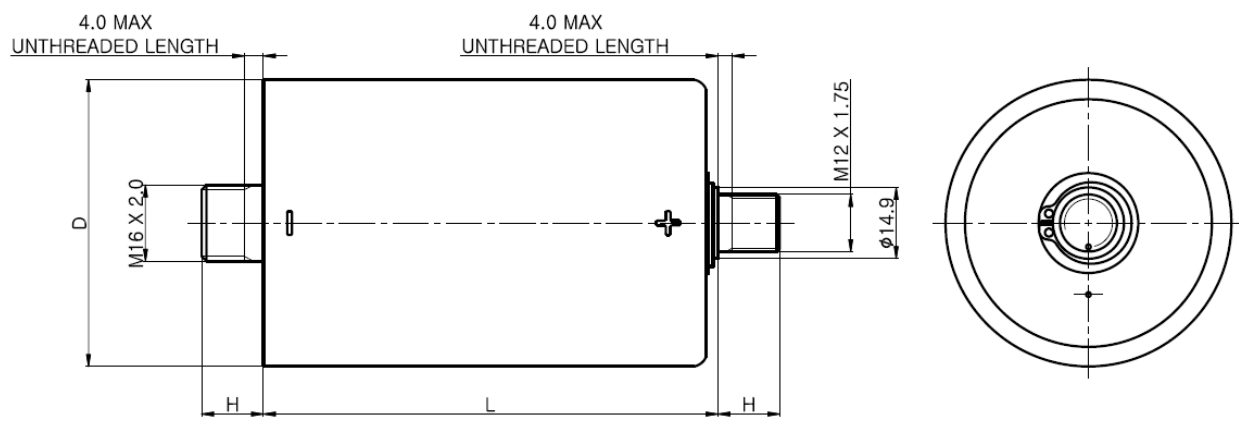
Safety & Certification	
RoHS	Compliant
REACH	Compliant
UL	Complies to 810A, Certificate No.: BBBG2.MH46340

THERMAL

Characteristics	ESHSR-3000C0-002R7A5T
Typical Thermal Resistance, R_{th} (Housing)	2.6 °C/W
Typical Thermal Capacitance, C_{th}	580 J/°C
Cont. Current to $\Delta T = 15^{\circ}C$	148 A
Cont. Current to $\Delta T = 40^{\circ}C$	243 A

PHYSICAL

Drawing



See Note on Mounting¹⁰

Dimensions	ESHSR-3000C0-002R7A5T
D (± 0.2)	60.2 mm
L (± 0.3)	139.0 mm
H (± 0.125)	13.0 mm
Nominal Weight	535 g

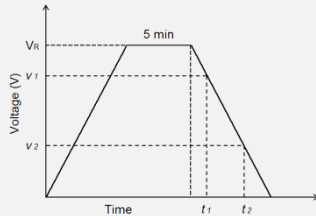
Shock & Vibration	
Shock Specification	SAE J2464
Vibration Specification	ISO 16750 (Table 14)

NOTE
1. Surge Voltage

- > Absolute maximum voltage, not repeated and for no longer than 1 second.

2. Rated Capacitance

- > Constant current charge with 10mA/F to V_R
- > Constant voltage charge at V_R for 5min
- > Constant current discharge with 10mA/F to 0.1V

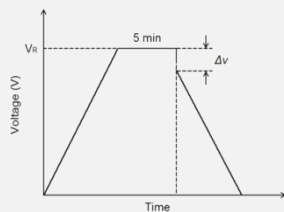


$$C = \frac{I \times (t_2 - t_1)}{v_1 - v_2}$$

Where v_1 is the measurement starting voltage, $0.8 \times V_R$ (V);
 v_2 is the measurement end voltage, $0.4 \times V_R$ (V);
 t_1 is the time from discharge start to reach v_1 (s);
 t_2 is the time from discharge start to reach v_2 (s);
 I is the absolute value of the discharging current (A).

3. ESR (Equivalent Series Resistance)

- > ESR_{DC}
 - Constant current charge to V_R
 - Constant voltage charge at V_R for 5min
 - Constant current discharge to 0.1V



$$R_d = \frac{\Delta v}{I}$$

Where R_d is the ESR_{DC} (Ω);
 Δv is the voltage drop for 10ms (V);
 I is the discharge current (A).

4. Average (or Typical)

- > Percentage spread that may be present in one shipment

5. Leakage Current

- > The capacitor is charged to the rated voltage at 25°C.
- > Leakage current is the current at 72 hours that is required to keep the capacitor charged at the rated voltage

6. Max. Current

- > Current for 1sec discharging from rated voltage to half rated voltage under constant current discharging mode.

$$I_{Max.} (A) = \frac{\frac{1}{2}V_R}{\Delta t / C + R_d}$$

Where Δt is the discharge time (sec) and Δt is 1 sec in this case;
 C is the capacitance (F);
 R_d is the ESR_{DC} (Ω);
 V_R is the rated voltage (V).

- > Max. Current **should not** be used in normal operation and is only provided as a reference value.

7. Energy & Power

- > Max. Stored Energy at $V_R = \frac{1}{2}CV_R^2$

Where C is the capacitance (F);
 V_R is the rated voltage (V).

- > Usable Specific Power, IEC 62391-2 (W/kg) = $\frac{0.12 \cdot V^2}{ESR_{DC} \cdot Mass}$

- > Impedance Match Specific Power (W/kg) = $\frac{0.25 \cdot V^2}{ESR_{DC} \cdot Mass}$

- > Gravimetric Specific Energy (Wh/kg) = $\frac{E_{Max.}}{Weight}$

8. Lifetime

- > End-of-Life Conditions
 - Capacitance: -30% from rated min. value
 - ESR: +100% from max. ESR value

9. Endurance

- > Conditions
 - Temperature: $65 \pm 2^\circ C$
 - Test duration : 2500 (+48/-0) h
 - Applied voltage: $V_R \pm 0.02V$
 - Capacitance and ESR measurement are made at 25°C

10. Mounting

- > Mounting should be designed in such a way as to not place undue mechanical stress on the terminals
- > Do not exceed the max torque value of 8Nm when assembling threaded type cells.
- > Provide adequate spacing in between cells to ensure required insulation strength for the application.
- > Provide clearance above the safety vent and do not position anything above the safety vent that may be damaged by vent rupture.
- > Welding recommendation for weldable cells available on www.nesscap.com under Support > Download.

The contents of this document are subject to change without notice. Values presented are thought to be accurate at the time of writing. Nesscap does not guarantee that the values are error-free, nor does Nesscap make any other representation, warranty or guarantee that the information is accurate, correct, reliable or current. For more information, you can reach us at one of following contacts

 Nesscap Energy Inc. Suite 3800, Royal Bank Plaza, South Tower, 200 Bay Street, P.O. Box 84, Toronto, Ontario, M5J 2Z4 CANADA	 Nesscap Energy Inc. S24040 Camino Del Avion #A118, Monarch Beach, California, 92629 USA	 Nesscap Co., Ltd. 17, Dongtangiheung-ro 681beon-gil, Giheung-gu, Yongin-si, Gyeonggi-do REPUBLIC OF KOREA	 Nesscap China Room 1608, Block N, Cangson Building, Chegongmiao, Futian District, Shenzhen City, P.R.C CHINA	 Nesscap Energy EASTERN EUROPE 10A, prospect 60-letiya Oktyabrya Moscow, 117036 RUSSIA	 Nesscap Energy GmbH Beerengarten 4 D-86938 Schondorf GERMANY
marketing@nesscap.com			info@nesscap-energy.de		

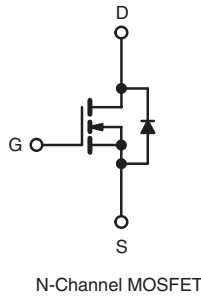
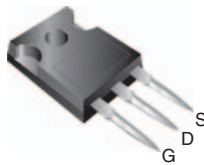
Appendix C

MOSFET Datasheet

Power MOSFET

PRODUCT SUMMARY	
V_{DS} (V)	500
$R_{DS(on)}$ (Ω)	$V_{GS} = 10\text{ V}$ 0.40
Q_g (Max.) (nC)	150
Q_{gs} (nC)	20
Q_{gd} (nC)	80
Configuration	Single

TO-247



FEATURES

- Dynamic dV/dt Rating
- Repetitive Avalanche Rated
- Isolated Central Mounting Hole
- Fast Switching
- Ease of Paralleling
- Simple Drive Requirements
- Lead (Pb)-free Available


RoHS*
COMPLIANT

DESCRIPTION

Third generation Power MOSFETs from Vishay provide the designer with the best combination of fast switching, ruggedized device design, low on-resistance and cost-effectiveness.

The TO-247 package is preferred for commercial-industrial applications where higher power levels preclude the use of TO-220 devices. The TO-247 is similar but superior to the earlier TO-218 package because its isolated mounting hole. It also provides greater creepage distances between pins to meet the requirements of most safety specifications.

ORDERING INFORMATION	
Package	TO-247
Lead (Pb)-free	IRFP450PbF
	SiHFP450-E3
SnPb	IRFP450
	SiHFP450

ABSOLUTE MAXIMUM RATINGS $T_C = 25\text{ }^\circ\text{C}$, unless otherwise noted				
PARAMETER	SYMBOL	LIMIT	UNIT	
Drain-Source Voltage	V_{DS}	500	V	
Gate-Source Voltage	V_{GS}	± 20		
Continuous Drain Current	V_{GS} at 10 V	$T_C = 25\text{ }^\circ\text{C}$	A	
		$T_C = 100\text{ }^\circ\text{C}$		
Pulsed Drain Current ^a	I_{DM}	56		
Linear Derating Factor		1.5	W/ $^\circ\text{C}$	
Single Pulse Avalanche Energy ^b	E_{AS}	760	mJ	
Repetitive Avalanche Current ^a	I_{AR}	8.7	A	
Repetitive Avalanche Energy ^a	E_{AR}	19	mJ	
Maximum Power Dissipation	$T_C = 25\text{ }^\circ\text{C}$	P_D	190	W
Peak Diode Recovery dV/dt^c	dV/dt	3.5	V/ns	
Operating Junction and Storage Temperature Range	T_J, T_{stg}	- 55 to + 150	$^\circ\text{C}$	
Soldering Recommendations (Peak Temperature)	for 10 s	300 ^d		
Mounting Torque	6-32 or M3 screw	10	lbf · in	
		1.1	N · m	

Notes

- Repetitive rating; pulse width limited by maximum junction temperature (see fig. 11).
- $V_{DD} = 50\text{ V}$, starting $T_J = 25\text{ }^\circ\text{C}$, $L = 7.0\text{ mH}$, $R_G = 25\text{ }\Omega$, $I_{AS} = 14\text{ A}$ (see fig. 12).
- $I_{SD} \leq 14\text{ A}$, $dI/dt \leq 130\text{ A}/\mu\text{s}$, $V_{DD} \leq V_{DS}$, $T_J \leq 150\text{ }^\circ\text{C}$.
- 1.6 mm from case.

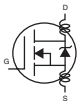
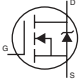
* Pb containing terminations are not RoHS compliant, exemptions may apply

IRFP450, SiHFP450

Vishay Siliconix



THERMAL RESISTANCE RATINGS				
PARAMETER	SYMBOL	TYP.	MAX.	UNIT
Maximum Junction-to-Ambient	R_{thJA}	-	40	°C/W
Case-to-Sink, Flat, Greased Surface	R_{thCS}	0.24	-	
Maximum Junction-to-Case (Drain)	R_{thJC}	-	0.65	

SPECIFICATIONS $T_J = 25\text{ }^\circ\text{C}$, unless otherwise noted						
PARAMETER	SYMBOL	TEST CONDITIONS	MIN.	TYP.	MAX.	UNIT
Static						
Drain-Source Breakdown Voltage	V_{DS}	$V_{GS} = 0\text{ V}$, $I_D = 250\text{ }\mu\text{A}$	500	-	-	V
V_{DS} Temperature Coefficient	$\Delta V_{DS}/T_J$	Reference to $25\text{ }^\circ\text{C}$, $I_D = 1\text{ mA}$	-	0.63	-	V/°C
Gate-Source Threshold Voltage	$V_{GS(th)}$	$V_{DS} = V_{GS}$, $I_D = 250\text{ }\mu\text{A}$	2.0	-	4.0	V
Gate-Source Leakage	I_{GSS}	$V_{GS} = \pm 20\text{ V}$	-	-	± 100	nA
Zero Gate Voltage Drain Current	I_{DSS}	$V_{DS} = 500\text{ V}$, $V_{GS} = 0\text{ V}$	-	-	25	μA
		$V_{DS} = 400\text{ V}$, $V_{GS} = 0\text{ V}$, $T_J = 125\text{ }^\circ\text{C}$	-	-	250	
Drain-Source On-State Resistance	$R_{DS(on)}$	$V_{GS} = 10\text{ V}$ $I_D = 8.4\text{ A}^b$	-	-	0.40	Ω
Forward Transconductance	g_{fs}	$V_{DS} = 50\text{ V}$, $I_D = 8.4\text{ A}^b$	9.3	-	-	S
Dynamic						
Input Capacitance	C_{iss}	$V_{GS} = 0\text{ V}$, $V_{DS} = 25\text{ V}$, $f = 1.0\text{ MHz}$, see fig. 5	-	2600	-	pF
Output Capacitance	C_{oss}		-	720	-	
Reverse Transfer Capacitance	C_{rss}		-	340	-	
Total Gate Charge	Q_g	$V_{GS} = 10\text{ V}$ $I_D = 14\text{ A}$, $V_{DS} = 400\text{ V}$, see fig. 6 and 13 ^b	-	-	150	nC
Gate-Source Charge	Q_{gs}		-	-	20	
Gate-Drain Charge	Q_{gd}		-	-	80	
Turn-On Delay Time	$t_{d(on)}$	$V_{DD} = 250\text{ V}$, $I_D = 14\text{ A}$, $R_G = 6.2\text{ }\Omega$, $R_D = 17\text{ }\Omega$, see fig. 10 ^b	-	17	-	ns
Rise Time	t_r		-	47	-	
Turn-Off Delay Time	$t_{d(off)}$		-	92	-	
Fall Time	t_f		-	44	-	
Internal Drain Inductance	L_D	Between lead, 6 mm (0.25") from package and center of die contact 	-	5.0	-	nH
Internal Source Inductance	L_S		-	13	-	
Drain-Source Body Diode Characteristics						
Continuous Source-Drain Diode Current	I_S	MOSFET symbol showing the integral reverse p - n junction diode 	-	-	14	A
Pulsed Diode Forward Current ^a	I_{SM}		-	-	56	
Body Diode Voltage	V_{SD}	$T_J = 25\text{ }^\circ\text{C}$, $I_S = 14\text{ A}$, $V_{GS} = 0\text{ V}^b$	-	-	1.4	V
Body Diode Reverse Recovery Time	t_{rr}	$T_J = 25\text{ }^\circ\text{C}$, $I_F = 14\text{ A}$, $dI/dt = 100\text{ A}/\mu\text{s}^b$	-	540	810	ns
Body Diode Reverse Recovery Charge	Q_{rr}		-	4.8	7.2	μC
Forward Turn-On Time	t_{on}	Intrinsic turn-on time is negligible (turn-on is dominated by L_S and L_D)				

Notes

- Repetitive rating; pulse width limited by maximum junction temperature (see fig. 11).
- Pulse width $\leq 300\text{ }\mu\text{s}$; duty cycle $\leq 2\%$.

TYPICAL CHARACTERISTICS 25 °C, unless otherwise noted

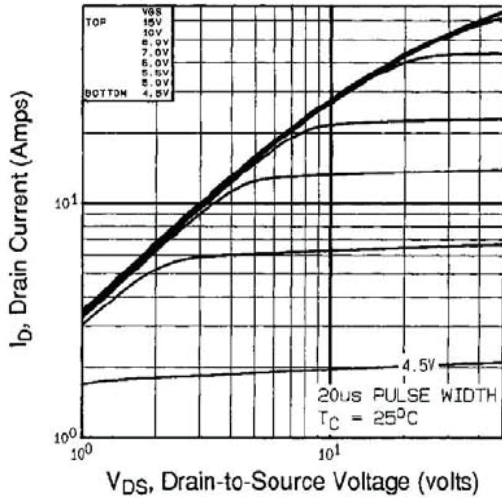


Fig. 1 - Typical Output Characteristics, $T_C = 25\text{ }^\circ\text{C}$

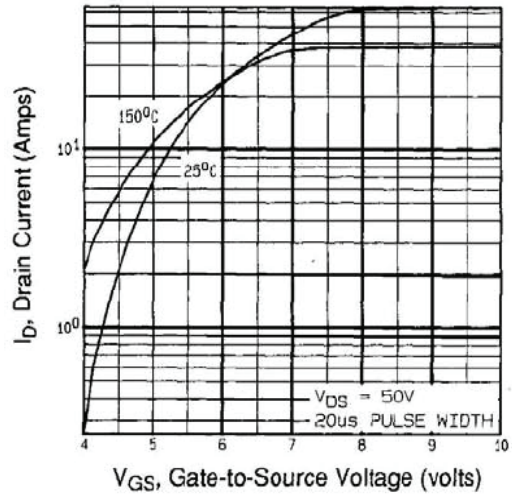


Fig. 3 - Typical Transfer Characteristics

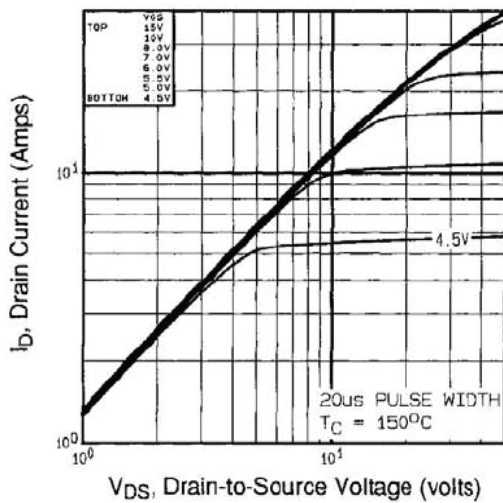


Fig. 2 - Typical Output Characteristics, $T_C = 150\text{ }^\circ\text{C}$

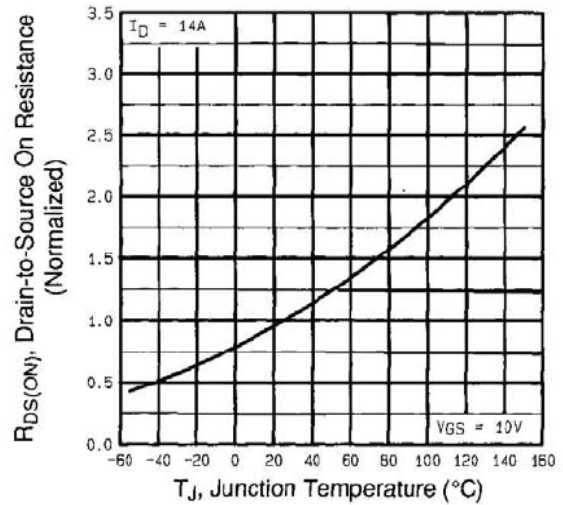


Fig. 4 - Normalized On-Resistance vs. Temperature

IRFP450, SiHFP450

Vishay Siliconix

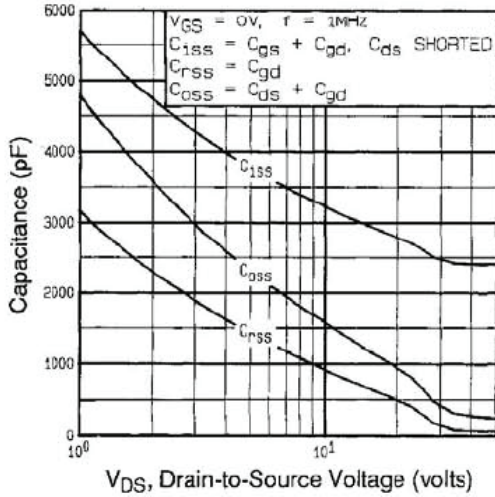


Fig. 5 - Typical Capacitance vs. Drain-to-Source Voltage

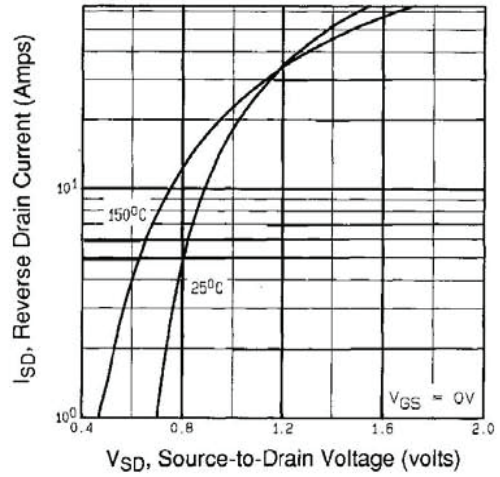


Fig. 7 - Typical Source-Drain Diode Forward Voltage

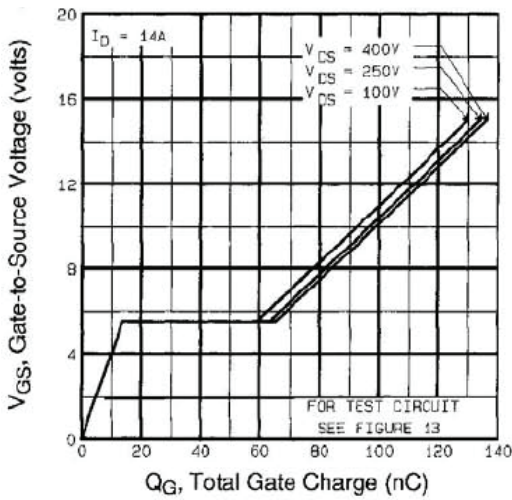


Fig. 6 - Typical Gate Charge vs. Gate-to-Source Voltage

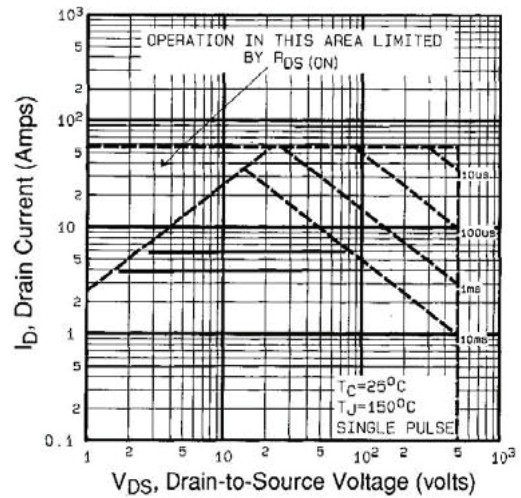


Fig. 8 - Maximum Safe Operating Area

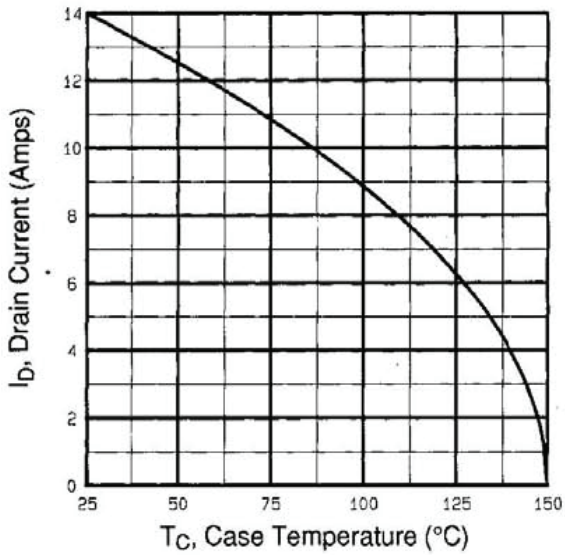


Fig. 9 - Maximum Drain Current vs. Case Temperature

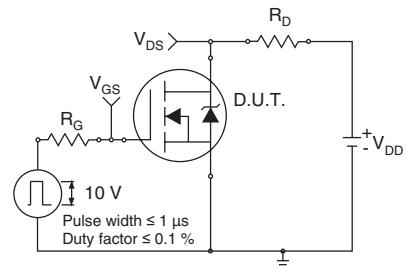


Fig. 10a - Switching Time Test Circuit

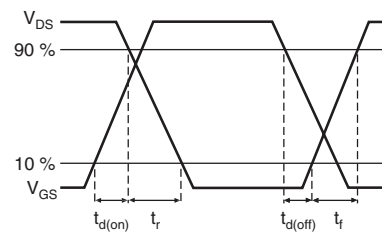


Fig. 10b - Switching Time Waveforms

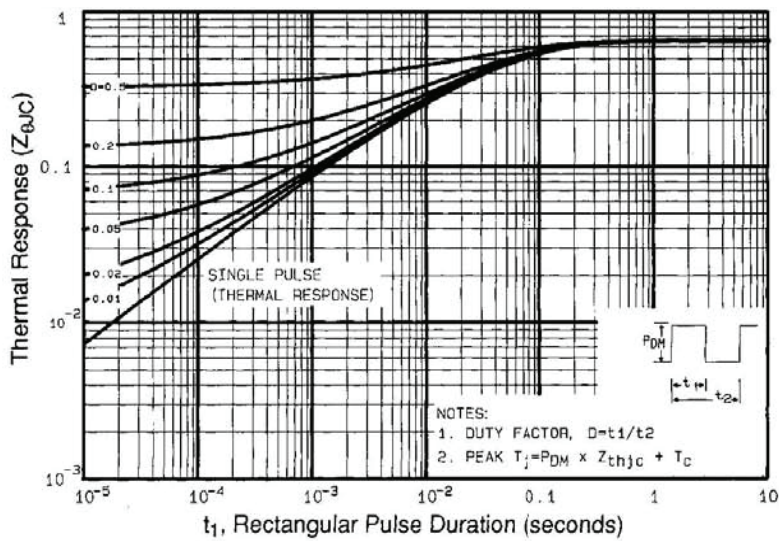


Fig. 11 - Maximum Effective Transient Thermal Impedance, Junction-to-Case

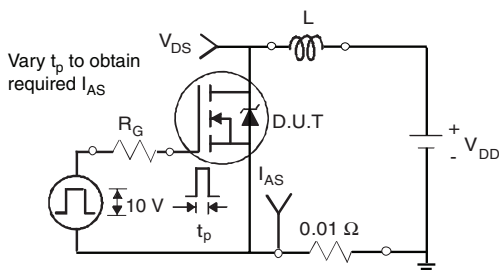


Fig. 12a - Unclamped Inductive Test Circuit

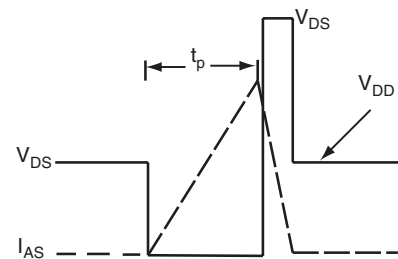


Fig. 12b - Unclamped Inductive Waveforms

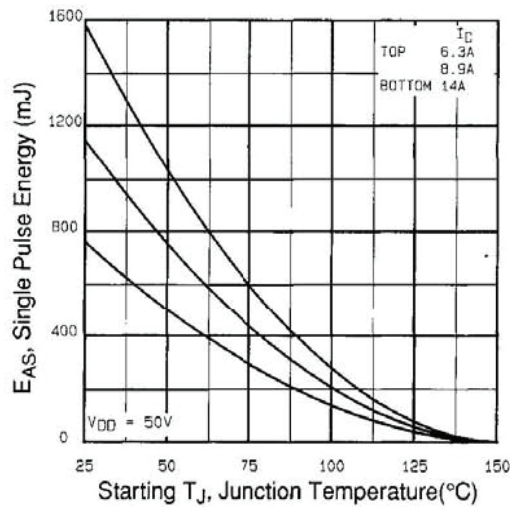


Fig. 12c - Maximum Avalanche Energy vs. Drain Current

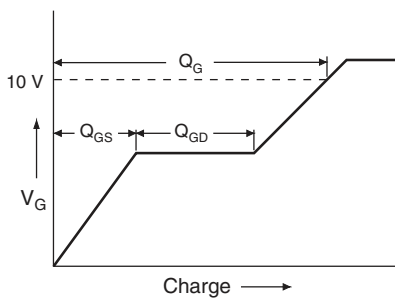


Fig. 13a - Basic Gate Charge Waveform

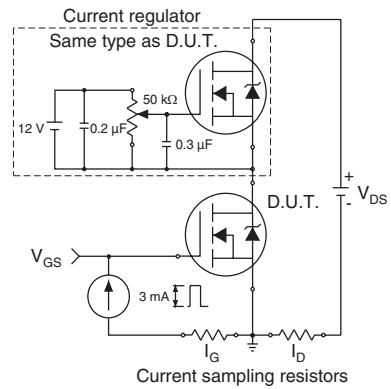
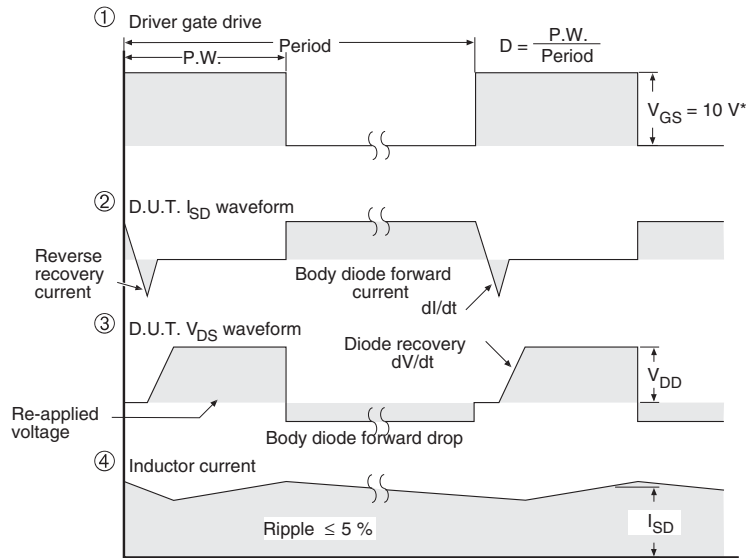
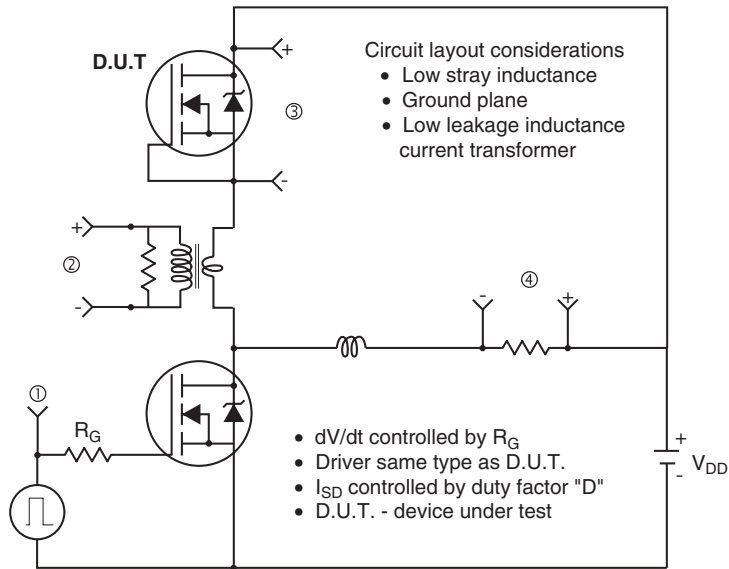


Fig. 13b - Gate Charge Test Circuit

Peak Diode Recovery dV/dt Test Circuit



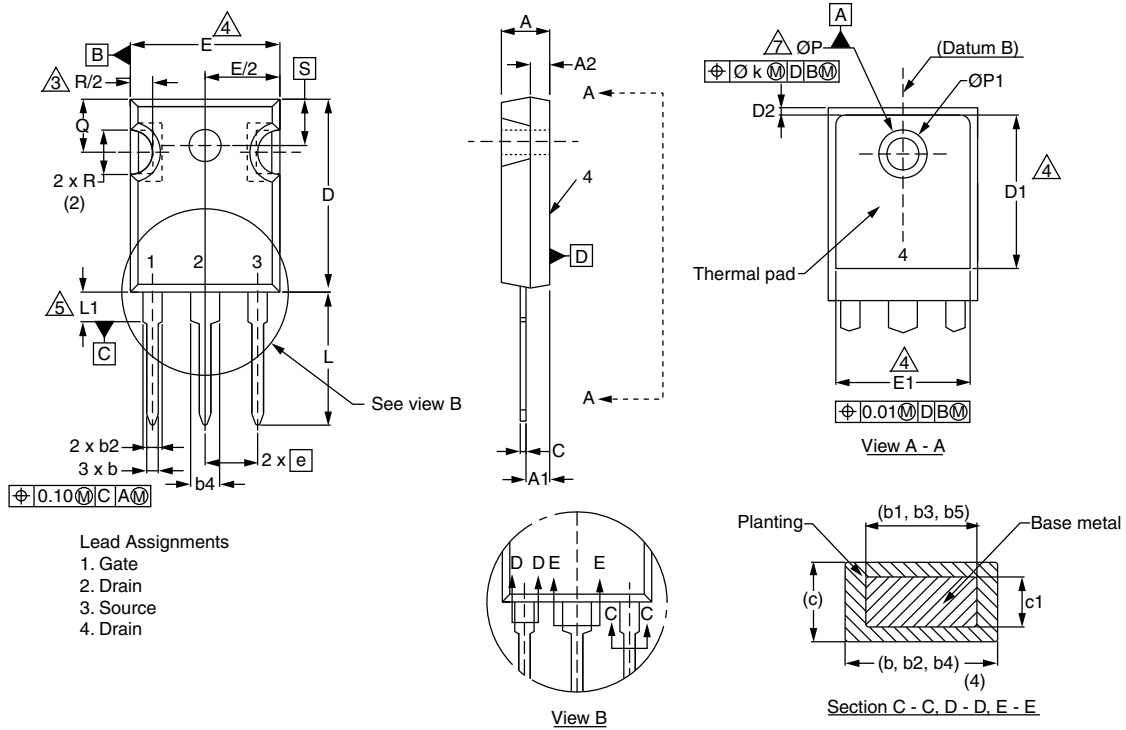
* $V_{GS} = 5 V$ for logic level devices

Fig. 14 - For N-Channel

Vishay Siliconix maintains worldwide manufacturing capability. Products may be manufactured at one of several qualified locations. Reliability data for Silicon Technology and Package Reliability represent a composite of all qualified locations. For related documents such as package/tape drawings, part marking, and reliability data, see <http://www.vishay.com/ppg?91233>.



TO-247AC (High Voltage)



DIM.	MILLIMETERS		INCHES	
	MIN.	MAX.	MIN.	MAX.
A	4.58	5.31	0.180	0.209
A1	2.21	2.59	0.087	0.102
A2	1.17	2.49	0.046	0.098
b	0.99	1.40	0.039	0.055
b1	0.99	1.35	0.039	0.053
b2	1.53	2.39	0.060	0.094
b3	1.65	2.37	0.065	0.093
b4	2.42	3.43	0.095	0.135
b5	2.59	3.38	0.102	0.133
c	0.38	0.86	0.015	0.034
c1	0.38	0.76	0.015	0.030
D	19.71	20.82	0.776	0.820
D1	13.08	-	0.515	-

DIM.	MILLIMETERS		INCHES	
	MIN.	MAX.	MIN.	MAX.
D2	0.51	1.30	0.020	0.051
E	15.29	15.87	0.602	0.625
E1	13.72	-	0.540	-
e	5.46 BSC		0.215 BSC	
Ø k	0.254		0.010	
L	14.20	16.25	0.559	0.640
L1	3.71	4.29	0.146	0.169
N	7.62 BSC		0.300 BSC	
Ø P	3.51	3.66	0.138	0.144
Ø P1	-	7.39	-	0.291
Q	5.31	5.69	0.209	0.224
R	4.52	5.49	0.178	0.216
S	5.51 BSC		0.217 BSC	

ECN: X13-0103-Rev. D, 01-Jul-13
DWG: 5971

Notes

1. Dimensioning and tolerancing per ASME Y14.5M-1994.
2. Contour of slot optional.
3. Dimension D and E do not include mold flash. Mold flash shall not exceed 0.127 mm (0.005") per side. These dimensions are measured at the outermost extremes of the plastic body.
4. Thermal pad contour optional with dimensions D1 and E1.
5. Lead finish uncontrolled in L1.
6. Ø P to have a maximum draft angle of 1.5 to the top of the part with a maximum hole diameter of 3.91 mm (0.154").
7. Outline conforms to JEDEC outline TO-247 with exception of dimension c.
8. Xian and Mingxin actually photo.





Disclaimer

ALL PRODUCT, PRODUCT SPECIFICATIONS AND DATA ARE SUBJECT TO CHANGE WITHOUT NOTICE TO IMPROVE RELIABILITY, FUNCTION OR DESIGN OR OTHERWISE.

Vishay Intertechnology, Inc., its affiliates, agents, and employees, and all persons acting on its or their behalf (collectively, "Vishay"), disclaim any and all liability for any errors, inaccuracies or incompleteness contained in any datasheet or in any other disclosure relating to any product.

Vishay makes no warranty, representation or guarantee regarding the suitability of the products for any particular purpose or the continuing production of any product. To the maximum extent permitted by applicable law, Vishay disclaims (i) any and all liability arising out of the application or use of any product, (ii) any and all liability, including without limitation special, consequential or incidental damages, and (iii) any and all implied warranties, including warranties of fitness for particular purpose, non-infringement and merchantability.

Statements regarding the suitability of products for certain types of applications are based on Vishay's knowledge of typical requirements that are often placed on Vishay products in generic applications. Such statements are not binding statements about the suitability of products for a particular application. It is the customer's responsibility to validate that a particular product with the properties described in the product specification is suitable for use in a particular application. Parameters provided in datasheets and / or specifications may vary in different applications and performance may vary over time. All operating parameters, including typical parameters, must be validated for each customer application by the customer's technical experts. Product specifications do not expand or otherwise modify Vishay's terms and conditions of purchase, including but not limited to the warranty expressed therein.

Except as expressly indicated in writing, Vishay products are not designed for use in medical, life-saving, or life-sustaining applications or for any other application in which the failure of the Vishay product could result in personal injury or death. Customers using or selling Vishay products not expressly indicated for use in such applications do so at their own risk. Please contact authorized Vishay personnel to obtain written terms and conditions regarding products designed for such applications.

No license, express or implied, by estoppel or otherwise, to any intellectual property rights is granted by this document or by any conduct of Vishay. Product names and markings noted herein may be trademarks of their respective owners.